

# **STUDIES ON ABSORPTION OF SO<sub>2</sub> IN REGENERATIVE IONIC LIQUIDS AND Ca-BASED SLURRIES**

**Ph.D. Thesis**

**AVANISH KUMAR**

**ID No. 2013RCH9066**



**DEPARTMENT OF CHEMICAL ENGINEERING  
MALAVIYA NATIONAL INSTITUTE OF TECHNOLOGY JAIPUR**

**December 2018**

# STUDIES ON ABSORPTION OF SO<sub>2</sub> IN REGENERATIVE IONIC LIQUIDS AND Ca-BASED SLURRIES

Submitted in  
fulfillment of the requirements for the degree of

*Doctor of Philosophy*

by

**Avanish Kumar**  
**ID: 2013RCH9066**

Under the Supervision of  
**Prof. S. K. Jana**



**DEPARTMENT OF CHEMICAL ENGINEERING**  
**MALAVIYA NATIONAL INSTITUTE OF TECHNOLOGY JAIPUR**

**December 2018**

**© Malaviya National Institute of Technology Jaipur-2018.**

**All rights reserved.**

## DECLARATION

I, Avanish Kumar, declare that this thesis titled, “Studies on Absorption of SO<sub>2</sub> in Regenerative Ionic Liquids And Ca-Based Slurries” and the work presented in it, are my own. I confirm that:

- This work was done wholly or mainly while in candidature for a research degree at this university.
- Where any part of this thesis has previously been submitted for a degree or any other qualification at this university or any other institution, this has been clearly stated.
- Where I have consulted the published work of others, this is always clearly attributed.
- Where I have quoted from the work of others, the source is always given. With the exception of such quotations, this thesis is entirely my own work.
- I have acknowledged all main sources of help.
- Where the thesis is based on work done by myself, jointly with others, I have made clear exactly what was done by others and what I have contributed myself.

Date: 10-12-2018

Avanish Kumar  
(2013RCH9066)

## CERTIFICATE

This is to certify that the thesis entitled “Studies on Absorption of SO<sub>2</sub> in Regenerative Ionic Liquids And Ca-Based Slurries” being submitted by Avanish Kumar (2013RCH9066) is a bonafide research work carried out under my supervision and guidance in fulfillment of the requirement for the award of the degree of **Doctor of Philosophy** in the Department of Chemical Engineering, Malaviya National Institute of Technology, Jaipur, India. The matter embodied in this thesis is original and has not been submitted to any other University or Institute for the award of any other degree.

Place: Jaipur  
Date: 10-12-2018

Prof. S. K. Jana  
Professor  
Dept. of Chemical Engineering  
MNIT Jaipur

## ACKNOWLEDGEMENT

*I am grateful to the almighty, the most benevolent and merciful, for giving me the strength and zeal to complete this endeavor. Tremendous praise for God, who is forever a torch of guidance for knowledge seekers and whole humanity.*

*Foremost, I would like to express my sincere gratitude to my supervisor **Prof. S. K. Jana**, Dept. of Chemical Engineering, Malaviya National Institute of Technology, Jaipur for the continuous support of my Ph.D. study and research, for his patience, motivation, enthusiasm, and immense knowledge. His nonpareil guidance helped me in all the time of research and writing of this thesis. I could not have imagined having a better advisor and mentor for my Ph.D. study.*

*I would to thank former Director **Prof. I. K. Bhatt** and current Director **Prof. Uday Kumar Yaragatti** of MNIT Jaipur for establishing and maintaining Department of Material Research Centre and providing equipment's facilities like XRD, <sup>1</sup>H NMR, Fe-SEM etc. that help me in my Ph.D work.*

*I am highly thankful to **Prof. Kailash Singh** Head, Department of Chemical Engineering for providing infra-structure support and facilities. All DREC members **Prof. Dilip Sharma, Dr. P. Pandit, Dr. U.K. Arum Kumar** and **Dr. Virendra Saharan** for their continuous evaluation and suggestions throughout my Ph.D. studies.*

*I am indebted to **Dr. Sandip Chaudhary** and **Dr. R. K. Joshi**, Assistant Professor, Department of Chemistry, MNIT Jaipur for granting me permission to use some apparatus of their laboratories for conducting some experiments.*

*A non-payable debt to my mother **Smt. Manju Sinha** and father **Shri Yougeshwar Prasad Singh** for their unflagging love, blessings and moral support throughout my research work. They prayed for me, shared the burdens and made sure that I sailed through smoothly. Their boundless affection has been my great strength during the moment of stress. I thank them for being my strength always.*

*The constant co-operation, inspiration and moral support accorded by my soul mate **Mrs. Swati Dubey** is beyond any acknowledgement. Her patience and love enabled*

*me to complete this work. My deepest gratitude goes for standing by me like a rock during critical periods and helping me a great deal to fulfill my scientific pursuits and preparation of this manuscript. I have no doubt in my mind that without her invaluable guidance and help, this stupendous work would not have been completed.*

*It is impossible to express my sincere and heartfelt thanks to my adorable sister **Mrs. Jyoti Kumari**, brother **Mr. Chandan Kumar**, niece **Miss Avani Singh**, and sister in law **Mrs. Khushboo Kumari & Ms. Shripriya Dubey** for their persistent co-operation, patience, moral support and endurance. I would also like to express my gratitude and indebtedness to my father in law **Shri Ganesh Shankar Dubey** for his strong inspiration, encouragement, blessings and to mother in law **Late Uma Dubey** for offering me silent wishes.*

*I wish to thank my colleagues **Mr. Prshant Shrivastava** who help me in fabrication of experimental set-up, **Mr. Lokesh Kumar** for his contribution in thesis writing. I cannot leave this acknowledgment without thanking my some Ph.D colleagues, **Mr. Avinash Shrivastava, Mahesh Paliwal, Munsaf Ali, Lalit Yadav** of Chemistry Department for their suggestions in conducting chemistry part of my Ph.D work.*

*I feel extremely thankful to all the non-teaching staff of the Department namely **Mr. Ramesh Sharma** and **Mr. Rajiv Goswami** also deserve mention for helping me with the experimental set-up and acquisitions of reagents and other requirements.*

*I sincerely thank all those people whose names I have not mentioned here, but directly or indirectly have contributed in making this thesis a success.*

**Dec. 2018**

**Avanish Kumar**

## ABSTRACT

The present work is concerned with the experimental studies of absorptive removal of sulfur dioxide from simulated gaseous mixtures using two different systems. In the first of these two variants, it was decided to find the performance of a contactor different from those conventionally used in FGD processes. In the other, experimental data were generated for the desulfurization operation using a series of low cost hydroxyammonium ionic liquids for which important design information is not available in the literature. While ionic liquids possess several desired properties, viz., low vapor pressure, high temperature stability, a strong solvent capacity to many compounds, etc. However, generally, these solvents are costly. Raw materials used for the synthesis of hydroxyammonium ionic liquids used in this study are however available at a substantially low cost and can be synthesized using a very simple process.

For the discussion of experimental results, information on reaction kinetics is found to be essentially required. That under the present experimental conditions, the gas absorption operation accompanied by chemical reaction follows the kinetics reported in the literature was verified through the application of the conventional methodology. For determination of percent resistance to mass transfer, liquid phase physical mass-transfer coefficient and gas phase mass transfer coefficients are required. Values of these parameters have been determined experimentally.

A chemical analysis of samples was performed for finding out the percentage of lime ( $\text{Ca(OH)}_2$ ) present in it. It was found to be nearly 96% by weight. XRD confirms the presence of  $\text{CaCO}_3$  as a major impurity. Particle-size distributions (PSDs) of reactant  $\text{Ca(OH)}_2$  sample were measured using a Mastersizer 2000E.

Desulfurization experiments were performed in a bubble column reactor made of a  $10.5 \times 10^{-2}$  m internal diameter and  $74.0 \times 10^{-2}$  m height glass column fitted with a gas-distributor plate at the bottom. A ZRJFAY36, Fuji, Japan make infrared  $\text{SO}_2$  analyzer was used to measure the  $\text{SO}_2$  concentration at the inlet and exit of the reactor. An air compressor and a vacuum pump were used to adjust the  $\text{SO}_2$  concentration in the feed gas



by diluting with compressed air and to remove the exhaust gas from the glass column, respectively.

For absorption studies using ionic liquids, a series of hydroxyammonium ionic liquids were synthesized by neutralization of mono- or tri-ethanolamine with lactic- or salicylic acid using ethanol as the solvent. Lactic acid dissolved in ethanol in a dropping funnel was added drop wise into a round bottom flask containing mono ethanol amine, also dissolved in ethanol and the contents stirred continuously using a magnetic stirrer. The round bottom flask was connected to a reflux condenser. Solvent ethanol was then removed from the product by subjecting it to vacuum evaporation. All the synthesized ILs were liquid at room temperature except 2- hydroxyethyl ammonium salicylate (MSIL).

Physico-chemical properties of the synthesized ionic liquids were measured for evaluating its suitability for its use as a solvent. The properties of the solvents measured in this study were density, viscosity, surface tension and refractive index. Densities of these ionic liquids were marginally higher than that of water, but viscosity values were observed to be substantially higher 252 to 364 MPa.s. Measured values of refractive index, useful for identification of an unknown substance or its concentration in a given liquid mixture, were found to vary in the range 1.457 to 1.511. Surface tension values of the synthesized ILs, another important parameter of a good absorbing solvent, were found to vary from 44 to 56 mN/m. In addition to this, for obtaining information about the micro structure of the synthesized ionic liquids and chemical interaction between the absorbed  $\text{SO}_2$  and the IL solvents, FT-IR and  $^1\text{H}$  NMR spectra of the virgin and exhausted ILs were measured. FT-IR and  $^1\text{H}$  NMR spectra of the  $\text{SO}_2$ -absorbed ILs and gas-free ILs indicated that there was no difference in the proton chemical shift and no new absorption bands in the two spectra. These results suggested that the absorbed  $\text{SO}_2$  gas was present in the molecular state without any chemical reaction.

Absorption experiments were performed in a semi-batch mode. A lean gaseous mixture of sulfur dioxide with air was allowed to pass through the empty column, and when the flow rate reached a steady value, a batch of ionic liquid solvent was carefully poured into the column. The concentration of sulfur dioxide at the reactor inlet and its variation with the propagation of reaction at the exit of the reactor displayed on the data

logger was recorded. Three sets of data were collected for each of the variables studied. The variables studied were: superficial velocity of the gaseous mixture, the volume of ionic liquid fed into the reactor and concentration of sulfur dioxide in the feed gas. Reactor performance was analyzed with reference to the variables.

Trial experiments were also performed using aqueous solutions of NaOH, NaClO, DMSO and pure water for verification of the information reported in the literature and the regeneration characteristics of the absorbents.

Effects of *superficial velocity of gas* on transient values of the SO<sub>2</sub> removal efficiency by the ionic liquids were studied for three different superficial velocities, viz.,  $3.85 \times 10^{-2}$ ,  $5.77 \times 10^{-2}$  and  $7.7 \times 10^{-2} \text{ m s}^{-1}$ . At the beginning of the reactor operation, the value of SO<sub>2</sub> removal efficiency started increasing and then approximately remained constant at about 89 percent. With an increase in the superficial velocity of the gas, the intensity of turbulence in the short bubble column contactor increased. This leads to an increase in the mass-transfer coefficient value for gas absorption. The Increased amount of SO<sub>2</sub> was thereby absorbed from each bubble during its rise through the pool of liquid and SO<sub>2</sub> removal efficiency was thereby increased. However, reduced contact time resulting from increased gas velocity lowered the rate of gas absorption from each bubble. These opposing factors possibly off-set each other's effects and maximum removal efficiency remained unchanged at about 89 percent. While studying the effects of the *nature of constituting ions* in the ILs on percent SO<sub>2</sub> removal efficiency, it was observed that when either 2-hydroxyethylammonium or tri-(2-hydroxyethyl) ammonium cation was associated with the lactate anion, each attained the same magnitude of the transient values of maximum SO<sub>2</sub> absorption efficiency. For Tri (2-hydroxyethyl)ammonium lactate (TLIL), it was marginally higher than that with 2-hydroxyethylammonium lactate (MLIL). Due to the very poor absorption behavior, Tri (2-hydroxyethyl)ammonium salicylate (TSIL) is not considered as a desired alternative absorbent. Hence, further experiments were not performed with this IL. With an increase in the *volume of IL fed into the reactor*, the exit concentration was found to reduce when values of all other variables remained unchanged. The beneficial effect of longer contact time due to the larger depth of solvent in the column possibly outweigh the negative effects of reduced intensity of turbulence, and the maximum SO<sub>2</sub> removal efficiency was

thereby increased with an increase in the volume of IL fed into the reactor. Percent of SO<sub>2</sub> removal efficiency by the MLIL was found to reduce with an increase in *its initial concentration in the feed gas*. At a constant temperature, the solubility of SO<sub>2</sub> in the ionic liquid increased as its concentration in the feed gas was increased. Moles of SO<sub>2</sub> absorbed from each gas bubble and hence the rate of absorption, at a fixed superficial velocity of the gas, increases with an increase in its concentration in the feed gas. Although total moles absorbed from a single gas bubble increased with an increase in the concentration of SO<sub>2</sub> in the feed gas, transient values of the percent removal of SO<sub>2</sub> reduced because of the definition used for its calculation, the concentration of SO<sub>2</sub> in the feed gas appears in the denominator.

The ionic liquid (IL) used in the experiments that got exhausted by absorption of SO<sub>2</sub>, was regenerated by subjecting it to desorption under vacuum using a rotary evaporator (BUCHI, Switzerland, Rotavapor R-210). Level of vacuum generated by the vacuum pump and the temperature of the water bath was adjusted to 100 mbar and 303 K, respectively. Application of vacuum was continued till the difference between the successive weights was negligibly small.

*Recyclability of the regenerated ionic liquids* was studied as these played a significant role in the economic feasibility of the process. The virgin ILs were found to get exhausted in a very short period during first absorption operation. But unlike conventional solvents, both the ionic liquids, MLIL and TLIL, were observed not to show any reduction in their absorption capacities even after successive absorption (performed for 60 min) and regeneration operations. The residual amount of ethanol present in virgin ILs was believed to form an additional hydrogen bond with the amine group of ionic liquid and thereby caused a reduction in the absorption behavior of each solvent. During the regeneration process, this residual amount of ethanol got evaporated, and the absorption capacity of the ILs was thereby increased.

Temperature stability of the ionic liquid MLIL was determined through measurement of its decomposition temperature by TGA analysis. For this measurement, a platinum sample holder was employed. Decomposition of MLIL was found to be 230 °C. This value agreed well with that reported in the literature.

The *second part of this investigation* was devoted to studies on absorption of SO<sub>2</sub> in Ca-based slurries in bubble column slurry and slurry-foam reactors. The variables studied were: effects of initial solids loading in the feed slurry, superficial velocity of the gas, the volume of slurry charged into the reactor, the initial concentration of solute in the feed gas and that of different types and concentrations of surfactants on transient SO<sub>2</sub> removal efficiency. Other experiments performed were: measurements of the gas holdup in the bubble column, gas phase mass transfer coefficient, physical mass-transfer coefficient values for liquid phase and characterization of FGD products, viz., XRD, SEM, TGA and FTIR analyses.

A *comparison* of the conversions obtained in the *slurry-foam reactor* in the presence of different types (cationic, anionic and non-ionic) of surfactants with those obtained from a conventional short *slurry bubble-column reactor* showed that in the slurry-foam reactor, SO<sub>2</sub> removal efficiency was decreased marginally by about 1%. With an increase in the *initial loading of Ca(OH)<sub>2</sub> and CaCO<sub>3</sub>*, the time required for complete consumption of these reactants was found to increase proportionately. Although the consequent increase in solid-liquid interfacial area was expected to cause an increased rate of solid dissolution, the rate of SO<sub>2</sub> absorption and reaction were found to remain unaffected. This was attributed to the high gas phase resistance at the very low partial pressure of SO<sub>2</sub>. SO<sub>2</sub> removal efficiency was found to be lower when the feed was a saturated solution of lime as compared to the slurry.

In the presence of sparingly soluble fine suspended particles of lime, particle dissolution and the reaction occurs in parallel within the film surrounding the gas bubbles and consequent shifting of the reaction plane towards the gas-liquid interface cause an increase in the rate of reaction. For the same solids loading of Ca(OH)<sub>2</sub> and CaCO<sub>3</sub>, SO<sub>2</sub> removal efficiency was found to be lower in the case of CaCO<sub>3</sub> even when compared on the basis of mass ratio of CaO present in the reactants. Substantially lower solubility of CaCO<sub>3</sub> as compared to Ca(OH)<sub>2</sub> was considered to be the main reason for this. As the *superficial velocity of the gas is increased*, the rate of reaction increased proportionally and the time required for complete consumption of a given mass of reactant *B* reduced proportionally. However, the transient value of maximum SO<sub>2</sub> removal efficiency was observed to be attained at the lowest velocity of the gas. With CaCO<sub>3</sub> slurry, the removal

efficiency was found to increase as the gas velocity is increased in its lower range, possibly due to an increase in the dissolution rate of suspended particles induced by higher intensity of agitation by the gas bubbles. In the higher range of gas velocities, the effect of the reduced residence time of bubbles possibly outweighed the beneficial effect of turbulence and the increased value of mass-transfer coefficient. With an increase in the *concentration of SO<sub>2</sub> in the feed gas*, gas phase resistance to mass transfer reduces and interfacial concentration of sulfur dioxide in the liquid phase increased. This increased the rate of gas absorption and reaction, and, the concentration of dissolved solid in the liquid phase is thereby reduced at a faster rate. This phenomenon resulted in more solid to dissolve in the liquid to restore its solubility. Thus, the rate of gas absorption, solid dissolution and its reaction increased with an increase in the concentration of SO<sub>2</sub> in the feed gas.

Experiments with calcium carbonate slurry showed that in addition to the gas-phase resistance to SO<sub>2</sub> absorption, the dissolution rate of calcium carbonate in the liquid phase played an important role in determining the rate of reaction. The position of the reaction plane in the film was established by the rate of diffusion of absorbed SO<sub>2</sub> and that of dissolved calcium carbonate. When the inlet SO<sub>2</sub> concentration was increased, the flux of SO<sub>2</sub> was enhanced. However, the dissolution rate of calcium carbonate does not increase so fast to accommodate the effect of increased flux of SO<sub>2</sub>. Therefore, the reaction plane within the liquid film gets shifted further away from the gas-liquid interface, and the reaction rate is decreased. Although total moles of SO<sub>2</sub> absorbed and reacted with component *B* increased with an increase in the initial concentration of SO<sub>2</sub>, its maximum removal efficiency reduced as the inlet concentration was increased from 250 ppm to 1500 ppm, owing to the definition used for its calculation. In order to find a suitable solution to obviate *the choking problem caused by the FGD products*, CaSO<sub>3</sub> and CaSO<sub>4</sub> · 2H<sub>2</sub>O, desulfurization of the simulated gaseous mixture was studied in a foam-bed reactor. The orifices on the gas distributor plate of the *bubble column contactor* in the present investigation were found to get choked at the time of product withdrawal for solids loading beyond 8 kg m<sup>-3</sup>. But in the foam-bed reactor with a surfactant concentration of only 4 ppm CTAB, no such choking was observed up to 16 kg m<sup>-3</sup> of solids loading. Beyond this, experiments were not performed in this investigation.

Addition of a surfactant was found to reduce the SO<sub>2</sub> removal efficiency, in all probability, due to the reduction in surface turbulence. This phenomenon restricts the movement of fresh reactants to the interface and causes a lowering in the rate of gas absorption. But at the above concentration of CTAB, no reduction in the SO<sub>2</sub> removal efficiency was observed and height of foam column being only about 0.010 to 0.012 mm, foam breaking was also not required.

Experiments were also performed by addition of higher concentration of other type of surfactants. However, when SO<sub>2</sub> was absorbed in distilled water in the presence or absence of surfactants there appeared no marked difference in its exit concentration. Partial surface coverage of the particles with the surfactant molecules, leading to a reduced rate of its dissolution and additional resistance formed on the liquid film of the alkaline solution was considered to cause a reduction in the absorption rate of SO<sub>2</sub>.

FGD products obtained from the bubble column and foam-bed reactors were *characterized* using *FTIR analysis*. The product obtained from the bubble column reactor and those from the foam-bed reactor with the use of Triton X-100 and Tween 80 as additives were calcium sulfate hemihydrates, but with the use of Teepol, calcium sulfate dihydrate (gypsum) was obtained. It was observed from the *thermogravimetric analyses (TGA)* that weight loss was about 20 percent at 170 °C for the product obtained with Teepol as the additive while it was about 6.11 percent at 150 °C for the other products. These findings confirm that the products were calcium sulfate dihydrate and hemihydrates, respectively. These conclusions were drawn from the XRD analysis as well. *SEM micrographs* of the FGD products obtained in the presence and absence of surface active agents showed that the morphology of the product crystals was needle-shaped and rod-like depending on the type of surfactant additives. The size estimation of the particles was performed using ImageJ software.

---

## CONTENTS

	PAGE NO.
<i>DECLARATION</i>	<i>i</i>
<i>CERTIFICATE</i>	<i>ii</i>
<i>ACKNOWLEDGEMENT</i>	<i>iii</i>
<i>ABSTRACT</i>	<i>v</i>
<i>CONTENT</i>	<i>xii</i>
<i>LIST OF TABLES</i>	<i>xx</i>
<i>LIST OF FIGURES</i>	<i>xiii</i>
CHAPTER 1 INTRODUCTION	1
CHAPTER 2 LITERATURE REVIEW	7
2.1 Flue gas desulfurization techniques	8
2.2 Absorption of SO <sub>2</sub> in conventional contactors	9
2.2.1 Stirred cell/Stirred tank	9
2.2.2 Liquid-jet/Laminar jet absorber	13
2.2.3 Packed bed	14
2.2.4 Sieve tray	16
2.2.5 Spray scrubber	16
2.2.6 Bubble column reactor-Packed/tapered/multistage/bubbling reactor	21
2.2.6.1 Absorption of SO <sub>2</sub> in bubbling reactor	25
2.3 Absorption of SO <sub>2</sub> in presence of a surface active agent	26
2.3.1 Absorption of SO <sub>2</sub> in presence of a surfactant (foam-bed reactor) and elimination of choking problem of distributor nozzles	27
2.4 Regenerative absorbent for flue gas desulfurization	28
2.4.1 Ionic liquids (ILs) as regenerative absorbents for SO <sub>2</sub>	29
2.4.1.1 Synthesis of ILs and its use for SO <sub>2</sub> solubility measurement	29

---

2.5	Reactor and reaction modeling for SO <sub>2</sub> absorption accompanied by chemical reaction	37
2.5.1	Gas-liquid systems	37
2.5.2	Gas-liquid-solid systems	39
2.5.3	Enhancement factor for solid dissolution	41
2.5.4	Modeling without a solid-liquid mass-transfer coefficient	42
2.5.5	Rate based models	43
2.6	Important aspects of bubble column and foam-bed reactors	46
2.6.1	Hydrodynamics and design parameters of bubble column reactors	47
2.6.1.1	Design and Scale-up	47
2.6.1.2	Fluid dynamics and regime analysis	47
2.6.1.3	Gas hold-up	51
2.6.1.4	Bubble characteristics	51
2.6.1.5	Mass transfer coefficient	53
2.6.2	Hydrodynamics and design parameters of foam-bed reactors	53
2.7	FGD byproduct utilization	54
2.7.1	Utilization of FGD gypsum are found mainly in the following aspects	55
2.8	Objectives for the present study	57
APPENDIX 2A		
2A.1		58
CHAPTER 3 THEORETICAL CONSIDERATIONS		62
3.1	Reaction schemes and kinetic constants of the systems studied in the present investigation and in other alkaline and aqueous systems	63
3.1.1	SO <sub>2</sub> absorption in pure water	63
3.1.2	Concept multiple reaction planes within the liquid film	64



---

3.1.2.1	SO <sub>2</sub> absorption in NaOH solution	64
3.1.2.2	SO <sub>2</sub> absorption in Ca(OH) <sub>2</sub> solution	66
3.1.2.3	SO <sub>2</sub> absorption in CaCO <sub>3</sub> solution	68
3.2	Ionic liquid and its utilization for SO <sub>2</sub> absorption	71
3.2.1	Proposed reactions scheme for synthesis of ionic liquid	71
3.2.2	Proposed scheme of association of ILs liquid into it	71
3.2.3	Axial mixing of gas and liquid phases in the bubble column and its effect on the rate of gas absorption reaction	72
3.3	Working equation for estimation of SO <sub>2</sub> removal efficiency	73
3.4	Conversion calculation of component <i>B</i>	73
3.5	Conditions to verify that absorption of SO <sub>2</sub> in Ca-based slurries occur with instantaneous reaction	74
3.6	Determination of controlling resistance for gas absorption; percent of total resistance in gas phase	75
3.7	Development of expression for calculation of parameter value	75
3.7.1	Estimation of liquid-side volumetric physical mass-transfer coefficient for SO <sub>2</sub> absorption	75
3.7.2	Expressions for estimation of gas-side mass-transfer coefficient for SO <sub>2</sub> absorption	76
3.7.3	Specific interfacial area in a gas-liquid dispersion	77
3.7.3.1	Working equations for estimations of 'a' using experimental data	77
3.7.3.2	Other methods for estimation of interfacial area	79
3.7.4	Gas hold-up	80
3.7.5	Solid-liquid interfacial area	80
3.7.6	Solid-liquid mass-transfer coefficient	80

3.8	Rate of gas absorption	81
3.9	Mass balance verification in the reactor	83
APPENDIX 3A		
3A.1	Single reaction plane model for gas absorption calculation	84
3B.1	Enhancement factor expressions based on film, penetration surface renewal theory	88
3C.1	Axial dispersion model	89
3C.2	Reported correlation for calculating gas phase mixing in bubble columns	91
3C.3	Sample calculation for dispersion coefficient and Peclet number for gas and liquid phase for MLIL and Ca(OH) <sub>2</sub> slurry	92
3D.1	Chemical method of determining the concentration of dissolved oxygen (Winkler Method)	95
CHAPTER 4 EXPERIMENTAL: MATERIALS AND METHODS		
4.1	An overview of the experiments performed	97
4.2	Gas-Liquid system	98
4.2.1	Ionic liquids-synthesis, application as absorbent for SO <sub>2</sub> removal and regeneration	98
4.2.1.1	Synthesis of ionic liquid	98
4.2.1.2	Absorption studies of SO <sub>2</sub> using the synthesized ionic liquid as the solvent	102
4.2.1.3	Removal of ethanol from virgin IL and regeneration of exhausted IL	106
4.2.2	SO <sub>2</sub> absorption experiments performed using other solvents	108
4.3	Gas-liquid-solid systems	109

---

4.3.1	Dimensions and materials of construction of foam column	110
4.3.2	Experiments performed in bubble column reactor (BCR)	111
4.3.3	Experiments performed in foam-bed reactor (FBR)	112
4.4	Characterization of ionic liquids	112
4.4.1	Physical properties of ionic liquids	112
4.4.2	FT-IR and <sup>1</sup> H NMR spectra – micro structure of the synthesized ionic liquids	113
4.4.3	Characterization of FGD products and estimation of parameter values	113
4.4.3.1	FT-IR	113
4.4.3.2	TGA	114
4.4.3.3	XRD	114
4.4.3.4	FE-SEM	114
4.4.4	Measurement of parameter values	115
4.4.4.1	pH of slurry with time in bubble column	115
4.4.4.2	Gas hold-up in bubble column slurry reactor	115
4.4.4.3	Particle size distribution (PSD) of Ca(OH) <sub>2</sub> and CaCO <sub>3</sub> and its size analysis	115
4.4.4.4	Volumetric liquid side mass transfer coefficient	115
4.4.4.5	Volumetric gas-side mass-transfer coefficient	116
4.4.4.6	Solid-liquid mass-transfer coefficient	117
APPENDIX 4A		
4A.1	Chemical analysis of hydrated lime samples for estimation of percentage of hydrated lime content	118
APPENDIX 4B		
4B.1	Molar rate of absorption of SO <sub>2</sub> from experimental data	121
4B.2	Liquid side mass-transfer coefficient from experimental data	121

4B.3	Gas-side mass transfer coefficient from experimental data	122
4B.4	Sample calculation for verification of instantaneous reaction	123
4B.5	Percent gas phase resistance from experimental data	124
4B.6	Checking from the experimental data whether the system is gas-film controlling	125
4B.7	Solid-liquid interfacial area from experimental data	125
4B.8	Sample calculation for solid-liquid mass transfer coefficient from experimental data	126
4B.9	Mass balance verification from experimental data	126
4B.10	Transient percent removal efficiency from experimental data	128
CHAPTER 5 RESULTS AND DISCUSSION		129
PART I: IONIC LIQUID- Characterization of synthesized ILs, absorption of SO <sub>2</sub> in ILs and solvent regeneration		130
5.1	Characterization of synthesized ILs	130
5.1.1	FT-IR and <sup>1</sup> H NMR spectra of ILs for micro structure analysis	132
5.2	Absorption of SO <sub>2</sub> in IL	137
5.2.1	Effect of different variables on the removal efficiency of SO <sub>2</sub>	138
5.2.1.1	Effect of the nature of constituting ions in the ILs on percent SO <sub>2</sub> removal efficiency	138
5.2.1.2	Effect of superficial velocity of gas on transient SO <sub>2</sub> removal efficiency	141
5.2.1.3	Effect of volume of solvent on percent SO <sub>2</sub> removal efficiency	143
5.2.1.4	Effect of initial concentration of SO <sub>2</sub> in feed gas on mass of SO <sub>2</sub> absorbed	146
5.2.1.5	Comparison of transient SO <sub>2</sub> removal efficiency of	

---

virgin and regenerated ILs	148
PART II: Absorption of SO <sub>2</sub> in aqueous slurries of Ca(OH) <sub>2</sub> and CaCO <sub>3</sub>	150
5.3 Effect of different variables on SO <sub>2</sub> removal efficiency by Ca(OH) <sub>2</sub> and CaCO <sub>3</sub> slurries in bubble column and foam-bed reactors	150
5.3.1 Simultaneous variation of exit concentration of SO <sub>2</sub> , pH of reactant slurry and gas hold-up with time in bubble column reactor for a typical experimental run	150
5.3.2 Gas hold-up in bubble column	151
5.3.3 Effect different variables on SO <sub>2</sub> removal efficiency	152
5.3.3.1 Effect of initial concentration of sulfur dioxide in feed gas on its removal efficiency	152
5.3.3.2 Effect of superficial velocity of gas	154
5.3.3.3 Effect of initial solid loading	157
5.3.3.4 Comparison of removal efficiency in bubble column and foam-bed reactors	159
5.4 Characterization of Reactant and FGD products	162
5.4.1 Analysis of Ca(OH) <sub>2</sub> and CaCO <sub>3</sub> sample	162
5.4.1.1 Particle size distribution of Ca(OH) <sub>2</sub> and CaCO <sub>3</sub> sample	162
5.4.1.2 XRD analysis of Ca(OH) <sub>2</sub> sample	164
5.4.2 XRD analysis of FGD products obtained from bubble column reactor	165
5.4.3 FT-IR spectra of FGD product in presence and absence of surface active agent	167
5.4.4 TGA of the products in presence and absence of surface active agent	168
5.4.5 Morphology of FGD products in presence and absence of surface active agent	171

---

APPENDIX 5A		
5A	Experimental data for the absorption of SO <sub>2</sub> in ILs	177
5B	Experimental data for the absorption of SO <sub>2</sub> in aqueous slurries of Ca(OH) <sub>2</sub> and CaCO <sub>3</sub>	194
5C.1	Experimental oxygen absorption data for the estimation of liquid-side mass-transfer coefficient	214
CHAPTER 6	CONCLUSIONS AND RECOMMENDATIONS FOR FUTURE WORK	215
NOTATIONS		218
REFERENCES		

---

## LIST OF TABLES

<b>Table number(s)</b>	<b>Title</b>	<b>Page number(s)</b>
2.1	Flow regimes in a bubble column and parameter estimation	50
2.2	Correlations for gas hold-up, rise velocity, bubble size and mass-transfer coefficient	51
2.3	Utilization of FGD gypsum in different areas in 2010	55
2A.1	Literature review based on reactor and absorbent used and flue gas composition	58
3B.1	Enhancement factor expressions based on film, penetration and surface removal theories	88
3C.2.1	Reported experimental studies on gas phase mixing in bubble columns	91
4.1	Reagents and their corresponding ILs synthesized	101
5.1	Physical properties of synthesized ILs at 303 K	131
5.2a	Particle size distribution of Ca(OH) <sub>2</sub> sample	162
5.2b	Particle size distribution of CaCO <sub>3</sub> sample	163
5.3	Size analysis of FGD crystals using FE-SEM	171
5A.1a	Variation of SO <sub>2</sub> absorption efficiency of virgin TLIL, MLIL and TSIL with time	177
5A.1b	Variation of SO <sub>2</sub> absorption efficiency of 1 <sup>st</sup> regenerated TLIL, MLIL and TSIL with time	178
5A.2	Complete SO <sub>2</sub> absorption characteristics of MLIL, TLIL and TSIL after 1 <sup>st</sup> regeneration of these ILs	180

---

5A.3	Effect of superficial velocity of gas on percent SO <sub>2</sub> removal efficiency of virgin MLIL	181
5A.4	Effect of Superficial velocity of gas on percent removal efficiency of 1 <sup>st</sup> regenerated MLIL	182
5A.5	Effect of volume of virgin MLIL on exit concentration of SO <sub>2</sub>	183
5A.6	Effect of volume of regenerated MLIL after first absorption on its transient SO <sub>2</sub> removal efficiency	184
5A.7	Effect of initial concentration of SO <sub>2</sub> in feed gas on its percent removal efficiency by virgin MLIL	186
5A.8	Effect of initial concentration of SO <sub>2</sub> in feed gas on its percent removal efficiency of 1 <sup>st</sup> regenerated MLIL	188
5A.9	Variation of percent SO <sub>2</sub> removal efficiency of TLIL with time for three consecutive absorption regeneration cycles	190
5A.10	Variation of percent SO <sub>2</sub> removal efficiency of MLIL with time for three consecutive absorption cycle	192
5B.1	Variation of concentration of SO <sub>2</sub> in exit gas, pH of absorbent and gas hold-up with time	194
5B.2	Variation of gas hold-up with superficial velocity of gas in slurry bubble column	196
5B.3	Effect of initial SO <sub>2</sub> concentration in the feed gas on its percent removal efficiency by Ca(OH) <sub>2</sub> slurry	197
5B.4	Effect of initial SO <sub>2</sub> concentration of inlet gas on its percent removal efficiency by calcium carbonate slurry	199
5B.5	Effect of superficial velocity of gas on SO <sub>2</sub> removal efficiency by Ca(OH) <sub>2</sub> slurry	201



---

5B.6	Effect of superficial velocity of gas on SO <sub>2</sub> removal efficiency by CaCO <sub>3</sub> slurry	203
5B.7	Effect of initial solids loading on percent SO <sub>2</sub> removal efficiency by Ca(OH) <sub>2</sub> slurry	205
5B.8	Effect of initial solid loading on SO <sub>2</sub> removal efficiency by CaCO <sub>3</sub> slurry	207
5B.9	Comparison of percent SO <sub>2</sub> removal efficiency by use of distilled water as absorbent in bubble column and foam-bed reactor	209
5B.10	Comparison of percent SO <sub>2</sub> removal efficiency by use of Ca(OH) <sub>2</sub> slurry as absorbent in bubble column and foam-bed slurry reactor	210
5B.11	Comparison of percent SO <sub>2</sub> removal efficiency by use of CaCO <sub>3</sub> slurry as absorbent in bubble column and foam-bed slurry reactors	212
5C.1	Variation of concentration of dissolved O <sub>2</sub> and liquid-side mass-transfer coefficient of pure oxygen with time in bubble column absorber	214

---

## LIST OF FIGURES

<b>Figure no(s)</b>	<b>Title</b>	<b>Page no(s)</b>
2.1	Schematic of possible flow regimes in bubble column	48
2.2	Gas flow regime map in a bubble column contactor	49
3.1	Typical concentration profiles in the gas and liquid film for absorption of SO <sub>2</sub> in NaOH or Ca(OH) <sub>2</sub> solution	66
3.2	Typical concentration profiles in the gas and liquid films for absorption of SO <sub>2</sub> in Ca(OH) <sub>2</sub> slurry	67
3.3	Typical concentration profiles in the liquid film for absorption of SO <sub>2</sub> in CaCO <sub>3</sub> slurry - One reaction plane model	69
3.4	Typical concentration profiles in the liquid film for absorption of SO <sub>2</sub> in CaCO <sub>3</sub> slurry- Two reaction plane model	70
3.5	Typical concentration profiles in the liquid film for absorption of SO <sub>2</sub> in CaCO <sub>3</sub> saturated solution	70
3.6	Ball stick model of proposed interaction between MLIL and SO <sub>2</sub>	71
3.7	Concentration profile for instantaneous reaction with varying concentration of reactant by Two-film theory	82
3A.1	Concentration profile for instantaneous reaction	85
4.1	Line diagram of experimental setup for synthesis of Ionic liquids	98
4.2	Photograph of experimental set-up for synthesis of ionic liquids	99

---

4.3	Pictures of Synthesized IL (a) TLIL, (b) MLIL and (c) TSIL	101
4.4	Schematic line diagram of the experimental setup for desulfurization experiment	103
4.5	Details of gas distributor plate	104
4.6	Top view and side view of the reactor-top enclosure with the material inlet and exit ports	104
4.7	Photograph of experimental set-up used for desulfurization of gaseous mixture	105
4.8	A line diagram of the experimental setup for regeneration of exhausted ionic liquid	106
4.9	A photograph of the experimental set-up for regeneration of exhausted IL	107
4.10	Detail of foam breaking plate	110
5.1	DSC analysis of MLIL	131
5.2a	FT-IR of virgin MLIL	132
5.2b	FT-IR of virgin TLIL	133
5.2b	FT-IR of virgin TSIL	134
5.2d	<sup>1</sup> H NMR spectra of virgin MLIL	134
5.3a	FTIR analysis of MLIL (a) before absorption and (b) after absorption	135
5.3b	<sup>1</sup> H NMR spectra of MLIL (a) before absorption and (b) after absorption	136
5.4a	Variation of SO <sub>2</sub> absorption efficiency of virgin TLIL, MLIL and TSIL with time	138

---

5.4b	Variation of SO <sub>2</sub> absorption efficiency of 1 <sup>st</sup> regenerated TLIL, MLIL and TSIL with time	139
5.4c	Complete SO <sub>2</sub> absorption characteristics of MLIL, TLIL and TSIL after 1 <sup>st</sup> regeneration of these ILs	140
5.5a	Effect of superficial velocity of gas on percent SO <sub>2</sub> removal efficiency by virgin MLIL	141
5.5b	Effect of superficial velocity of gas on percent removal efficiency by 1 <sup>st</sup> regenerated MLIL	142
5.6a	Effect of volume of virgin MLIL on exit concentration of SO <sub>2</sub>	143
5.6b	Effect of volume of regenerated MLIL after first regeneration on its transient SO <sub>2</sub> removal efficiency	144
5.7a	Effect of initial concentration of SO <sub>2</sub> in feed gas on its percent removal efficiency by virgin MLIL	146
5.7b	Effect of initial concentration of SO <sub>2</sub> in feed gas on its removal efficiency by use of regenerated (after 1 <sup>st</sup> absorption) MLIL	147
5.8a	Variation of percent SO <sub>2</sub> removal efficiency by TLIL with time for three consecutive absorption cycle	148
5.8b	Variation of percent SO <sub>2</sub> removal efficiency by MLIL with time for three consecutive absorption regeneration cycles	149
5.9	Variation of concentration of SO <sub>2</sub> in exit gas, pH of absorbent and gas hold-up with time in the bubble column reactor	150
5.10	Variation of gas hold-up with superficial velocity of gas in the slurry bubble column	152
5.11a	Effect of initial SO <sub>2</sub> concentration in the feed gas on its percent removal efficiency by Ca(OH) <sub>2</sub> slurry	153

---

5.11b	Effect of initial SO <sub>2</sub> concentration of inlet gas on percent removal efficiency by CaCO <sub>3</sub>	153
5.12a	Effect of superficial velocity of gas on SO <sub>2</sub> removal efficiency by Ca(OH) <sub>2</sub> slurry	155
5.12b	Effect of superficial velocity of gas on percent SO <sub>2</sub> removal efficiency by CaCO <sub>3</sub> slurry	156
5.13a	Effect of initial solids loading on percent SO <sub>2</sub> removal efficiency by Ca(OH) <sub>2</sub> slurry in a bubble column reactor	157
5.13b	Effect of initial solids loading on SO <sub>2</sub> removal efficiency by limestone slurry in a bubble column reactor	158
5.14a	Comparison of percent SO <sub>2</sub> removal efficiency by use of distilled water as absorbent in bubble column and foam-bed reactors	159
5.14b	Comparison of percent SO <sub>2</sub> removal efficiency by use of Ca(OH) <sub>2</sub> slurry as absorbent in bubble column and foam-bed slurry reactors	160
5.14c	Comparison of percent SO <sub>2</sub> removal efficiency by use of CaCO <sub>3</sub> slurry as absorbent in bubble column and foam-bed slurry reactors	161
5.15	XRD analysis of Ca(OH) <sub>2</sub> sample	164
5.16a	XRD pattern of product obtained by SO <sub>2</sub> absorption in bubble column using Ca(OH) <sub>2</sub> slurry	165
5.16b	XRD pattern of the product, obtained by SO <sub>2</sub> absorption in bubble column reactor using CaCO <sub>3</sub> slurry	166
5.17a	FT-IR analysis of the FGD the products, obtained by SO <sub>2</sub> absorption in bubble and foam-bed contactors using Ca(OH) <sub>2</sub>	167

---

	slurry	
5.17b	FT-IR analysis of the FGD the products, obtained by SO <sub>2</sub> absorption in bubble and foam-bed contactors using CaCO <sub>3</sub> slurry	168
5.18a	TGA of the FGD product, obtained by SO <sub>2</sub> absorption in bubble column- and foam-bed reactors using Ca(OH) <sub>2</sub> slurry	169
5.18b	TGA of the FGD product, obtained by SO <sub>2</sub> absorption in bubble column- and foam-bed reactors using CaCO <sub>3</sub> slurry	170
5.19a	SEM image of the FGD product, obtained by SO <sub>2</sub> absorption in bubble column reactors using Ca(OH) <sub>2</sub> slurry (without surfactant)	172
5.19b	SEM image of the FGD product, obtained by SO <sub>2</sub> absorption in bubble column reactors using CaCO <sub>3</sub> slurry (without surfactant)	173
5.20a	SEM image of the FGD product, obtained by SO <sub>2</sub> absorption in foam-bed reactor using Ca(OH) <sub>2</sub> slurry (surfactant: Triton X-100)	174
5.20b	SEM image of the FGD product, obtained by SO <sub>2</sub> absorption in foam-bed reactor using CaCO <sub>3</sub> slurry (surfactant: Triton X-100)	174
5.21a	SEM image of the FGD product, obtained by SO <sub>2</sub> absorption in foam-bed reactor using Ca(OH) <sub>2</sub> slurry (surfactant: Tween 80)	175
5.21b	SEM image of the FGD product, obtained by SO <sub>2</sub> absorption in foam-bed reactor using CaCO <sub>3</sub> slurry (surfactant: Tween 80)	175
5.22a	SEM image of the FGD product, obtained by SO <sub>2</sub> absorption in foam-bed reactor using Ca(OH) <sub>2</sub> slurry (surfactant: Teepol)	176

---

5.22b	SEM image of the FGD product, obtained by SO <sub>2</sub> absorption in foam-bed reactor using CaCO <sub>3</sub> slurry (surfactant: Teepol)	176
-------	---	-----

**CHAPTER- 1****INTRODUCTION**

Incessantly escalating concern world over on environmental protection requires no special mention (De Visscher, A., 2013; Ghosh et al., 2017). The most important reason of this concern on air pollution is certainly related to the increasing energy demand from fossil fuels, especially burning low to medium grade high sulfur content lignite coals keeping pace with that of world population growth (Bhoi et al., 2016). These fuels when burnt in fired boilers, emits Giga tones of SO<sub>2</sub> to the atmosphere each year (Arif et al., 2015). While in the form of acid rains, this brings damage to vegetation, to the buildings, monuments and aquatic lives, in the gaseous state, it seriously affects human organs (Park and Park, 2016). Probably the first attempt on acid rain reduction was enacted through the clean air act amendment in 1990 although the legislation on SO<sub>2</sub> emission was introduced by the USA and Japan Governments in the early seventies of the nineteenth century (Wang et al., 2005). Over the years, many other countries have framed their environmental laws on SO<sub>2</sub> emission control strategies and, some countries, e.g., Denmark, even imposed high environmental levy per unit mass of sulfur emitted to the atmosphere (Mc Kinney et al., 2007).

On the basis of the most recent emission estimates, India has surpassed the U.S. to be the world's second largest SO<sub>2</sub> emitting country, after China, since 2010 (Lu et al., 2010, 2011). The coal-fired power sector is the single largest contributor, accounting for ~50% of the national SO<sub>2</sub> emissions and ~70% of the emission increment during 1996–2010. In particular, during 2005–2012, SO<sub>2</sub> emissions increased rapidly by 71% from 3354 to 5738 Gg, with an annual average growth rate (AAGR) of 8.0% (Lu et al., 2013).

For controlling the emission of SO<sub>2</sub>, various flue-gas desulfurization (FGD) technologies have been evolved through extensive research and development over the last three decades to improve its removal efficiency, the economy of separation and trouble-free operation (Wang et al., 2005). The existing FGD processes are conventionally classified either as once-through technology if the spent sorbent is disposed of as a waste or utilized as a byproduct and regenerative technology if it, the absorbent, is regenerated for reuse and the released SO<sub>2</sub> is either liquefied for sale or



converted to other salable products (Pandey et al., 2005). Each of the once-through and regenerative technologies is once again classified as either wet or dry that specifically signify not to the actual process, but that the solid waste or byproduct regenerated in the FGD unit is a wet or dry substance, respectively (Karatepe, N., 2000). In reality, regenerative technologies are very infrequently employed, as these are known to incur higher plant and operating costs (Shang et al., 2011). Among the different, once through technologies, wet FGD with lime stone forced oxidation (LSFO) is the most widely accepted technology in commercial ventures, especially in most European and Japanese plants. This is so because in these countries it is essential that the by-product must have to be high-quality gypsum, suitable for wallboard manufacture and that limestone, a substantially low-cost reagent can be used for the desulfurization process (Hamm et al., 2004, Lou et al., 2011).

On the other hand, hydrated lime, considered to be a rather costlier reagent must be used in the dry or semi-dry FGD processes, limestone being not reactive under this condition. The reaction products generated in these processes are not considered to be useful (Karatepe N., 2000) as these comprise of a mixture of calcium sulfite, calcium sulfate and unreacted lime. The process suffers from low efficiency and requires disposal of large tonnages of solid waste, and, therefore not consistent with the principles of sustainable development.

Varieties of solvents, solutions and slurries in quite different types of contactors have been employed for the removal of sulfur dioxide from gaseous mixtures. These absorbents can be broadly classified into aqueous solutions containing Na-salts, aqueous or non-aqueous solutions containing N-bearing chemicals, ionic liquids (ILs) and slurries of lime, limestone or that of magnesium hydroxide. The reported absorption operations were carried out under a variety of experimental conditions by different investigators, and a number of different reaction kinetics and reactor models have been proposed. Plant capacity, type of fuel, sulfur to fuel ratio; salability, selling price and availability of the market for the desulfurization product and its disposal cost if not sellable, including its effect on the environment, are considered to be the important factors for the selection of a desulfurization process. A comparison of high potential processes from the view point of technical, economical and environmental aspects is considered to be very important. Different mass-transfer mechanisms on flue gas desulfurization have been reported in the literature. While absorption of  $\text{SO}_2$

in most of the aqueous solutions and slurries are reported to occur and modeled according to either penetration or film theories with instantaneous reaction occurring in two reaction planes (Hikita et al., 1977; 1978, Sada et al., 1982) close to the interface, fractional order (Gao et al., 2010) or first, pseudo-first and second order (Basu and Datta, 1987) kinetics with single reaction plane and surface-renewal theories have also been used to model the absorbers.

FGD processes using slurries of lime or lime stone are rather low-cost processes and are used by industries where SO<sub>2</sub> discharge rate is low. Specific equipments for handling slurries, viz., spray scrubbers, slurry bubble columns and agitated vessels are the preferred contactors for this purpose. Grinding of lime or lime stone, slurry preparation, separation of sludge, dewatering and disposal of solids are the typical handling and economic considerations associated with the process. Choking of the gas distributor plate is a very critical operational difficulty of the process. Concentrated SO<sub>2</sub> gas can be recovered by calcining the product and later used for the manufacture of H<sub>2</sub>SO<sub>4</sub>. Among the Na-containing absorbents, the aqueous solution of Na<sub>2</sub>CO<sub>3</sub> or NaHCO<sub>3</sub> is used in many industries. Product Na<sub>2</sub>SO<sub>4</sub> is sold as a byproduct. Laboratory studies of the use of NaClO or NaClO<sub>2</sub> have been reported to possess high efficiency for simultaneous removal of SO<sub>2</sub> and NO<sub>x</sub>. However, the solution obtained is likely to be highly acidic and require corrosion resistant equipments and post-treatment of the liquid. Use of N-based bases, e.g., the aqueous solution of dimethyl aniline has been adopted by many industries. The solvent is regenerated by steam stripping from the sulfated product and recycled. Other nitrogen bases reported for these purposes are ethylene diamine, urea etc. The latter reagent produces (NH<sub>4</sub>)<sub>2</sub>SO<sub>4</sub> which can be sold as a byproduct.

The most effective method of removal and recovery in a pure state of the desired component from a gaseous mixture is possibly by selective absorption in a regenerative liquid solvent (Shannon et al., 2014). The interaction between the solute and the solvent should be moderate conforming to physical absorption such that absorption capacity is adequately high and that the solvent is regenerative (Qu et al., 2013). Absorptive removal of a component from a flue gas also requires that the absorber be operated at a relatively higher temperature and that the solvent possess the required chemical and thermal stability, available at low cost, and, has a negligibly low vapor pressure at the relatively high operating temperature (Duan et al., 2011). In

the past decade, low temperature molten organic salts, customarily called ionic liquids (ILs), have emerged as environmentally benign solvents for absorptive removal of various acid gases (Liu et al., 2013). It is very important that contrary to the conventional organic solvents, the desired properties of the ILs can be custom-built by suitably selecting the structures of their cations and anions to yield the best performance for the desired separation process (Yuan et al., 2007). It has also been observed that ILs having the same anion yielded the same solubility for SO<sub>2</sub> (Anderson et al., 2006). While Henry's Law constant for SO<sub>2</sub> is less than 2 bar, that for CO<sub>2</sub> is ~30 bar and therefore, the former gas present in a very low concentration can be fully removed although concentration of CO<sub>2</sub> in flue gases are substantially higher and simultaneously get absorbed in the liquid (Li et al., 2015). It may, however, be observed that most of the investigations on absorption of SO<sub>2</sub> in ILs focus on its solubility studies or estimation of absorption capacity and percent SO<sub>2</sub> removal efficiency by the different ILs using a very small volume of this solvent at a fixed value of this gas rate (Huang et al., 2014). Reported information in the literature on the detailed investigation for generation of experimental data on conventional laboratory scale studies for the effects of different variables on percent SO<sub>2</sub> removal useful for further studies on a pilot plant scale or otherwise are meagre.

Although the studies on absorption of SO<sub>2</sub> and other acid gases (Gupta et al., 1986) have been performed in different types of equipments, e.g., stirred cell, laminar jet absorber, packed bubble column, bubbling reactors, etc., the wet FGD operations are almost exclusively carried out in spray scrubbers (Brogen and Karlson, 1997). However, the spray nozzles are prone to choking and cause serious operational problems. While stirred cell and laminar jet absorbers are important for theoretical studies and reactor modeling aspects, the packed bubble columns are not truly suited for slurry reactions. In the reported studies, only a single nozzle has been used for entry of gaseous mixture into the bubbling reactors, and this configuration, therefore is not a true replica of plant scale equipment. It may be observed that slurry reactions incorporating sparingly soluble reactive particles, e.g., carbonation of hydrated lime, are conveniently carried out in industries in bubble column reactors (Perez-Lopez et al., 2008) for the production of precipitated calcium carbonate. This equipment is therefore considered to be highly suitable for slurry reactions and gas-liquid contacting being very intense; it can yield high SO<sub>2</sub> removal efficiency. Additionally,

limestone being available at very low cost, aqueous slurries of this reagent is the most favored absorbent for desulfurization operations in industries. In the open literature, however, although one can find a bubble column reactor to have been employed for SO<sub>2</sub> absorption using NH<sub>4</sub>HCO<sub>3</sub> solution (Li et al., 2013), experimental performance data on this reactor for SO<sub>2</sub> absorption using CaCO<sub>3</sub> slurry as the absorbing media is meagre.

It may be observed that treatment of large tonnages of SO<sub>2</sub> using limestone slurries generates impure gypsum amounting to about three times of the quantity of SO<sub>2</sub> treated annually and in most of the cases it causes a serious disposal problem, this being a solid waste. Also, the absorption of SO<sub>2</sub> from flue gases in calcium-based slurries is almost exclusively carried out in spray scrubbers in the concerned industries, and there are reports that several critical operational problems arise. In the open literature, experimental performance data of a slurry bubble column contactor for this system is not reported while it is conventionally used for other slurry reactions as mentioned above. In all probability, use of a three-phase foam- slurry reactor for this system with the addition of a suitable surfactant (Rennie and Evans, 1962; Kelekar and Bhagwat, 2006) in a very low concentration level would be advantageous, as it may obviate the choking problem. Also, experimental data on the absorption of SO<sub>2</sub> in IL solvents in conventional laboratory scale process equipment as functions of different operating variables reported in the open literature are meagre.

The objective of the present work is to synthesize a series of regenerative low-cost hydroxyammonium ionic liquids and study its SO<sub>2</sub> removal efficiency in a conventional bubble column contactor as functions of different operating variables, study the regeneration of the exhausted ILs and its suitability for recycling. The other objective of this work is to experimentally study the performances of a bubble column (Ca(OH)<sub>2</sub> or CaCO<sub>3</sub>) slurry reactor, with and without the addition of a surfactant, for absorptive removal of SO<sub>2</sub> from a simulated gaseous mixture with respect to different operating parameters, *viz.* initial solids loading, superficial velocity of gas, volume of slurry charged into the reactor and concentration of sulfur dioxide in the feed gas. It is also intended to find out suitable conditions for eliminating the gas-distributor choking problem.

*In the present thesis*, Chapter 2 comprises of review of reported literature in the areas of synthesis of ionic liquids, absorption of sulfur dioxide from gaseous mixtures by

use of these solvents, its regeneration and reuse for further absorption. Usages of calcium-based slurries, alkalis and N-containing bases for this purpose reported in the literature have also been discussed. Merits and demerits of different types of contactors studied for flue gas desulfurization, hydrodynamics and design parameters of the bubble column and foam-bed reactors and utilization of FGD products are discussed in brief. Conclusions are then drawn for objectives of present studies. Chapter 3 describes the theoretical considerations concerned with the absorption of sulfur dioxide in different types of solvents, rate expressions, and, expressions for the estimation of parameter values. Chapter 4 describes the methodology, material and experimental setup used for the study of the performances of the bubble column and foam-bed reactors using IL and Ca-based slurries. Experimental details of characterization of reactants and products, and, that of estimation of parameter values have been discussed. Sample calculations for determination of the values different kinetic and mass transfer parameters have been shown. Chapter 5 describes the experimental results and detailed discussions pertaining to the variables used and all critical observations. Results of characterization of reactants and products for both the systems studied have been discussed in detail. Chapter 6 comprises the conclusions and recommendations for future work.

**CHAPTER- 2****LITERATURE REVIEW**

Socio-economic and environmental problems in the form of acid rain, smog formation, lungs disorder and such other problems caused by the emission of  $\text{SO}_2$  led to extensive studies of flue gas desulfurization (FGD) techniques. Diverse types of process equipment and a number of organic and aqueous solvents, solutions and slurries have been employed for studies on the emission control of this acidic oxide. While several solvents are extensively used in industries for  $\text{CO}_2$  absorption, and the solvents are reused after their regeneration, no such process for  $\text{SO}_2$  gas has yet been reported. Since last about one decade, ionic liquids have been reported to be a potential solvent for different acid gases, viz.,  $\text{CO}_2$ ,  $\text{SO}_2$  and  $\text{H}_2\text{S}$ . Further studies on finding a suitable regenerative solvent or the ways to alleviate the current plant operational problems. One needs a detailed search on all the relevant reported literature.

Reported information related to the understanding of the reaction mechanisms and estimation of parameter values for determination of the rate of  $\text{SO}_2$  absorption in bubble column and foam-bed contactors are also included in this chapter. The literature reported on FGD studies broadly comprises of the following aspects:

1. Current industrial techniques of flue gas desulfurization (FGD) practiced in industries.
2. Performance of different types of contactors, viz., Spray absorbers, bubbling reactors, laminar jet absorbers, packed column reactors, etc.
3. Absorbents used for removal of  $\text{SO}_2$ , e.g., aqueous alkaline solutions, slurries, ionic liquids, etc.
4. Synthesis of ionic liquids and its use for absorption of  $\text{SO}_2$ .
5. Models for  $\text{SO}_2$  absorption in gas-liquid and gas-liquid-solid systems.
6. Important aspects of a bubble column and a foam-bed reactor.
7. Utilization of the FGD products.
8. Objectives of the present work.

A comprehensive review of the literature focusing on all of the above aspects is presented in the following sections. These incorporate the information on equipments

and absorbents used for studies of desulfurization, experimental findings, reaction mechanisms, rate equations, plant operational problems and product utilization/disposal aspects.

It appears justified, first to present a brief review the different techniques of FGD currently in use in different industries and then proceed for a detailed literature review on the above-mentioned aspects.

## **2.1 Flue gas desulfurization techniques**

For controlling the emission of  $\text{SO}_2$ , various flue-gas desulfurization (FGD) technologies have been evolved through extensive research and development over the last three decades to improve its removal efficiency, the economy of separation and trouble-free operation. The existing FGD processes are conventionally classified either as

- I. Once-through technology, if the spent sorbent is disposed of as waste or utilized as a byproduct ;
- II. Regenerative technology, if it is regenerated for reuse and the released  $\text{SO}_2$  is either liquefied for sale or converted to other salable products.

Each of the once-through and regenerative technologies is once again classified as either

- (i) Dry
- (ii) Semi-dry, or
- (iii) Wet processes

(i) and (iii) specifically signify not to the actual process, but that the solid waste or byproduct generated in the FGD unit is a dry or wet substance, respectively. In reality, regenerative technologies are very infrequently employed, as these are known to incur higher plant and operating costs. Among the different once through technologies, wet FGD with lime stone forced oxidation (LSFO) is the most widely accepted technology in commercial ventures, especially in most European and Japanese plants, as in these countries it is essential that the byproduct must be a high-quality gypsum, suitable for wall board manufacture; and that limestone, a substantially low-cost reagent can be used for the desulfurization process. On the other hand, hydrated lime, considered to be a rather costlier reagent must be used in the dry or semi-dry FGD process, limestone being not reactive under this condition. The reaction product generated in

these processes comprises of a mixture of calcium sulfite where its sulfate and unreacted lime are not considered to be a useful byproduct. The process suffers from low efficiency and requires disposal of large tonnages of solid waste, and therefore not consistent with the principles of sustainable development.

## **2.2 Absorption of SO<sub>2</sub> in conventional contactors**

Contactors of diverse configurations have been used by different investigators for studies of desulfurization of flue gases. The equipment for experimental studies was chosen based on the specific experimental conditions used by the investigators. These include a laminar jet absorber, stirred cell, laminar falling film, packed bed and spray towers (Sada et al., 1980; Basu and Dutta, 1987; Olausson et al., 1993; Schultes, M., 1998; Dagaonkar et al., 2001). The first three of these equipment types were used mainly to study the absorption mechanism in alkali solutions and alkaline slurries. While packed beds were used for gas-liquid systems and stirred cell absorbers were employed for the well-defined surface area to facilitate mass transfer calculations and agitated contactors and spray towers for performing slurry reactions. Bandyopadhyay and Biswas (2006, 2007) and Meikap et al. (2002) used modified bubble columns for absorption of SO<sub>2</sub> from simulated gaseous mixtures. Olausson et al. (1993); Gomez et al. (2007); Marocco (2010) reported pilot plant scale studies on the performance of a spray tower for the removal of SO<sub>2</sub> from flue gases. Enhancement of the rate of absorption due to the presence of fine reactive particles has been reported by Uchida et al. (1975), Sada et al. (1977, 1983), Laohavichitra et al. (1982) and Scala, F. (2002), to name a few.

### **2.2.1 Stirred cell / Stirred tank**

Sada et al. (1977) studied simultaneous absorption of SO<sub>2</sub> and CO<sub>2</sub> into Ca(OH)<sub>2</sub> slurry in a stirred-tank reactor with a plane gas-liquid interface both singly and separately. The authors found that in the process of simultaneous absorption of SO<sub>2</sub> and CO<sub>2</sub>, the solubility of sulfur dioxide being more than 25 times larger than carbon dioxide, then, CO<sub>2</sub> could almost be regarded as an inert gas. The reaction of SO<sub>2</sub> with hydroxyl ion was considered to be instantaneous, and the reaction rate was found to be much greater than the corresponding reaction with CO<sub>2</sub>. The rate constant for the reaction involving SO<sub>2</sub> was considered to be larger by a factor of 10<sup>4</sup> than that involving CO<sub>2</sub>. The authors proposed a two reaction-plane model for absorption of



SO<sub>2</sub> in Ca(OH)<sub>2</sub> slurry considering that the reaction of various species occurs at two different reaction planes. The authors argued that the model of Uchida et al. (1975) was better in its predictions than the model reported by Ramachandran and Sharma (1969).

Sada et al. (1979) performed the absorption for lean SO<sub>2</sub> & NO<sub>2</sub> by exploiting aqueous slurries of fine Ca(OH)<sub>2</sub> and Mg(OH)<sub>2</sub> particles in a stirred vessel with a gas-liquid interface at a temperature of 25 °C and 1 atm pressure. That absorption process using Ca(OH)<sub>2</sub> slurries was found to be almost gas-film controlled. On the contrary, for Mg(OH)<sub>2</sub> slurry system, the absorption process was diffusion controlled across the liquid film, and *the absorption rate increased with solid concentration*.

Sada et al. (1981) performed the absorption of dilute SO<sub>2</sub> into an aqueous slurry of CaSO<sub>3</sub> using a stirred vessel with a plane gas-liquid interface. It was assumed that reaction on the solid surface facilitated the SO<sub>2</sub> absorption which helped in deriving the enhancement factor. The reaction between absorbed SO<sub>2</sub> with dissolved solid was assumed to be an irreversible instantaneous reaction, and between absorbed SO<sub>2</sub> with the solid particle, it was irreversible first order.

Sada et al. (1983) investigated CO<sub>2</sub> absorption using Ca(OH)<sub>2</sub> and Mg(OH)<sub>2</sub> slurries in a bubble column reactor at a temperature of 308 K and 0.1013 MPa pressure. Volumetric mass-transfer coefficient & effective gas-liquid interfacial areas were determined. It was found that with an increase in the concentration of slurry liquid-side physical mass-transfer coefficient decreased. Effective gas-liquid interfacial area and the rate of chemical absorption reached their maximum values at an optimum concentration of lime reactant particles.

Uchida et al. (1984) investigated SO<sub>2</sub> absorption into melamine slurry at 20°C in a stirred-tank contactor with a plane gas-liquid interface. The melamine slurries concentration were 1.0 to 10 wt. %. The absorption rate was calculated using the equations given by Uchida and Wen (1977). The absorption rate increased with an increase in the stirrer speed. In this system, the authors had considered the dissolution rate to be fast and the absorption process to be controlled by the diffusion of SO<sub>2</sub> either in gas film or liquid film. Melamine floated on the slurry surface under the prevailing the experimental conditions, and it caused a reduction in the effective gas-liquid interfacial area.

Sada et al. (1987) investigated the influence of suspended particles on parameters including gas holdup, volumetric liquid-side mass-transfer coefficient & gas-liquid interfacial area in a bubble column for sodium sulfite/sulfate solutions in which several loadings of coarse nylon particles & fine alumina particles were suspended. It was observed that a slurry bubble column with suspended coarse particles had a lower gas-liquid interfacial area as compared to a two-phase bubble column; particularly at high superficial gas velocity. Effects of suspended fine and coarse particles on the liquid-side mass-transfer coefficient were observed not to be significantly different within the range of experimental conditions used by the investigators.

Lancia et al. (1994) proposed a model for absorption of lean SO<sub>2</sub> into limestone slurry. The absorption model was developed using the two-film theory. The authors performed experiments in a stirred vessel in which a mixture of SO<sub>2</sub> and N<sub>2</sub> was bubbled into the limestone slurry with pH as the variable ranging from 3.6 to 6.0. The partial pressure of SO<sub>2</sub> was varied from 44.6 to 190 Pa. However, it is observed from the experimental setup that there is no exhaust line for venting excess gas leaving the reactor. All the reactor exit gas passes into the analyzer, but it has been observed that only a limited volume of gas can pass through the analyzer depending on the particular make. The authors did not provide any kinetic or reactor performance data useful for either pilot plant study or an industrial scale absorber design. The feed slurry was very dilute, with the maximum slurry concentration being only 1 g CaCO<sub>3</sub> per litre of solvent. The concentration of SO<sub>2</sub> in the exit gas was measured using a UV analyzer. The concentration of a dissolved Ca<sup>2+</sup> ion in the exit liquid stream from the reactor was calculated by EDTA titration using murexide as an indicator. The model predicted values were found to fit well with the experimental results.

Chang and Rochelle (1981) reported the results of their experimental studies of the pure and lean SO<sub>2</sub> absorption into pure water, HCl solution & NaCl solution in a continuous stirred-tank reactor. The authors developed a model for the rate of absorption of SO<sub>2</sub> in the liquid phase by using surface renewal theory & instantaneous reaction mechanism. Experimental data showed that in the case of the SO<sub>2</sub>-HCl system, the change in gas phase SO<sub>2</sub> concentration did not affect the value of mass transfer enhancement factor if temperature and HCl concentration remained unchanged.

Hikita and Konishi (1983) studied the absorption of lean SO<sub>2</sub> into an aqueous solution of sodium carbonate in baffled agitated vessel operated batch-wise at 25°C. The experimental results were examined with the chemical absorption theory based on the Leveque model. The model predicted values were found to fit well with the measured values of absorption and desorption rates.

Chu et al. (2001) studied the absorption of dilute SO<sub>2</sub> & that of a mixture of SO<sub>2</sub> and NO into an aqueous solution of KMnO<sub>4</sub>/NaOH in a stirred tank reactor at 50°C. It was found that in the SO<sub>2</sub>-(KMnO<sub>4</sub>-NaOH) system, the SO<sub>2</sub> absorption rate increased with an increase in the NaOH concentration. In the (SO<sub>2</sub>+NO)-(KMnO<sub>4</sub>+NaOH) system, NO absorption rate decreased quite significantly with increase in SO<sub>2</sub> concentration. However, an increase in the concentration of NO had no influence on the absorption rate of SO<sub>2</sub>.

Bravo et al. (2002) studied the absorption of SO<sub>2</sub> from its mixtures with N<sub>2</sub> into limestone slurries. The reactor used was a stirred tank with an almost flat gas-liquid interface of area  $67.7 \times 10^{-4} \text{ m}^2$ , and the liquid was stirred at 400 rpm. A semi-batch reactor was used for experiments in which the gas-phase was passed continuously through a batch of CaCO<sub>3</sub> slurry. The experimental data demonstrated a considerable reduction in the rate of sulfur dioxide absorption as the CaCO<sub>3</sub> disappeared by the reaction from the slurry and that the flux of SO<sub>2</sub> across the gas-liquid interface did not change significantly with the operating temperature. The SO<sub>2</sub> flux across the gas-liquid interface was also observed to be practically independent of the CaCO<sub>3</sub> content by weight in the feed slurry and of the particle size of CaCO<sub>3</sub> in it, within the range tested, although the one assayed in this study was limited.

Gao et al. (2010) studied the gas-liquid system characteristics for SO<sub>2</sub> absorption in ammonium sulfite solution. A stirred tank reactor was used for performing the experiments. The authors found that the absorption was controlled by both the gas and liquid films when ammonium sulfite concentration was lower than 0.05 g mol/l and mainly by gas film at greater temperature. It was observed that absorption rate was of zero-order in regards to ammonium sulfite and the rate increased as the concentration of sulfur dioxide was increased. The reaction was of 0.6<sup>th</sup> order with respect to the concentration of SO<sub>2</sub>. The absorption rate was also found to increase with an increase in the temperature of operation. Under the experimental conditions, the absorption rate of SO<sub>2</sub> increased with an increase in the (NH<sub>4</sub>)<sub>2</sub>SO<sub>3</sub> concentration from 0.03 to 0.05 g

mol/l. From this observation, the authors concluded that the reaction was controlled concurrently by both gas- and liquid-film. On the contrary, the absorption rate of  $\text{SO}_2$  became nearly constant as the concentration of  $(\text{NH}_4)_2\text{SO}_3$  was raised above 0.05 gmol/l. In the latter case, the reaction might not be influenced by the liquid- film and appeared to be zero-order with regards to concentration of  $(\text{NH}_4)_2\text{SO}_3$ .

### **2.2.2 Liquid jet/Laminar jet absorber**

Bjerle et al. (1972) investigated absorption of  $\text{SO}_2$  into  $\text{CaCO}_3$  slurry using a laminar jet absorber and determined the value of gas phase mass-transfer coefficient from experimental data. The liquid in this type of absorber had very short contact time with the gas, and solid dissolution seemed to not effect on the rate of the absorption. Under the experimental conditions, unsteady state mass transfer occurred into the liquid jet and the area for mass transfer in a liquid jet being well-defined, penetration theory was used by the authors for the theoretical determination of the rate of gas phase mass transfer and hence the value of mass-transfer coefficient.

Sada et al. (1979) performed absorption studies of lean  $\text{SO}_2$  gas into an aqueous solution of  $\text{Na}_2\text{CO}_3$  in a stirred vessel with a plane gas-liquid interface. The process of absorption was analyzed in terms of a two reaction plane model. The reaction between sulfur dioxide & sodium carbonate was believed to be instantaneous and a gas-phase controlled process. The theoretical model was developed with the assumption of film theory. The authors considered desorption of the reactant product  $\text{CO}_2$  as an important factor in the reaction kinetics in the development of the model for gas absorption.

Hikita and Konishi (1978) performed the pure  $\text{SO}_2$  absorption into aqueous ammonia & aqueous ammonium sulfite solutions in a liquid jet column at a temperature of  $25^\circ\text{C}$ . Penetration theory was used by the authors for the development of a model for determining the rate of absorption. The reaction was considered to be instantaneous, and two reaction-plane model was used to describe the reaction mechanism. The theoretical rate of absorption predicted from the model was found to agree well with the experimental data.

Babu et al. (1984) measured the sulfur dioxide absorption rate of into  $\text{Ca}(\text{OH})_2$  solutions by the application of a laminar jet apparatus. Gas-liquid contact times were varied between 10 & 25 milliseconds. The hydroxyl ion concentrations in the

Ca(OH)<sub>2</sub> solutions were varied between 0.025 & 0.041 g-ion/l, and the concentration of SO<sub>2</sub> in the mixture of nitrogen and sulfur dioxide was varied between 0.96 and 2.86 percent by volume. For these conditions, the reaction was assumed to be instantaneous. Experimental data was in good agreement with the predictions from penetration theory.

Van Dam et al. (1999) reported a kinetic study for the absorption of SO<sub>2</sub> in a laminar falling film reactor. Parabolic velocity profiles were assumed in both the phases. A model was developed based on the following assumptions: axial transport in both gas and liquid phase was convective, radial transport in both phases was diffusive, permanent regime velocity profiles in both phases, first-order reversible reaction in the liquid phase. For the organic solvents, N-Methyl-2-pyrrolidone and N-N'-Dimethyl propylene urea, the experimental absorption flux was about 80% of the maximum value, achieved with NaOH solution. This high value of absorption flux was promising to the authors for the use of these kinds of solvents that was indicative of the development of a new regenerable process for sulfur dioxide removal.

### **2.2.3 Packed bed**

Schultes (1998) studied the SO<sub>2</sub> absorption into NaOH solution in a packed column. The author presented a model and compared the theoretical predictions with the experimental data. The author showed the nature of variation of the height of the gas phase transfer unit (HTU<sub>OV</sub>) with the enhancement factor for gas absorption and temperature of reactor operation. Height of gas phase transfer unit dropped with an increase in the enhancement factor until it attained the value of 100 and decreased with an increase in reactor operation temperature. The authors concluded that a constant HTU<sub>OV</sub> value could be achieved at increasing absorption temperatures only with increasing enhancement factors, i.e. with increased concentrations of sodium hydroxide solution.

Ebrahimi et al. (2003) developed a steady-state model based on the rate for the design & simulation of the packed column for the sulfur dioxide absorption into an aqueous solution of NaHCO<sub>3</sub>/Na<sub>2</sub>CO<sub>3</sub> and desorption of CO<sub>2</sub>. The absorption rate, enhancement factors & concentration profiles of all the involved chemical species were assessed. The model was based on the film theory absorption of gas. The authors

observed that with the increasing SO<sub>2</sub> concentration in the flue gas from 1000 to 2000 ppm, the degree of desulfurization decreased from 95 to 89.5%.

Ju-Hui et al. (2008) studied the effect of the concentration of ferric sulfate solution on SO<sub>2</sub> absorption efficiency in a packed column. It was found that the SO<sub>2</sub> absorption efficiency increased with increasing concentration of ferric sulfate & decreased with the acidity of the spraying solution. As the hydrolysis of ferric ions occurs in solution, the removal efficiency of SO<sub>2</sub> augmented slowly with increasing Fe(III) concentration. Taking into account the hydrodynamic and mass transfer characteristics of the packed column, the enhancement factor (*E*) was found to depend on the concentration of the ferric ions and pH of the solution. The authors established that these results could be used for the simulation and design of SO<sub>2</sub> scrubbers.

Zhang et al. (2010) investigated a novel process for FGD in a packed column with simultaneous production of polymeric ferric sulfate (PFS), using the FeSO<sub>4</sub> solution as absorbent, sulfur dioxide (SO<sub>2</sub>) in flue gas as raw material & sodium chlorate (NaClO<sub>3</sub>) as oxidant. The results indicated that SO<sub>2</sub> removal efficiency in a packed column could be maintained at a high level, with more than the average value of 95%. Liquid PFS of fine quality was manufactured in the packed column reactor. Solid PFS by-product was obtained in a spray-drying column by use of the high-temperature inlet flue gas and the parameters for measuring its quality were estimated. The liquid & solid PFS byproducts were used to treat three types of wastewater & it was found that two types of synthesized PFS were comparable or superior to commercially available solid PFS for reduction of chemical oxygen demand of impure water and the performance of liquid PFS was found to be better than solid PFS.

Fang et al. (2011) used a counter-current packed column and operated it under continuous mode for the NO<sub>x</sub> and SO<sub>2</sub> absorption in urea solutions. On the basis of high removal efficiency SO<sub>2</sub>, the NO<sub>x</sub> removal efficiencies for different experimental conditions were determined. The results showed that Urea solution was a promising absorbent for simultaneous desulfurization & denitration of gaseous mixtures. It exhibited high SO<sub>2</sub> removal efficiency (almost 100% desulfurization efficiency) & more than 40% denitration efficiency. The degree of oxidation of nitrogen oxides, additives and other factors had a great influence on the denitration efficiency. The capacity of NO<sub>x</sub> removal efficiency of four additives was in the order, NaClO<sub>2</sub>>

$\text{KMnO}_4 > \text{NaClO} > \text{H}_2\text{O}_2$ . The investigators concluded that using different oxidants, 52.6% to 97.8%  $\text{NO}_x$  removal efficiencies could be achieved.

#### **2.2.4 Sieve tray**

Chien and Chu (2000) investigated the effect of various parameters on absorption efficiency of  $\text{SO}_2$  and  $\text{NO}_x$  for lesser  $\text{NaClO}$  solution concentration under acidic conditions in a bench-scale sieve tray column. The authors achieved the maximum removal efficiencies of  $\text{NO}_x$  and  $\text{SO}_2$  as 36-72% and 88-100%, respectively for the united  $\text{SO}_x/\text{NO}_x$  removal system.

#### **2.2.5 Spray scrubber**

Dantuluri et al. (1990) reported the growth of a comprehensive model for the sulfur dioxide absorption from a lean gaseous mixture into  $\text{Ca}(\text{OH})_2$  slurry in a spray scrubber FGD system. In this study, the model was developed by taking into account the surface area of the calcium hydroxide particles. A sensitivity analysis was then conducted to measure the sensitivity of the model to the surface area at a particle radius of 2, 3, 4 & 6 micrometres.

Brogren and Karlsson (1997) developed a model based on penetration theory to measure the dynamic rate of sulfur dioxide absorption into a limestone slurry droplet in a spray scrubber. The model included both instantaneous equilibrium reactions & reactions with finite rates for lime stone dissolution, sulfite oxidation, gypsum crystallization & the hydrolysis reaction of  $\text{CO}_2$ . The high value of physical mass transfer coefficient was considered near the nozzle due to high droplet velocity & for a high degree of turbulence because of the high pressure atomization. The authors found that except near the top of the spray scrubber, sulfur dioxide absorption was primarily a liquid-side controlled process.

Frandsen et al. (2001) studied the effects of the introduction of an organic acid into the slurry of limestone with fine particle-size distributions (PSD) in a wet FGD pilot plant. The authors also studied the optimization of the plant with regards to the degree of desulfurization, slurry pH profiles & the residual limestone content of the gypsum product. Of the different organic acids tested, adipic acid was preferred to citric acid, as the investigators obtained a greater  $\text{SO}_2$  removal rate. Additionally, adipic acid did not appear to affect the gypsum dewatering properties significantly. Simulations suggested that DBA (a mixture of adipic, glutaric & succinic acid) was just as active

as the adipic acid in optimizing wet FGD plants, though the degradation rates of glutaric and succinic acids were not examined. Using limestone with a smaller average particle-size, higher SO<sub>2</sub> removal efficiency and a lower residual limestone level in the slurry was achieved by the investigators. At a holding tank pH between 5.88 & 5.90, degree of desulfurization increased but the residual limestone content in the product gypsum increased from 19 to 30 wt.%. The authors determined that the choice of optimization method should be centred on a distinct technical & economical evaluation of a given wet flue gas desulfurization plant.

Chien et al. (2000) investigated the absorption kinetics of low concentration of SO<sub>2</sub> & NO from flue gas in an aqueous solution of acidic sodium chlorite using a bench-scale spraying sieve tray wet scrubber. The NO<sub>x</sub> absorption rate increased with increasing NO<sub>x</sub> and NaClO<sub>2</sub> concentrations, and with decreasing pH value of the absorbing solutions. The NO<sub>x</sub> absorption rate was not significantly affected by operating temperature & the range of gas-liquid contact time used in the study. The existence of ClO<sub>2</sub> in the NaClO<sub>2</sub> solutions for the cases of simultaneous absorption of SO<sub>2</sub> and NO<sub>x</sub> was also observed, and the mass balances of N and S species were pretty fine.

Nygaard et al. (2004) carried out two measurement campaigns at a power plant which had a capacity of 620 MW & was equipped with a wet FGD plant using a counter-current spray absorber with five spray levels. The predictable decrease in SO<sub>2</sub> concentrations alongside the height of the absorber was found in the spray section (from height 26.5 to 36.2 m) although the sulfur dioxide concentration above the holding tank and below the gas inlet was quite low, perhaps because of long local residence times in the region. Horizontal variations, because of somewhat different flow conditions near the column wall were investigated and the sulfur dioxide concentrations were observed to be higher near the wall. Measurements at different gross loads depicted that the sulfur dioxide gas phase concentration at a given position inside the absorber was roughly related to the L/G ratio in the measuring interval. Turning off one of the lower spray levels, while burning coal with low S content, did not lower the overall removal efficiency of the absorber. However, the concentration of SO<sub>2</sub> in the gas phase in the lower part of the absorber was increased by a factor of 2–3. Measurements of slurry pH at various positions showed a decrease of approximately 0.5 units from the upper to the lower part of the absorber.



Gomez et al. (2007) developed a CFD model and compared the model predicted values with the actual industrial data for the SO<sub>2</sub> absorption and O<sub>2</sub> & CO<sub>2</sub> desorption. The model was applied for simulation of the flue gas desulfurization plant of the Teruel power station situated in Andorra (Teruel, Spain) that included both the spray scrubber & the oxidation tank. The power station was fired with high-S coal (up to 4.5 percent) which generated flue gases with SO<sub>2</sub> concentrations ranging between 4000-6500 ppm. The FGD system power station was designed for a desulfurization volume of 1.4 million Nm<sup>3</sup>/hr of flue gas for desulfurization efficiency in excess of 90%.

Erdöl-Aydin and Nasün-Saygili (2007) presented a model for the reaction between sulfur dioxide & trona based slurries. The model predicted values were found to well agree with the experimental data. It was concluded that at high stoichiometric ratios of Na/S in the feed streams, the diffusion of SO<sub>2</sub> from the gas bulk to the droplet interface lead to increasing absorption & with decreasing ratio of this quantity, the absorption efficiency decreased. An elevation in the temperature was observed to cause a diminution in the absorption efficiency. At the stoichiometric ratio of Na/S = 2, SO<sub>2</sub> removal efficiency was found to be approximately 90%.

Dou et al. (2008) used an electrostatic spraying absorber (ESA) as the reactor, where sulfur dioxide was absorbed into an aqueous slurry of reactive Ca(OH)<sub>2</sub>. The absorption process was measured by using the two-film theory of mass-transfer. The absorption process was reported to be controlled by both liquid and gas side resistances. The ESA characteristics were examined for the applied voltage ranging from -10 to 10 kV at various slurry flow rates. The removal efficiency of sulfur dioxide did not depend on the polarity of the applied voltage. Slightly greater efficiency was achieved with the conduction charging configuration as compared to the induction charging configuration. A model for external mass-transfer incorporating an enhancement factor was proposed for approximation of the absorption efficiency. Predicted values of SO<sub>2</sub> removal efficiency were reported to produce good agreement with the experimental data.

Dou et al. (2009) performed experiments in a spray tower for the sulfur dioxide removal from flue gases using limestone slurry. Sulfur dioxide concentration in the flue gas was about 2500 ppm. The parameters studied by the investigators included droplet size, pH value of the slurry, gas and liquid phase flow rates, and, limestone concentration. Two film theory was assumed to define the mass transfer mechanism.

SO<sub>2</sub> removal efficiency was found to increase as the pH value of the slurry was increased from 5.0 to 6.0. Absorption of SO<sub>2</sub> at lower pH values was reported to increase the utilization efficiency of absorbent and eliminate the sulfite ions responsible for scaling and plugging problems. The SO<sub>2</sub> removal efficiency reduced substantially when the pH was too low and led to very high residual limestone content in the gypsum produced. The authors observed that the SO<sub>2</sub> removal efficiencies greatly increased with increasing the L/G ratios, and it reached 96% at L/G ratios of higher than 13.

Kallinikos et al. (2010) developed a dynamic model for desulfurization of power plant exhausts using a wet process. Limestone dissolution, crystallization of calcium sulfite & gypsum & oxidation of sulfite ions were taken into account for simulation of the model for a spray tower. For the development of the mathematical model, the authors made several assumptions, viz., (i) dissolution of limestone occurred both in the feed tank and in the column, (ii) all CaCO<sub>3</sub> fed into the system reacted and its concentration in the exit stream was nil, (iii) oxidation of SO<sub>3</sub><sup>2-</sup> to SO<sub>4</sub><sup>2-</sup> occurred both in the feed tank and in the column, and, it was catalyzed by the presence of typical transition metals like Mn<sup>2+</sup>, (iv) the absorption rate of SO<sub>2</sub> was affected both by the mass-transfer resistances developed across the gas and liquid films as well as by the chemical reaction rate, (v) desorption rate of CO<sub>2</sub> was considered to be affected only by the mass-transfer resistances developed across the liquid film, (vi) CaSO<sub>3</sub> crystallization occurs in the tower, while its dissolution occurred in the feed tank, and, (vii) gas absorption could be described by the two film theory. Typical operating parameters were flue gas volumetric flow rate (700m<sup>3</sup>/s), inlet sulfur dioxide concentration (14,500 mg/Nm<sup>3</sup>), desired exit concentration of sulfur dioxide (400 mg/Nm<sup>3</sup>), volumetric flow rate of fresh air to the tank (7m<sup>3</sup>/s), and flow rate of the feed slurry (around 12 m<sup>3</sup>/s).

Marocco (2010) illustrated a computational fluid dynamic (CFD) model of a counter-current Open Spray Tower desulfurization reactor & its application in the simulation of full-scale industrial equipment. The two-phase gas-liquid reactor was simulated using a Euler–Lagrange approach and a commercial CFD code. Physical absorption was modeled by applying dual film theory. The aqueous phase chemistry was taken into account for the instantaneous equilibrium reactions of eight dissolved species into

a slurry droplet. The numerical results were found to agree well with the measured values of pressure drop & SO<sub>2</sub> removal efficiency.

Jia et al. (2011) used the two film theory to develop a mathematical model of an ammonia-based wet FGD process. Experimental data were collected for the operating conditions including pH, liquid/gas ratio & SO<sub>2</sub> concentration. The model predicted values for the desulfurization system for several 220 tons/hr boilers were found to compare well to that of the corresponding measured data. This model could predict well the absorption performance of an ammonia-based wet FGD process, appeared to be useful for designing of SO<sub>2</sub> absorbers with ammonia absorbent.

Codolo (2012) presented his experimental data on the removal efficiency of SO<sub>2</sub> in a spray tower. The variables studied were the superficial velocity of the gas, L/G ratio, size of spray nozzles and height of the tower. The effect of the height of tower on the removal efficiency was calculated through experiments inside a spray tower. Two sets of five nozzles were used, with the diameter of orifices 2.4 and 3.2 mm, and only one nozzle with the orifice diameter of 5.6 mm. The removal efficiency significantly increased up to a height of about one meter and then almost remained constant. Removal efficiencies obtained with 2.4 mm diameter nozzles were higher than those with 3.2 mm dia nozzles. This was attributed to the smaller diameter droplets and larger specific gas-liquid interfacial area for a given liquid rate produced with the smaller diameter nozzle than that with the larger size nozzle. The results depicted the effect of the gas velocity and L/G ratio and tower height on the SO<sub>2</sub> removal efficiency and that of the gas velocity on the volumetric gas-side mass-transfer coefficient.

Shen et al. (2013) presented a novel Mg-based wet FGD process in which sodium thiosulphate was applied to inhibit the oxidation of desulfurization product. Effects of various operating variables on desulfurization efficiency of flue gas were experimentally studied in a spray scrubber. The results demonstrated that the magnesium-based wet FGD process was more suitable for low SO<sub>2</sub> concentration flue gas and indicated that the addition of Na<sub>2</sub>S<sub>2</sub>O<sub>3</sub> could somewhat increase the desulfurization process & the MgSO<sub>3</sub> content in the byproduct could be maintained above 95% when the thiosulphate to sulfite ratio was controlled above 1:6. A desulfurization process model was recognized by the two-film theory of mass transfer. The computed values of mass-transfer coefficients were in good agreement with the

experimental values & the absorption process was observed to be gas-film diffusion controlled.

Zhu et al. (2015) presented a concise model for wet FGD system using limestone slurry in a spray tower. The expressions for droplet motion & mass balance for SO<sub>2</sub> were incorporated into the model equations. The predicted values were well validated with the experimental data for the height of the spray tower required for reducing the concentration of SO<sub>2</sub> from its inlet value to the desired exit value. The effect of operating parameters on the absorption height was also examined. The results showed that absorption height decreased with an increase in the liquid to gas ratio and pH value of the slurry. The required height was found to increase with increasing droplet diameter, gas flow rate, gas temperature, inlet SO<sub>2</sub> concentration and absorption efficiency. As the most sensitive parameter, the droplet diameter was found to be most vital for the sound prediction of absorption height. It was concluded that this model could give engineering guidance to design a spray tower absorber.

#### **2.2.6 Absorption studies of SO<sub>2</sub> in bubble column reactor-Packed/ tapered/ multistage/ bubbling reactor**

Mashelkar and Sharma (1970) investigated the mass transfer parameters of packed bubble columns & compared with those of the unpacked bubble columns. The performances of bubble & packed bubble columns were also examined for systems in which there is a considerable variation in the superficial velocity of gas as the gas traverses the column (Abraham and Sawant, 1990; Krishna et al., 1994; Sawant et al., 1979). This occurs as the gas traverses pass through a column of the convergent-divergent cross-section. The system considered was the absorption of CO<sub>2</sub> in aqueous sodium carbonate-bicarbonate buffer. This corresponds to the situation of gas absorption followed by a slow chemical reaction. The theory of absorption with reaction was applied to get the values of the effective interfacial area, the gas-side & the liquid-side mass transfer coefficients. The mass transfer characteristics of the bubble columns operated in semi-batch, co-current & counter-current modes in a wide range of superficial gas and liquid velocities were found to be equivalent. Several other investigators (Kantarci et al., 2005; Shulman and G molstad, 1950) concluded from the results of their studies that gas bubble columns display mass-transfer rates of the same order of magnitude as packed columns at low liquid rates but at higher liquid rates, mass-transfer rates are found to be much higher in a bubble column & packed

columns are found to be inefficient. Also, in a bubble column, the effective interfacial area is a function of the liquid properties like viscosity, the nature of ions and ionic strength. Provided these properties were kept nearly equal; the effective interfacial area remains practically unchanged in a packed column irrespective of the reacting species & the kinetics of the reaction.

Braulick et al. (1965) studied the air oxidation of aqueous sodium sulfite solutions in simple bubble contacting columns of 3, 4, and 6-in. diameter. Superficial gas mass velocities, up to 300 lbm/ (hr)(sq. ft) were used. Contacting action was described in detail, and comparisons with air-water data show the marked influence of small, ionic bubbles. Mass transfer rates and dynamic gas holdup data were presented, and the former were compared with mass transfer data obtained from bubble-cap trays. Gas holdup and mass transfer rates were found to increase with gas flow rates and with the submergence diameter ratio. The mass transfer characteristics of the gas-sparged bubble column were found to be equivalent to those of stirred vessels. Also, at gas rates in the turbulent contacting regimes, essentially complete back-mixing of the liquid was observed.

Halhouli et al. (1999) used a bubble column for desulfurization of flue gas (sulfur dioxide concentration: 1000-2000 ppm) by bubbling the gas through iodine in methanol solution. In this, iodine was used as the oxidizing agent and methanol as the solvent. The experimental results were compared with those obtained from the bromine in water and bromine in methanol systems. Methanol was used to avoid bromine stripping from the water. Bromine and iodine were regenerated by the electrolysis of the resulting hydrobromic and hydroiodic acids. Sulfuric acid and hydrogen gas were the products of the electrolysis process. The use of iodine in this study produced a higher desulfurization rate than that obtained using bromine as the oxidant.

Meikap et al. (2002) performed experimental investigations on the scrubbing of SO<sub>2</sub> in the modified multi-stage bubble column scrubber (MMSBCS) using water as the absorbent and achieved almost 100% removal efficiency of SO<sub>2</sub> without any additives or pretreatment. The investigators made several simplifying assumptions for development of a mathematical model for the system they studied. Partial back mixing of each of the two phases viz., gas and liquid, were assumed. The gas samples was analyzed for sulfur dioxide concentration by absorbing SO<sub>2</sub> in tetrachloromercurate

and the latter solution was analyzed for SO<sub>2</sub> concentration using a UV-VIS spectrophotometer. The high efficiency of the process was attributed to the multi-stage operation.

Meikap et al. (2002) developed a realistic model for the absorption of SO<sub>2</sub> in a modified multi-stage bubble column scrubber (MMSBCS). Experimental results indicated that the performance of the simple bubble column for scrubbing of SO<sub>2</sub> using water as the scrubbing medium were predicted by using theoretical equations based on physical mass-transfer process. It was observed from the experimental investigation that air-SO<sub>2</sub> mixture in the MMSBCS without using any additives or pre-treatment could result in very high percentage removal of SO<sub>2</sub>. This high efficiency was attributed to the multi-stage operation. For modified multi-stage bubble column, the experimental results showed clearly the staging effect, which led to almost 100% removal efficiency.

Tang et al. (2004) presented a novel FGD process in which an organic amine was applied to absorb SO<sub>2</sub> from flue gas in a bubbling contactor. The vapor-liquid equilibrium model of absorption of SO<sub>2</sub> from the flue gas by an organic amine was recognized & the vapor-liquid equilibrium of the sulfur dioxide-ethylene-diamine-phosphoric acid-water system was first predicted. For a 0.3 g mol/l ethylene-diamine buffer solution system, the predicted values were found to validate with the experimental data well. It was established that their model was significantly good to forecast vapor liquid equilibrium under the experimental conditions. Using an ethylene-diamine-phosphoric acid aqueous solution as the absorbent, some operating conditions including temperature, gas to liquid ratio, pH value reaction medium, concentration of the absorbing reagent & liquid flow rate used in the absorption & de-absorption studies were performed in a laboratory packed tower. The optimized conditions calculated for the system studied were stated. The authors claimed that the novel FGD method reported in this paper had leads of high desulfurization efficiency along with low investment.

Bandyopadhyay and Biswas (2006) performed experimental investigations on the scrubbing of SO<sub>2</sub> (of initial concentration in the range of 400 to 1780 ppm) in a tapered bubble column scrubber using water and sodium alkali (in the range of concentrations of  $2.0 \times 10^{-4}$  to  $5.0 \times 10^{-3}$  kg mol/m<sup>3</sup>). Increase in gas flow rate decreased

the percentage removal of SO<sub>2</sub>, while the increase in liquid flow rate increased the percentage removal.

Liu and Xiao (2006) performed the absorption of SO<sub>2</sub> into limestone slurry containing suspended reactive particles in a bubbling reactor with continuous feeding of both gas and liquid phases at a constant pH and high temperature (50°C). An absorption model with a single reaction plane based on the film model was developed. The effects of limestone particle size, concentration of limestone, acetic acid additive, and inlet SO<sub>2</sub> concentration on the concentration distribution of different chemical species in the liquid film and SO<sub>2</sub> absorption rate were investigated. Increasing the concentration of limestone slurry, use of acetic acid additives into the system, decreasing the limestone particle size or inlet SO<sub>2</sub> concentration caused the reaction plane in the liquid film to shift towards the gas-liquid interface. Model predictions were found to fit the experimental data well.

Jin et al. (2006) presented a study that attempted to generate chlorine dioxide (ClO<sub>2</sub>) gas continuously by chlorate–chloride process and to utilize it further to clean up SO<sub>2</sub> and NO<sub>x</sub> gases simultaneously from the flue gas in the lab-scale bubbling reactor. Experiments were carried out to examine the effects of various operating parameters like inlet SO<sub>2</sub> and NO concentrations, pH of the reaction medium and ClO<sub>2</sub> feed rate on the SO<sub>2</sub> and NO<sub>x</sub> removal efficiencies at 45°C. Complete oxidation of NO into NO<sub>2</sub> occurred on passing sufficient ClO<sub>2</sub> gas into the scrubbing solution. SO<sub>2</sub> removal efficiency of about 100% and NO<sub>x</sub> removal efficiency of 66–72% were achieved under optimized conditions. NO<sub>x</sub> removal efficiency decreased slightly with increasing pH and NO concentration. Input SO<sub>2</sub> concentration had marginal catalytic effect on NO<sub>2</sub> absorption. No improvement in the NO<sub>x</sub> removal efficiency was observed on passing excess of chlorine dioxide into the scrubbing solution.

Zhao et al. (2009) performed experiments of simultaneous removal of SO<sub>2</sub> and NO from simulated flue gas, using NaClO<sub>2</sub> solution as the absorbent, in a self-designed bubbling reactor. Under the optimal experimental conditions, high removal efficiencies of both the gaseous species were obtained. The mechanism of simultaneous removal based on NaClO<sub>2</sub> solution was proposed by analyzing the reaction products. Limitations of the desulfurization and denitrification process using NaClO<sub>2</sub> solutions were computed by thermodynamic methods. Experimental results of reaction kinetics for simultaneous desulfurization & denitrification depicted that the

oxidation-absorption processes of SO<sub>2</sub> & NO were divided into two zones, explicitly the fast & slow reaction zones. In the slow reaction zones both the reactions were of zero order, whereas in the fast reaction zones, the reaction order, rate constant and activation energy of the reaction of SO<sub>2</sub> with the absorbent were 1.4, 1.22 (g mol l<sup>-1</sup>)<sup>0.4</sup> s<sup>-1</sup> and 66.25 kJ·g mol<sup>-1</sup>, respectively. The corresponding quantities for the NO reaction were 2, 3.15 10<sup>3</sup> (g mol l<sup>-1</sup>)<sup>-1</sup>· s<sup>-1</sup>, and 42.50 kJ g mol<sup>-1</sup>.

### 2.2.6.1 Absorption of SO<sub>2</sub> in a bubbling reactor

Zhao et al. (2010) investigated the simultaneous removal of SO<sub>2</sub> and NO from flue gas in a bubbling reactor using a solution of a mixture of NaClO and NaClO<sub>2</sub>. The various influencing factors, such as g molar ratio of NaClO to NaClO<sub>2</sub>, solution pH, reaction temperature, SO<sub>2</sub> and NO concentrations on removal efficiencies of SO<sub>2</sub> and NO were studied experimentally. The optimal conditions established were, g molar ratio of NaClO to NaClO<sub>2</sub> = 4.0, solution pH = 5.5, reaction temperature = 50 °C. Under the optimal operating conditions, the removal efficiencies of SO<sub>2</sub> and NO attained 100% and 85%, respectively. The investigators proposed the reaction mechanism of simultaneous desulfurization and denitration using the mixed reagents.

Li et al. (2013) used a bubble column reactor for studies of the absorption of SO<sub>2</sub> from a gaseous mixture into aqueous NH<sub>4</sub>HCO<sub>3</sub> solutions with different concentrations accompanied by an instantaneous irreversible chemical reaction. The investigators also proposed mass transfer models based on Danckwerts surface-renewal model as well as the penetration theory for surface stretch proposed by Angelo et al. (1966). They obtained analytical expressions for time-average mass transfer coefficient & enhancement factor. The model predicted values were found to agree well with the experimental results.

Zhao et al. (2014) used Fenton reagent for simultaneous desulfurization & denitrogenation of flue gas in a bubbling reactor. The influence of reaction temperature, the concentration of each component in the Fenton reagent, initial pH value, gas flow rate, initial concentrations of SO<sub>2</sub> & NO in flue gas on removal efficiencies was investigated systematically. The optimum operating parameter values obtained by the investigators were, temperature: 328 K, flow rate of flue gas: 0.02 m<sup>3</sup>/h at 0.1 MPa, 328 K, H<sub>2</sub>O<sub>2</sub> concentration: 11.0% (w/w), concentration of Fe(II) 2.8 mg mol/L, and solution pH: 3.0. The simultaneous removal efficiencies of 100% for



SO<sub>2</sub> & more than 90% for NO were attained under the established optimal experimental conditions. A reaction mechanism of desulfurization & denitrogenation was proposed. Several thermodynamic parameter values were thought based on the basic thermodynamic principle to authenticate the viability of the oxidation reactions of SO<sub>2</sub> & NO with Fenton reagent.

### **2.3 Absorption of SO<sub>2</sub> in the presence of a surface active agent**

Hikita et al. (1977) studied pure SO<sub>2</sub> absorption into aqueous sodium bisulfite, sodium hydroxide, and sodium sulfite solutions with & without the addition of a surface active agent at 25°C in a liquid jet column. For absorption of sulfur dioxide into sodium hydroxide solution, the rate of absorption without a surface active agent was observed to be more than that into the solution containing the surface active agent. This was attributed to the presence of the interfacial turbulence. The absorption rates attained by the authors with no surface active agent were in good agreement with the predictions from the model developed on the basis of the penetration theory.

Hikita et al. (1978) studied the absorption of pure sulfur dioxide into aqueous ammonia and that into aqueous ammonium sulfite solutions containing ammonium bisulfite at 25°C in a liquid jet column. The absorption rates obtained with and without the addition of a surface active agent for these systems were found to be the same. These results indicated the absence of the interfacial turbulence and were well validated with the theoretical predictions based on the penetration theory.

Vazquez et al. (1988) studied the effects of liquid flow rate, NaOH concentration, column length & presence of  $5 \times 10^{-3}$  wt. % of the surfactant SLS on the pure SO<sub>2</sub> absorption rate by aqueous NaOH solution in a sphere & cylinder column. The presence of SLS was reported to prevent axial turbulence which enhanced the rate of mass transfer in longer columns and was almost independent of the liquid flow rate. The enhancement factor due to the reaction between SO<sub>2</sub> & NaOH in comparison to the process of physical absorption was investigated for the systems with excess OH<sup>-</sup> in the exit flow stream. *The experimental results acquired in the presence of a surfactant were satisfactorily detailed with a single reaction plane model based on the film theory. Those obtained in the absence of surfactant were best described by a two reaction-plane model based on the surface renewal theory.*

Garcia-abuin et al. (2015) studied the absorption of pure SO<sub>2</sub> in a bubble column with or without the addition of a surfactant (HTAB AND DTAB) in pure water and solutions of calcium hydroxide and sodium hydroxide. In each of the alkaline solutions, an increase in sulfur dioxide loading in comparison to that in water was observed. But, this enhancement was marginal due to the very high gas solubility of SO<sub>2</sub> in water. The authors did not find any significant influence of the presence of surfactant on the absorption rate of SO<sub>2</sub>. It was concluded that this may be due to the very high reaction rate between sulfur dioxide and sodium hydroxide, the latter being present in very high concentration. The negative effect of surfactant upon gas diffusivity in the liquid phase was negligible in comparison to the positive effect caused by chemical reaction.

### **2.3.1 Absorption of SO<sub>2</sub> in presence of a surfactant (foam-bed reactor) and elimination of choking problem of distributor nozzles**

Foam-bed reactors have been reported to possess several important advantages as mass-transfer equipment (Jana, 2007). The most important of these, likely to be useful for desulfurization of flue gases, is the elimination of the choking problems of spray nozzles in the case of a spray tower or orifices on the gas distributor plate of a bubble column reactor. Jana, (2007) reported that at the time of carbonation of hydrated lime slurry in a semi-batch bubble column reactor, the orifices on the gas-distributor plate got choked. But when the same experiments were performed in a foam-bed reactor, the addition of a surfactant, say CTAB, in ppm level, eliminating the choking problem.

Absorption of SO<sub>2</sub> from lean gaseous mixtures using solutions or slurries of the hydroxides of alkali and alkaline earth metals investigated by numerous investigators (Hikita et al, 1977; Vázquez et al., 1988; García-Abuín et al., 2015) produced in each and every case a higher rate of absorption of SO<sub>2</sub> than those obtained using the same solution but in presence of a surfactant. Therefore, there remains a research gap to find out whether the addition of a small amount of surfactant may eliminate the choking problem and at the same time does not affect the rate of absorption of SO<sub>2</sub>.

#### **2.4. Regenerative absorbents for flue gas desulfurization**

Various regenerative absorbents that are used for SO<sub>2</sub> absorption include magnesium oxide, ammonia-based absorbents, sodium alkali based absorbents, etc. Aqueous sodium sulfite and sodium bi-sulfite solutions reported to have been used for absorption of sulfur dioxide from flue gas. Regeneration of the solvent produced a concentrated SO<sub>2</sub> stream, which was converted into a saleable product such as liquid SO<sub>2</sub>, sulfuric acid, or elemental sulfur.

Pandey et al. (2005) reported the use of ammonium sulfite in place of sodium sulfite. This process was able to achieve more than 95% SO<sub>2</sub> removal efficiency from flue gases generated from high-sulfur fuels. Installation of the required plant for this process was reported to be expensive but relatively cheaper to operate.

Nolan (2000) made a comparative study and showed that the operating cost for this process is similar to that of a limestone-based FGD process.

Yeager (1980) used an aqueous solution of citric acid for the capture of the SO<sub>2</sub>. Citric acid was regenerated with concomitant formation of elemental sulfur. This regeneration was achieved by treating the used sorbent with H<sub>2</sub>S.

Satriana (1981) reported the use of dilute ammonium hydroxide for SO<sub>2</sub> scrubbing from flue gas. The ammonium salt produced was crystallized from the concentrated spent scrubber liquor. It was suggested that this could be used as a valuable constituent for fertilizer formulations.

Karatepe (2000) made a comparative study of the different processes and reported that among the processes studied, the one which needs the highest amount of capital investment was the sodium-based scrubber process with regeneration. With respect to capital investment, this process was followed by the ammonia-based scrubber process, the limestone-lime sludge process with gypsum end product, the spray dry processes (lime and soda-ash) & the dry alkali injection processes, Ca & Na based.

### 2.4.1 Ionic liquids (ILs) as regenerative absorbents for SO<sub>2</sub>

The following aspects are discussed in brief in the following paragraphs.

- (i) Synthesis of ILs and its use for SO<sub>2</sub> solubility measurements
- (ii) Use of ILs for flue gas desulfurization
- (iii) Investigations on g molecular level interactions between the IL and the SO<sub>2</sub> g molecules

#### 2.4.1.1. Synthesis of ILs and its use for SO<sub>2</sub> solubility measurements

Ionic liquids are g molten organic salts at ambient temperature and consist of big organic cations & inorganic or organic anions. Because of the distinct properties such as negligible vapor pressure, high thermal stability & excellent solvent power for a varied range of both organic & inorganic materials, ionic liquids have been considered environment friendly solvents as water and supercritical CO<sub>2</sub>. As a result, ILs are considered as a new generation “green solvent”. It offers an extensively high potential application in many fields like catalysis (Hallett and Welton, 2011), electrolysis (Armand et al., 2009), extraction (Huddleston et al., 1998), membrane separation (Noble and Gin, 2011), biocatalysts and nano-phase materials (Yang and Pan, 2005) gas absorption (Bates et al., 2002; Duan et al., 2011; Guo et al., 2011; Shiflett and Yokozeki, 2009), etc. As far as the application of ILs in gas absorption is concerned, ILs have been proposed to be more effective & environmentally benign alternative to traditional desulfurization solvents for the separation of SO<sub>2</sub> from flue gas, according to some pioneering works (Huang et al., 2006; Wu et al., 2004).

Wu et al. (2004) described a novel method for desulfurization of a simulated flue gas in which an IL: 1,1,3,3-tetramethylguanidinium lactate (TMGL) was used to absorb SO<sub>2</sub>. The IL was synthesized by direct neutralization of 1,1,3,3-tetramethylguanidinium (TMG) with lactic acid using ethanol as the solvent. To gain some knowledge on the nature of the interaction between the virgin IL and the SO<sub>2</sub> g molecules in the SO<sub>2</sub> absorbed in the IL, the investigators performed <sup>1</sup>H NMR and FTIR analyses of the absorbent before and after absorption of SO<sub>2</sub>. New bands formed at 1230 cm<sup>-1</sup> and 957 cm<sup>-1</sup> in the product g molecules were assigned to sulfate S=O, and S-O stretches, respectively. The equilibrium SO<sub>2</sub> absorption capacity of this IL for 8% by volume of SO<sub>2</sub> with N<sub>2</sub> at 40°C and 1 atm total pressure was 0.978 g mol of SO<sub>2</sub> per g mol of IL. For pure SO<sub>2</sub>, at 40°C and 1.2 atm total pressures this ratio was observed to be 1.7.

The absorbed SO<sub>2</sub> could be reversibly desorbed, and the regenerated solvent could be reused for absorption of SO<sub>2</sub>, and the cycle could be repeated. The practical utility of this IL was limited because of its relatively low thermal stability. Hence, only a fraction of the absorbed gas could be thermally released before degradation of the IL occurred (Duan et al., 2011).

Huang et al. (2006) examined the absorption of SO<sub>2</sub> gas in TMG (Tetramethyl guanidine), and BMIM (1-butyl-3-methylimidazolium) based ILs. The SO<sub>2</sub> absorption capacity of the ILs using pure SO<sub>2</sub> gas at 1 bar and 20 °C, g mol of SO<sub>2</sub> per g mol of IL, was found to be 1.33, 1.50, 1.27, 1.18, 1.60 in [BMIM][BTA], [BMIM][BF<sub>4</sub>], [TMG][BF<sub>4</sub>], [TMG][BTA] and [TMGB2][BTA], respectively. However, when experiments were performed with 10 g mole percent SO<sub>2</sub> in N<sub>2</sub>, only 0.007, 0.005, 0.064, 0.061, 0.080 g mol of SO<sub>2</sub> per g mol of IL was absorbed at the same pressure and temperature.

Huang et al. (2008) also performed experiments to absorb SO<sub>2</sub> from a mixture of 10% SO<sub>2</sub> in N<sub>2</sub> in 1,1,3,3-tetramethylguanidine(TMGG)-based ILs, [TMGG]BF<sub>4</sub>, [TMGGPO]BF<sub>4</sub>, [TMGGPO2]BF<sub>4</sub>, [TMGG]Tf<sub>2</sub>N and [TMGGHB2]Tf<sub>2</sub>N and got the absorption capacities of 0.06, 0.131, 0.167, 0.057 and 0.074 g mol fraction, respectively.

Ren et al. (2010) found that task-specific ILs ([TMG]L and [MEA]L) could chemically absorb SO<sub>2</sub> when the g mole ratio of SO<sub>2</sub> to the IL was less than 0.5; when the g mole ratio was greater than 0.5, the IL could physically absorb SO<sub>2</sub>. The normal ILs ([BMIM][BF<sub>4</sub>], [BMIM][PF<sub>6</sub>], and [TMG][BF<sub>4</sub>]) could only physically absorb SO<sub>2</sub>. For the task-specific ILs to absorb SO<sub>2</sub>, before at a g mole ratio of SO<sub>2</sub> to IL less than 0.5, the viscosity and density increase, and the conductivity decrease with an increase of the g mole ratio of SO<sub>2</sub> to IL. After that, the conductivity and density increase, and the viscosity decrease with further increase in the g mole ratio of SO<sub>2</sub> to IL. However, for the normal ILs, the conductivity and density increase and the viscosity decrease with an increase of the g mole ratio of SO<sub>2</sub> to IL.

Shang et al. (2011) used new anions for the synthesis of three new guanidine-based ionic liquids (GBILs). These investigators synthesized [1,1,3,3-tetramethylguanidinium][phenol] ([TMG][PHE]), [1,1,3,3-tetramethylguanidinium][imidazole] ([TMG][IM]) and [1,1,3,3-

tetramethylguanidinium][2,2,2-trifluoroethanol] ([TMG][TE]) and determined the SO<sub>2</sub> absorption and desorption characteristics of these ILs. The absorption capacities of ILs were found to be 2.58- 4.132 g mol SO<sub>2</sub>/g mol IL at 20°C and 2.24-3.17 g mol SO<sub>2</sub>/g mol IL at 40°C. CO<sub>2</sub> absorption characteristics of these new ILs were also studied. It was observed that only 0.502 g mol CO<sub>2</sub> per g mol IL was absorbed at 20 °C. By performing <sup>1</sup>H NMR, <sup>13</sup>C NMR and FTIR analyses, the investigators concluded that the synthesized GBILs could absorb SO<sub>2</sub> by both physical and chemical interactions while physical absorption played the important role at the experimental conditions used by them. Low temperature favored high absorption capacity and could be reused after regeneration.

Anderson et al. (2006) measured the solubility of SO<sub>2</sub> in 1-n-hexyl-3-methylimidazolium bis(trifluoromethylsulfonyl) imide ([hmim][Tf2N]) and 1-n-hexyl-3-methylpyridinium bistrifluoromethylsulfonyl) imide ([hmpy]-[Tf2N]) in the temperature range 25-60 °C and at pressures up to 4 bar. The experiments were carried out in a magnetic suspension balance. It had a working range of vacuum of 500 bar and -200 to 350 °C with an accuracy of 2μg. The absence of any major impurity in the ILs was confirmed by <sup>1</sup>H, and <sup>13</sup>C NMR analyses and approximate water content was determined by Karl Fischer titration or by coulometry. The investigators used the virial equation of state for estimation of the density of the SO<sub>2</sub> gas. The authors also showed that although the solubility of SO<sub>2</sub> was much larger than CO<sub>2</sub> in these ILs at a particular temperature and pressure, the numerical value of this quantity is quite close when compared at the same reduced pressure defined as  $P_{\text{reduced}}=P_{\text{actual}}/P_{\text{saturation}}$ .

Hallett and Welton (2011) reported that in recent years, ionic liquids were being studied increasingly to remove acid gases such as CO<sub>2</sub>, SO<sub>2</sub> and H<sub>2</sub>S from gaseous mixtures. Compared to the traditional industrial solvents, ionic liquids present significant advantages, especially in complex systems, as they could be tuned by appropriate selection of the structures of their cations and anions (Rogers and Seddon, 2003).

Guo et al. (2010, 2011) synthesized CaprolactamTetrabutyl Ammonium Halide Ionic liquid by using different g mole ratios of caprolactam (CPL) and tetrabutyl ammonium bromides (TBAB) and used for the absorption studies of SO<sub>2</sub> and H<sub>2</sub>S. The solubility of SO<sub>2</sub> in g mole fraction unit in [CPL][TBAB] (1:1) was reported to be

0.680 at 298.2 K and decreased to 0.351 at 373.2 K.

Duan et al. (2010) measured the pH of a binary mixture of CPL-TBAB IL and solvents (water, ethanol, and 2-propanol) in the range of ionic liquid concentrations from  $(5.0 \times 10^{-3}$  to 0.80)  $\text{g mol} \cdot \text{L}^{-1}$  and temperature range from 296.15 to 325.65 K. The results showed that the range of the pH values was from 5.12 to 6.93. The authors also used pure ionic liquid for the absorption of NO and NO<sub>2</sub> gas (Duan et al., 2011). The binary mixture of CPL-TBAB IL and water was used by the same author for the absorption of SO<sub>2</sub>. The CPL-TBAB ionic liquid and water are completely miscible in all proportions under ambient conditions. A second phase appeared when SO<sub>2</sub> was introduced into the solution. The solubility of SO<sub>2</sub> in CPL-TBAB/water ( $4 \text{ g mol l}^{-1}$ ) was 0.523 g per g of the solution at 293.2 K. Physical properties of CPL-Halide IL, such as *melting points, heats of fusion and heat capacities* were measured by differential scanning calorimeter (DSC) (Jiang et al., 2013).

Liu et al. (2013) prepared five eutectic ionic liquids (EILs) using caprolactam (CPL) and low g molecular weight organic compounds (acetamide, imidazole, furoic acid, benzoic acid, o-toluic acid) which were denoted as CPL-acetamide (1:1), CPL-imidazole (1:1), CPL-furoic acid (1:1), CPL-benzoic acid (1:1) and CPL-o-toluic acid (2:1), respectively. Their properties such as melting point, density, viscosity, conductivity, and decomposition temperature and the solubility behavior of SO<sub>2</sub> in these EILs at 30-70 °C was explored. The viscosity of the EILs was found to decrease in the order: CPL-furoic acid (1:1) > CPL-o-toluic acid (2:1) > CPL-benzoic acid (1:1) > CPL-acetamide (1:1) > CPL-imidazole (1:1) at all the measured temperatures. The solubility of pure SO<sub>2</sub> in CPL-imidazole (1:1) was 0.624 g/g of mixture mass fraction at 30 °C and 1 atm. while it decreased to 0.341 g/g of the mixture at 70 °C. The SO<sub>2</sub> absorption capacities of CPL-organic amines were higher than CPL-organic acids.

Lee et al. (2010) synthesized BMIm (1-butyl-3-methylimidazolium), HMIm (1-hexyl-3-methyl imidazolium) and EMIm (1-ethyl-3-methyl imidazolium) based ionic liquid by varying the halide group viz; [BMIm]Br, [BMIm]Cl, [BMIm]I, [EMIm]Cl, [HMIm]Cl, [OMIm]Cl, [BMPyri]Cl and [BMPyrr]Cl and the solubility of SO<sub>2</sub> was found to be 2.06, 2.11, 1.91, 2.03, 2.19, 2.19, 2.22 and 2.22 g mol SO<sub>2</sub> per g mol IL, respectively. The solubility of SO<sub>2</sub> increased in the order of Br > Cl > I. It was

proposed that the primary interaction of the halide occurs with the C<sub>2</sub>-H of the imidazolium and the S atom of SO<sub>2</sub>.

Li et al. (2017) synthesized amine-functionalized ILs [NH<sub>2</sub>emim][OAc] and [NH<sub>2</sub>emim][BF<sub>4</sub>]. The conventional imidazole-based ILs [bmim][OH] and [bmim][BF<sub>4</sub>] with low viscosity were also prepared. Subsequently, the amine-functional ILs were mixed with the conventional ILs to investigate the absorption performance. In this study, the SO<sub>2</sub> absorption capacities of IL mixtures were determined using simulated flue gas with lean SO<sub>2</sub> gas. The investigators observed that the mixture of ionic liquids absorbed SO<sub>2</sub> reversibly, and the absorption capacity *remained unchanged after even 12 cycles*, but the viscosity and density of the mixtures increased by 2-3 percent in each cycle.

Shiflett and Yokozeki (2009) developed a ternary equation of state (EOS) model for the CO<sub>2</sub>/SO<sub>2</sub>/1-butyl-3-methylimidazoliummethyl sulphate ([BMIM][MeSO<sub>4</sub>]) system. The authors proposed that the enhanced selectivity of [BMIM][MeSO<sub>4</sub>] for CO<sub>2</sub> over SO<sub>2</sub> was significantly higher than 1-hexyl-3-methylimidazoliumbis(trifluoromethylsulphonyl)imide ([HMIM][Tf<sub>2</sub>N]). Through this work, the investigators made a quantitative demonstration for the selectivity and *simultaneous capture* of CO<sub>2</sub>/SO<sub>2</sub> mixture.

Mondal and Balasubramanian (2016) examined the anion dependence of SO<sub>2</sub> capture in eight ionic liquids, 1-butyl-3-methylimidazolium ([BMIM]<sup>+</sup>) as the cation, and chloride ([Cl]<sup>-</sup>), nitrate ([NO<sub>3</sub>]<sup>-</sup>), tetrafluoroborate ([BF<sub>4</sub>]<sup>-</sup>), hexafluorophosphate ([PF<sub>6</sub>]<sup>-</sup>), triflate ([CF<sub>3</sub>SO<sub>3</sub>]<sup>-</sup>), bis(trifluoromethanesulfonyl)imide ([NTf<sub>2</sub>]<sup>-</sup>), acetate ([OAc]<sup>-</sup>), and thiocyanate ([SCN]<sup>-</sup>) as anion, using g molecular dynamics simulations and quantum chemical calculations. On the basis of the solvation free energy and binding energies of SO<sub>2</sub> in ILs, they found the IL containing the *thiocyanate* anion to be the most suited for SO<sub>2</sub> absorption.

Qu et al. (2013) synthesized two kinds of phosphate ionic liquids and studied the absorption capacity for SO<sub>2</sub>. Absorption capacities of [Bmim][DBP] and [Emim][DEP] were found to be 2.8 and 2.7 g mol SO<sub>2</sub> per g mole ILs, respectively at ambient temperature and normal pressure. After 4 cycles of absorption and desorption, absorption capacity of the ILs were found to remain unchanged. According to the structure of two phosphate based ionic liquids before and after SO<sub>2</sub> absorption,



confirmed by FT-IR spectrum and  $^1\text{H}$  NMR analyses, absorption of  $\text{SO}_2$  occurred by purely physical absorption. It was concluded that the anion containing the phosphate-based group might had a great  $\text{SO}_2$  philicity, with the free electrons on the oxygen which interact with Lewis acidic sulfur of  $\text{SO}_2$ . As a result, the absorption capacity of  $\text{SO}_2$  in the ionic liquids was improved.

Huang et al. (2013), synthesized less viscous IL: hydroxylammoniumdicarboxylate ionic liquids (ILs), imethyl ethanolammoniumdimalate ([DMEA][dimalate]), dimethylethanol ammoniumdimalonate ([DMEA][dimalonate]) and dimethylethanolammoniumdiglutarate ([DMEA][diglutarate]). They mixed these with free DMEA and water to form novel hybrid solvents for  $\text{SO}_2$  absorption. The mixed absorbents exhibited a low viscosity in the range of 6–13 mPa s at 313.2 K. A certain amount of  $\text{SO}_2$  was introduced into the Equilibrium Cell (with an initial  $\text{SO}_2$  partial pressure of about 1.2 bar), and the pressure change in the equilibrium chamber was recorded online until it became constant. The equilibrium solubilities of  $\text{SO}_2$  at corresponding  $\text{SO}_2$  partial pressures are 0.255 at 0.002 bar for [DMEA][glutarate] (1.2:1), 0.254 at 0.004 bar for [DMEA][malonate] (1.2:1) and 0.264 at 0.002 bar for [DMEA][malate] (1.6:1), respectively.

Huang et al. (2013) determined the solubility of  $\text{SO}_2$  in [N2224][dimalonate], [N2224][disuccinate], and [N2224][dimalate]. These could absorb 0.2, 0.04 and 0.12 gram of  $\text{SO}_2$  per gram of IL at pressures as low as 5kPa, respectively. The IL film was coated on the QCM crystal of 5.0 MHz. During the experiments, the QCM frequency was recorded when  $\text{SO}_2$  was injected into the measuring cell of the QCM apparatus and kept at a pressure of 40 kPa. After the frequency was reduced to a steady state, the absorption equilibrium was thought to be realized.

Bicak (2005) prepared 2-hydroxyethylammonium formate ionic liquid by mixing equimolar mixture of formic acid and 2-hydroxyethylamine and determined its physical properties such as viscosity, ionic conductivity, heat stability and solvation abilities. Its melting temperature was  $-82\text{ }^\circ\text{C}$ . It was *thermally stable* up to  $150\text{ }^\circ\text{C}$ .

Yuan et al. (2007) synthesized nine different types of hydroxyl ammonium ionic liquids. These authors observed that the solubility of  $\text{SO}_2$  in these ILs were quite high at ambient pressure. The solubility of  $\text{SO}_2$  in tris-(2-hydroxyethyl) ammonium lactate was 0.4957 g mol fraction, but the solubility of  $\text{SO}_2$  sharply decreased as the

temperature was increased. They found the absorption and desorption of SO<sub>2</sub> in these ILs were practically reversible.

Ren et al. (2011) used a task-specific IL, monoethanolaminium lactate ([MEA]L), to study the absorption of SO<sub>2</sub> and its oxidation by O<sub>2</sub> present in simulated flue gases (1.65 vol% SO<sub>2</sub> and 11.5 vol.% O<sub>2</sub>) with and without ash and activated carbon in [MEA]L. It was found that the presence of O<sub>2</sub> in the simulated flue gas did not influence the absorption of SO<sub>2</sub> by [MEA]L, but it causes, to a very small extent, the oxidation of SO<sub>2</sub>. The authors also observed the effect of sulfuric acid in [MEA]L on the absorption of SO<sub>2</sub> and the regeneration of the exhausted [MEA]L. The main reason was the possible oxidation of SO<sub>2</sub> and its conversion to sulfuric acid when water vapor remained in the flue gas. It was observed that the presence of sulfuric acid could reduce the absorption of SO<sub>2</sub> in [MEA]L greatly and effect the reuse of the IL. However, when NaOH, CaO, or CaCO<sub>3</sub> was added into the mixture of [MEA]L & H<sub>2</sub>SO<sub>4</sub>, sulfuric acid was altered into the corresponding salts, precipitated & separated by filtration, and then [MEA]L could be regenerated (Ren et al., 2012).

Li et al. (2015) studied the effect of the presence of low concentration SO<sub>2</sub> on the capture of CO<sub>2</sub> from flue gases using 1-ethyl-3-methylimidazolium acetate [C<sub>2</sub>mim][OAc] ionic liquid. Experiments were performed with a flue gas composition of 15% by volume of CO<sub>2</sub> with 0.2% SO<sub>2</sub>. It was found that the absorption capacity of CO<sub>2</sub> in the absence of SO<sub>2</sub> was 0.221 g mol CO<sub>2</sub>/g mol IL. But, in the presence of 0.2% SO<sub>2</sub>, CO<sub>2</sub> absorption capacity decreased to 0.167 g mol CO<sub>2</sub>/g mol IL, which is about 25% of the initial absorption capacity. The investigators explained the microscopic mechanism of the absorption of the two gases through quantum chemical calculation. In comparison to a CO<sub>2</sub> g molecule, a SO<sub>2</sub> g molecule possess high g molecular polarity and dipole moment that result in strong affinity with the sorbent.

Mohammadi and Foroutan (2014) studied the effects of anion types (PF<sub>6</sub><sup>-</sup>, BF<sub>4</sub><sup>-</sup>, NO<sub>3</sub><sup>-</sup>, Cl<sup>-</sup> and Br<sup>-</sup>) on SO<sub>2</sub> gas absorption by five ionic liquids (ILs) containing the 1-ethyl-3-methyl imidazole cation using g molecular dynamic simulations. These ILs belong to two different groups: liquid crystals and plastic crystals. It was reported that the diffusion coefficient of the cation in the SO<sub>2</sub> absorbed IL and in pure IL was higher than that of the anions and much lesser than SO<sub>2</sub> g molecules. They also observed that the presence of SO<sub>2</sub> in the ILs caused an increase in the conductivity, diffusion

coefficients, heat capacity and density of the ionic species in comparison to those in the pure ILs.

Prasad and Senapati (2009) presented a g molecular level detail of the interactions of ILs with SO<sub>2</sub>, CO<sub>2</sub>, and N<sub>2</sub> and demonstrated its consequences to the differential gas solubility. Their predicted results showed that the IL anion-gas interactions act as the key role in deciding the gas solubility in ILs, especially for polar gases like SO<sub>2</sub> while the cation plays only a secondary role. The authors also showed that regular solution assumption applied to N<sub>2</sub> solubility and that the original fluid structures of the ILs remain unaltered by the absorption of gas g molecules.

Tian et al. (2014) synthesized two kinds of hydrophobic task-specific ILs, 1-(2-diethyl-aminoethyl)-3-methylimidazolium hexafluorophosphate ([Et<sub>2</sub>NEmim][PF<sub>6</sub>]) and 1-(2-diethyl-aminoethyl)-1-methylpyrrolidinium hexafluorophosphate ([Et<sub>2</sub>NEmpyr][PF<sub>6</sub>]). Compared with [Et<sub>2</sub>NEmpyr][PF<sub>6</sub>], the absorption of SO<sub>2</sub> by [Et<sub>2</sub>NEmim][PF<sub>6</sub>] could reach the absorption equilibrium rapidly. The investigators observed that [Et<sub>2</sub>NEmim][PF<sub>6</sub>] had high SO<sub>2</sub> absorption capacity, up to 2.11 g mol SO<sub>2</sub> per g mole IL (for pure SO<sub>2</sub> gas) and 0.94 g mol SO<sub>2</sub> per g mole IL (for 3% SO<sub>2</sub> gas) in the presence of moisture at 30 °C. [Et<sub>2</sub>NEmim][PF<sub>6</sub>] was found to possess much lower viscosity, substantially higher thermal stability and SO<sub>2</sub> absorption rate than [Et<sub>2</sub>NEmpyr][PF<sub>6</sub>]. The recycling of [Et<sub>2</sub>NEmim][PF<sub>6</sub>] with or without water were tested for five cycles & no obvious losses of absorption capacities were determined.

Wang et al. (2011) proposed a novel method for the synthesis of the multiple-site capture of SO<sub>2</sub> by the use of azole-based ILs by neutralizing various azoles with phosphonium hydroxide. The influence of pressure on the SO<sub>2</sub> absorption by two kinds of typical azole-based ILs [P66614][Tetz] and [P66614][Im] was also studied. It was shown that the g molar ratios of SO<sub>2</sub> to IL for [P66614][Tetz] and [P66614][Im] decreased from 3.72 to 1.54 and 4.80 to 2.07, respectively, as the pressure reduced from 1.0 to 0.1 bar.

Zeng et al. (2014) synthesized a series of thermally stable pyridinium-based ILs, viz., N-butylpyridinium tetrafluoroborate ([C<sub>4</sub>Py][BF<sub>4</sub>]), N-octylpyridinium tetrafluoroborate ([C<sub>8</sub>Py][BF<sub>4</sub>]), N-hexylpyridinium tetrafluoroborate ([C<sub>6</sub>Py][BF<sub>4</sub>]), 1-butyl-3-methylpyridinium tetrafluoroborate ([C<sub>4</sub><sup>3</sup>MPy][BF<sub>4</sub>]), 1-octyl-3-

methylpyridinium tetrafluoroborate ( $[C_8^3MPy][BF_4]$ ), 1-hexyl-3-methylpyridinium tetrafluoroborate ( $[C_6^3MPy][BF_4]$ ), Nbutylpyridiniumthiocyanate ( $[C_4Py][SCN]$ ) & N-butylpyridiniumbis (trifluoromethylsulfonyl)imide ( $[C_4Py][Tf_2N]$ ). It was found that among the investigated ILs  $[C_2Py][SCN]$  had the highest absorption capacity of 0.841 g SO<sub>2</sub> per g of IL at 1 atm and 25 °C and claimed that this was much higher than those reported for most of the imidazolium-based ILs. Furthermore, the higher selectivity for SO<sub>2</sub>/CO<sub>2</sub>, SO<sub>2</sub>/N<sub>2</sub> and SO<sub>2</sub>/O<sub>2</sub> of the  $[C_4Py][SCN]$  indicated that  $[C_4Py][SCN]$  had excellent selectivity for SO<sub>2</sub> absorption compared to other imidazolium-based ILs. Especially SO<sub>2</sub>/CO<sub>2</sub> selectivity of  $[C_4Py][SCN]$  was found to be two times higher than that of  $[C_4Py][BF]$ . Meanwhile, the presence of water in the ILs had a slightly negative effect on the SO<sub>2</sub> absorption capacity, but the absorption capacity of  $[C_4Py][SCN]$  hardly altered with & without water. The spectroscopic investigations depicted that the SO<sub>2</sub> was *physically absorbed* by the pyridinium-based ILs.

Cui et al. (2015) synthesized acyl amino-based ILs and used for the absorption of SO<sub>2</sub> at 0.1 to 1 bar partial pressure. The absorption capacity achieved was 4.5 g mol SO<sub>2</sub> per g mol IL at 1 bar but at 0.1 bar it reduced to 1.7 g mol SO<sub>2</sub> per g mol IL. The effect of water in the ILs on the absorption of SO<sub>2</sub> was investigated at ambient pressure and 20 °C. SO<sub>2</sub> was bubbled through water to obtain SO<sub>2</sub> gas with 100 percent humidity, which was then bubbled through IL. The SO<sub>2</sub> absorption capacity of [P66614]-[Phth] was 4.32 g mol SO<sub>2</sub> per g mole IL at 20 °C, and 1 bar for SO<sub>2</sub> gas containing 100% humidity and this value was very close to 4.40 g mol SO<sub>2</sub> per g mole IL for dry SO<sub>2</sub> gas. Spectroscopic investigations and quantum chemical calculations showed that dramatic enhancement in SO<sub>2</sub> absorption capacity was originated from the strong N...S interaction and enhanced C=O...S interactions between acyl amino-based anion and SO<sub>2</sub>.

## **2.5 Reactor and reaction modeling for SO<sub>2</sub> absorption accompanied by chemical reaction**

### **2.5.1 Gas-liquid systems**

Hikita et al. (1977) measured rates of absorption of SO<sub>2</sub> in aqueous solutions of NaOH and Na<sub>2</sub>SO<sub>3</sub> solutions, without and with a surface active agent in a liquid jet Column. Rates of absorption were found to be more in the solution containing no surface active

agent for which the investigators developed a model based on penetration theory. It was shown that in  $\text{Na}_2\text{SO}_3$  solution, reaction occurs at one reaction plane while that in the  $\text{NaOH}$  solution it occurs at two different reaction planes. The average rate of absorption  $N_A$  of the solute gas  $A$  for this case could be calculated using the expression,  $N_A = \beta(2A_i\sqrt{D_A/\pi t})$  where  $\beta = 1/\text{erf}(\sigma)$ . The parameter  $\sigma$  was a dimensionless quantity defined by the equation:

$$2\text{erfc}\left(\frac{\sigma_2}{\sqrt{r_B}}\right)\exp\left[\left(\frac{1}{r_C}-1\right)\sigma_1^2+\left(\frac{1}{r_B}-\frac{1}{r_C}\right)\sigma_2^2\right]=\sqrt{r_B}q_B\text{erf}\sigma_1\text{-----(I)}$$

$$\text{erfc}\left(\frac{\sigma_2}{\sqrt{r_{E3}}}\right)\exp\left[\left(\frac{1}{r_{E2}}-1\right)\sigma_1^2+\left(\frac{1}{r_{E3}}-\frac{1}{r_{E2}}\right)\sigma_2^2\right]-2\text{erfc}\left(\frac{\sigma_2}{\sqrt{r_{E2}}}\right)\exp\left[\left(\frac{1}{r_C}-1\right)\sigma_1^2+\left(\frac{1}{r_{E3}}-\frac{1}{r_C}\right)\sigma_2^2\right]$$

$$+\sqrt{\frac{r_{E3}}{r_{E2}}}\text{erf}\left(\frac{\sigma_2}{\sqrt{r_{E2}}}\right)-\text{erfc}\left(\frac{\sigma_1}{\sqrt{r_{E2}}}\right)\exp\left[\left(\frac{1}{r_{E2}}-1\right)\sigma_1^2\right]=\sqrt{r_{E3}}q_E\text{erf}(\sigma_1)\text{-----(II)}$$
(2.1)

Hikita and Konishi (1983) showed that absorption of  $\text{SO}_2$  in aqueous  $\text{Na}_2\text{CO}_3$  solution occurs by a combination of irreversible instantaneous and reversible instantaneous steps with simultaneous desorption of  $\text{CO}_2$ . The experimental results were analyzed using the chemical absorption theory based on the Leveque model.

Sada et al. (1979) carried out the absorption of lean  $\text{SO}_2$  in aqueous solutions of  $\text{Na}_2\text{CO}_3$  using a stirred vessel with a gas-liquid interface. The process of  $\text{SO}_2$  absorption and  $\text{CO}_2$  desorption was analyzed in terms of a two-reaction plane model which states that the reactant  $\text{CO}_3^{2-}$  cannot co-exist with the reaction product  $\text{HSO}_3^-$ . Rate of absorption was expressed by the equation,

$$N_{A_1} = \phi_{A_1} k_{LA_1} C_{A_1 i} \quad (2.2)$$

$$\text{Where, } \phi_{A_1} = \frac{z_L}{z_1} = 1 + \frac{D_{B,III} C_{B0}}{D_{A_1} C_{A_1 i}} \quad (2.3)$$

The rate of  $\text{CO}_2$  desorption was expressed as

$$N_{A_2} = \frac{D_{A_2}}{z_L} \left[ \frac{D_B}{D_{A_2}} C_{B0} - \left( \phi_{A_1} + 1 - \frac{1}{\phi_{A_1}} \right) C_{A_2 i} \right] \quad (2.4)$$

Hikita et al. (1983) used the Leveque model to describe the diffusion of all the species in the liquid phase. This model is non-linear and cannot be solved analytically. The

approximate analytical solution can be obtained by replacing the diffusivity ratios in the exact analytical solution based on the film model by the two-third roots of these ratios.

Chang and Rochelle (1981) reported that many of the previous work used pure SO<sub>2</sub> as the gas phase in which the SO<sub>2</sub> hydrolysis reaction was highly depressed and could only enhance the physical absorption rate about 10%. SO<sub>2</sub> concentration in the stack gas being in the range of 1000-4000 ppm, *effect of hydrolysis reaction is very important*. Sulfur dioxide and bisulfite diffusivities being different, models not taking into account the hydrolysis reaction incur some error. The authors showed that a very good approximation to the results of the penetration theory could be obtained by making use of the film theory and replacing the diffusivity ratios by their square roots. The SO<sub>2</sub> absorption rate may be calculated using the expression

$$N_{SO_2} = \phi k_l^0 a ([SO_2]_i - [SO_2]_0) \quad (2.5)$$

where,  $\phi$  is the enhancement factor, calculated using the expression:

$$\phi = 1 + \left( \frac{D_{HSO_3^-}}{D_{HSO_2}} \right)^{1/2} \left( \frac{[HSO_3^-]_i - [HSO_3^-]_0}{[SO_2]_i - [SO_2]_0} \right) + \left( \frac{D_{SO_3^{2-}}}{D_{SO_2}} \right)^{1/2} \left( \frac{[SO_3^{2-}]_i - [SO_3^{2-}]_0}{[SO_2]_i - [SO_2]_0} \right) \quad (2.6)$$

Chang and Rochelle, (1985) showed that for the conditions of interest for FGD applications (i.e. *low SO<sub>2</sub> partial pressure*), the *reversibility* of the SO<sub>2</sub> hydration reaction has to be taken into account.

### 2.5.2 Gas-liquid-solid systems

Ramachandran and Sharma (1969) presented an analysis using the film theory of mass transfer for absorption of gas into slurry containing fine suspended particles. The following simple reaction scheme was used to model the dissolution and reaction steps.



It was shown that two types of problems might be encountered:

Case 1. *Solid dissolution in the liquid film next to the gas-liquid interface is unimportant:*

This corresponds to the case when the concentration of the solids in the slurry is relatively small or when the reactant particle-size is large as compared to the thickness of the liquid film. Under these circumstances, the extent of solid dissolution while the species  $B$  diffuses in the film can be considered negligible. Solid dissolution and chemical reaction are assumed to occur in series. These assumptions are assumed to be valid when:

$$\frac{k_s A_p D_A^2}{4k_L^2 D_B} \ll 1 \quad (2.8)$$

The reaction scheme for this case involves the following steps (Ramachandran and Sharma, 1969):

- I. Diffusion of the gaseous species  $A$  through the gas film.
- II. Dissolution of the solid species  $B$ .
- III. Diffusion and the simultaneous chemical reaction of the absorbed gas with the dissolved  $B$  in the liquid film near the gas-liquid interface.

The rates of the various steps are the same under steady-state conditions.

The rates of steps (1) and (2) are given by:

$$\begin{aligned} R' &= k_G a [P_{Ab} - P_{Ai}] \\ &= k_s A_p [C_{BS} - C_{Bi}] \end{aligned} \quad (2.9)$$

where  $R'$  = rate of absorption of  $A$ , g g moles of gas absorbed/s cm<sup>3</sup> dispersion.

Eliminating  $P_{Ai}$  &  $C_{Bi}$ , from the equation 2.9, final rate of absorption is as follows:

$$R' = \frac{HP_{AB} + \frac{D_B}{D_A} C_{BS}}{\frac{H}{k_G} + \frac{1}{k_L a} + \frac{D_B}{D_A} \frac{1}{k_s A_p}} \quad (2.10)$$

Case 2. *The solid dissolution in the liquid film is important.*

When the average diameter of the particles is considerably less than the thickness of the liquid film,  $\left(d_p \leq \frac{1}{10} \delta\right)$ , solid dissolution in the film becomes important for usual values of  $k_{st}$ , and, solid dissolution and chemical reaction steps become parallel. This

phenomenon increases the local concentration of the reactive species  $B$  in the film and thereby enhances the rate of gas absorption.

### 2.5.3 Enhancement factor for solid dissolution

Uchida et al. (1975) modified the model of Ramachandran and Sharma (1969) with the assumption that the rate of dissolution of the solid is enhanced by the reaction between the absorbed gas and the suspended particles in the liquid. The enhancement factor for the rate of solid dissolution based on the film model is presented below. A material balances for species  $A$  yields:

$$D_A \frac{d^2 C_A}{dx^2} - \frac{k_{sl}}{R_{BA}} \left( 1 + \frac{R_{BA} C_A^* D_A}{C_{B0} D_B} \right) A_p C_{BS} = 0 \quad \text{at } 0 \leq x \leq \lambda \quad (2.11)$$

Due to the presence of the absorbed gas  $A$  in the region  $0 \leq x \leq \lambda$ , the rate of solid dissolution is enhanced by the value of  $\left( 1 + \frac{z C_A^* D_A}{C_{BS} D_B} \right)$ .

Under these circumstances, the rate of absorption of gas  $A$  was reported to be

$$\bar{R} = m D_A C_A^* \coth m\lambda + \frac{m D_B C_{BS}}{z} \left( \coth m\lambda - \frac{1}{\sinh m\lambda} \right) \quad (2.12)$$

where  $m = \sqrt{k_s A_p / D_B}$ .

$\lambda$  was calculated by use of the equation:

$$\frac{D_B C_{BS}}{z} \left( \coth m\lambda + \coth m(\delta - \lambda) - \frac{1}{\sinh m\lambda} \right) - \frac{D_A C_A^*}{\sinh m\lambda} = 0 \quad (2.13)$$

Uchida et al. (1981) modified their (Uchida et al., 1975) previously published model by assuming the *penetration theory* in place of film theory for the absorption of gas  $A$  in a slurry containing particles of  $B$  with instantaneous chemical reaction. The pertinent differential equations and the relevant initial and boundary conditions were obtained by writing mass balances over a small volume element in the liquid phase:

$$\frac{\partial C_A}{\partial t} = D_A \frac{\partial^2 C_A}{\partial x^2} - \frac{1}{z} k_s A_p \left( \sqrt{\frac{D_B}{D_A}} + z \sqrt{\frac{D_A}{D_B}} \frac{C_A}{C_B} \right) C_{BS} \quad (2.14)$$



,where the enhancement factor for solid dissolution,  $\beta_d$ , was assumed to be given by

$$\beta_d = \sqrt{\frac{D_B}{D_A}} + z \sqrt{\frac{D_A}{D_B}} \frac{C_A}{C_{BS}} \quad (2.15)$$

The differential equations were written for a moving boundary problem; and after its solution and further simplification, the quantity of gas absorbed into slurry through unit area in contact time  $t$  for an instantaneous irreversible reaction, and its enhancement factor were obtained as follows:

$$R_A = 2(1 + q_B) \sqrt{\frac{D_A}{\pi}} \left\{ \left( \frac{\pi k_s A_p t}{2} + \frac{1}{4} \sqrt{\frac{\pi}{k_s A_p t}} \right) \operatorname{erf} \sqrt{k_s A_p t} + \frac{1}{2} \exp(k_s A_p t) \right\} C_A^* \quad (2.16)$$

$$\beta = (1 + q_B) \left\{ \left( \sqrt{\frac{k_s A_p t}{2}} + \frac{1}{4} \sqrt{\frac{\pi}{k_s A_p t}} \right) \operatorname{erf} \sqrt{k_s A_p t} + \frac{1}{2} \exp(k_s A_p t) \right\} \quad (2.17)$$

#### 2.5.4 Reactor modeling without the use of solid-liquid mass-transfer coefficient

Yagi and Hikita (1987) critically analyzed the work of Sada et al. (1977) as well as that of Uchida et al. (1975). Their study provides a different view for dealing with *gas absorption with instantaneous chemical reaction; instead of using a mass transfer coefficient for solid dissolution*, they used the diffusion coefficient of the gaseous solute, in two dimensions, and stated that this diffusion rate depended upon the interparticle distance and hence on the size and concentration of the particles. However, the enhancement factor for the case of instantaneous reaction

$$\beta = 1 + \frac{D_A}{D_B} \frac{\left\{ B_s \left( 1 - \frac{W}{\rho} \right) + \frac{W}{M_w} \right\}}{\nu A_i} \quad (2.18)$$

was found to be infinite. Consequently, the authors suggested that their results are only qualitative, as they did not assume shrinkage of particles. The authors provided an expression for the upper bound value of the enhancement in the specific rate, by assuming that all the particles are present in “completely dissolved form” so that the extra reactant contained in the solid phase can be treated as being immediately available to the liquid phase.

Pasiuk-Bronikowska and Rudzinski (1991) developed a model for SO<sub>2</sub> absorption into aqueous slurry neglecting the solid dissolution into the gas-liquid mass transfer

boundary layer, and got satisfactory results. In their model, they considered the presence of reacting solids  $\text{Ca}(\text{OH})_2$  and  $\text{CaSO}_3$  & applied the film theory to predict the absorption rate of  $\text{SO}_2$  and the enhancement factor value. The model equations take into account the material & charge balances for diffusing ionic species, without considering the effect of the electric potential gradient on the ions diffusion. The electroneutrality in the liquid phase was described as:

$$0 = [H^+] - [OH^-] - [HSO_3^-] - 2[SO_3^{2-}] - [an^-] + [Ca^{2+}] + [CaOH^+] + [cat^+] \quad (2.19)$$

The g molar balances of diffusing and reacting species within the liquid film were written, according to the law of conservation of atoms, for S(IV), calcium and the inert ions:

$$\begin{aligned} \frac{d}{dx} \left( D_{HS} \frac{d[SO_{2aq}^0]}{dx} + D_{BS} \frac{d[HSO_3^-]}{dx} + D_S \frac{d[SO_3^{2-}]}{dx} \right) &= 0 \text{-----}(I) \\ \frac{d}{dx} \left( D_{CA} \frac{d[Ca^{2+}]}{dx} + D_{CaOH} \frac{d[CaOH^+]}{dx} \right) &= 0 \text{-----}(II) \\ \frac{d^2}{dx^2} [Cat^+] &= 0 \text{-----}(III) \\ \frac{d^2}{dx^2} [an^-] &= 0 \text{-----}(IV) \end{aligned} \quad (2.20)$$

This approach was critically explained by Rochelle (1992), who pointed out that neglecting the effect of the electric potential gradient generates a non-zero flux of charge into the liquid film. To avoid this discrepancy, Rochelle observed that it was more correct to make the explicit assumption that the charge flux is zero, by excluding any relationship forcing charge balance at the interface. According to Rochelle's approach, ion diffusion is not affected by the gradient of the electric potential, yet the error introduced in the calculation of the mass transfer fluxes & the enhancement factor is negligible (Glasscock and Rochelle, 1989).

### 2.5.5 Rate based models

Lancia et al. (1994) focused their work on the influence of the electric potential on ionic diffusion in the mass transfer boundary layer. They examined absorption of  $\text{SO}_2$  in  $\text{CaCO}_3$ -containing systems by means of the film theory and explained the concentration profiles of the different species in the liquid film. The *total material balances* approach reported by Olander (1960) was followed. Species conservation

equations for calcium, carbonate and sulphite ions reported by the investigators were as follows:

$$\begin{aligned} \frac{dN_{Ca^{2+}}}{dx} &= 0 \text{-----(I)} \\ \frac{dN_{H_2CO_3}}{dx} + \frac{dN_{HCO_3^-}}{dx} + \frac{dN_{H_2CO_3^{2-}}}{dx} &= 0 \text{-----(II)} \\ \frac{dN_{SO_2}}{dx} + \frac{dN_{HSO_3^-}}{dx} + \frac{dN_{SO_3^{2-}}}{dx} &= 0 \text{-----(III)} \end{aligned} \tag{2.21}$$

The gas phase material balance for SO<sub>2</sub> in the bubble column was shown to be:

$$\int_{P_{SO_2in}}^{P_{SO_2out}} \frac{1}{N_s} dp_{SO_2} = -\frac{RTaV}{G} \tag{2.22}$$

where,  $N_s$  is the total flux of sulfites, g mol/m<sup>2</sup> s and  $G$  is gas flow rate, m<sup>3</sup>/s

Lancia et al. (1997) developed a model for SO<sub>2</sub> absorption from a mixture of SO<sub>2</sub> and N<sub>2</sub> using a bubbling reactor and aqueous suspensions of limestone. Their model was based on the film theory and was proposed to describe liquid-side mass transfer and to evaluate the enhancement factor. It was assumed that the liquid-side resistance to diffusion was concentrated within a film and the thickness of which depended on the fluid dynamics conditions.

Brogren and Karlsson (1997) developed a model based on the *penetration theory* to calculate the dynamic absorption rate of sulfur dioxide into a droplet of limestone slurry. The model deliberated that both the instantaneous equilibrium reactions of the slurry and the reactions with finite rates. It was based on the assumption that neither precipitation nor dissolution of calcium sulphite or sulfate took place in the liquid film around the limestone particle. Additionally, oxidation of sulfite to sulfate in the film was overlooked. It was shown (Rochelle 1992; Brogren and Karlsson, 1997) that as long as the mass flux equations are combined with an expression for flux of charge, the impact of any electric potential gradient on the flux of ions might be disregarded under FGD conditions. The flux  $J$  can, therefore, be expressed as follows:  $J_k = -D_k \nabla C_k$  where the diffusion constant  $D_k$  is constant. To avoid using rate constants fixed at randomly high values of the equilibrium reactions, mass balances for individual concentrations were combined to balance for total sulfite, total carbonate, total calcium, total magnesium and total sulfate as follows:

$$0 = \sum_{k=1}^n -D_k \nabla^2 C_k - \frac{2}{b} D_k C_k \quad (2.22)$$

Species involved in the combined balances were for total sulfite:  $SO_2$ ,  $HSO_3^-$ ,  $SO_3^{2-}$ ,  $CaSO_3^0$  and  $MgSO_3^0$ ; total carbonate:  $HCO_3^-$ ,  $CO_3^{2-}$ ,  $CaHCO_3^+$ ,  $MgHCO_3^+$ ,  $CaCO_3^0$ ; total calcium:  $Ca^{2+}$ ,  $CaSO_3^0$ ,  $CaHCO_3^+$ ,  $CaSO_4^0$  total magnesium:  $Mg^{2+}$ ,  $MgSO_3^0$ ,  $MgHCO_3^+$ ,  $MgSO_4^0$  and total sulfate:  $SO_4^{2-}$ ,  $CaSO_4^0$ ,  $MgSO_4^0$ . Similarly, a balance for the net charge was needed:

$$0 = \sum_{k=1}^n -z_k D_k \nabla^2 C_k - \frac{2}{b} z_k D_k C_k \quad (2.23)$$

where, the species involved were:  $H^+$ ,  $OH^-$ ,  $Ca^{2+}$ ,  $Mg^{2+}$ ,  $SO_4^{2-}$ ,  $HSO_3^-$ ,  $SO_3^{2-}$ ,  $HCO_3^-$ ,  $CO_3^{2-}$ ,  $CaHCO_3^+$ ,  $MgHCO_3^+$  and  $Cl^-$ .

Scala and D'Ascenzo (2002) discussed the case of gas absorption followed by an instantaneous irreversible chemical reaction into a rigid droplet containing sparingly soluble, fine reactant particles, assuming slow reactant particle dissolution which means that particle shrinkage is negligible. Conditions are also given for the applicability of the model. More recently, Scala (2002) developed a model for an infinitely deep quiescent liquid and for an agitated liquid using the film theory. The theoretical treatment was based on the following simplifying assumptions: both gaseous & solid reactants have a low solubility in the liquid, the reaction between the two species was irreversible & instantaneous, the influence of the product species on the process is negligible, solid particle dissolution was low, so that particles shrinkage could be neglected, solid particles are spherical, uniform in size & uniformly dispersed in the liquid phase & do not agglomerate, solid particles are fine, viz., their size are smaller than the typical reactant diffusional length scale, there was no existence of surface kinetic resistance to particle dissolution, which was fully controlled by mass transfer, solid particles were non-diffusing & the liquid around the particles could be considered stagnant as proposed by Mehra (1996), the heats of reaction and dissolution can be neglected, interfacial effects are negligible. Two cases were analyzed, namely, an infinitely deep quiescent liquid and an agitated liquid. The gas-liquid interface was planar, and the concentrations of diffusants were uniform

over any plane parallel to the interface. Reactants diffuse only in the direction perpendicular to the interface.

## **2.6 Important design aspects of Bubble column- and foam-bed reactors**

In the present investigation, experiments were performed in a bubble column reactor. Both gas-liquid and gas-liquid-solid systems were studied in this contactor. Hence, a brief review of the important features of a bubble column is presented below.

A bubble column reactor is basically a cylindrical vessel with a gas distributor at the bottom. For gas-liquid and gas-liquid-solid systems, it can be operated either in semi-batch or in continuous mode. The inlet and exit ports are situated depending on the mode of operation. The gas is sparged in the form of bubbles into either a liquid phase or a liquid–solid suspension. These reactors are generally referred to as slurry bubble column reactors when a solid phase exists. In general, bubble columns are usually applied in industrial practice as absorbers and reactors because of their low cost, ease of maintenance, simplicity of operation & the ease with which the liquid residence time can be varied (Doraiswamy and Sharma, 1984; Sharma and Mashelkar, 1968; Adewuyi et al., 1999; Öztürk et al., 1987; Reilly et al., 1986).

The lack of moving parts, smaller floor space, large interfacial area & high heat and mass transfer coefficients are few of the advantages that bubble columns provide (Li and Prakash, 1997; Öztürk et al., 1987; Saxena et al., 1990). Although, bubble columns suffer from considerable liquid back-mixing, some back mixing in the gas phase, and bubble coalescence. Back mixing can affect the distribution of residence time in the reactor & therefore affect the reaction selectivity & yield. To overcome two shortcomings, bubble columns are a lot packed with a variety of packings (Gopal and Sharma, 1982; Sharma and Mashelkar, 1968; Wang and Fan, 1978). By filling a bubble column with packings, the interfacial area increases due to a continual break up of bubbles and the liquid back mixing also reduces. Other disadvantages of bubble columns include a rapid reduction of effective interfacial area at high height-to-diameter ratios (say,  $> 15$ ) and relatively high-pressure drop of the gas because of the high static head of the liquid (Doraiswamy and Sharma, 1984).

The literature on bubble column primarily emphasizes on design and scale-up, fluid dynamics and regime analysis, and, estimation of parameter values, viz., gas holdup,

bubble characteristics, mass- and heat transfer coefficients, etc. These aspects are described in brief in the following sections.

## **2.6.1 Hydrodynamics and design parameters of bubble column reactor**

### **2.6.1.1 Design & Scale-up**

Accurate and successful design and scale-up require an improved understanding of multiphase fluid dynamics and its influences on the performance of a bubble column. Industrial bubble columns usually operate with a length-to-diameter ratio, or aspect ratio of at least 5 (Kumar et al., 1976). The effects brought about by the selection of column dimensions have found interest in bubble column reactor design. First, the use of large diameter reactors is desired because large gas throughputs are involved. Additionally, large reactor heights are required to obtain large conversion levels (Krishna et al., 1997). The design and scale-up of bubble column reactors generally depend on the quantification of three main phenomena: (i) heat and mass transfer characteristics; (ii) mixing characteristics; (iii) chemical kinetics of the reacting system. Thus, the reported studies emphasize the requirement of improved understanding of the multiphase fluid dynamics and its influence on phase holdups, mixing and transport properties (Degaleesan et al., 2001). More specifically, in order to design bubble column reactors, the following hydrodynamic parameters are required: specific gas-liquid interfacial area, axial solids dispersion coefficients, sauter mean bubble diameter, axial dispersion coefficients of the gas and liquid, overall heat transfer coefficient between slurry and immersed heat transfer internals, mass transfer coefficients for all the species, gas holdups, physicochemical properties of the liquid medium. The aspects are briefly discussed below:

### **2.6.1.2 Fluid dynamics and regime analysis**

The fluid dynamic characterization of bubble column reactors has a significant effect on the operation and performance of bubble columns. Parameter values strictly depend on the regime prevailing in the column. The flow regimes in bubble columns are classified and maintained based on the superficial gas velocity employed in the column. Three types of flow regimes are commonly observed in bubble columns: the homogeneous or bubbly flow regime; the heterogeneous or churn-turbulent flow regime and slug flow regime (Hyndman et al., 1997). The bubbly flow regime also called the homogeneous flow regime is attained at low superficial gas velocities,

approximately less than 5 cm/s in semi-batch columns (Hills, J. H., 1974). This flow regime is illustrated by bubbles of relatively uniform small sizes & rise velocities (Schumpe and Grund, 1986). There is practically no bubble coalescence or break-up, thus bubble size in this regime is almost completely dictated by the sparger design and system properties (Thorat and Joshi, 2004). Kawagoe et al. (1976) found that the gas holdup in the bubbly flow regime increases linearly with increasing superficial gas velocity.

The churn-turbulent regime, also called the heterogeneous regime is maintained at higher superficial gas velocities (greater than 5 cm/s in batch columns). This flow regime is thus sometimes referred as coalesced bubble flow regime, indicating the much different sizes of the bubbles (Schumpe and Grund, 1986). As a matter of fact, by bubble coalescence and break-up, a wide bubble size distribution is attained. Matsuura and Fan (1984) reported that this regime consisted of a mixture of small and larger bubbles with diameters ranging from a few millimetres to a few centimetres. It has been shown that the gas-liquid mass transfer coefficient is lower at churn-turbulent (heterogeneous) regime as compared to homogeneous flow.

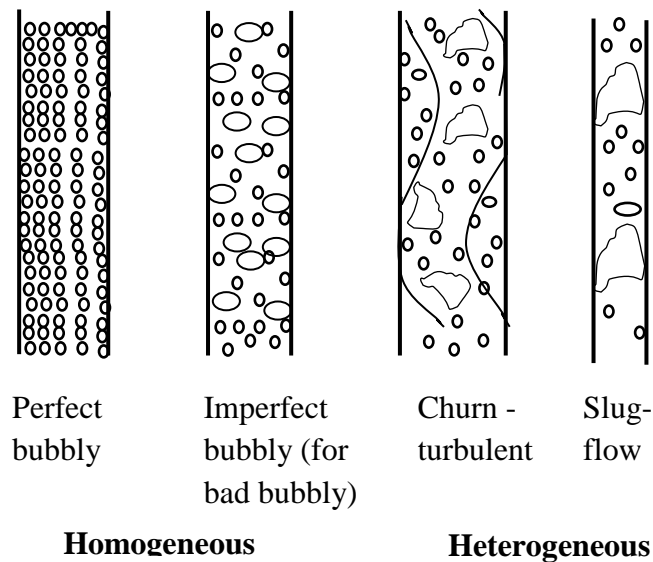


**Figure 2.1: Schematic of possible flow regimes in bubble column**

However, despite this fact, bubble columns are mostly operated under heterogeneous flow conditions in the chemical industry and the interpretations of effective interfacial area measurements, the design parameter estimations and reactor modeling concepts have been based on the assumption of two distinct bubble classes (Schumpe and Grund, 1986). For these models, information on the holdup fractions, contributions to

the overall flow, rise velocity and superficial gas velocity fractions are required for small and large bubbles.

Figure 2.1 best illustrates the differences between the possible regimes discussed. In order to illustrate the flow regimes, unfortunately, it is impossible to provide definite quantitative ranges for superficial velocities. Various studies performed with different systems & operating conditions give different results for finding regime boundaries and regime transitions. For instance, Hyndman et al. (1997) proposed that below 4 cm/s superficial velocity, a bubbly flow regime prevails. Schumpe and Grund (1986) suggested that homogeneous (bubbly) flow prevails for superficial velocities lower than 5 cm/s while Bukur and Daly (1987) observed the churn-turbulent flow regime for gas superficial velocities between 2 and 5 cm/s.

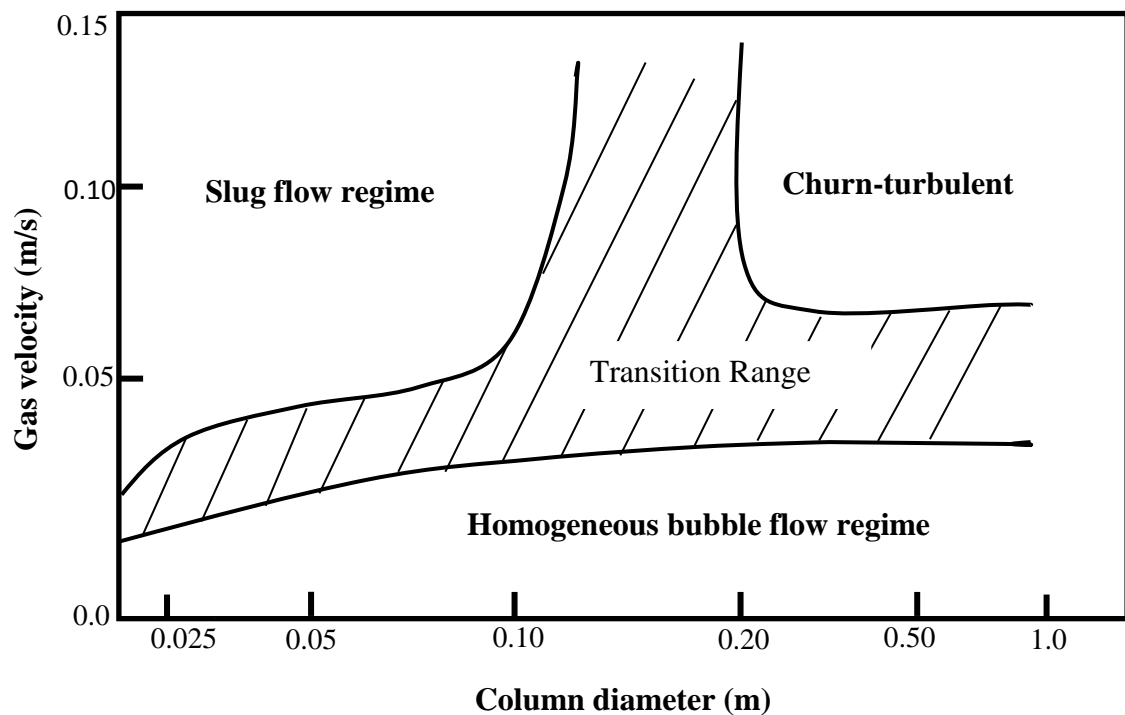


**Figure 2.2: Gas flow regime map in a bubble column contactor**

One such flow regime map presented by Deckwer et al. (1980) has been shown in Figure 2.2. The map explains quantitatively the dependence of flow regimes on column diameter & superficial velocity of the gas and is valid for both bubble and slurry bubble columns with a batch (stationary) liquid phase operated with a low viscosity



**Table 2.1 Flow regimes in a bubble column and parameter estimation.**

S. N.	Flow regime	Range of $u_g$ or $d_c$	Remarks
1.	Homogeneous or, bubbly flow	$u_g < 0.05$ m/s, $d_c$ is not important. gas is uniformly distributed using multi-orifice nozzles. Constant bubble residence time.	Uniform bubble size or having a very narrow distribution, uniform distribution (no radial and axial gradients) of gas holdup. Mass transfer parameters are determined on a single bubble size.
2.	Transition regime	$u_g$ depends on $d_c$ , and physical properties of gas and liquid.	Critical gas hold-up depends on $h_d/d_c$ and $d_0$ .
3.	Heterogeneous or churn turbulent flow	$u_g > 0.05$ m/s, $d_c > 0.15$ m; residence time of bubbles of different size is different in the dispersion. Residence time of bubbles, etc is determined on the assumption of two distinct bubble classes.	Radial gas-holdup profile with maxima at the centre (density of dispersion being less than that at the wall) creates strong circulation and back mixing.  Coalescence and bubble break up generates wide distribution of bubbles size and <i>the mass transfer rate is governed by the latter.</i>
4.	Slug flow	$d_c < 0.15$ m; $u_g > 0.05$ m/s. With increasing gas velocity, large gas bubbles in the form of slugs are formed.	Wall effect is important. Large bubbles are stabilized by the column and mixing is poor. Strongly affects mass transfer parameters.

liquid phase. The shaded regions in the figure indicate the transition regions between various flow regimes. However, the exact boundaries associated with the transition regions would depend on the system studied. Flow regimes in a bubble column are

typically divided into four types and specified in terms of the superficial velocity of gas ( $u_g$ ) and column diameter ( $d_c$ ) as shown in Table 2.1.

### 2.6.1.3 Gas hold-up

The spatial variation of the gas holdup, i.e. gas holdup profile is another important factor which gives rise to pressure variation and thus liquid recirculation. Since liquid recirculation plays an important role in mixing, and, heat and mass transfer, predictions of radial gas holdup profiles would lead to better understanding of these phenomena and thus more reliable bubble column scale-up. The magnitude of gas holdup radial gradients depends on superficial gas velocity, column diameter, physical properties of the system and operating conditions (Wu et al., 2001).

There exist various correlations in literature in order to predict the gas holdup in both two-phase and three-phase slurry bubble columns. In Table 2.2, several frequently used gas holdup correlations for bubble and slurry bubble columns are summarized. In the subsections below, the findings of various studies on the effects of these factors are presented.

### 2.6.1.4 Bubble characteristics

**Table 2.2 Correlation for gas hold-up, bubble rise velocity, bubble size and liquid side mass transfer coefficient in bubble column**

Bubble populations, bubble holdup and rise velocities of bubbles have significant impact on altering the hydrodynamics, as well as heat and mass transfer coefficients

Parameters	Correlation	Reference
Gas hold-up	$\varepsilon_g = \frac{V_g}{0.3 + 2V_g}$	Joshi and Sharma, 1979
	$\varepsilon_g = \frac{1}{2 + (0.35/V_g)/(\rho_1\sigma/72)^{1/3}}$	Hughmark, 1967
	$\varepsilon_g = 1.07F_r^{1/3}$	Kawase and Moo-Young, 1987

	$\frac{\varepsilon_g}{1 + \varepsilon_g} 0.0625 \left( \frac{V_g}{u_1 g} \right)$	Kawase et al., 1992
Bubble rise velocity	$u_{b,small} = \frac{g\rho}{18\mu} d_b^2 Re_e < 1$ Stoke's equation	Moo-Young and Blanch, 1981
	$u_b = \frac{g\rho}{18\mu} d_b^2$ Hadamard-Rybczynski equation	Moo-Young and Blanch, 1981
	$u_{b,sm} = u_{b,sm0} \left[ 1 + \frac{1.073}{u_{b,sm0}} \phi_s \right]$	Li and Prakash, 2000
Bubble size	$d_b = \left[ \frac{6\sigma}{g(\rho_l - \rho_g)} \right]^{1/3}$ for low gas flow rates	Miller, 1974
	$d_b = 0.19 d_o^{0.48} Re_o^{0.32}$ , $Re_o$ is the orifice Reynolds number and $Re_o = \frac{4Q\rho_g}{\pi d_o \mu_g}$	Moo-Young and Blanch, 1981
	$d_b = 0.18 d_o^{0.5} Re_o^{0.333}$ ; $Re < 2000$	Leibson et al., 1956
	$V_b = \left( \frac{4\pi}{3} \right)^{1/3} \left( \frac{15\mu_l Q}{2\rho_l g} \right)^{3/4}$	Kumar and Kuloor, 1970
	$\frac{d_b}{d_o} = 3.23 \left( \frac{4\rho_l Q}{\mu_l \pi d_o} \right)^{-0.1} \left( \frac{Q^2}{d_o^5 g} \right)^{0.21}$	Bhavaraju et al., 1978
Liquid side mass transfer coefficient	$\frac{k_l a V_g}{g} = 14.9 \left( \frac{V_g \mu_l}{\sigma} \right)^{1.76} \left( \frac{\mu_l^4 g}{\rho_l \sigma^3} \right)^{-0.248} \left( \frac{\mu_g}{\mu_l} \right)^{0.243} \left( \frac{\mu_l}{\rho_l D_{AB}} \right)^{-0.604}$	Hikita et al., 1981

in a bubble column. The average bubble size in a bubble column has been determined to be governed by gas velocity, liquid properties, gas distribution, operating pressure

& column diameter. The rise velocity of a single gas bubble depends on its size. In the following subsections, the results of various studies on bubble size, rise velocity and bubble holdups are presented:

### 2.6.1.5 Mass transfer coefficient

The overall mass transfer rate per unit volume of the dispersion in a bubble column is, in general, governed by the liquid-side mass transfer coefficient,  $k_l a$  assuming that the gas side resistance is negligible. Assuming the bubbles are spherical, the specific gas–liquid interfacial area is in relation with the gas holdup,  $\varepsilon_g$ , and the sauter mean bubble diameter,  $d_{bs}$  by

$$a_s = \frac{6\varepsilon_g}{d_{bs}} \quad (2.24)$$

Thus, a detailed knowledge of the gas holdup & bubble size distribution is required to find the specific gas–liquid interfacial area (Daly et al., 1992). It is a well-established fact that the volumetric mass-transfer coefficient,  $k_l a$ , enhances with gas velocity, gas density & pressure while reduces with increasing solid concentration & liquid viscosity. It is also reported that the existence of ions in solution increase  $k_l a$ , due to small bubbles and existence of large bubbles should be evaded in industrial columns for effective mass transfer.

## 2.6.2 Hydrodynamics and design parameters of foam-bed reactor

Foam bed contactors have been employed extensively during the past few decades for studies of its performance for carrying out various separation processes/ reactions. A foam-bed contactor is a device in which a reactive gas/ mixture of gases is brought into contact with a liquid solvent or a solution containing a reactive species (the liquid being self-foaming or containing a surfactant for generation of stable foam) in which mass transfer occurs with or without a chemical reaction.

A foam-bed reactor has the following important features:

- It can be operated in various modes: semi-batch, continuous flow, recycled, co-current, and countercurrent
- A large amount of gas can be contacted with a small amount of liquid

- It can be conveniently used as a slurry reactor and fouling problem is less even with a sticky material because of presence of surfactant in the liquid
- Gas-liquid contact time is sufficiently high
- Gas pressure drop for flow through the reactor is low to moderate
- Gas-liquid interfacial area and gas hold-up are higher than in any other type of contactor
- For certain systems, e.g. precipitation reactions with a pure gas, only a marginal cost is incurred for the surfactant used in generation of a stable foam as the solvent can be completely recycled back into the reactor.

By virtue of these promising features, a foam-bed reactor beckoned many investigators to exploit its potential for various practical gas-liquid/ gas-liquid-solid systems. Under certain conditions, the performance of a foam-bed reactor is far superior to that of the conventional contactors (Helsby and Birt, 1955; Metzner and Brown, 1956).

That reaction rates and conversion of reactants for carbonation of hydrated lime slurry can be increased substantially in a slurry foam reactor, has been reported by Jana and Bhaskarwar (2010). It is also reported that under the experimental conditions, fouling and distributor choking observed in a bubble column slurry reactor could be eliminated by using a foam-slurry reactor.

## **2.7 FGD byproduct utilization**

FGD gypsum can be produced from flue gas desulfurization (FGD) processes that use lime or limestone directly for wet scrubbing of flue gas (Rosenberg, 1986). The major component is calcium sulfate dihydrate ( $\text{CaSO}_4 \cdot 2\text{H}_2\text{O}$ ) and its physical and chemical properties are similar to natural gypsum. After conversion it can get five patterns and seven kinds of morphological variants. FGD gypsum usually contains about 8-12% attached water, particle-size distribution is relatively concentrated, with a diameter between 30-60  $\mu\text{m}$  and the value of pH in aqueous medium is generally around 5-9 (Wang and Deng, 2015). FGD gypsum can be used as setting retarders in cement (Tzouvalas et al., 2004; Chandara et al., 2009), a substitute for natural gypsum in wallboards and concrete blocks manufacturing (Leiva et al., 2010; Yazici, 2007), in land applications (Alva, A.K., 1994) and agriculture (Shainberg et al., 1989)

According to the European Coal Combustion Products Association (ECOBA, 2010), in the year 2009 FGD-gypsum was the second largest byproduct (21%) generated in the EU15 countries. The EU15 comprised the following 15 countries: Austria, Belgium, Denmark, Finland, France, Germany, Greece, Ireland, Italy, Luxembourg, Netherlands, Portugal, Spain, Sweden, United Kingdom). The amount of FGD-gypsum produced in Europe (EU15) was approximately 10 kilo tones in 2010. The FGD gypsum utilization in different areas is shown in Table 2.3.

**Table 2.3. Utilization of FGD gypsum in different area in Europe in the year 2010**

<b>Area of application</b>	<b>Percent utilization</b>
Set retarder for cement	5.98
Projection plaster	6.78
Plaster boards	50.56
Gypsum Blocks	2.50
Self-levelling floor screeds	12.71
Other uses	0.523
Reclamation, Restoration	10.00
Temporary stockpile	6.55
Disposal	4.37

### **2.7.1 Utilization of FGD gypsum are found mainly in the following aspects.**

1. *As setting time retarder of cement:* Chandara et al.(2009), Kallinikos et al.(2010) and Tzouvalas et al. (2004) studied the use of FGD gypsum in cement to adjust its setting time. It was observed to satisfy the national standards of setting time of cement and workability of concrete by use of this cement was found to be good compared with the use of natural gypsum for setting time retarder of cement. But,

for using as a cement retarder, FGD gypsum dosage is generally relatively low about 3~5%.

2. *Preparation of gypsum board*: FGD gypsum is extensively used to produce various kinds of gypsum plasterboards as seen from Table 1 above. Ben Mansour et al.(2013) studied the use of Tunisian gypsum plaster (Meknassi region) which ranks second worldwide, for the production of gypsum plasterboards. They found that the plaster exhibits an interesting behavior on the between thermal conductivity and temperature for buildings walls. Zhang et al. (2016) prepared thermal insulation gypsum plaster using flue gas desulfurization gypsum, thermal conductivity of this material being 0.18 W/mK.
3. *Calcium sulfate hemihydrates*: This can occur in two different forms: alpha- and beta-hemihydrate. The use of the alpha form is very limited, because of its brittleness as a building material (Yu and Brouwers, 2011). Beta form is exclusively used but owing to the high specific area of the beta form of hemihydrates, water needs to be used in excess during the preparation of the composite. For example, the weight ratio noted w/p, where w is defined as the mass of water and p as the mass of plaster, is at least equal to 0.4 for plasterboard preparation while in the stoichiometric proportions w/p is equal to 0.2 (Yu and Brouwers, 2012).
4.  *$\alpha$ -Calcium sulfate hemihydrate production*:  $\alpha$ -HH has been widely used in ceramics, g molding, special binder systems, industrial arts & architecture, as well as in the construction industry. The explorations in technologies for large-scale production of  $\alpha$ -HH from FGD gypsum are of great significance.  $\alpha$ -HH is commercially produced by autoclave methods such as the SICOWA-ProMineral autoclaving process & the Omega process (Guan et al., 2011).
5. *Preparation of composite binder*: Martias et al. (2014) investigated on the effects of the addition of glass fibers, mica & vermiculite to the mechanical properties of a gypsum-based composite at room temperature & during a fire test.

## 2.8 OBJECTIVES FOR THE PRESENT STUDY

It is therefore observed that treatment of Giga tons of SO<sub>2</sub> using limestone slurries generates impure gypsum amounting to about three times of the quantity of SO<sub>2</sub> treated annually and in most of the cases it causes a serious disposal problem, this being a solid waste. Also the absorption of SO<sub>2</sub> from flue gases in calcium based slurries is almost exclusively carried out in spray scrubbers in the concerned industries. These find several critical operational problems. In the open literature experimental performance data of a slurry bubble column contactor for this system is not reported while it is conventionally used for other slurry reactions as mentioned above. Use of a three phase foam- slurry reactor for this system with the addition of a suitable surfactant in a very low concentration level is likely to be advantageous, as it may obviate the choking problem.

Based on the above review of literature the following objectives were decided for the present studies:

1. *To synthesize low cost regenerative ionic liquids for absorptive separation of SO<sub>2</sub> from flue gases and recover it by desorption. Pure SO<sub>2</sub> gas thus recovered may be used for manufacture of suitable products and the regenerated ionic liquid recycled to the absorber.*
2. *To generate experimental reactor performance data for the absorption of SO<sub>2</sub> using calcium based slurries in a bubble column contactor with reference to different operating variables to find the possibility of using an alternative equipment for this purpose.*
3. *To study the absorption of SO<sub>2</sub> in calcium based slurries in a foam bed reactor which in addition to higher rate of reaction, may obviate the reported operational problems associated with a spray scrubber. The filtrate after separating the product solid can be mixed with fresh slurry feed and recycled to the reactor conforming to zero discharge.*



## APPENDIX 2A

**Table 2A.1 Literature review based on reactor and absorbent used and flue gas composition**

Absorbing liquid and gas phase composition	Proposed models of		Contactor	References
	Mass Transfer	Reaction Kinetics		
Calcium carbonate slurry SO <sub>2</sub> :0.01-1 vol. % in N <sub>2</sub>	Two film theory	Instantaneous	Laminar jet absorber	Bjeerle et. al. 1972
Calcium carbonate slurry SO <sub>2</sub> : Pure	Two film theory	Instantaneous		Uchida et. al 1975
NaOH, sodium sulfite, sodium bisulfite, ammonia, ammonium sulfite solution(with/without surface active agent, Emulgen 147 or Scourol) SO <sub>2</sub> : Pure	Penetration theory	Instantaneous		Hikita et.al. 1977; Hikita et.al. 1978
Aqueous sodium carbonate (0-300 g mol/m <sup>3</sup> ) SO <sub>2</sub> : 0.12-0.7 atmin N <sub>2</sub>	Two film theory	Instantaneous	Stirred tank	Sada et. al. 1979
Aqueous dispersion of Dimethylaniline SO <sub>2</sub> : 1.2-2.3 vol% in N <sub>2</sub>	Two film theory	Instantaneous		Bhattachary S. 1996

Ca(OH) <sub>2</sub> (0-16 wt%) & Mg(OH) <sub>2</sub> (0-16 wt%) SO <sub>2</sub> : Pure	Two film theory	Instantaneous		Dagaonkar et. al. 2001
(NH <sub>4</sub> ) <sub>2</sub> SO <sub>3</sub> solution (0.03-0.05 g mol/l) SO <sub>2</sub> : 1000-4000 ppm in N <sub>2</sub>	Two film theory	zero-order with respect to the concentration of ammonium sulfite		Gao et. al., 2010
Pure water, HCl, NaCl, NaOH, NaSO <sub>3</sub> solution SO <sub>2</sub> : 0.0002-0.98 bar in N <sub>2</sub>	Surface renewable theory	Instantaneous		Chang and Rochelle, 1981; Chang & Rochelle, 1985
Aqueous sodium carbonate (39.8-994 g mol/ m <sup>3</sup> ) SO <sub>2</sub> : 3.45 – 5.45 kPa in N <sub>2</sub>	Leveque model	Instantaneous		Hikita and Konishi 1983
Dimethylaniline in kerosene (0.7807 g mol/l) SO <sub>2</sub> : 0.351 – 3.141 vol.% in air	Penetration theory	Pseudo-first order	Laminar falling film	Basu and Dutta 1987
Limestone slurry (0.3 – 1.0 kg m <sup>-3</sup> ) SO <sub>2</sub> : 48.6-190 Pa in N <sub>2</sub>	Film theory	Instantaneous	Bubbling reactor	Lancia et. al. 1994

Dimethyl sulfoxide SO <sub>2</sub> : 1806-2806 ppm in N <sub>2</sub>	NA	NA	Absorption apparatus (micro scale)	Li et. al., 2003
Pure water SO <sub>2</sub> : 600-1500 ppm in air	N/A	First order	Modified multi-stage bubble column scrubber	Meikap et. al., 2002
NaHCO <sub>3</sub> /Na <sub>2</sub> CO <sub>3</sub> solution SO <sub>2</sub> : 1000-2000 ppm in air	Two film theory	Instantaneous	Packed column	Ebrahimi et. al., 2003
Limestone slurry (10 wt%) SO <sub>2</sub> : 991 ppm in air	NA	NA	Jet bubbling reactor	Zheng et. al., 2003
Water and dilute sodium alkali SO <sub>2</sub> :400-1780 ppm in air	Two film theory	Instantaneous	Tapered and Spray-cum-bubble column	Bandyopadhyay and Biswas 2006a, 2006b,2007
Mg(OH) <sub>2</sub> slurry (0.2 - 2.0 kg/ m <sup>3</sup> ) SO <sub>2</sub> :0.608-0.963 kPa in N <sub>2</sub>	NA	Instantaneous	Bubbling reactor	Mondal, M.K., 2007
CaCO <sub>3</sub> (1 -7 wt %)	Two film	Instantaneous	Spray tower	Olausson et al.,

SO <sub>2</sub> : 100 – 1000 ppm in air	theory	s		1993
Limestone slurry SO <sub>2</sub> : 2800 ppm in air	Penetration theory	Instantaneous		Gerbec and Stergarsek 1995
Limestone slurry SO <sub>2</sub> : 200 Pa in air	Penetration theory	Both finite and instantaneous		Brogren and Karlsson 1997
Limestone slurry (5 – 10 kg m <sup>3</sup> ) SO <sub>2</sub> : 1500 – 5000 ppm in air	Stagnant-film theory	Instantaneous		Warych and Szymanowski, 2001
Limestone slurry (333 g/l) SO <sub>2</sub> : 4437 - 6163 ppm in air	NA	NA		Gomez et al., 2007
Limestone slurry (11- 18 wt%) SO <sub>2</sub> : 1000 mg/m <sup>3</sup> in air	Two film theory	Instantaneous		Dou et al., 2009
Suspension of water and limestone (15 wt%) SO <sub>2</sub> : 930 ppm in air	Two film theory	Instantaneous		Marocco, 2010; Marocco and Inzoli, 2009

## CHAPTER- 3

## THEORITICAL CONSIDERATIONS

Chapter 3 is concerned with the detailed understanding of the absorption phenomena of sulfur dioxide from its mixture with air into ionic liquids, alkali solution and slurries of hydrated lime and calcium carbonate. The rate of dissolution of suspended particles in the slurry and that of SO<sub>2</sub> in the various absorbents is desired to be predicted. This necessitates a brief discussion on the methods of determination of the associated parameter values. The overall presentation in this chapter aims to gain a deep insight into the physical picture actually prevalent in the reactor, to understand the reaction mechanisms and find assistance in explaining the experimental results.

Absorption and partial hydrolysis of SO<sub>2</sub> in water are known to be a reversible phenomenon. In an alkaline solution, however, this reaction is *instantaneous* and known to occur irreversibly. The latter is, therefore, a mass-transfer controlled process and *kinetics is therefore irrelevant* (Danckwerts, P.V. 1966).

Slow reactions are known to occur in the bulk of the liquid and values of volumetric mass-transfer coefficient,  $k_l^0 a$ , are important for the calculation of the rate of mass transfer. But, fast and instantaneous reactions occur at the gas-liquid interface. *Separate values* of interfacial area per unit volume of dispersion,  $a$ , and volume of gas-liquid dispersion,  $V_d$ , for estimation of total interfacial area available in the entire volume of dispersion, and, the liquid side mass-transfer coefficient in presence of chemical reaction,  $k_{lr}$ , are required for the estimation of enhancement factor and subsequently for the rate of gas absorption for the cases associated with these reaction kinetics.

When absorption of SO<sub>2</sub> is accompanied by an instantaneous chemical reaction that occurs in a solution, rate of moles of this solute absorbed being equal to that reacted, then, the *rate of reaction*,  $R_A$  in k mole/m<sup>2</sup> s, of this mass-transfer controlled process is *calculated* using the equation,

$$R_A = k_l^0 \Delta C \cdot E_{inst} \quad (3.1)$$

where,  $\Delta C$  is the amount of gas phase component A required to saturate unit volume of the bulk liquid corresponding to a partial pressure of this component prevailing at

the gas-liquid interface,  $k_l^0$  is the liquid phase mass-transfer coefficient for physical absorption (which is defined as “when absorbed gas does not react with any of the component of the absorbing liquid, the prevailing mass-transfer coefficient is called physical mass-transfer coefficient”) and  $E_{inst}$  is the enhancement factor for gas absorption with instantaneous chemical reaction.

Equation (3.1) may be rewritten alternatively as,

$$R_A = k_{lr} \Delta C \quad (3.2)$$

Where,  $k_{lr}$  is the liquid phase mass transfer-coefficient for chemical absorption which is equal to  $k_l^0 E_{inst}$ .

In the case of an *irreversible instantaneous* reaction of dissolved  $A$  with a single reactant  $B$  in solution, as shown later in this chapter by Eqn. (3.48), the rate expression for equal diffusivity values takes the form:

$$R_A = k_l^0 (C_{A_i} + C_{B_0} / z) \quad (3.3)$$

where,  $C_{A_i} + C_{B_0} / z$  represents  $\Delta C$  in eqn. (3.3).

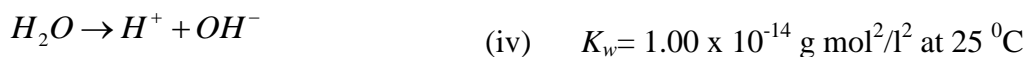
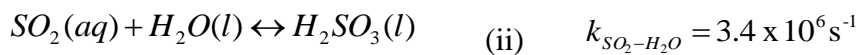
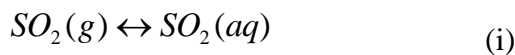
Rate of absorption of  $SO_2$ ,  $\bar{R}_A$ , in  $k \text{ mole m}^{-3} \text{ s}^{-1}$  is therefore calculated using the expression,

$$\bar{R}_A = R_A \cdot a = k_l^0 a \Delta C \quad (3.4)$$

### 3.1 Reaction schemes and kinetic constants of the systems studied in the present investigation and in other alkaline and aqueous systems

#### 3.1.1. $SO_2$ absorption in pure water

When  $SO_2$  is absorbed into pure water, it is partially and reversibly hydrolyzed as follows:



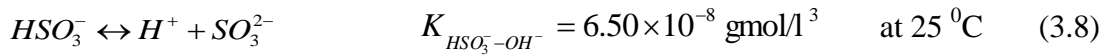
$k_{SO_2-H_2O}$  is the forward reaction rate constant (Chang and Rochelle, 1981) and  $K_w$  is thermodynamic equilibrium constant (Lancia et al., 1994). The concentration of  $H_2O$  being constant, the equilibrium constant for the absorption of  $SO_2$  in water may be written as,

$$K_{SO_2-H_2O} = \frac{[H^+][HSO_3^-]}{[SO_2]} \quad K_{SO_2-H_2O} = 1.7 \times 10^{-2} \text{ gmole/l} \quad \text{at } 20^\circ\text{C} \quad (3.6)$$

The value of this constant at  $25^\circ\text{C}$  is  $1.39 \times 10^{-2} \text{ g mol/l}$ . The value of solubility of  $SO_2$ , which is the equilibrium saturation concentration  $[SO_2]$ , at  $20^\circ\text{C}$  and 1 atm being  $1.82 \text{ g mol/l}$ , the concentrations of different species may be obtained from Eqn. (3.7).

$$[H^+] = [HSO_3^-] = (1.7 \times 10^{-2} \times 1.82)^{1/2} = 0.175 \text{ g mol/l} \quad (3.7)$$

The second ionization occurring in the hydrolysis reaction of  $SO_2$  may be written (Lancia et al. 1997) as,

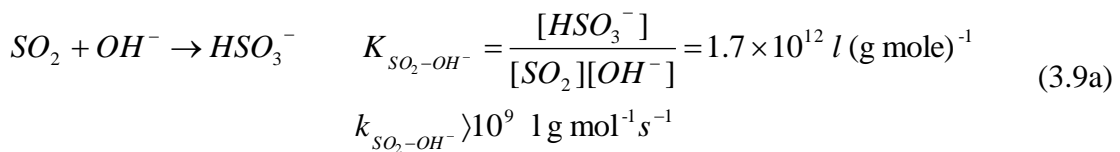


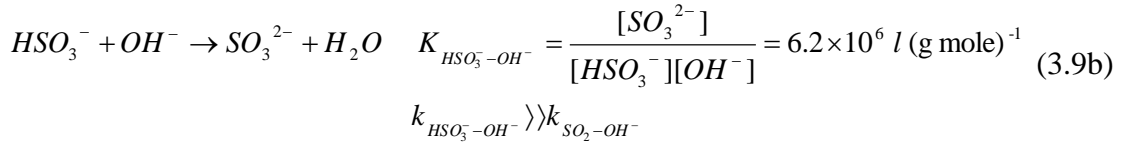
### 3.1.2. Concept of multiple reaction planes within the liquid film

Reaction of absorbed  $SO_2$  with  $OH^-$  occurs through a set of parallel reactions. Reaction rate constants of some reactions being enormously larger than others and all the reacting species cannot coexist. The concept of two reaction planes within the liquid film has therefore been conceived. Particularly for absorption of  $SO_2$  in alkaline solutions and slurries, various investigators (Hikita et al., 1972, Hikita et al., 1977, Sada et al., 1979) proposed a two reaction plane theory to model the reactions, and the details of this are discussed below.

#### 3.1.2.1. $SO_2$ absorption in NaOH solution

When sulfur dioxide is absorbed into aqueous alkaline solution, the following two reactions should be considered (Hikita et al., 1977):





The values of equilibrium constants  $K_{SO_2 - OH^-}$  and  $K_{HSO_3^- - OH^-}$  for reactions (3.9a) and (3.9b) shown above are at 25°C and infinite dilution. These values were estimated from the dissociation constant  $k_{SO_2 - OH^-}$  and  $k_{HSO_3^- - OH^-}$  of sulfurous acid. Reaction (3.9a) is very fast, with a rate constant exceeding  $10^9$  l/g mol s (Saal R.N.J., 1928). Reaction (3.9b) has very much higher rate constant than reaction (3.9a) since it is a proton transfer reaction. Thus both the reactions, (3.9a) and (3.9b), may be regarded as instantaneous reactions. In strong alkaline solutions reaction (3.9a) is followed by (3.9b) and the overall reaction is



Mechanism of chemical absorption for the above reaction depends on the ratio of the equilibrium constants,  $K_1/K_2$ . For this reaction, the value of the ratio of  $K_1/K_2 \rightarrow \infty$ . Hence,  $HSO_3^-$  cannot coexist with  $OH^-$  and the reaction (3.10) never takes place directly. Two reaction planes are formed within the liquid film, and the reaction  $SO_2 + SO_3^{2-} + H_2O \rightarrow 2HSO_3^-$  occurs at the first reaction plane and  $HSO_3^- + OH^- \rightarrow SO_3^{2-} + H_2O$  takes place at the second reaction plane. On the other hand, in region III (Figure 3.1), no chemical reaction occurs. Only  $OH^-$  and  $SO_3^{2-}$  diffuse physically.



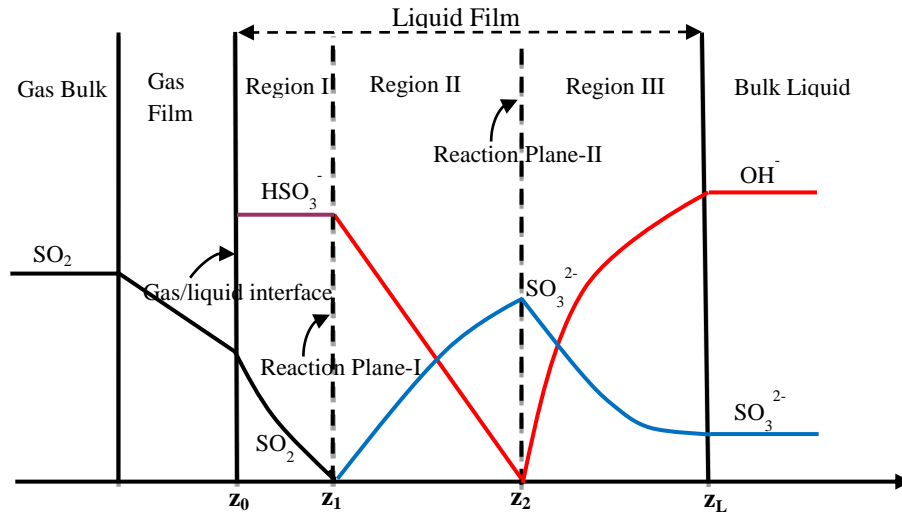
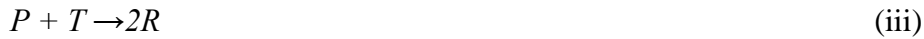


**Figure 3.1** Typical concentration profiles in the gas and liquid films for absorption of  $\text{SO}_2$  in  $\text{NaOH}$  or  $\text{Ca}(\text{OH})_2$  solution (Hikita et al., 1977)

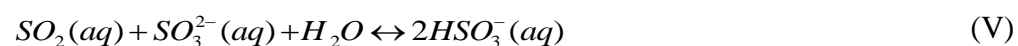
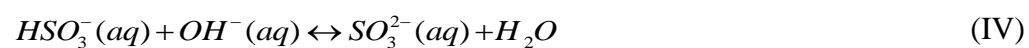
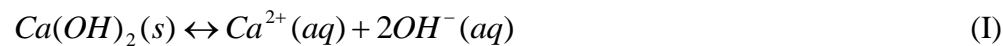
Reactions (3.9a), (3.9b) and (3.10) may be expressed symbolically as,

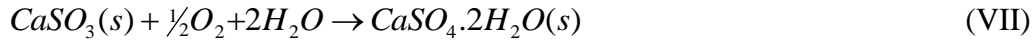


Concentration profiles of different reactant and product species in the liquid film are shown in Figure 3.1.

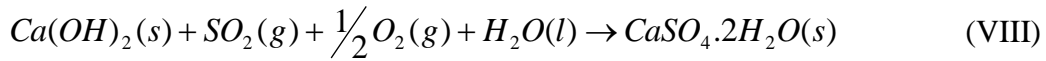
### 3.1.2.2 $\text{SO}_2$ absorption in $\text{Ca}(\text{OH})_2$

The desulfurization reactions between  $\text{SO}_2$  and calcium hydroxide slurry (Sada et al., 1979, 1980 and Dagaonkar et al. 2001) are written as follows:





The overall reaction is



Concentration profiles of the different ionic species in the liquid film for reaction of  $\text{SO}_2$  in a saturated hydrated lime *solution* are shown in Figure 3.1 and that in the slurry containing suspended particles of sparingly soluble particles are shown in Figure 3.2.

It has been mentioned above that in the process of sulfur dioxide absorption in alkaline solutions with no suspended particles,  $\text{HSO}_3^-$  cannot coexist with  $\text{OH}^-$  and hence reaction by eqn. (3.10) never takes place directly. Reactions (3.9a) and (3.9b) take place at two differently located planes in two reaction planes model. However, in the slurry process being considered here, both dissolved  $\text{SO}_2$  and  $\text{HSO}_3^-$  produced by reaction (3.13V) within the film can react with  $\text{OH}^-$ , supplied by the dissolution of solid particles within the liquid film itself and therefore the dissolved  $\text{SO}_2$  is consumed according to reactions (3.13III) and (3.13V) simultaneously (Sada et al. 1977).

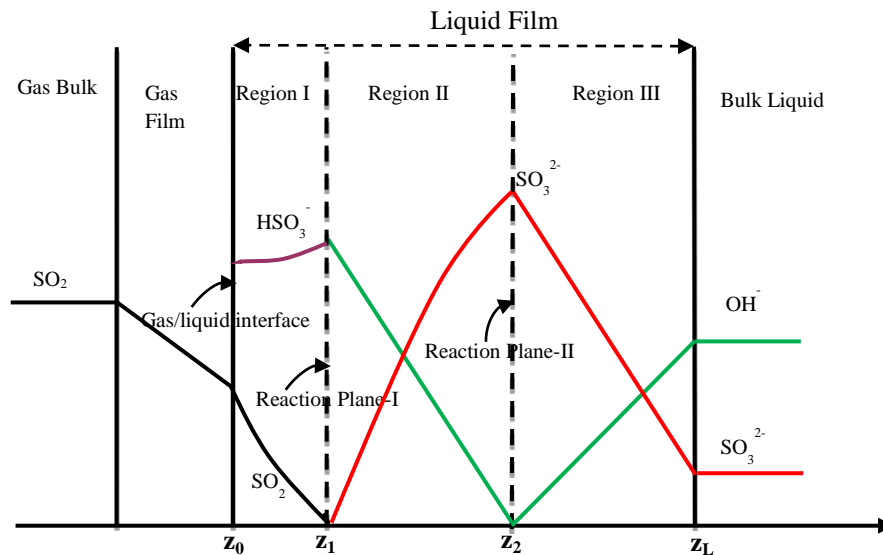


**Figure 3.2 Typical concentration profiles in the liquid films for absorption of  $\text{SO}_2$  in  $\text{Ca}(\text{OH})_2$  slurry (this is proposed by a comparison with the  $\text{Mg}(\text{OH})_2\text{-SO}_2$  system, Sada et al. 1981, Figure 3b)**

### 3.1.2.3. SO<sub>2</sub> absorption in CaCO<sub>3</sub> slurry

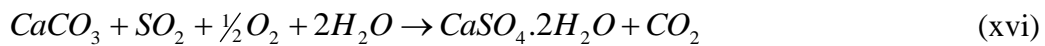
The reaction mechanism between SO<sub>2</sub> and calcium carbonate slurry is represented by the following set of equations (Sada et al. 1980, Liu and Xiao, 2006):



Diffusion of dissolved chemical species in liquid film



The overall reaction is



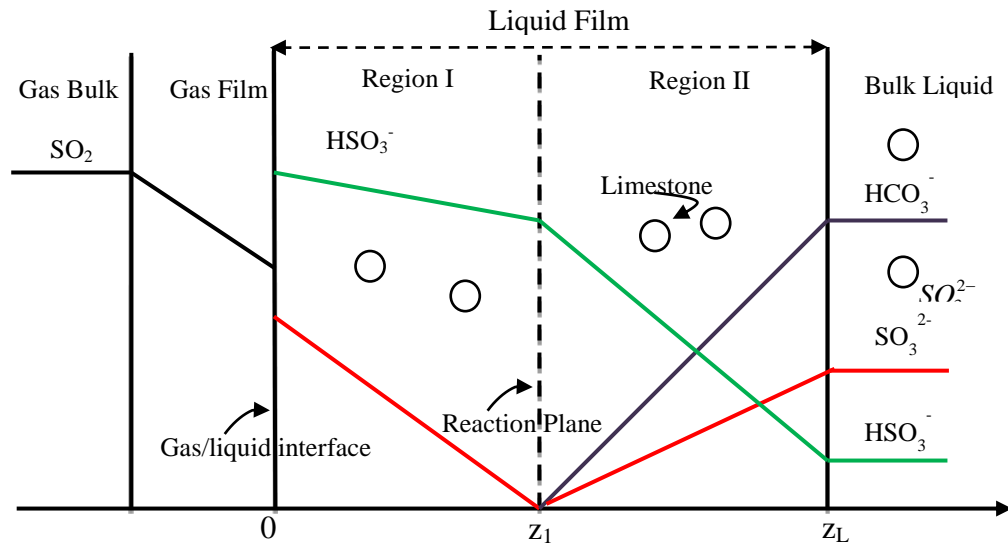


**Figure 3.3 Typical concentration profiles in the liquid film for absorption of  $\text{SO}_2$  in  $\text{CaCO}_3$  slurry - One reaction plane model (Liu and Xiao, 2006)**

The reactant species  $\text{CO}_3^{2-}$  and reaction product  $\text{HSO}_3^-$  cannot coexist because the chemical equilibrium constant for the ionic reaction between these two species is estimated to be approximately  $10^3$  (Sada et al., 1980). Assuming that the reaction (3.14xiii) is irreversible and instantaneous, it follows that there exist two reaction planes in the liquid film. That is, at one reaction plane  $\text{SO}_2$  reacts according to reaction (3.14xiv) and (3.14xv) and at another plane reaction (3.14xiii) takes place (Sada et al., 1980). The overall reaction is (3.14xvi) (Zheng et al., 2003).

Concentration profiles of the different ionic species in the liquid film for the reaction of  $\text{SO}_2$  in the slurry containing sparingly soluble suspended particles of this reactant are shown in Figures 3.3 and 3.4. That in saturated calcium carbonate *solution* is shown in Figure 3.5.

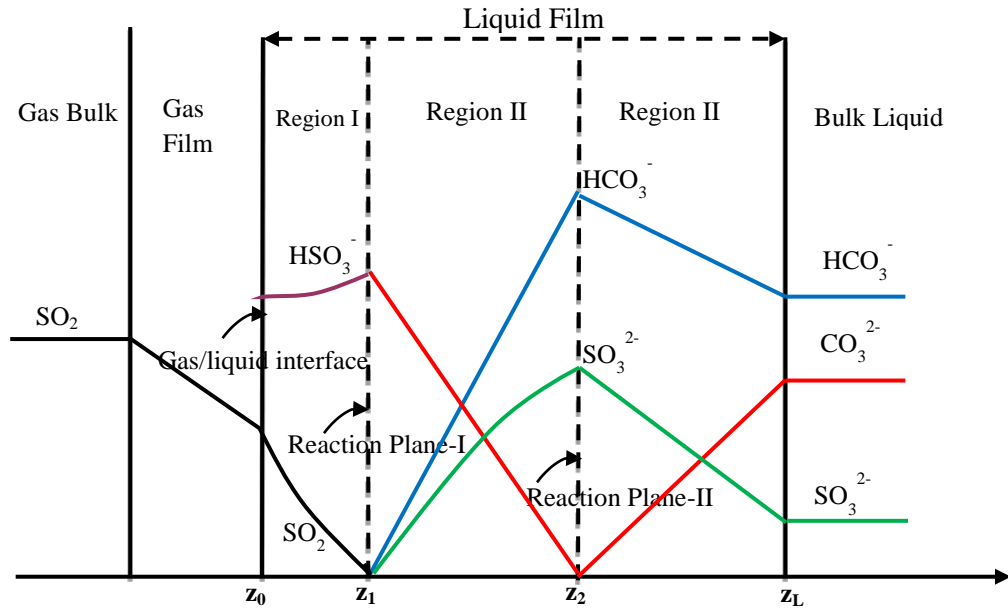


Figure 3.4 Typical concentration profiles in the liquid film for absorption of  $\text{SO}_2$  in  $\text{CaCO}_3$  slurry- Two reaction plane model (Sada et al., 1981)

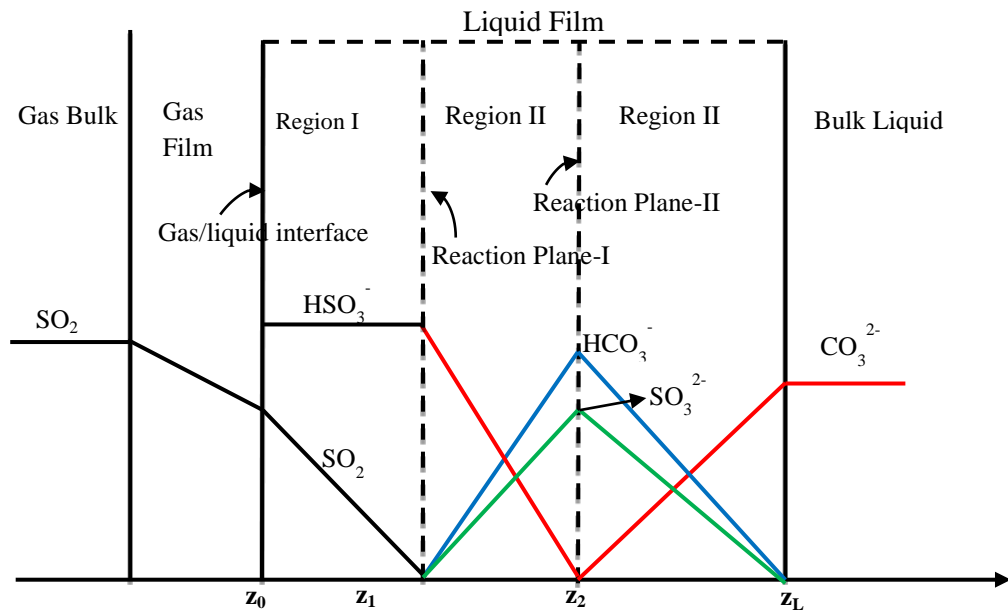
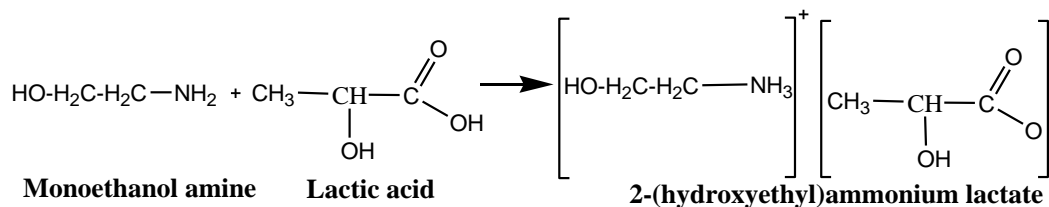


Figure 3.5 Typical concentration profiles in the liquid film for absorption of  $\text{SO}_2$  in  $\text{CaCO}_3$  saturated solution (Sada et al., 1981)

### 3.2. Ionic liquid and its utilization for SO<sub>2</sub> absorption

#### 3.2.1. Proposed reaction Scheme for synthesis of ionic liquid

Formation of ionic liquid by the reaction between monoethanolamine and lactic acid occurs according to the following reaction (Yuan et al., 2007):



#### 3.2.2. Proposed scheme of association of IL with SO<sub>2</sub> absorbed into it

Absorption of SO<sub>2</sub> by MLIL is considered to be a physical phenomenon and that SO<sub>2</sub> gas remains in the molecular state due to hydrogen bond, Coulombic interaction, etc. (Qu et al. 2013; Huang et al. 2006). It is proposed that the oxygen atom of SO<sub>2</sub> gas forms a hydrogen bond with the hydrogen atom of the hydroxyl group as shown below by a ball stick model. Similar pattern for the interaction between SO<sub>2</sub> and IL has been reported by Prasad and Senpati (2009).

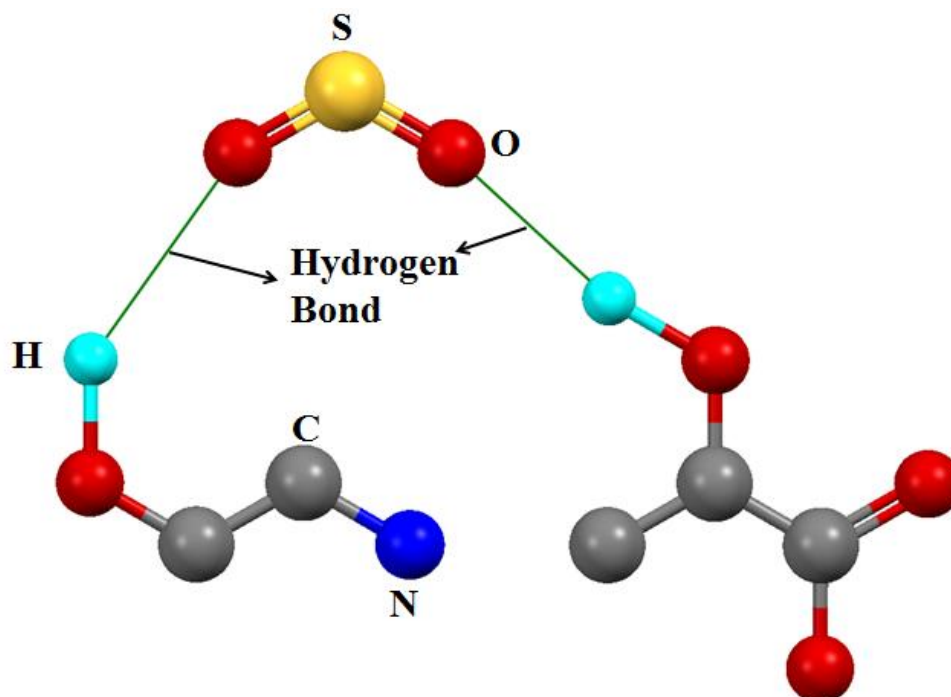


Figure 3.6 Ball stick model of proposed interaction between MLIL and SO<sub>2</sub>

### 3.2.3. Axial mixing of gas and liquid phases in the bubble column and its effect on the rate of gas absorption and reaction

Mixing in the gas as well as that in the liquid phase in a bubble column determines its mass transfer efficiency under the given experimental conditions. Gas phase mixing is important especially when the mass-transfer process is gas-phase controlled. This is true for the liquid phase as well. The degree of mixing is determined using the dispersion model. It is observed from the reported correlations (Towell and Ackerman, 1972; Field and Davidson, 1980; Mangartz and Pilhofer, 1981) that the extent of axial gas phase mixing increases with an increase in the superficial gas velocity and increasing the column diameter. Kantak et al. (1994) reported that the gas phase mixing decreased with increasing liquid viscosity and the reported studies indicate that a decrease in the turbulence in the bubble column causes a decrease in the extent of axial gas-phase mixing.

Gas phase mixing in bubble columns has usually been modeled as plug flow (Stern et al., 1983; Vuuren and Heydenrych, 1985; Herbolzheimer and Iglesia, 1994) although few other authors have reported that this should not be considered as negligible. The most common approach to model the non-ideal mixing behavior in bubble column contactors is the 1-D axial dispersion model (ADM). In this model, all the parameters leading to the axial gas mixing are lumped into a single parameter called the axial gas-phase dispersion coefficient ( $D_g$ ). In the present investigation, the ionic liquid used for desulfurization being highly viscous and superficial gas used is low, the extent of turbulence and axial gas-phase mixing is approximated to be in the plug flow region. A large number of correlations have been proposed by various investigators for estimation of  $D_g$ , and a few of these are shown in Appendix 3B. Most of the reported work claims that  $D_g$  is a function of column diameter  $d_c$  and superficial velocity of gas  $u_g$  or the actual gas velocity  $u_g/\varepsilon_g$ .

To determine the intensity of mixing in the short bubble column reactor, one finds the value of Peclet number ( $Pe$ ) for each of the phases.

$$\text{For gas phase, } Pe_g = \frac{h_{disp} u_g}{D_g \varepsilon_g} \text{ and,} \quad (3.15)$$

$$\text{For liquid phase, } Pe_l = \frac{u_g d_c}{D_l} \quad (3.16)$$

A value of  $Pe \rightarrow \infty$  indicates plug flow while  $Pe \rightarrow 0$  indicates complete mixing.

These criteria have been used to determine the extent of mixing and its effect on the high gas-phase resistance to absorption of  $SO_2$  is especially important in the case absorption by ionic liquids. Increased value of viscosity of the absorbing liquid cause a reduction in the value of gas hold-up,  $\varepsilon_g$ . Reported correlations for estimation of  $D_g$  have been shown in Appendix 3C, Table 3C.2.1

### 3.3 Working Equation for estimation of $SO_2$ removal efficiency

During the semi-batch operation of the bubble column contactor, the exit concentration of  $SO_2$  varies with time depending on the additional amount of  $SO_2$  required to saturate the absorbing solvent at the prevailing partial pressure of the solute or consumption rate of the liquid phase reactant. Using the available experimental set-up, the exit concentration of  $SO_2$  could be measured over a minimum time interval of 10 s. Transient values of  $SO_2$  removal efficiency can, therefore, be calculated from the experimental data using eqn. (3.17):

$$\eta(t) = \frac{C_{in} - C_e(t)}{C_{in}} \times 100 \quad (3.17)$$

where,  $\eta(t)$  = % of transient  $SO_2$  removal efficiency

$C_{in}$  = concentration of  $SO_2$  at the inlet to the reactor (invariant) at the start of each time step  $\Delta t$ , ppm

$C_e(t)$  = exit concentration of  $SO_2$  at the end of each small time step  $\Delta t$ , ppm

In the present investigation, exit concentration of  $SO_2$  at an interval of 10 sec being available, this time interval has been used in the calculation of  $SO_2$  conversion.

### 3.4. Conversion calculation of component B

The extent of time-dependent conversion of the reactant  $B$ , for various operating conditions, is a measure of the performance of a reactor.

Percentage conversion ( $X$ ) of the dissolved species  $B$  at any time ' $t$ ' may be written as

$$X = \frac{m_B^T(0) - m_B^T(t)}{m_B^T(0)} \times 100 \quad (3.18)$$



$$= \frac{C_B^T(0) - C_B^T(t)}{C_B^T(0)} \times 100 \quad (3.19)$$

,where  $m_B^T(t)$  and  $m_B^T(0)$  are the total loading of unreacted  $B$  (both dissolved in solution and also present as particles) at time  $t$  and that initially present in slurry volume  $V_{sl}$ , respectively.  $C_B^T(t)$  and  $C_B^T(0)$  are the respective total molar loadings of component  $B$  per volume of the solvent (water in this case). The particles being sparingly soluble, the expressions for

$m_B^T(t)$  and  $C_B^T(t)$  are written as follows :

$$m_B^T(t) = C_B^T(t) \cdot M_B \cdot V_l \quad (3.20)$$

$$C_B^T(t) = C_B(t) + \sum_i (n_{pi} \frac{\pi d_{pi}^3}{6}) \frac{\rho_B}{M_B} \frac{V_{sl}}{V_l} \quad (3.21)$$

Instantaneous values of  $C_B^T(t)$ ,  $C_B(t)$ , and  $d_{pi}(t)$  can be calculated by solving the unsteady- state material-balance equations for components  $A$  and  $B$  in solution, and the volume balance for the suspended particles of component  $B$ , written for a semi-batch operation of the slurry or slurry-foam reactor.

### 3.5. Conditions to verify that absorption of $SO_2$ in Ca-based slurries occur with the instantaneous reaction:

The following conditions should satisfy (Ridgway et al. 1991) so that the reaction of absorbed  $SO_2$  in  $Ca(OH)_2$  or  $CaCO_3$  slurry occurs instantaneously,

$$Ha \gg 1 \text{ and } Ha > 10E_{inst} \quad (3.22)$$

$$\text{where, } Ha = \frac{\sqrt{D_A k_1 C_{B0}}}{k_l^0} \quad (3.23)$$

$$\text{and } E_{inst} = 1 + \frac{D_B C_{B0}}{R_{BA} D_A C_{Ai}} \quad (3.24)$$

Several expressions for the enhancement factors for other mass-transfer models have been shown in Appendix 3B, Table 3B.1.

### 3.6. Determination of controlling resistance for gas absorption: percent of total resistance in the gas phase

If  $k_l^0$  is the liquid phase mass transfer coefficient for physical absorption of gas, then liquid phase resistance to physical absorption is calculated as  $1/k_l^0$ . For estimation of gas phase resistance, liquid phase resistance is made negligibly small by absorbing a gas (here  $\text{SO}_2$ ) into a strong alkaline liquid, say  $\text{NaOH}$ , in which it reacts instantaneously. In the presence of an enhanced rate of gas absorption, if  $E_{inst}$  is the enhancement factor, the modified value of the liquid-phase resistance now becomes  $1/k_l^0 E_{inst}$ .

Considering that the overall resistance to mass transfer on liquid phase basis is written as

$$\frac{1}{K_l} = \frac{1}{k_l^0 E_{inst}} + \frac{1}{k_g H}, \quad (3.25)$$

where,  $H$  is the Henry's constant for gas absorption,  $k_g$  the gas-phase mass transfer coefficient and  $1/k_g H$  the gas-phase resistance to mass transfer, percent of gas-phase resistance to mass transfer,  $\beta$ , may be calculated using the expression:

$$\beta = \frac{\frac{1}{k_g H}}{\frac{1}{k_l^0 E_{inst}} + \frac{1}{k_g H}} \times 100 \quad (3.26)$$

### 3.7. Development of expressions for calculation of parameter values

#### 3.7.1 Estimation of liquid side volumetric physical mass-transfer coefficient for $\text{SO}_2$ absorption

The value of  $k_l^0$  may be obtained through the estimation of  $k_l^0 a$ . Pure oxygen, hence resistance to mass transfer is nil, is absorbed in deoxygenated water to satisfy physical absorption. For the unsteady state absorption of oxygen, the expression obtained from the following treatment may be used for estimation of volumetric liquid phase mass-transfer coefficient  $k_{l\text{O}_2}^0 a$  for physical absorption of oxygen.

The value of  $k_l^0$  required for verification of the condition of instantaneous reaction is obtained through estimation of  $k_l^0 a$ . For the unsteady state absorption of oxygen, the required expression is obtained as follows (Akita and Yoshida, 1973).

The governing unsteady-state mass balance eqn. for absorption of oxygen in water may be written as,

$$V_l \frac{\partial C_{O_2}}{\partial t} = k_{lO_2}^0 a' (C_{O_2}^* - C_{O_2}) V_l \quad (3.27)$$

where,  $a'$  is the gas-liquid interfacial area per unit volume of solvent.

Eqn. (3.27) may be rearranged and integrated to obtain an expression for  $k_{lO_2}^0 a'$  as follows

$$\int_{C_{O_2i}}^{C_{O_2f}} \frac{dC_{O_2}}{(C_{O_2}^* - C_{O_2})} = k_{lO_2}^0 a' \int_0^t dt \quad (3.28)$$

$$\text{Or, } k_{lO_2}^0 a' = \frac{1}{t} \ln \frac{(C_{O_2}^* - C_{O_2f})}{(C_{O_2}^* - C_{O_2i})} \quad (3.29)$$

Eqn. (3.29) may be written more specifically to signify that the interfacial area,  $a$ , associated with  $k_{lO_2}$  is expressed per unit volume of dispersion as follows:

$$k_{lO_2}^0 a = \frac{1 - \varepsilon_G}{t} \ln \frac{(C_{O_2}^* - C_{O_2f})}{(C_{O_2}^* - C_{O_2i})} \quad (3.30)$$

The values of  $C_{O_2i}$ ,  $C_{O_2f}$  and  $\varepsilon_G$  are determined experimentally to obtain the value of  $k_{lO_2}^0 a$ .

Liquid side volumetric physical mass-transfer coefficient for absorption of  $SO_2$  can be determined from that of  $O_2$  using the expression:

$$k_{lSO_2}^0 a = k_{lO_2}^0 a \left( \frac{D_{SO_2}}{D_{O_2}} \right)^{2/3} \quad (3.31)$$

### 3.7.2 Expressions for estimation of the gas-phase mass-transfer coefficient, $k_{gSO_2} \cdot a$ for $SO_2$ absorption

The rate of gas absorption in the bubble column may, therefore, be calculated using the expression:

$$W_{SO_2} = R_{SO_2} \cdot a \cdot V_{disp} = k_{gSO_2} \cdot a \cdot (p_{SO_2b} - p_{SO_2i}) \cdot V_{disp} \quad (3.32)$$

where,  $R_{SO_2}$  is the moles of  $SO_2$  absorbed per unit interfacial area per unit time,  $a$  the interfacial area per unit volume of dispersion and  $V_{disp}$  the volume of dispersion. Moles of  $SO_2$  absorbed per unit time,  $W_{SO_2}$ , has been determined experimentally.

Eqn. (3.32) may, therefore, be rearranged to obtain,

$$\frac{W_{SO_2}}{V_{disp}} = k_{gSO_2} \cdot a \cdot (p_{SO_2b} - p_{SO_2i}) \quad (3.33)$$

For an instantaneous, purely gas-phase controlled reaction all the gas reaching the gas-liquid interface reacts at the interface itself and  $p_{SO_2i}$  tends to zero.  $k_g a$  can therefore be calculated using the expression,

$$k_{gSO_2} \cdot a = \frac{W_{SO_2}}{V_{disp} \cdot p_{SO_2b}} \quad (3.34)$$

Molar rate of absorption of  $SO_2$  is calculated from experimental data. A mass balance on  $SO_2$  over the reactor may be written as follows:

$$W_{SO_2} = \frac{Q_{tot} \cdot (p_{SO_2in} - p_{SO_2out})}{RT} \quad (3.35)$$

Where,  $p_{SO_2in}$  is ppm of  $SO_2$  in the feed gas  $\times 10^{-6}$  atm/ ppm.

$W_{SO_2}$  can be substituted from Eqn. (3.35) into (3.34) and the value of  $k_{gSO_2} \cdot a$  calculated from the resulting expression.

### 3.7.3. Specific interfacial area, $a$ , in a gas-liquid dispersion

#### 3.7.3.1. Working equations for estimation of ‘ $a$ ’ using experimental data

Interfacial area is possibly the most important parameter governing the reactor performance when gas absorption is accompanied by an instantaneous chemical reaction. It is reported to be a function of column diameter, operating variables and physicochemical properties of the system. However, for gas absorption accompanied by slow or instantaneous reaction, the rate of mass transfer is estimated by use of the volumetric mass transfer coefficient,  $k_l a$ .

There are two important methods used extensively for the determination of interfacial area in a bubble column reactor:

- (i) *Physical, and*

(ii) *Chemical.*

Use of a chemical method produces an assessment of interfacial area,  $a$ , based on the entire volume of the reactor but physical processes give a local value of the interfacial area.

**Physical method:** While the optical methods based on reflection, refraction and diffraction can be applied for direct measurements, the most widely used physical method is based on the estimation of  $d_s$ .

**Chemical method:** Reaction model, kinetic parameters, solubility and diffusivity are required for estimation of  $a$  by this method. But the main disadvantage of this method is that for each material system, ‘ $a$ ’ is to be determined separately (ref: bubble column reactors, Wolf-Dieter Deckwer, Germany, John Wiley and Sons). For an irreversible gas-liquid reaction,  $m^{\text{th}}$  order in  $A$  and  $n^{\text{th}}$  order in  $B$ :



$$\text{The local rate of reaction is } R_A = k_{mn} C_A^m \cdot C_B^n \quad (3.37)$$

When the concentration of  $B$  virtually remains uniform everywhere within the reaction mass, the reaction is said to be pseudo-  $m^{\text{th}}$  order in  $A$ .

The condition for this situation is,

$$Ha = \sqrt{M} = \sqrt{(2/m+1)D_A k_{mn} (C_{Ai})^{m-1} (C_{B0})^n / k_l^2} \ll C_{B0} / zC_{Ai} \quad (3.38)$$

and,

$$\sqrt{M} > 3 \quad (3.39)$$

The rate of absorption per unit area is

$$R_A = C_{Ai} \sqrt{2/(m+1)D_A k_{mn} (C_{Ai})^{m-1} (C_{B0})^n} \quad (3.40)$$

Conditions for pseudo-  $m^{\text{th}}$  order reaction and rate expressions for absorption per unit interfacial area for different values of  $m$  and  $n$  have been presented in tabular form by Danckwerts and Sharma (1970) and for brevity shown in Appendix 3A of this thesis.

$R_A$  is calculated using Eqn. (3.40) or the system specific equation given in Appendix 3A. Total rate of absorption  $R_A \cdot A_T$  is determined experimentally as a combined quantity and total interfacial area  $A_T$  is calculated accordingly. For a sparged absorber,

it is ensured that the difference between the volumes of gas entering and leaving the absorber is negligible.

For a typical second order reaction with  $m=n=1$ , if condition (3.38) is satisfied, but the reaction is not first enough to satisfy condition (3.39), rate of absorption per unit volume of dispersion is calculated using the expression,

$$R_A \cdot a = a \cdot C_{Ai} \sqrt{D_{AB} k_2 C_{B0} + k_l^0} \quad (3.41)$$

Experimentally,  $R_A \cdot a$  is measured as a combined quantity for different values of  $k_2 C_{B0}$ . At constant hydrodynamic conditions, a graph of  $(R_A a)^2$  against the variable  $k_2 C_{B0}$  produces a straight line with the slope  $(a C_{Ai})^2 D_{AB}$  and an intercept equal to  $(a C_{Ai} k_l^0)^2$ . This is the well-known Danckwert's plot.  $D_{AB}$  being known,  $k_l^0$  can be calculated using the values of slope and intercept.

**Cases when kinetics not essential for estimation of  $a$ :**  $R_A$  may be calculated without any knowledge of Kinetics of reaction. A wetted wall column or a stirred cell with known interfacial area is used to measure the rate of absorption,  $R_A$ . Gas rate and stirring speed in the stirred cell should be varied to confirm that  $R_A$  is independent of  $k_l$  and liquid volume.

### 3.7.3.2 Other methods for estimation of $a$

The interfacial area,  $a$ , that combines with  $k_l$  or  $k_l^0$  is defined with respect to the dispersion volume,  $V_d$ , and has the units of area per unit volume of dispersion.

$$a = \frac{A_{td}}{V_{disp}} = \frac{A_{td}}{V_l + V_g} = \frac{A_{td} \cdot \epsilon_G}{V_g} \quad (3.42)$$

where,  $A_{td}$  is the total area of all the bubbles at any time in the dispersion = (average area of each bubble)(no of bubbles in dispersion). It has been assumed here that bubble breakup and its coalescence do not occur in the short bubble column reactor.

Specific interfacial area per unit volume of dispersion,  $a$ , and per unit volume of solvent  $a'$ , are related by the expression

$$a' = a / \epsilon_l \quad (3.43)$$

### 3.7.4 Gas hold-up

Gas holdup in the bubble column has been calculated using the expression:

$$\varepsilon_g = \frac{h_d - h_l}{h_d} \quad (3.44)$$

where,  $h_l$  is the clear liquid height in the column for a given volume of feed solvent and  $h_d$ , the height of dispersion, measured as a function of superficial velocity of the gas at constant values of solvent volume.

### 3.7.5 Solid-liquid interfacial area

The total surface area of particles,  $A_p$ , may be calculated as follows:

$$A_p = \sum_{i=1}^n A_{pi} = \sum_{i=1}^n \frac{6w_i}{\rho_p d_{pi}} \quad (3.45)$$

Where,  $w_i$  = weight of particles in  $i^{\text{th}}$  fraction

$d_{pi}$  = average diameter of particles in  $i^{\text{th}}$  fraction

$\rho_p$  = density of particle

### 3.7.6 Solid-liquid mass-transfer coefficient

According to Uchida et al. 1975, a solid-liquid mass-transfer coefficient value in the presence of a chemical reaction becomes larger and rate of dissolution of particles is thereby enhanced. A brief review of this has been presented in Chapter 2. Rate of dissolution of particles increases with an increase in the superficial velocity of the gas, etc. Under given experimental conditions  $k_{sl}$  is calculated by a stoichiometric mass balance of  $\text{SO}_2$  absorbed and reacted with the dissolved lime under steady state conditions.

$$\text{Rate of dissolution of particles, } R_B = k_{sl} \cdot A_{sl} \cdot V_{disp} (C_{B0} - C_{B\lambda}) \quad (3.46)$$

where,  $A_{sl}$  is the total solid-liquid interfacial area in the reacting slurry per unit volume of dispersion. Under steady state conditions, rate of absorption of  $\text{SO}_2$  equals the rate of its reaction. Rate of dissolution of particles,  $R_B$ , is therefore obtained from a stoichiometric balance. The reaction being instantaneous, the concentration of species  $B$ ,  $C_{B\lambda}$  at reaction plane is considered to be negligibly small. Therefore, for the

uniform concentration of  $B$  from the interface to liquid bulk  $k_{sl}$  is obtained using the expression,

$$k_{sl} = \frac{R_B}{(A_{sl})(V_{disp})(C_{B0})} \quad (3.47)$$

### 3.8 Rate of gas absorption

Rates of absorption of  $SO_2$  depend on the concentration profiles of the different reactant species in the reactor. The possible cases are discussed below:

Assuming that a steady rate of gas absorption attains instantaneously after the start of experiments, two film theory may be used to calculate the rate as follows:

Using the two film theory, the instantaneous rate of absorption may be written as (Danckwerts, P.V., 1970),

$$R_A = k_{gSO_2}(P_{Ab} - P_{Ai}) = k_{ISO_2}^0 C_{Ai} E_{inst} = k_{ISO_2}^0 C_{Ai} \left( 1 + \frac{D_B C_{B0}}{z D_A C_{Ai}} \right) = k_{ISO_2}^0 \left[ C_{Ai} + \frac{D_B C_{B0}}{z D_A} \right] \quad (3.48)$$

and if Henry's law is obeyed,

$$P_{Ai} = H C_{Ai} \quad (3.49)$$

Substituting eqn. (3.49) in (3.48) and rearranging one gets,

$$k_{gSO_2} \cdot P_{Ab} - k_{gSO_2} P_{Ai} = k_{ISO_2}^0 \left[ \frac{P_{Ai}}{H} + \frac{D_B C_{B0}}{z D_A} \right] \quad (3.50)$$

$$\text{or, } P_{Ai} \left[ k_G + \frac{k_l}{H} \right] = k_{gSO_2} P_{Ab} - \frac{k_{ISO_2}^0 D_B C_{B0}}{z D_A} \quad (3.51)$$

$$P_{Ai} = H C_{Ai} = \frac{H \left[ k_{gSO_2} P_{Ab} - \left( \frac{k_{ISO_2}^0 D_B C_{B0}}{z D_A} \right) \right]}{H k_{gSO_2} + k_{ISO_2}^0} \quad (3.52)$$

$$\text{Condition 1, if, } k_{gSO_2} P_{Ab} > \frac{k_{ISO_2}^0 D_B C_{B0}}{z D_A} \quad (3.53)$$

Thus Rate of absorption

$$R_A = k_{gSO_2} (P_{Ab} - P_{Ai}) \quad (3.54)$$



Substituting the expression for  $p_{Ai}$  from Eqn. (3.52) and rearranging one gets,

$$R_A = \left( p_{Ab} + \frac{D_B C_{B0} H}{z D_A} \right) / \left( \frac{H}{k_{ISO_2}^0} + \frac{1}{k_{gSO_2}} \right) \quad (3.55)$$

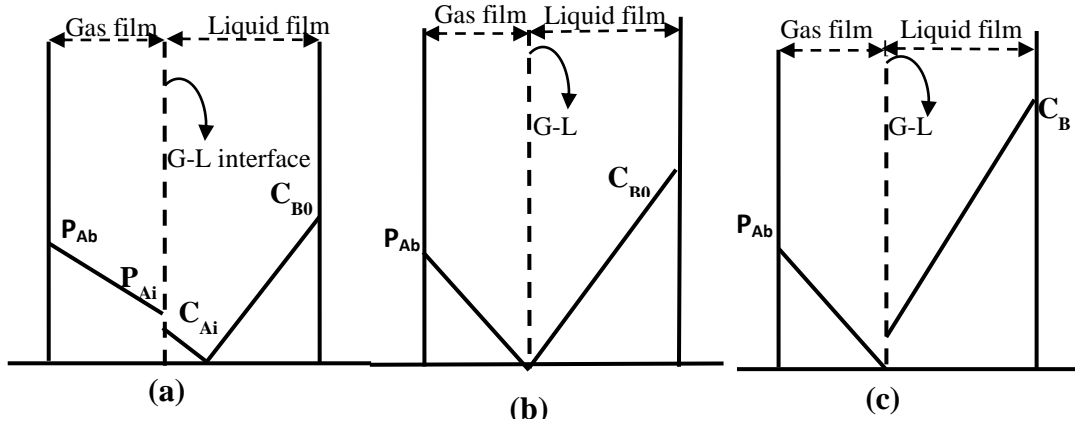


**Figure 3.7** Concentration profiles for instantaneous reaction with varying concentration of reactant by Two-film theory (Figure 5.13, p-149, Danckwerts, P.V. 1970); (a): condition 1, (b): condition 2, (c) condition 3

$$\text{Condition 2: } k_{gSO_2} p_{Ab} = \frac{k_{ISO_2}^0 D_B C_{B0}}{z D_A} \quad (3.56)$$

$$\text{Rate of absorption: } R_A = k_{gSO_2} p_{Ab} = \frac{k_{ISO_2}^0 D_B C_{B0}}{z D_A} \quad (3.57)$$

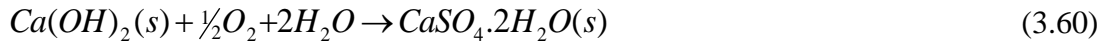
$$\text{Condition 3: } k_{gSO_2} p_{Ab} < \frac{k_{ISO_2}^0 D_B C_{B0}}{z D_A} \quad (3.58)$$

The absorption process is entirely controlled by the transport of A across the gas film (Eq. 5.178, p-149, Danckwerts, 1970). As it has already been determined from independent analysis that the system is strongly gas phase controlled, the rate of absorption is calculated using the expression,

$$R_A = k_g p_{Ab} \quad (3.59)$$

### 3.9 Mass balance verification in the reactor

The overall reaction occurring in the reactor for absorption of SO<sub>2</sub> in Ca(OH)<sub>2</sub> slurry may be written as,



Under steady state condition,

Moles of SO<sub>2</sub> absorbed and reacted in the bubble column reactor = Moles of hydrated lime dissolved and reacted.

This mass balance for SO<sub>2</sub> is made for the period from the start of the experiment to till the break through point is reached, and pH becomes less than 7. At and below this pH, SO<sub>2</sub> gets primarily absorbed in H<sub>2</sub>O, and under this condition, the reaction is known to be reversible and instantaneous.

Under steady state condition,

$$\begin{aligned} \text{Moles of SO}_2 \text{ absorbed} \\ = \frac{(Q_{gtot}) (1000/60)(C_{SO_2in} - C'_{SO_2out})}{RT} \times 10^{-6} \text{ atm/ppm} \times \Delta t \end{aligned} \quad (3.61)$$

here,  $Q_{gtot}$  has the unit of lpm and

$C'_{SO_2out}$  is the concentration of SO<sub>2</sub> in exit gas at steady state in ppm.

$$\begin{aligned} \text{Mass of lime reacted} &= M_B \cdot (\text{moles of lime reacted}) \\ &= M_B \cdot (\text{moles of SO}_2 \text{ reacted}) \end{aligned} \quad (3.62)$$

Alternatively, one can calculate moles of SO<sub>2</sub> absorbed using the instantaneous experimental data as,

$$\text{Moles of SO}_2 \text{ absorbed} = \int_0^{t_{bt}} \frac{(Q_{gtot}) (1000/60)(C_{SO_2in} - C_{SO_2out}) \times 10^{-6}}{RT} dt \quad (3.63)$$

where,  $t_{bt}$  = breakthrough time (time at which pH of slurry just attained a neutral value), s

$$Q_{gtot} = \text{total inlet gas flow rate, m}^3/\text{s}$$

### APPENDIX 3A

#### 3A.1 SINGLE REACTION PLANE MODEL FOR GAS ABSORPTION CALCULATION

A single reaction plane model for gas absorption calculation was proposed by Ramachandran and Sharma (1969). An attempt was made to use this simple model for estimation of the rate of gas absorption for present experimental conditions. However, it was observed that the model assumes no gas-side resistance. Additionally, it was found that one can get a positive value of the rate of absorption only if the solids loading is very high and  $\rho_{\text{solid}} = 1$ .  $\rho_{\text{Ca(OH)}_2}$  being 2.21, this model equations could not be used for calculation. However, the detail formulation is shown below.

##### Modeling of a slurry-bubble column reactor

Unsteady state material balance equation for component *A* in a semi-batch reactor may be written as,

$$\frac{\partial C_A}{\partial t} = D_A \frac{\partial^2 C_A}{\partial x^2} - k_{sl} A_p C_{B0} \quad (3A.1)$$

where  $C_A$  is concentration of *A* in the film

For the instantaneous reaction, there being no accumulation of *A* within the film, material balance equation (1) reduces to

$$D_A \frac{d^2 C_A}{dx^2} - k_{sl} A_p C_{B0} = 0 \text{ at } 0 \leq x \leq \lambda \quad (3A.2)$$

Similarly, the material balance equation for component *B* is

$$\frac{\partial C_B}{\partial t} = D_B \frac{\partial^2 C_B}{\partial x^2} + k_{sl} A_p (C_{B0} - C_B) \quad (3A.3)$$

where  $C_B$  is concentration of *B* in the film

Following a similar reason as for *A*, the reduced form of equation (3A.3) is rewritten as,

$$D_B \frac{d^2 C_B}{dx^2} + k_s A_p (C_{Bs} - C_B) = 0 \text{ at } \lambda \leq x \leq \delta \quad (3A.4)$$

The boundary condition for the solution of equation (3A.2) and (3A.4) are,

$$\text{at } x=0, C_A = C_{Ai}, -D_A \left[ \frac{dC_A}{dx} \right]_{x=0} = R_A \quad (3A.5)$$

$$\text{at } x=\lambda, C_A = C_B = 0, -D_A \left[ \frac{dC_A}{dx} \right]_{x=\lambda} = -D_B \left[ \frac{dC_B}{dx} \right]_{x=\lambda} \quad (3A.6)$$

$$\text{at } x=\delta, C_B = C_{B0} \quad (3A.7)$$

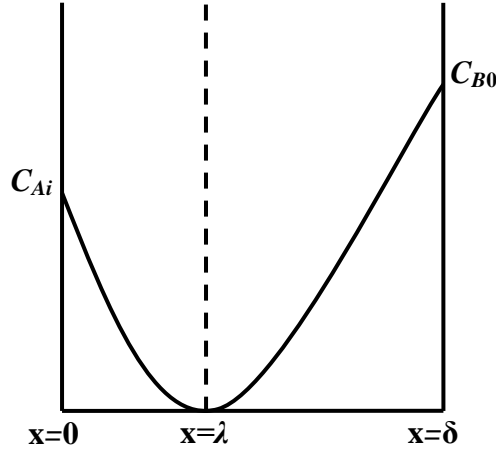


**Figure 3A.1 Concentration profile for the instantaneous reaction**

Solution of equation (3A.2) subject to boundary conditions (3A.5) and (3A.6) is obtained as,

$$C_A = C_{Ai} \left[ 1 - \frac{x}{\lambda} \right] - \left( \frac{k_{sl} A_P C_{B0}}{2D_A} \right) x(\lambda - x) \quad (3A.8)$$

Solution of equation (4) subject to boundary condition (3A.6) and (3A.7) is obtained as

$$C_B = C_{B0} \left[ 1 - \frac{\text{Sinh} \sqrt{\frac{k_{sl} A_P}{D_B}} (\delta - x)}{\text{Sinh} \sqrt{\frac{k_{sl} A_P}{D_B}} (\delta - \lambda)} \right] \quad (3A.9)$$

Specific rate of chemical reaction,  $R$

$R$  can be calculated by using equation (3A.5) as follows:

Differentiating equation (3A.8) with respect to  $x$ , we get

$$\frac{dC_A}{dx} = C_{Ai} \left[ -\frac{1}{\lambda} \right] - \left( \frac{k_{sl} A_P C_{B0}}{2D_A} \right) (\lambda - 2x) \quad (3A.10)$$

$$\left[ \frac{dC_A}{dx} \right]_{x=0} = C_{Ai} \left[ -\frac{1}{\lambda} \right] - \left( \frac{k_{sl} A_P C_{B0}}{2D_A} \right) (\lambda) \quad (3A.11)$$

Substituting equation (3A.11) in equation (3A.5), we get

$$R = -D_A \left[ \frac{dC_A}{dx} \right]_{x=0} = \left[ \frac{D_A C_{Ai}}{\lambda} \right] + \left( \frac{k_{sl} A_P C_{B0}}{2} \right) (\lambda) \quad (3A.12)$$

For calculation of reaction rate R using concentration profile for B, equation (3A.6) can be used as follows;

$$\text{i.e. } -D_A \left[ \frac{dC_A}{dx} \right]_{x=\lambda} = -D_B \left[ \frac{dC_B}{dx} \right]_{x=\lambda}$$

using equation (10)

$$\begin{aligned} -D_A \left[ \frac{dC_A}{dx} \right]_{x=\lambda} &= \left[ \frac{D_A C_{Ai}}{\lambda} + \left( \frac{k_{sl} A_P C_{B0}}{2} \right) (\lambda - 2x) \right]_{x=\lambda} \\ &= \left[ \frac{D_A C_{Ai}}{\lambda} + \left( \frac{k_{sl} A_P C_{B0}}{2} \right) \lambda - \left( \frac{k_{sl} A_P C_{B0}}{2} \right) 2x \right]_{x=\lambda} \\ &= R_A + k_{sl} A_P C_{B0} \lambda \end{aligned} \quad (3A.13)$$

Differentiating equation (3A.9) with respect to  $x$  and substituting  $x=\lambda$ , we get

$$\left[ \frac{dC_B}{dt} \right]_{x=\lambda} = C_{B0} \sqrt{\frac{k_{sl} A_P}{D_B}} \coth \sqrt{\frac{k_{sl} A_P}{D_B}} (\delta - \lambda) \quad (3A.14)$$

Using equation (6), (13) and (14)

$$\begin{aligned} R_A &= C_{B0} \sqrt{D_B k_{sl} A_P} \coth \sqrt{\frac{k_{sl} A_P}{D_B}} (\delta - \lambda) + C_{B0} k_{sl} A_P \lambda \\ &= \left[ \frac{D_A C_{Ai}}{\lambda} \right] + \left( \frac{k_{sl} A_P C_{B0}}{2} \right) (\lambda) \end{aligned} \quad (3A.15)$$

The total surface area of particles,  $A_p$ , can be calculated by the Eqn. (3.45).

*Condition for instantaneous reaction (Danckwerts, P. V., 1970)*

For the case of transient absorption into a quiescent liquid, the condition for the instantaneous reaction is

$$\frac{Q_o}{2C_{Ai}} \sqrt{\frac{\pi}{D_A t}} \left\langle \left\langle 1 + \frac{C_{B0}}{zC_A^*} \sqrt{\frac{D_B}{D_A}} \right. \right. \quad (3A.i)$$

Here,  $Q_o$  is the amount of gas which is absorbed per unit area in time  $t$  if the reactant in the neighbourhood of the surface retained its bulk concentration  $C_{BS}$  instead of becoming depleted by the reaction. The analogous expression for the absorption into an agitated liquid is

$$\frac{R_o}{k_l C_{Ai}} \left\langle \left\langle 1 + \frac{C_{B0}}{zC_{Ai}} \sqrt{\frac{D_B}{D_A}} \right. \right. \quad (3A.ii)$$

Where  $R_o$  is the rate at which gas would be absorbed if there were no depletion. Thus in the case of fast irreversible  $m, n^{\text{th}}$  order reaction we have for the quiescent liquid:

$$Q_o = C_{Ai} t \sqrt{\left\{ \frac{2k_{mn}}{(m+1)} (C_{Ai})^{m-1} (C_{B0})^n D_A \right\}} \quad (3A.iii)$$

And the condition for the instantaneous reaction is

$$\sqrt{\left\{ \frac{\pi k_{mn}}{2(m+1)} (C_{Ai})^{m-1} (C_{B0})^n \right\}} \left\langle \left\langle 1 + \frac{C_{B0}}{2C_{Ai}} \sqrt{\frac{D_B}{D_A}} \right. \right. \quad (3A.iv)$$

For the agitated liquid, we have

$$R_o = C_{Ai} \sqrt{\left\{ \frac{2k_{mn} (C_{Ai})^{m-1} (C_{B0})^n D_A}{(m+1)} \right\}} \quad (3A.v)$$

Condition (ii) becomes

$$\frac{1}{k} \sqrt{\left\{ \frac{2k_{mn} (C_{Ai})^{m-1} (C_{B0})^n D_A}{(m+1)} \right\}} \left\langle \left\langle 1 + \frac{C_{B0}}{zC_{Ai}} \sqrt{\frac{D_B}{D_A}} \right. \right. \quad (3A.vi)$$

If the above condition is satisfied, then the entire reaction occurs in the film. There being no accumulation of  $A$  and  $B$  in the film.

**APPENDIX 3B**

**Table 3B.1 Enhancement factor expressions based on film, penetration and surface renewal theories:**

Author	Mass Transfer Theory	Reaction scheme	Reaction plane Model	Expression for Enhancement factor, $E_i$
Olander, D. R. (1960)	Film theory	$A + B \rightarrow C$	One reaction plane	$E_{inst} = 1 + \frac{D_B}{D_A} \cdot \frac{C_{B0}}{C_{Ai}}$
Ozturk and Shah (1985)	Penetration theory	$A + B \rightarrow C$	One reaction plane	$E_{inst} = 1 + \sqrt{\frac{D_A}{D_B}} \left( 1 + \frac{D_B}{zD_A} \cdot \frac{C_{B0}}{C_{Ai}} \right)$
Chang and Rochelle (1981)	Surface Renewal theory	$A + B \rightarrow C$	One reaction plane	$E_{inst} = 1 + \sqrt{\frac{D_B}{D_A}} \cdot \frac{C_{B0}}{C_{Ai}}$
Vazquez et al. (1988)	Surface Renewal theory	$SO_2 + 2OH^- \rightarrow SO_3^{2-}$	One reaction plane	$E_{inst} = 1 + \frac{1}{2} \sqrt{\frac{D_{OH^-}}{D_{SO_2}}} \cdot \frac{C_{OH^-}^0}{C_{SO_2}^i}$

## APPENDIX 3C

## 3C.1 Axial Dispersion Model

An axial dispersion model is used to describe a non-ideal tubular reactor. Axial dispersion of the material analogous to analogy to Fick's law of diffusion is assumed to be superimposed on the flow through a tubular reactor. In addition to transport by bulk flow,  $u_g A_c C_{SO_2}$ , molecular and convective diffusion of every component through

the entire cross section of the reactor occurs at a rate equal to  $-D_g (A_c) \frac{\partial C_{SO_2}}{\partial z}$ .

Convective diffusion signifies either Aris-Taylor dispersion in laminar flow reactors or turbulent diffusion resulting from turbulent eddies.

The molar flow rate  $f_{SO_2}$  of the gas-phase component by both convection and dispersion is written (Fogler, H.S., 1999) as

$$f_{SO_2} = -D_g A_c \frac{\partial C_{SO_2}}{\partial z} + u_g A_c f_{SO_2} \quad (3C.1)$$

where,  $D_g$  is the effective dispersion coefficient ( $m^2/s$ ) and  $u_g$  ( $m/s$ ) is the superficial gas velocity. Correlations for the dispersion coefficients in both liquid and gas systems have been shown in Table 3C.2.

A mole balance on the gas-phase component yields,

$$-\frac{\partial f_{SO_2}}{\partial z} = A_c \frac{\partial C_{SO_2}}{\partial z} \quad (3C.2)$$

Substituting for  $F_T$  from and dividing by the cross-sectional area  $A_c$ , we have

$$\frac{\partial C_{SO_2}(t)}{\partial t} = D_g \frac{\partial^2 C_{SO_2}}{\partial Z^2} - \frac{u_g}{\varepsilon_g} \frac{\partial C_{SO_2}(t)}{\partial z} \quad (3C.3)$$

In the presence of absorption from the gas phase, eqn. (3C.3) takes the form,

$$\frac{\partial C_{SO_2}(t)}{\partial t} = D_g \frac{\partial^2 C_{SO_2}}{\partial Z^2} - \frac{u_g}{\varepsilon_g} \frac{\partial C_{SO_2}(t)}{\partial z} - \frac{k_l a}{\varepsilon_g} [HC_{SO_2}(t) - C_l(t)] \quad (3C.4)$$

Similarly, writing a mass balance on the dissolving component in the liquid phase, one obtains



$$\frac{\partial C_{so_2}(t)}{\partial t} = D_l \frac{\partial^2 C_{so_2}}{\partial Z^2} + \frac{k_l a}{\varepsilon_l} [HC_{so_2}(t) - C_l(t)] \quad (3C.5)$$

These fluctuations in concentration can result from different flow velocities, pathways and from molecular and turbulent diffusion.

Eqn. (3C.5) is first put into dimensionless form and using the Danckwerts boundary condition in dimensionless form, it is solved for exit trace concentration as a function of dimensionless time  $\Theta=t/\tau$  and then relate  $D_g$ ,  $\sigma^2$  and  $\tau$ . Using a pulse tracer experiment, the effluent trace concentration measured as function of time. The mean residence time and variance are calculated from these data and these are used to calculate  $D_g$ .

**3C.2 Reported correlation for calculating gas phase mixing in bubble columns**

**Table 3C.2.1 - Reported experimental studies on gas phase mixing in bubble columns**

Author	System	Column diameter, D (cm)	Superficial gas velocity (cm/s)	Dispersion coefficient, $D_g$ (m <sup>2</sup> /s)	Correlation
Towell and Ackerman (1972)	Air/ H <sub>2</sub> O	40.6-106	1.62-3.4	0.02-0.14	$D_g = 19.7d_c^2u_g$
Pilhofer et al. (1978)	Air/ H <sub>2</sub> O N <sub>2</sub> /n-Propanol Air/glycol	10	1-20	0.003-1	$D_g = 2.64u_s^{3.56}$
Field and Davidson (1980)	Air/ H <sub>2</sub> O	320	4.5 -5.5	1-8	$D_g = 56.4d_c^{1.33} \left( \frac{u_G}{\epsilon_g} \right)^{3.56}$
Mangartz and Pilhofer (1981)	Air / H <sub>2</sub> O N <sub>2</sub> /n-Propanol Air/glycol	10	1.5-10	0.01-1	$D_g = 50d_c^{1.5} \left( \frac{u_G}{\epsilon_g} \right)^3$
Wachi et al. (1990)	Air/ H <sub>2</sub> O	20-50	2.9-45.6	0.02-5	$D_g = 20d_c^{3/2}u_g$

### 3C.3 Sample calculation for dispersion coefficient and Peclet number for gas and liquid phase for MLIL and Ca(OH)<sub>2</sub> slurry

#### (a) Gas hold-up and distribution coefficient in bubble column when MLIL is used as a solvent

Gas hold-up is calculated by using the expression given by Hughmark, G.A. (1967):

$$\varepsilon_g = \frac{1}{2 + \frac{0.35}{u_G} \left( \rho_L \frac{\sigma}{72} \right)^{1/3}}$$

here, density of MLIL,  $\rho_{IL} = 1.172 \text{ g/cm}^3$

Surface tension of liquid,  $\sigma_{IL} = 43.81 \text{ dyne/cm}$

Superficial velocity of gas,  $u_G = 3.85 \times 10^{-2} \text{ m/s}$

$$\varepsilon_g = \frac{1}{2 + \frac{0.35}{3.85 \times 10^{-2}} \left( 1.172 \times \frac{43.81}{72} \right)^{1/3}} = 0.098$$

Gas hold-up was experimentally determined is equal to 0.1

#### (i) Gas phase mixing behavior is calculated by using the expression given by Mangartz and Pilhofer (1981):

$$D_g = 50 d_C^{1.5} \left( \frac{u_G}{\varepsilon_g} \right)^3$$

here,  $d_C = 0.105 \text{ m}$

$u_G = 3.85 \times 10^{-2} \text{ m/s}$

$\varepsilon_g = 0.1$

$$D_g = 50 \times 0.105^{1.5} \left( \frac{3.85 \times 10^{-2}}{0.1} \right)^3$$

$$D_g = 0.097 \text{ m}^2/\text{s}$$

Calculation for gas-phase Peclet number

$$Pe_g = \frac{h_D u_G}{D_g \varepsilon_g}$$

$h_D = \text{Dispersion height, m}$

$$Pe_g = \frac{3.19 \times 10^{-2} \times 3.85 \times 10^{-2}}{0.097 \times 0.1} = 0.127$$

The calculated value of Peclet number using the correlation (Table 3C.2) given by Wachi et al., (1990) comes out to be 0.472

Calculation for liquid-phase dispersion coefficient

Liquid phase dispersion coefficient is calculated by the correlation given by Meikap et al., (2002):

$$D_l = 0.678d_c^{1.4}u_G^{0.3} \quad \text{where, } d_c^{1.4}u_G^{0.3} < 400$$

$$d_c^{1.4}u_G^{0.3} = 0.105^{1.4} \times 3.85 \times 10^{-2}$$

$$d_c^{1.4}u_G^{0.3} = 0.016$$

$$D_l = 0.678 \times 0.016 = 0.0108 \text{ m}^2/\text{s}$$

Calculation for liquid-phase Peclet number

$$Pe_l = \frac{u_G d_c}{D_l}$$

$$Pe_l = \frac{3.85 \times 10^{-2} \times 0.105}{0.0108}$$

$$Pe_l = 0.374$$

**(b) Dispersion coefficient in Ca(OH)<sub>2</sub> slurry**

Gas-phase dispersion coefficient is calculated by using the expression given by Mangartz and Pilhofer 1981:

$$D_g = 50d_c^{1.5} \left( \frac{u_G}{\epsilon_g} \right)^3$$

$$\epsilon_g = 0.365 \text{ (experimental data)}$$

$$D_g = 50 \times 0.105^{1.5} \left( \frac{3.85 \times 10^{-2}}{0.365} \right)^3 = 2.0 \times 10^{-3} \text{ m}^2/\text{s}$$

Calculation for gas-phase Peclet number

$$Pe_g = \frac{h_D u_G}{D_g \epsilon_g}$$

$$\text{Dispersion height, } h_D = 3.96 \times 10^{-2} \text{ m}$$

$$Pe_g = \frac{3.96 \times 10^{-2} \times 3.85 \times 10^{-2}}{2.0 \times 10^{-3} \times 0.365} = 2.08$$

Calculation for liquid-phase dispersion coefficient

Liquid phase dispersion coefficient is calculated by the correlation given by Deckwer et al. 1974:

$$D_l = 0.678 d_c^{1.4} u_G^{0.3} \quad \text{where, } d_c^{1.4} u_G^{0.3} < 400$$

$$d_c^{1.4} u_G^{0.3} = 0.105^{1.4} \times 3.85 \times 10^{-2}$$

$$d_c^{1.4} u_G^{0.3} = 0.016$$

$$D_l = 0.678 \times 0.016 = 0.0108 \text{ m}^2/\text{s}$$

Calculation for liquid-phase Peclet number

$$Pe_l = \frac{u_G d_c}{D_l}$$

$$Pe_l = \frac{3.85 \times 10^{-2} \times 0.105}{0.0108} = 0.374$$

## APPENDIX 3D

**3D.1 Chemical method of determining the concentration of dissolved oxygen (Winkler Method)**

Winkler method was used to determine dissolved oxygen concentration for the determination of liquid-side volumetric mass-transfer coefficient. The detail of reagents and procedure are discussed below:

Reagents required:

1. Manganous sulphate (GR) solution- 48 g of  $MnSO_4 \cdot 4H_2O$  is dissolved in water and the solution is diluted to 100 ml.
2. Alkaline iodide- Na- azide (LR) solution- 50 gm  $NaOH$ , 15 gms  $KI$  and 1 gm  $NaN_3$  are dissolved in water and the solution is diluted to 100 ml.
3. Concentrated  $H_2SO_4$ .
4.  $Na_2S_2O_3$  (GR) solution- 6.205 gm (approx.) of  $Na_2S_2O_3$  is dissolved in 1 lit of water so that the solution is approximately 0.025 (N). The solution is to be standardized for every experiment in separate days.
5. Starch (LR) indicator solution- 0.5 gms of starch, 0.001 gm of  $HgI_2$  are triturated with 30 ml of cold water and it is slowly poured with stirring into 70 ml of boiling water. It is boiled for 3 minutes. The solution is allowed to cool and the supernatant clear liquid is decanted off.

Procedure:

Three stoppered bottles of 300 ml capacity are filled with sample and 1.5 ml  $MnSO_4$  alkaline iodide- Na- azide solution are added keeping the tip of the pipette in each case well below the surface of the liquid and the stoppers are replaced such that air bubbles from outside not enter into bottle. The contents are thoroughly mixed and allowed to stand. Mixing is repeated again and allowed to settle.

When further settling produces at least 100 ml of clear supernatant, the stoppers are removed carefully and 2 ml of concentrated  $H_2SO_4$  are added immediately by running the acid down the neck of the bottle, restoppered and mixed well to ensure uniform distribution of iodine in the bottle.

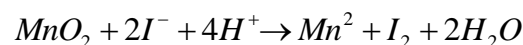
200 ml of the solution is taken and titrated immediately against standard  $Na_2S_2O_3$  solution adding 1 ml of starch indicator solution when the color becomes pale yellow and the titration is completed to the disappearance of the blue color. The error due to the displacement of sample by reagents is taken to be insignificant.

Reactions:

$MnSO_4$  is converted into white ppt. of  $Mn(OH)_2$ . Dissolved  $O_2$  oxidises some of the divalent  $Mn^{2+}$  to the tetravalent  $Mn^{4+}$  state and forms a brown ppt. of  $MnO_2$

Thus the dissolved  $O_2$  is converted into chemically oxide form.

In acidic medium  $MnO_2$  reacts with  $I^-$  to produce  $I_2$  and it is reduced to  $Mn^{++}$  state producing a viole solution.



Under acidic condition soluble and colorless.

1 lit 1(N)  $Na_2S_2O_3$  = 1 lit 1 (N)  $I_2$  = 1 lit 1(N)  $O_2$

Or 1 lit N/40  $Na_2S_2O_3$  = 1 lit 1 N/40  $I_2$  = 1 lit N/40  $O_2$

$$\text{Or, } \frac{117}{40} \text{ gm } I_2 = \frac{8}{40} \text{ gm } O_2 = \frac{1}{5} \text{ gm } O_2$$

$$\therefore 1 \text{ ml. N/40} = \frac{1}{5 \times 1000} \text{ gm } O_2 = \frac{1}{5} \text{ mg } O_2$$

$$\therefore V \text{ ml N/40 } Na_2S_2O_3 \text{ solution} = \frac{V}{5} \text{ mg } O_2$$

If 1 ml N/40 is required for 200 ml sample.

Then 200 ml sample contains  $\frac{1}{5} \text{ mg } O_2$

Or 1000 ml sample contains  $1 \text{ mg } O_2$

If V ml N/40 is required for 200 ml sample, then DO = V mg/lit.

General Case: From (1) 1 ml 1(N)  $Na_2S_2O_3$  =  $\frac{40}{5} \text{ mg } O_2$  in V ml sample =  $8 \text{ mg } O_2$  in

V ml sample.

Performances of a bubble column for desulfurization of simulated gaseous mixtures have been studied using various gas-liquid and gas-liquid-solid systems in relation to different variables/parameters. The objective is that the experimental results will justify and facilitate further studies in pilot plant scale, and, subsequent application in industries. In the following sections the details of the experimental setups and materials used, experimental procedure, methods of chemical analyses and sample calculations have been presented. The contents presented in this chapter may be broadly classified into four sections, (i) General considerations that narrate an overview of this chapter, (ii) various gas-liquid (especially ionic liquid) systems (iii) gas-liquid-solid systems used for desulfurization studies and (iv) additional experiments performed for determination of parameter values.

#### **4.1 An overview of the experiments performed**

Details of experimental studies undertaken in this work have been described in the following three sections with the section heading: gas-liquid systems, gas-liquid-solid systems and estimation of parameter values. Various liquid absorbents used for screening the performances of a bubble column reactor for selection of the most suitable solvent are, H<sub>2</sub>O, DMSO, NaClO and a series of hydroxyl ammonium ionic liquids. On the other hand, for the gas-liquid-solid systems, aqueous slurries of Ca(OH)<sub>2</sub> and CaCO<sub>3</sub> containing sparingly soluble fine suspended particles have been employed as absorbent. For experiments and discussion of the experimental results, values of the system parameters are essentially required. Some of these important parameters are, liquid-side mass-transfer coefficient, gas-side mass-transfer coefficient, gas holdup, liquid viscosity, size distribution of particles in the slurry reactor, etc. These are discussed in detail following the description of major experiments.

In the first of these sections, the details of experimental setups, materials used, the experimental procedure for the synthesis of ILs, absorption studies of SO<sub>2</sub> in these liquids and regeneration of the solvents have been presented.



## 4.2 Gas-liquid system

### 4.2.1 Ionic liquids – synthesis, the application as an absorbent for SO<sub>2</sub> removal and regeneration

The following experiments were performed for absorption studies of SO<sub>2</sub> in ILs:

- a. synthesis of ILs
- b. absorption of SO<sub>2</sub> in ILs: effects of
  - nature of cations and anions in ILs.
  - superficial velocity of gas
  - initial concentration of SO<sub>2</sub> in feed gas
  - volume of solvent charged into the reactor
- c. regeneration of exhausted ionic liquid

#### 4.2.1.1 Synthesis of ionic liquid

**Experimental Setup:** The experimental setup used for the synthesis of ILs is shown in Figure 4.1. It comprised of a two-necked round bottom flask of 1000 mL capacity, a dropping funnel of capacity 200 mL, a water-cooled condenser, a water bath, a peristaltic pump, a magnetic stirrer

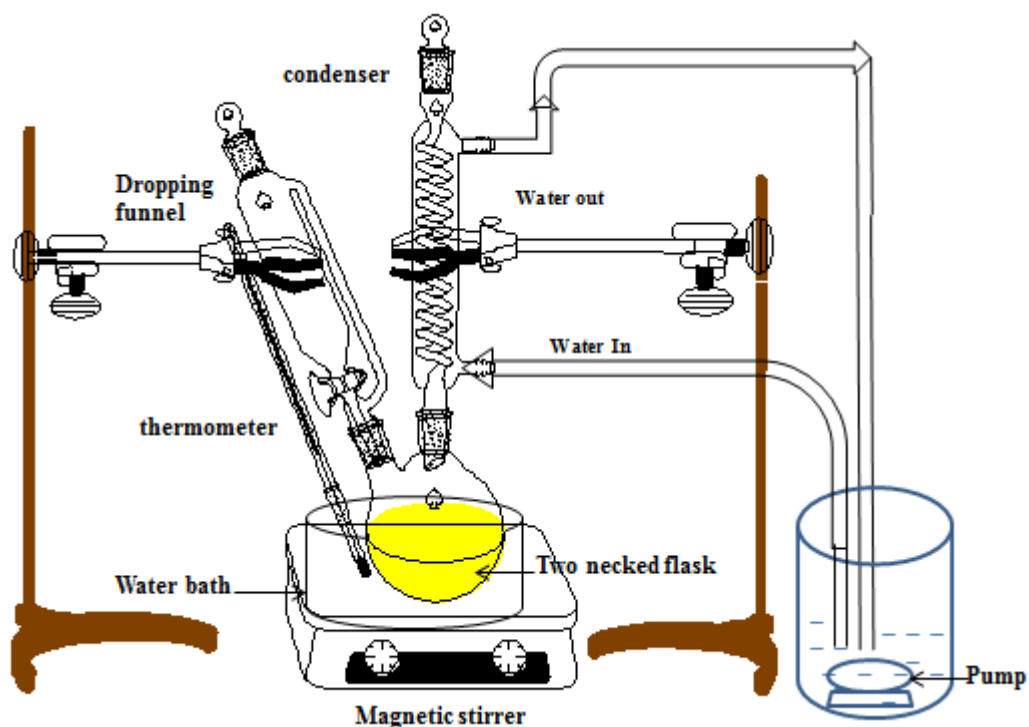


Figure 4.1 Line diagram of the experimental setup for the synthesis of Ionic liquids

and a thermometer to measure the temperature of the water bath. A photograph of the experimental setup used for the synthesis of the ionic liquid is shown in Figure 4.2.

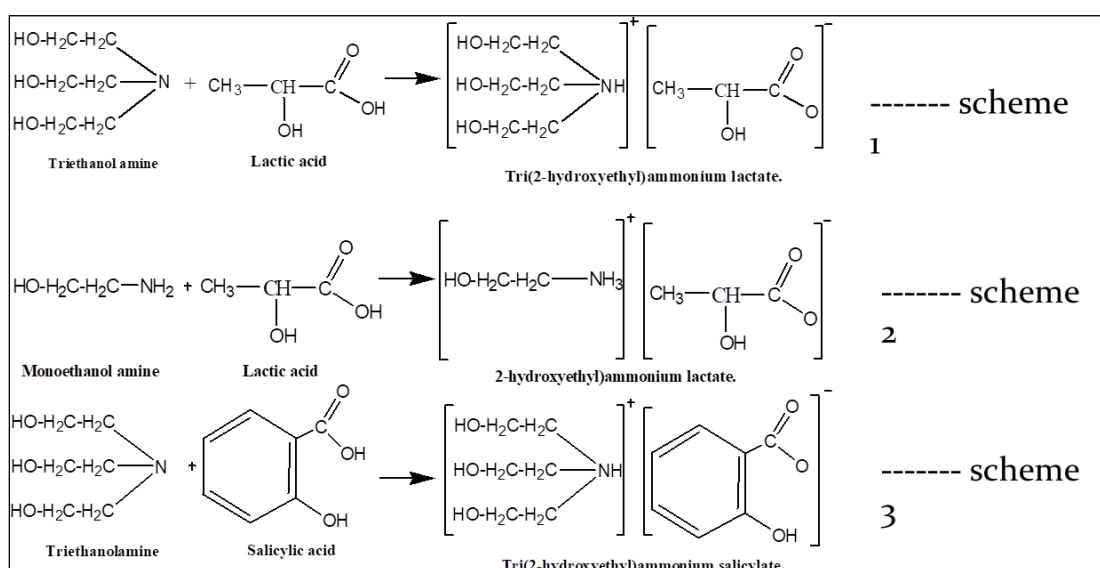
**Materials used:** The reagents used for the synthesis of ionic liquids were mono-ethanolamine and tri-ethanolamine as bases and DL-lactic acid (88%), salicylic acid or tartaric acid as the other reagent in the acid-base reaction. Ethanol was used as the solvent. All these reagents were of GR grade, make Merck India Ltd., Mumbai.



**Figure 4.2 Photograph of the experimental setup for the synthesis of ionic liquids**

**Procedure:** A series of hydroxyl ammonium ionic liquids were synthesized by neutralization of mono- or tri-ethanolamine with lactic- or salicylic acid using ethanol as the solvent. A scaling-up of the procedure reported by Yuan et al., 2007 with some modification was followed in this study. The synthesis procedure of 2-hydroxyethylammonium lactate is described below and the reaction involved is shown

in scheme 2 below. One mole of mono-ethanolamine was dissolved in 200 mL of ethanol in a 1000 mL round bottom flask and mixed thoroughly with gentle shaking (Figure 4.1). The flask was placed in a water bath maintained at 303 K and connected to a reflux condenser. A dropping funnel of 500 mL capacity was filled with a solution containing 1 mol of lactic acid dissolved in 200 mL of ethanol and fitted to the other neck of the round bottom flask. The contents in the flask were stirred at 400 rpm using a magnetic stirrer and lactic acid solution from the funnel added drop wise to the reaction mixture in the flask over a period of about 120 min. Stirring was continued, and the reaction was allowed to occur for 2 hrs. more after complete addition of the acid solution.



**Scheme 1, 2 and 3 for the synthesis of ionic liquid (a) TLIL (b) MLIL (c) TSIL, respectively**

The contents were then transferred to a 2000 mL volumetric flask fitted with a ground glass joint stopper. This experiment was repeated until the required volumes of ionic liquid for conducting several experiments were synthesized. The composite liquid containing the solvent ethanol was subjected to separation of ethanol under vacuum using a *rotavapor*. This operation is very similar to the regeneration of exhausted ionic liquid and the latter will be described later in this section.

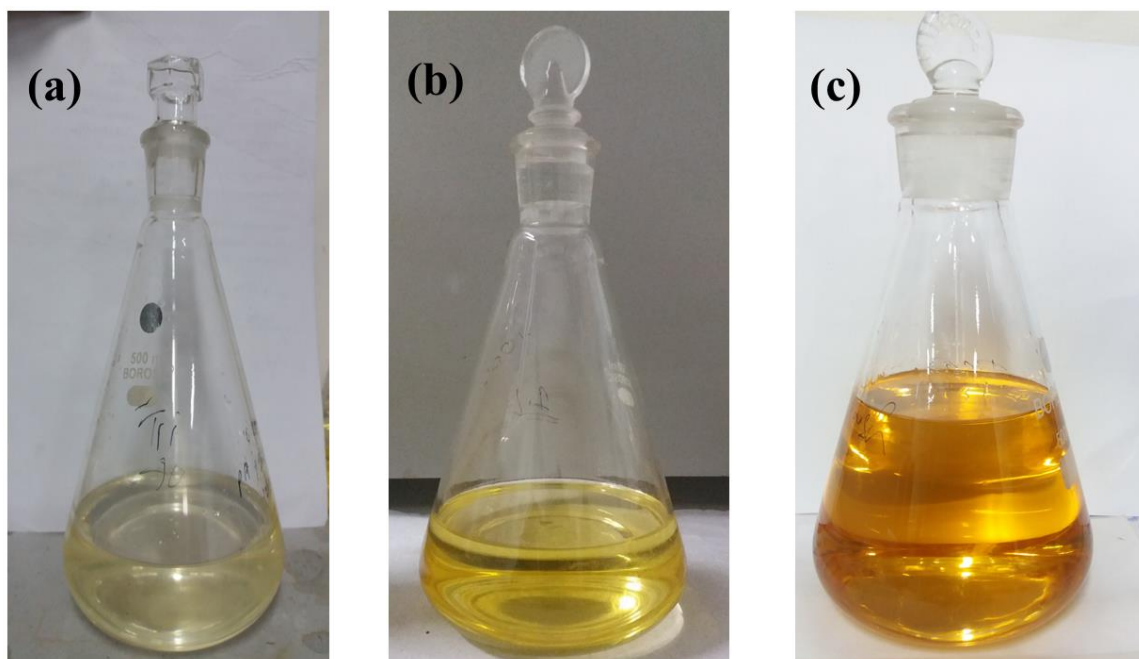


**Figure 4.3 Images of Synthesized IL (a) TLIL, (b) MLIL and (c) TSIL**

The similar procedure was followed for synthesis of the other ionic liquids. The synthesized ionic liquids were stored in stoppered volumetric flasks (Figure 4.3) for their physicochemical property evaluation and for conducting SO<sub>2</sub> absorption experiments.

**Table 4.1 Reagents and their corresponding ILs synthesized**

Base	Acid	Product
Triethanolamine	Lactic acid	Tri (2-hydroxyethyl)ammonium lactate (TLIL)
Monoethanolamine	Lactic acid	2- hydroxyethylammonium lactate (MLIL)
Triethanolamine	Salicylic acid	Tri (2- hydroxyethyl)ammonium salicylate (TSIL)
Monoethanolamine	Salicylic acid	2- hydroxyethyl ammonium salicylate

#### 4.2.1.2 Absorption studies of SO<sub>2</sub> using the synthesized ionic liquid as the solvent

**Setup** The setup used for the absorption of SO<sub>2</sub> from its mixture with air is shown schematically in Figure 4.4. It comprised of a glass column, SO<sub>2</sub> cylinder, air compressor, rotameter for air, rotameter for SO<sub>2</sub> and a mixer for SO<sub>2</sub> and air. The glass column, 0.74 m long and  $10.5 \times 10^{-2}$  m internal diameter were connected at the bottom to a glass cone with the help of flanges. A gas distributor plate,  $2.0 \times 10^{-3}$  m thick (Table 4.2) and made up of perspex was placed between these flanges. There were 31 holes of  $1.0 \times 10^{-3}$  m diameter and arranged in triangular pitch (Figure 4.5). A vacuum pump was used to remove exhaust gas from the glass column for feeding it to the neutralization tank. The top of the glass column was covered with a wooden lid and contains three ports: one for solvent feed inlet, kept closed at the time of reactor operation; the second for vent gas line connection to the vacuum pump and the third for exit gas sampling line connected to the SO<sub>2</sub> analyzer. A rubber gasket fitted to the wooden lid arrested any leakage of SO<sub>2</sub> from the column (Figure 4.6). A ZRJFAY36, Fuji, Japan make infrared SO<sub>2</sub> analyzer was used to measure the SO<sub>2</sub> concentration at the inlet to- and exit from the reactor. A photograph of the experimental setup is shown in Figure 4.7. The analyzer was calibrated periodically by using pure nitrogen for zero ppm and 4000 ppm calibrated SO<sub>2</sub> gas from a cylinder for setting 4000 ppm concentration in the analyzer.

**Table 4.2 Dimensions and materials of construction of bubble column**

##### **Glass column**

Material of construction: glass

Diameter of the column (I.D.):  $10.5 \times 10^{-2}$  m

Height of column: 0.74 m

##### **Gas distributor plate**

Material of construction: perspex

Thickness of plate:  $2.0 \times 10^{-3}$  m

Diameter of each hole:  $1.0 \times 10^{-3}$  m

Number of holes: 31

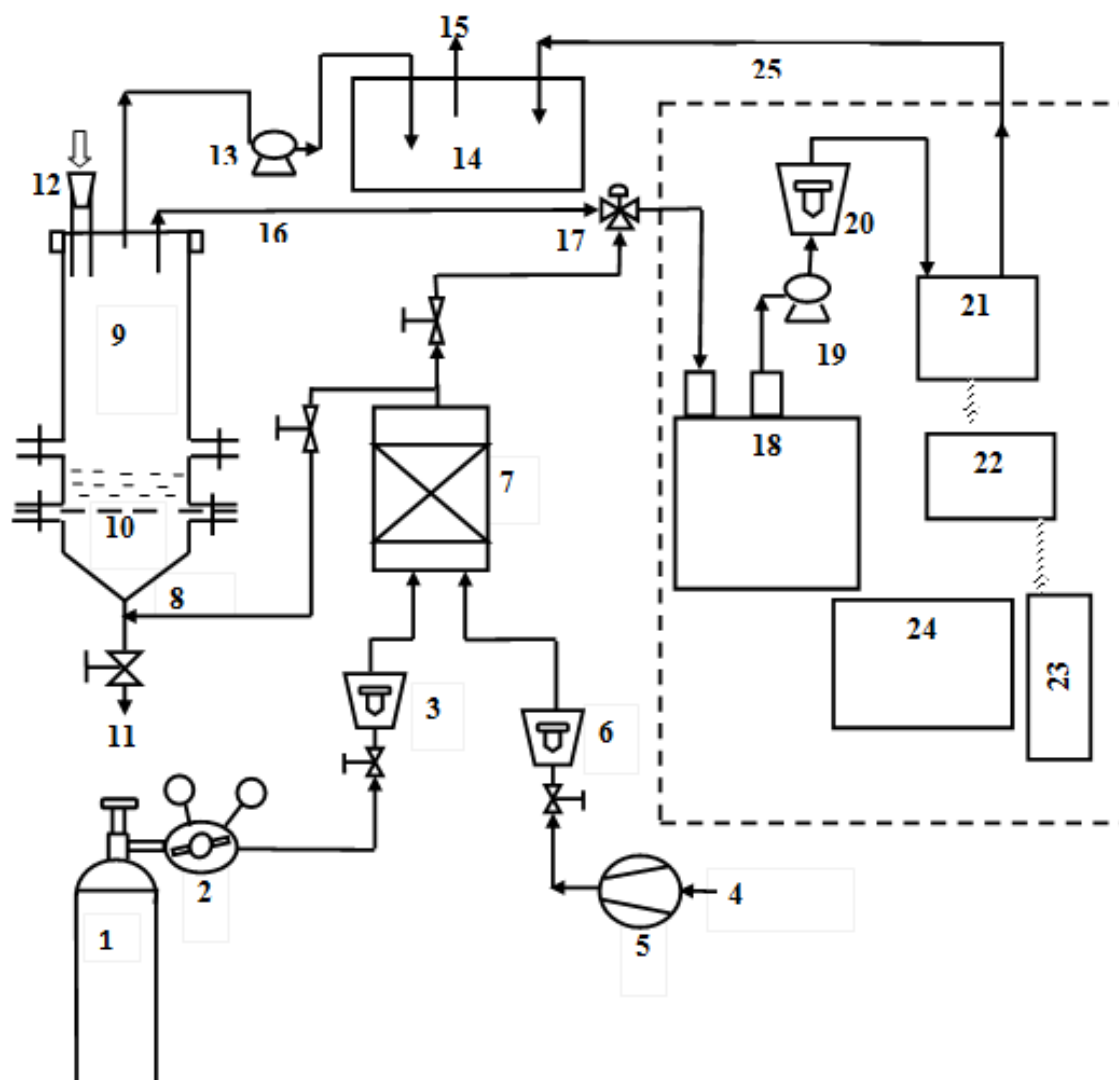
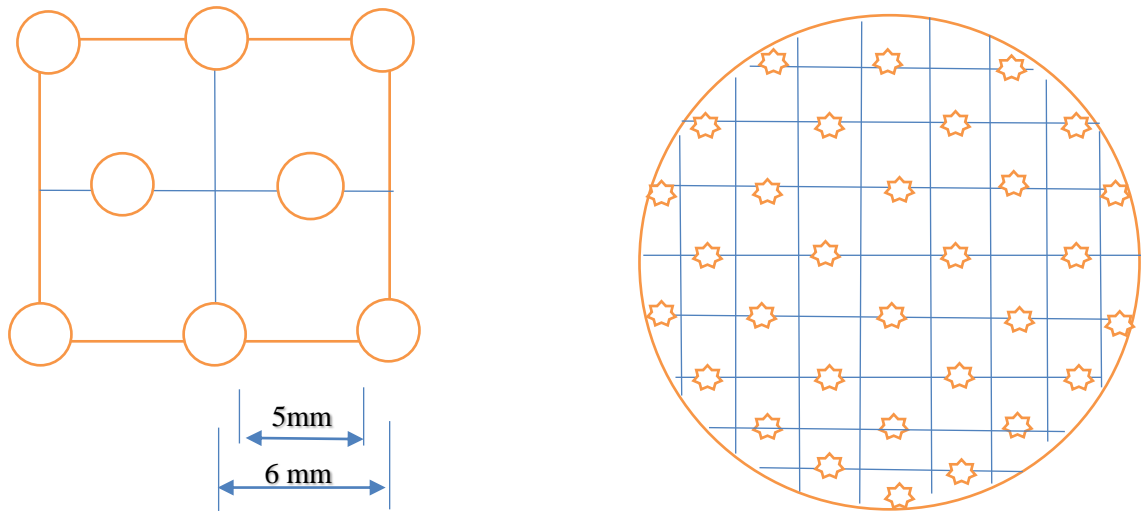


**Figure 4.4. Schematic line diagram of the experimental setup for desulfurization experiment** (1. Calibrated SO<sub>2</sub> cylinder; 2. High-pressure regulator; 3. Rotameter for calibrated SO<sub>2</sub> gas; 4. Air; 5. Compressor; 6. Rotameter for air; 7. Gas mixer; 8. Gas inlet line; 9. Glass column; 10. Gas distributor; 11. Drainage line; 12. Absorbent inlet; 13. Vacuum pump; 14. Neutralization tank; 15. Vent line; 16. Exit gas line for analysis; 17. Three-way valve; 18. Refrigerator; 19. Suction pump; 20. Rotameter; 21. SO<sub>2</sub> gas analyzer; 22. Data logger; 23. CPU; 24. Monitor)



☆ Indicates holes of dia.  $1 \times 10^{-3}$  m

Total plate area =  $132.73 \times 10^{-4}$  m<sup>2</sup>

Total holes area =  $1.71 \times 10^{-4}$  m<sup>2</sup>

**Figure 4.5. Details of gas distributor plate**

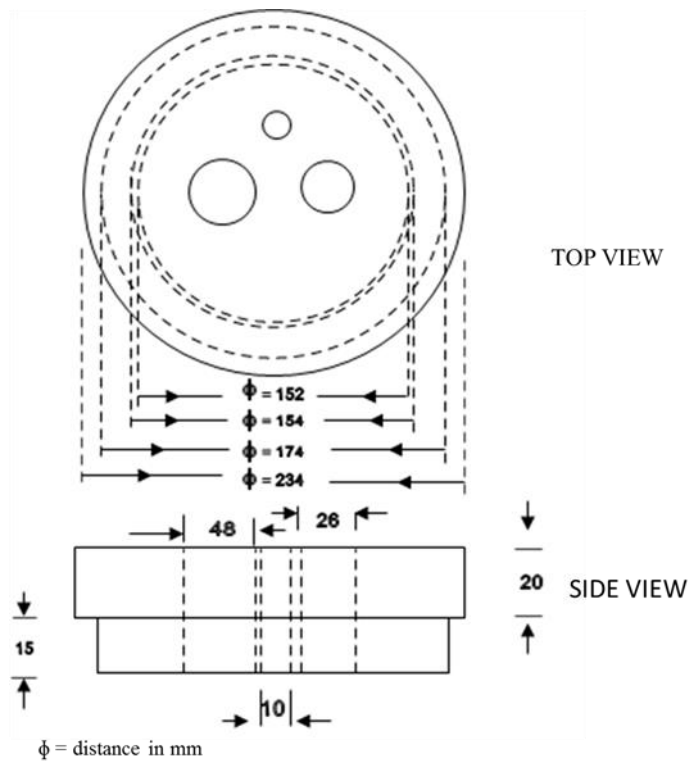


**Figure 4.6 Top and side view of the reactor-top enclosure with the material inlet and exit ports**

**Materials used:** The solute gas for absorption, 5000 ppm SO<sub>2</sub> in nitrogen and pure N<sub>2</sub> gas for purging of the SO<sub>2</sub> analyzer at the time of calibration (each being of Instrument Grade) were supplied by Dinesh Gases Pvt. Ltd., Jaipur. 4000 ppm calibrated SO<sub>2</sub> gas cylinder for calibration of the SO<sub>2</sub> analyzer was supplied by Alchemie Gases and Chemicals Pvt Ltd., Mumbai.

**Procedure:** In a typical run, at first the analyzer was allowed to warm up for the required period. The vacuum pump and the air compressor were switched on and the analyzer was then purged using nitrogen from an instrument grade nitrogen cylinder. Sulfur dioxide and air at the desired flow rate for a predetermined feed concentration of SO<sub>2</sub> was monitored by the respective calibrated rotameters were allowed to flow through the mixer and then into the reactor. When the flow rates of these gases became steady, fine adjustment of the rotameter readings for the desired inlet concentration of SO<sub>2</sub> into the reactor was made and the concentration displayed on the data logger was noted down. A definite volume of ionic liquid was poured carefully into the column through the feed inlet port and the latter closed



**Figure 4.7 Photograph of the experimental setup used for desulfurization of the gaseous mixture**

immediately with a rubber cork. Variation of exit concentration of sulfur dioxide displayed on the monitor indicated the progress of the reaction. Attainment of exit



SO<sub>2</sub> concentration equal to that of its inlet concentration indicated that the absorbent was completely exhausted. Gas inlets were closed, vacuum released and the exhausted solvent drained and stored in stoppard bottles for subsequent treatment. These experiments were repeated for the collection of experimental data for different feed gas flow rates and other variables studied in this work. Similar experiments were performed using TLIL and TSIL as absorbents.

Details of the experimental data collected, results of data analysis and its discussion are presented in Chapter 5.

#### 4.2.1.3 Removal of ethanol from virgin IL and regeneration of exhausted IL

**Apparatus:** For removal of the solvent (ethanol) and to obtain the regenerated IL, the setup used is shown in Figure 4.8. It comprised of a chiller, a vacuum release valve, a condenser, a receiving flask, a water bath, an evaporating flask, an impinger, a vacuum pump and a pressure gauge. A photograph of the experimental setup is shown in Figure 4.9.

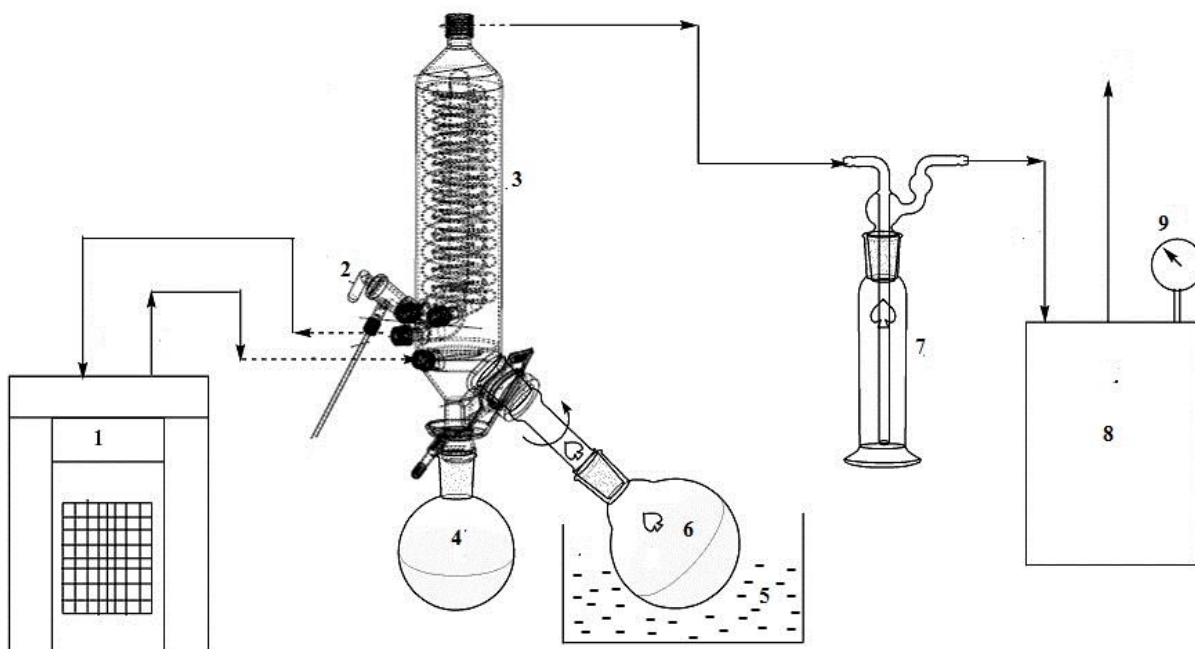


**Figure 4.8** A line diagram of the experimental setup for regeneration of exhausted ionic liquid (1-chiller, 2-vacuum release valve, 3-condenser, 4-receiving flask, 5-water bath, 6-evaporating flask, 7-impinger, 8-vacuum pump, 9-pressure gauge).

**Materials used:** Exhausted ionic liquids: Tri (2-hydroxyethyl)ammonium lactate (TLIL), 2- hydroxyethylammonium lactate (MLIL), Tri (2- hydroxyethyl)ammonium salicylate (TSIL), 2- hydroxyethyl ammonium salicylate with SO<sub>2</sub> absorbed into these liquids.

**Procedure:** The ionic liquid (IL) that was used for experiments and got exhausted by absorption of SO<sub>2</sub> was regenerated by subjecting it to desorption under vacuum (Figure 4.8). About 250 mL of exhausted IL was loaded into a 1000 mL round bottom flask, partially immersed in a water bath and connected to a rotary evaporator (BUCHI, Switzerland, Rotavapor R-210). Level of vacuum generated by the vacuum pump and the temperature of the water bath was gradually adjusted to 100 mbar and 303 K, respectively.

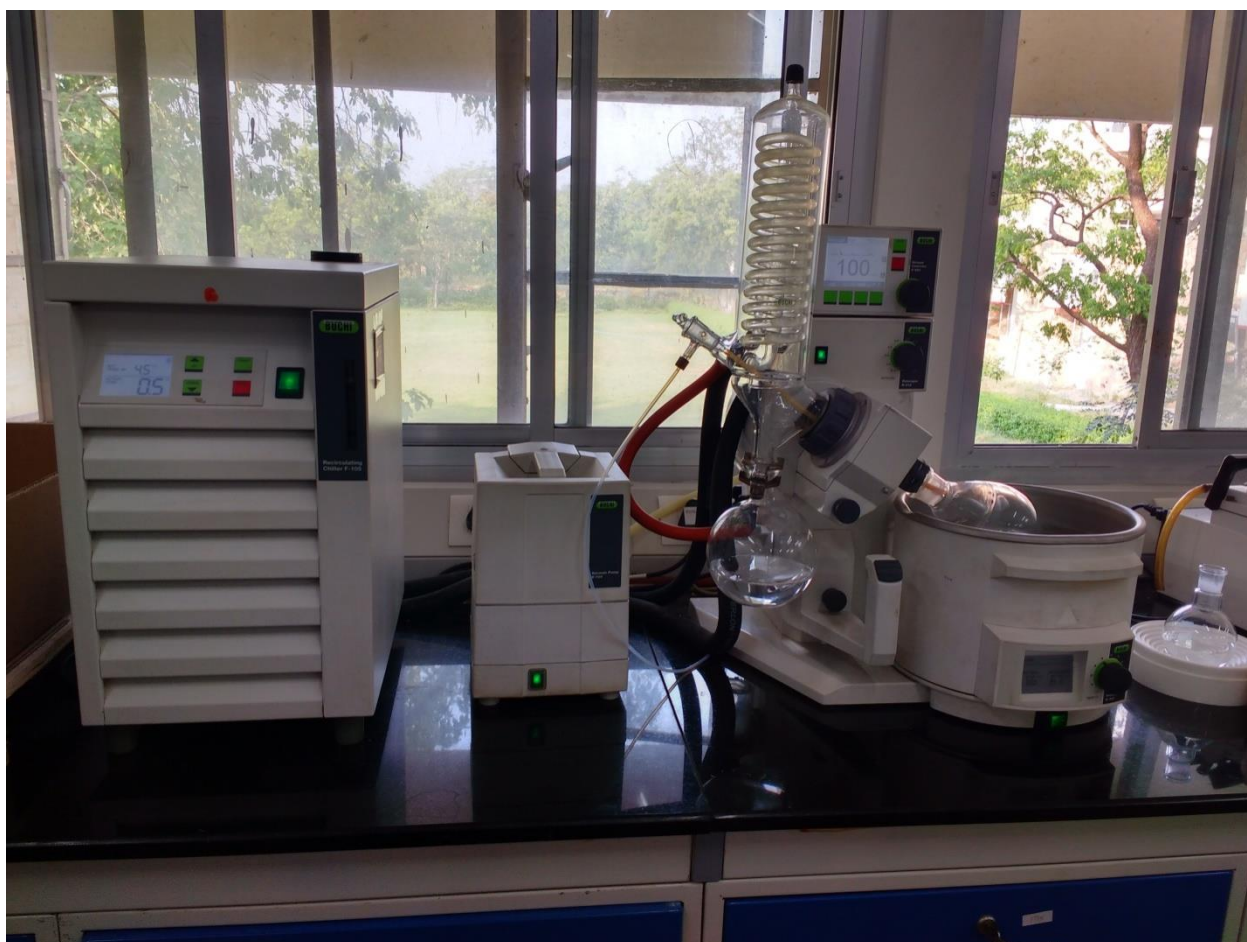


**Figure 4.9** Photograph of the experimental setup for regeneration of exhausted IL

The same procedure was followed for separation of ethanol from the newly synthesized ionic liquid during which ethanol vapor was condensed and collected in

the receiving flask; while at the time of regeneration of the exhausted ILs, the receiving flask remained dry. Application of vacuum was continued till the difference between the successive weights was negligibly small. The entire regeneration operation took about 40-45 min. At the end of separation of ethanol or desorption of SO<sub>2</sub>, valve (2) was opened to release the vacuum and then only the evaporating flask was detached from the system.

#### 4.2.2 SO<sub>2</sub> absorption experiments performed using other solvents

With the objective of finding a suitable solvent for SO<sub>2</sub> removal from flue gases, trial experiments were performed using the following solvents:

- a. aqueous solutions of NaClO and DMSO as the solvent, and
- b. pure water as the absorbent for a comparison of the experimental data with those obtained by use of other solvents.

The potential of these low-cost solvents for desulfurization of flue gases reported in the literature was experimentally verified in reference to different operating variables for carrying out further investigation.

**Materials used:** The solvents tried were, aqueous solutions of 1.6-4.0 % w/V NaClO and DMSO (40%) and pure water.

**Procedure:** The SO<sub>2</sub> analyzer was made ready as described above and 2.5 x 10<sup>-4</sup> m<sup>3</sup> of 1.6-4.0 % aqueous NaClO or 40% DMSO solution was poured into the semi-batch reactor. Measurement of the inlet and exit concentration of SO<sub>2</sub> and the transient values of the SO<sub>2</sub> removal efficiencies were determined following an identical procedure adopted in the SO<sub>2</sub> absorption experiments using the ionic liquids. The concentration of SO<sub>2</sub> in the feed gas was maintained at 1500 ppm. The results of the use of these solvents for SO<sub>2</sub> removal from gaseous mixtures are discussed in Chapter 5.

Use of water for absorptive removal of SO<sub>2</sub> from simulated gaseous mixtures has been reported in the literature to yield highly encouraging results. In the present investigation, transient values of the SO<sub>2</sub> removal efficiency from a gaseous mixture containing 500 ppm SO<sub>2</sub> was determined in the semi-batch bubble column reactor using 2.5 x 10<sup>-4</sup> m<sup>3</sup> of distilled water. Concentrations of the gaseous streams were measured using the same online SO<sub>2</sub> analyzer as mentioned before.

### 4.3 Gas-liquid-solid systems

The following experiments were performed to determine the performance of the bubble column slurry reactor for the absorption of SO<sub>2</sub> in Ca-based slurries. These experiments were also performed in a foam-bed reactor to determine advantages if any, that can be derived in such systems and to make a comparison of the performances of the two reactor configurations for absorptive removal of SO<sub>2</sub>.

**Experiments performed in bubble column reactor (BCR):** The variables studied in this type of reactor configuration were:

- Initial solids loading
- Superficial velocity of gas
- Initial concentration of SO<sub>2</sub> in feed gas

**Experiments performed in foam-bed reactor (FBR):** The following surfactants were used in the slurry-foam reactor

Nature of surfactant

- Cationic: Cetyl Trimethyl Ammonium Bromide (CTAB)
- Anionic: Sodium Dodecyl Sulfate (SDS), Teepol
- Non-ionic: Octyl Phenoxy Polyethoxy ethanol (Triton X-100), Tween 80.

**Estimation of parameter values:** The following parameter values required for analysis of experimental results were determined experimentally

- pH of slurry in the reactor and its variation with time
- Gas hold-up in the bubble column
- Particle-size distribution of Ca(OH)<sub>2</sub> test samples
- Gas-liquid interfacial area
- Volumetric liquid-side mass-transfer coefficient
- Volumetric gas-side mass-transfer coefficient
- Solid-liquid mass-transfer coefficient

**4.3.1 Dimensions and materials of construction of foam column**

The bubble column reactor used for the desulfurization of simulated flue gas was also used as a foam column reactor with the addition of a surfactant into the feed slurry. The dimensions of the glass column and the gas distributor plate of the foam-bed reactor therefore remained the same as that of the bubble column shown in Figure 4.4. Detail of the foam breaking plate is shown in Figure 4.10. The distributor plate has two parts attached with a hinge in which Part A remained fixed and Part B can be opened and closed before and after the addition of feed slurry respectively.

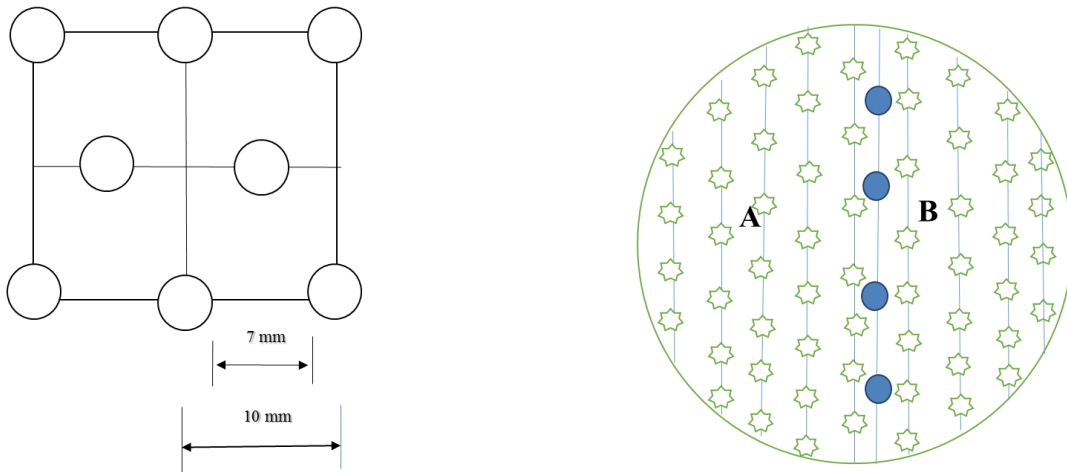
**Orifice plate for foam breaking**

Material of construction: perspex

Thickness of plate:  $2.0 \times 10^{-3}$  m

Diameter of each hole:  $3.0 \times 10^{-2}$  m

Number of holes: 57



☆ Indicates holes of dia.  $3 \times 10^{-3}$  m

Total plate area =  $86.59 \times 10^{-4}$  m<sup>2</sup>

Total holes area =  $4.029 \times 10^{-4}$  m<sup>2</sup>

● indicates hole for hinge

**Figure 4.10 Details of foam breaking plate**

### 4.3.2 Experiments performed in the bubble column reactor (BCR)

**Setup:** The experimental setup used for the absorption of SO<sub>2</sub> into Ca-based slurries is shown in Figure 4.4, it was same as that used for the absorption of sulfur-dioxide into ILs described in the section 4.2.1.2.

**Materials used:** Calcium hydroxide (GR, MERCK Ltd. Mumbai) and Calcium carbonate (AR, LobaChemie Mumbai) were used as absorbing reagents in the form of an aqueous slurry. The solute gas for absorption, 5000 ppm SO<sub>2</sub> in nitrogen and pure N<sub>2</sub> gas for purging of the SO<sub>2</sub> analyzer at the time of calibration (each being of Instrument Grade) were supplied by Dinesh Gases Pvt. Ltd., Jaipur. 4000 ppm calibrated SO<sub>2</sub> gas cylinder for calibration of the SO<sub>2</sub> analyzer was supplied by Alchemie Gases and Chemicals Pvt Ltd., Mumbai.

**Experimental:** (i) Slurry preparation: Calcium hydroxide being sparingly soluble in water and forms lumps when mixed with cold water was mixed with boiling-hot distilled water was used. A known amount of calcium hydroxide or calcium carbonate powder, say,  $1.0 \times 10^{-3}$  kg, was added to  $1.0 \times 10^{-4}$  m<sup>3</sup> was hot distilled in a  $2.5 \times 10^{-4}$  m<sup>3</sup> stoppered volumetric flask, shaken thoroughly and then intermittently for about half an hour. The volume of the cooled slurry was made up with distilled water and shaken for about another half an hour to obtain a saturated solution along with particles suspended in it.

Feed gas of the desired concentration obtained by mixing of 4000 ppm SO<sub>2</sub> in air with compressed air at the desired flow rate was brought to the steady state and the SO<sub>2</sub> analyzer was made ready following the same procedure as already described for experiments with ionic liquid solvents. The slurry was shaken thoroughly for complete mixing and then poured into the reactor. Exit concentration of SO<sub>2</sub> was recorded in the analyzer and the column was flushed with water immediately at the end of the experiment. The product slurry was collected in a 1000 mL volumetric flask, filtered using Whatmann 40 filter paper and the residue dried for measurement of its properties. These experiments were repeated for different variables studied in this work.

### 4.3.3 Experiments performed in the foam-bed reactor

**Setup:** The setup used for experiments in the bubble column reactor was employed for experiments in the foam-bed reactor as well except that a foam-breaker orifice plate connected to a thin copper rod was used for maintaining the desired foam height during experiments.

**Materials used:** CTAB (AR, LobaChemie Mumbai), Sodium dodecyl sulphate (GR, MERCK Ltd. Mumbai), Teepol (Sigma-Aldrich Switzerland), Triton X-100 (Thermo Fisher Scientific India Pvt. Ltd., Mumbai) and Tween 80 (GR, MERCK Ltd. Mumbai) were used as the foaming agents. Iso-amyl alcohol (GR, MERCK Ltd. Mumbai), an anti-foaming agent was used to maintain the desired foam height. In addition to these, all the reagents used for desulfurization of flue gas in a bubble column reactor were used for experiments in the foam-bed reactor as well.

**Procedure:** A known amount of surfactant was dissolved in  $5.0 \times 10^{-5} \text{ m}^3$  of distilled water in a  $2.5 \times 10^{-4} \text{ m}^3$  beaker.  $1.0 \times 10^{-4} \text{ m}^3$  of  $\text{Ca}(\text{OH})_2$  or  $\text{CaCO}_3$  slurry in distilled water was prepared in a  $2.5 \times 10^{-4} \text{ m}^3$  volumetric flask taking  $1.0 \times 10^{-3} \text{ kg}$  of one of these reagents following a similar procedure to that described for experiments in the bubble column reactor and the surfactant solution was added into it. The slurry volume was then made up to  $2.5 \times 10^{-4} \text{ m}^3$  with the gradual addition of distilled water and mix the contents thoroughly. Experiments in the slurry-foam reactor were performed following the same procedure as those in the bubble column slurry reactor except that a multi-orifice foam-breaking plate with iso-amyl alcohol applied on to its surface was kept hanging immediately after the slurry was fed into the reactor for maintaining a definite foam height. Experiments were repeated for different variables studied in this reactor.

## 4.4 Characterization of Ionic-liquids

### 4.4.1 *Physical properties of ionic liquids*

Physical properties are highly important in selecting a suitable absorbent for  $\text{SO}_2$  capture and determining the operational parameters for industrial scale applications. These properties of the ionic liquids, viz., density, viscosity, surface tension and refractive index have been measured for assessing the solvent properties. Liquid density was measured using a Kruss density meter (DS7800) make Kruss Optronics (Germany), viscosity by Brookfield viscometer make Brookfield (USA) and surface

tension by Drop Shape Analyzer make Kruss (Germany). Refractive index was measured using an Automatic Digital Refractometer, RX-7000i make (ATAGO, Japan). Because of the very high surface tension values of the ILs, gas bubbles rising through the pool of absorbent liquid burst immediately and no foaming could be observed on the liquid pool. The measured values of these properties are shown in Table 5.1.

#### **4.4.2 FT-IR and $^1\text{H}$ NMR spectra - micro structure of the synthesized ionic liquids**

To obtain information about the micro structure of the synthesized ionic liquids, chemical interaction between the absorbed  $\text{SO}_2$  and the IL solvents, Fourier-transform infrared spectroscopy (FT-IR) and Proton nuclear magnetic resonance ( $^1\text{H}$  NMR) spectra of the virgin and exhausted ILs were measured. FT-IR spectra were taken by a Perkin-Elmer (UATR 2) IR spectrometer, using a KBr disk. The structures of the synthesized ionic liquids were determined using  $^1\text{H}$  NMR spectroscopy on JEOL (ECS-400) 400 MHz spectrometer using DMSO as the solvent. The decomposition temperature of IL was analyzed by Thermogravimetric analysis (TGA) and Differential thermal analysis (DTA) (PerkinElmer STA6000, Waltham, Massachusetts U.S). Experimental results are presented in section 5.1 of chapter 5.

#### **4.4.3 Characterization of FGD products and estimation of parameter values**

The product obtained by desulfurization of flue gas in bubble column and foam-bed reactor, called FGD product, was characterized by FT-IR and Thermogravimetric analysis (TGA) to observe the nature of polymorph of calcium sulfate product and the morphology of the product was observed by Field Emission Scanning Electron Microscope (FE-SEM), and, X-Ray Diffraction (XRD) studies.

##### **4.4.3.1 FT-IR**

Fourier transform infrared spectroscopy (FTIR), (Perkin Elmer, Waltham, Massachusetts U.S) was used to evaluate bonding patterns of compounds present in the product at different temperatures.

Material amount: 1mg sample amount + 1g KBR powder

Machine source: Deuterium



The sample was prepared in a mortar and pestle and was fed to the Pelletizer. After preparation of the pellet, it was inserted into the FT-IR device. Experimental data are presented in Figures 5.17a and 5.17b.

#### 4.4.3.2 TGA

Thermogravimetric analysis (TGA) and Differential thermal analysis (DTA) were performed in a simultaneous TG-DTA (PerkinElmer STA6000, Waltham, Massachusetts U.S) analyzer by continuous heating of the sample of about 30 mg from room temperature to 950 °C with a heating rate of 20 °C/min in nitrogen atmosphere. Weight loss with temperature rise and thermal behavior were recorded. Experimental data are shown in Figure 5.18a and 5.18b.

#### 4.4.3.3 XRD:

Phase analysis was carried out by X-ray diffraction analysis (X'Pert Powder Analytical, Netherland, CuK $\alpha$  Radiations). Two-theta angle used for analysis was in the range of 10–60 with a scan step time of 0.800 per s.

Step size: (2theta) = 0.20

Temperature: 25 °C

Generator setting: 40Ma, 40Kv

Goniometer radius = 240 mm

Time period = 30 min

Maximum amount of sample taken = 1.1 g

Crystalline size is obtained from the equation below (Richardson, et al. 1989)

$$d = 0.89 \lambda / \beta \cos\theta$$

where,  $\beta$  is the full width at half maxima intensity and

$\lambda$  is the wavelength of X-Ray = 1.5405 Å

#### 4.4.3.4 FE-SEM

Surface morphology and elementary analysis were performed using a scanning electron microscope (SEM) (Nova Nano SEM 450, FEI, Netherland). Detail results of scanning of the surfaces of the samples are presented in chapter 5.

#### **4.4.4 Measurement of parameter values**

##### **4.4.4.1 pH of slurry with time in bubble column**

Variation of pH of reactant slurry is very important to understand the mechanism of reaction under varying conditions in the semi-batch reactor and to find out the most appropriate range of pH for carrying out this reaction in a continuous reactor. Experiments were carried out using  $\text{Ca}(\text{OH})_2$  or  $\text{CaCO}_3$  slurry for 5, 10, 15, 20, 25 and 30 minutes and the pH of the product slurry was measured using a Thermo Fisher Scientific pH meter.

##### **4.4.4.2 Gas hold-up in bubble column slurry reactor**

To determine gas holdup, the bubble column slurry reactor was operated using a definite concentration of  $\text{SO}_2$  gas. A specific gas rate and a known solids loading in the slurry, the same as those used in the gas absorption experiments were employed. Height of dispersion was measured on different sides of column using a measuring scale and an average value was taken. Gas flow was then stopped and the height of clear liquid was also measured at different locations and an average value was taken. Gas holdup was calculated using eqn. (3.44). Knowledge of bubble diameter and gas holdup enables one to calculate the gas-liquid interfacial area per volume of dispersion, which is important for the calculation of the rate of mass transfer.

##### **4.4.4.3 Particle size distribution (PSD) of $\text{Ca}(\text{OH})_2$ & $\text{CaCO}_3$ and their size analysis**

The PSDs play a significant role in calculating solid-liquid interfacial area. Particle-size distribution (PSDs) of reactant  $\text{Ca}(\text{OH})_2$  were measured using Mastersizer 2000 E.  $\text{Ca}(\text{OH})_2$  sample from MERCK Ltd. was used in performing the present experimental work and the particle size of the sample was measured using the above particle-size analyzer. The volume-average particle diameter, 6.84  $\mu\text{m}$ , of the samples obtained by particle size measurement was used for the estimation of solid-liquid interfacial area. Details of particle size distributions of lime are reported in section 5.4.1.1 of Chapter 5.

##### **4.4.4.4 Volumetric liquid side mass transfer coefficient**

Values of the volumetric liquid-side mass-transfer coefficient  $k_L a$  were required for estimation of the rate of gas absorption as well as for predicting the percent resistance

to mass transfer of different phases. In the present investigation, physical absorption of pure oxygen in water in the same semi-batch reactor as that used for studies of FGD was performed and the data were used to calculate the average values of the mass transfer coefficient for absorption of oxygen in water as shown in Chapter 3. The concentration of dissolved oxygen in the liquid sample was analyzed by using a Dissolved Oxygen Meter (Hanna Instruments India Pvt Ltd., Navi Mumbai, India) as well as analytically by Winkler's method (Appendix 4D.1). The same result was obtained by the two methods. Values of physical mass-transfer coefficient for absorption of SO<sub>2</sub> in water were obtained by the usual procedure as outlined in Chapter 3.

**Setup:** A pure oxygen gas cylinder was connected to the bubble column. The same bubble column used for other experiments presented in this work.

**Materials used:** Pure oxygen (Instrument Grade) was supplied by Dinesh Gases Pvt. Ltd., Jaipur. Fresh distilled water was prepared in the lab by using distilled water apparatus.

**Procedure:** The column was washed thoroughly. About  $1.0 \times 10^{-3} \text{ m}^3$  of distilled water was purged with pure nitrogen gas for about 20 minutes to a residual dissolved oxygen content of 0.5 mg/l. Pure oxygen at a rate of  $3.33 \times 10^{-4} \text{ m}^3/\text{s}$  as monitored by a calibrated rotameter, was allowed to flow into the bubble column reactor. When the flow rate of this gas became steady,  $2.5 \times 10^{-4} \text{ m}^3$  of the deoxygenated distilled water was poured carefully into the column. The flow of oxygen was closed after 1 min and the concentration of dissolved oxygen in the liquid was analyzed using the Dissolved Oxygen (DO) Meter as well as by Winkler's method. The experiment was repeated for other time intervals, e.g., 2 min, 3 min and so on and the concentrations of DO were determined using the same methods.

#### 4.4.4.5 Volumetric gas-side mass-transfer coefficient

**Setup:** The experimental setup used for performing FGD studies in the present investigation was also used for this study and reported previously in Figure 4.4.

**Materials used:** 2 (M) aqueous NaOH solution, 4000 ppm calibrated mixture of SO<sub>2</sub> and air supplied by Dinesh Gases Pvt. Ltd., Jaipur and compressed air.

**Procedure:** 4000 ppm SO<sub>2</sub> gas from the cylinder and compressed air at the desired flow rates were allowed to pass through the respective rotameters for obtaining a

definite concentration of SO<sub>2</sub> in the feed gas. The two gases were allowed to pass through a gas mixer and then enter into the empty glass column. The analyzer was made ready following a procedure described in section 4.2.2.1. 2.5 x 10<sup>-4</sup> m<sup>3</sup> of 2(M) NaOH solution was poured into the reactor and the concentration of SO<sub>2</sub> in the exit gas getting recorded in the data logger was observed. The experiment was discontinued when the exit concentration of SO<sub>2</sub> remained steady for a considerable period. The experiment was repeated for other superficial velocities of gas used for FGD studies. The experimental data were used to estimate the gas phase mass-transfer coefficient, rate of gas absorption and percent of gas phase resistance to mass transfer.

**4.4.4.6 Solid-liquid mass-transfer coefficient:** Solid-liquid mass-transfer coefficient values are required for estimation of the rate of dissolution of sparingly soluble particles in the slurry reactor. From knowledge of the inlet and steady-state exit concentration of SO<sub>2</sub> from the slurry reactor and the gas flow rates, the rate of absorption of SO<sub>2</sub> was determined. The stoichiometric equation for the reaction between SO<sub>2</sub> and Ca(OH)<sub>2</sub>/ CaCO<sub>3</sub> along with the rate of gas absorption determines the rate of dissolution of particles. Initial solids loading in the slurry, average initial particle size and percent of impurity present in the sample being known, solid-liquid mass-transfer coefficient was calculated using a material balance.

## APPENDIX 4A

**4A.1 Chemical Analysis of Hydrated Lime Samples for Estimation of Percentage of Hydrated Lime Content**

**Reagents:** (i) Standard sodium-thiosulphate solution, 0.1 N  
(ii) Standard iodine solution  
(iii) Starch-indicator solution

**Procedure**

About  $1.0 \times 10^{-3}$  kg of the hydrated lime sample, accurately weighed, was taken in a glass-stoppered conical flask and about  $3.0 \times 10^{-5}$  m<sup>3</sup> of boiling water was added to it. The mixture was shaken for about 10 minutes, cooled, and iodine solution added to it with the constant shaking of the flask till the violet color of iodine persists (indicating the presence of excess iodine after complete reaction with lime). The solution was transferred to a  $5.0 \times 10^{-4}$  m<sup>3</sup> volumetric flask and diluted with distilled water by making up the volume to the mark.

$2.5 \times 10^{-5}$  m<sup>3</sup> of the solution was pipetted out and the excess iodine was titrated with a standard sodium-thiosulphate solution adding starch indicator towards the end of the titration. A blank determination was also carried out using the same amount of iodine solution as with the sample.

**Working Equation for Estimation of Hydrated Lime Content in the Sample**

For convenience, the following analysis was followed in CGS units as it involves g equivalent weight, normality, etc.

Let the actual weight of hydrated lime taken for preparation of solution be  $M_H \times 10^{-3}$  kg.

We know that  $V_{thio}$  ml of a thiosulphate solution having normality, N, contains

$\frac{(V_{thio})(N)}{1000}$  g equivalents of thiosulphate. (N is normality of the thiosulphate solution =

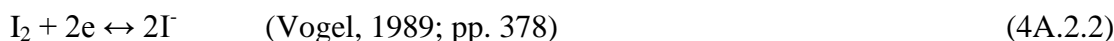
number of g equivalents of thiosulphate dissolved in 1000 ml of solution.)

1 g equivalent of thiosulphate  $\equiv$  1 g equivalent of iodine

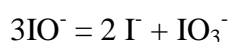
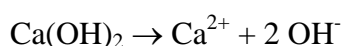
Thus,

$$\frac{(V_{thio})(N)}{1000} \text{ g equivalents of thiosulphate} = \frac{(V_{thio})(N)}{1000} \text{ g equivalents of iodine} \quad (4A.2.1)$$

Again, the following equation indicates that the equivalent weight of iodine is equal to the atomic weight, i.e. 126.905 g.



Reaction between  $I_2$  and  $Ca(OH)_2$  can be written to follow the steps shown below:



Thus, 1 g mol of  $I_2 = 2$  g equivalents of  $I_2$

$$2 \text{ g equivalents of } I_2 \equiv 2 \text{ g equivalents of } Ca(OH)_2 = 1 \text{ g mol of } Ca(OH)_2 \quad (4A.2.4)$$

(As equal number of equivalents of reactants react with each other).

$$\begin{aligned} \text{Therefore, } & \frac{(V_{thio})(N)}{1000} \text{ g equivalents of iodine} \\ & \equiv \frac{(V_{thio})(N)}{(1000)(2)} \text{ g moles of } Ca(OH)_2 \\ & = (74.1) \times \frac{(V_{thio})(N)}{(1000)(2)} \text{ g of } Ca(OH)_2 \end{aligned} \quad (4A.2.5)$$

Using equation (4A.2.1), it follows that

$$\begin{aligned} & \frac{(V_{thio})(N)}{1000} \text{ g equivalents of thiosulphate} \\ & \equiv (74.1) \times \frac{(V_{thio})(N)}{(1000)(2)} \text{ g of } Ca(OH)_2 \end{aligned} \quad (4A.2.6)$$

In the above procedure, for estimation of  $Ca(OH)_2$  in a lime sample,  $M_H$  g of lime was dissolved in 500 ml of solution. 25 ml of this lime solution was taken for titration and an excess (over that required to consume all the lime present in it) amount of iodine was added to it. Let the volume of thiosulphate required to titrate the excess iodine present be denoted by  $V_{th,s}$  and that for blank determination (with the volume of

iodine equal to that added per 25 ml of the 500 ml lime solution made), the volume of thiosulphate required to be denoted by  $V_{th,b}$ . Thus,  $(V_{th,b} - V_{th,s})$  ml is the lesser volume of thiosulphate consumed because of the reaction of iodine with  $\text{Ca(OH)}_2$  present in 25 ml of lime solution. Using equation (4.8.6), one can write

$(V_{th,b} - V_{th,s})$  ml of thio of normality  $N$

$$\begin{aligned} &\equiv \frac{(V_{th,b} - V_{th,s})(N)}{(1000)} \text{ g equivalents of thio} \\ &\equiv (74.1) \times \frac{(V_{th,b} - V_{th,s})(N)}{(2)(1000)} \text{ g of Ca(OH)}_2 \end{aligned} \quad (4A.2.7)$$

Therefore, 25 ml of solution contains  $(74.1) \times \frac{(V_{th,b} - V_{th,s})(N)}{(2)(1000)}$  g of  $\text{Ca(OH)}_2$  (4A.2.8)

$$\begin{aligned} \text{Or, 500 ml of solution contains } &(74.1) \times \frac{(V_{th,b} - V_{th,s})(N)}{(2)(1000)} \times \frac{500}{25} \text{ g of Ca(OH)}_2 \\ &= (0.741) (V_{th,b} - V_{th,s})(N) \text{ g of Ca(OH)}_2 \end{aligned} \quad (4A.2.9)$$

Since,  $M_H$  g of sample is present in 500 ml of solution,

$$\text{Percentage of hydrated lime by mass} = \frac{74.1(V_{th,b} - V_{th,s})(N)}{M_H} \quad (4A.2.10)$$

$$[\text{Percentage of lime by mass as CaO} = \frac{56.08(V_{th,b} - V_{th,s})(N)}{M_H} \text{ IS 1514: 1990 p. 6}].$$

## APPENDIX 4B

## SAMPLE CALCULATION

**4B.1 Molar rate of absorption of SO<sub>2</sub> from experimental data**

Molar rate of absorption of SO<sub>2</sub> was calculated from experimental data is described in chapter 3, section 3.7.2 and this can be calculated by

$$W_{SO_2} = \frac{Q_{gtot} \cdot (P_{SO_2in} - P_{SO_2out})}{RT}$$

Total gas flow rate,  $Q_{gtot} = 20 \text{ lpm} = 333.33 \text{ cm}^3/\text{s}$

Universal gas constant,  $R = 82.05 \text{ cm}^3 \text{ atm K}^{-1} \text{ mol}^{-1}$

$$P_{SO_2in} = 500 \text{ ppm} = 5 \times 10^{-4} \text{ atm}$$

$$P_{SO_2out} = 5 \text{ ppm} = 5 \times 10^{-6} \text{ atm}$$

Thus, substituting these values, we get

$$W_{SO_2} = \frac{333.33(5 \times 10^{-4} - 5 \times 10^{-6})}{82.05 \times 303} = 6.63 \times 10^{-6} \text{ g mol/s}$$

**4B.2 Liquid side mass-transfer coefficient from experimental data**

Liquid side mass-transfer coefficient for O<sub>2</sub> has been obtained using the expression:

$$k_{l,O_2}^0 a = \frac{1 - \varepsilon_G}{t} \ln \frac{C_{O_2}^* - C_{O_2i}}{C_{O_2}^* - C_{O_2f}}$$

Saturation concentration of O<sub>2</sub> in the water at 30 °C,  $C_{O_2}^*$

$$= 1.3 \times 10^{-6} \text{ g mol/cm}^3 \quad (\text{Deckwer, W. D., 1992})$$

$$C_{O_2i} = 2.5 \times 10^{-8} \text{ g mol/cm}^3 \text{ (Initial concentration of O}_2 \text{ in distilled water)}$$

$$C_{O_2t} = 5.2125 \times 10^{-7} \text{ g mol/cm}^3 \text{ at time, } t=60 \text{ s (by D.O. meter)}$$

$$\text{Thus, } k_{l,O_2}^0 a = \frac{1 - 0.22}{60} \ln \frac{1.3 \times 10^{-6} - 2.5 \times 10^{-8}}{1.3 \times 10^{-6} - 5.3125 \times 10^{-7}} = 6.61 \times 10^{-3} \text{ s}^{-1}$$

It was observed that as the concentration of O<sub>2</sub> in water approached its saturation value, the magnitude of mass-transfer coefficient reduced to significantly low values. In this study, this condition did not arise. Hence the average value of the mass-transfer



coefficient is determined for absorption of about 60% saturation concentration of O<sub>2</sub> in water. Thus the average liquid-side mass-transfer coefficient is

$$k_{l,O_2,avg}^0 a = 1.685 \times 10^{-3} \text{ s}^{-1}$$

Detail experimental data of dissolve O<sub>2</sub> and liquid-side mass-transfer coefficient of O<sub>2</sub> are mentioned in Table 5C.1 (Appendix 5C)

Liquid side mass transfer coefficient for SO<sub>2</sub> has been obtained using the expression:

$$k_{l,SO_2}^0 a = k_{l,O_2}^0 a \left( \frac{D_A}{D_{O_2}} \right)^{2/3}$$

$$a = 1.35 \text{ cm}^2/\text{cm}^3 \text{ (Sada et. al., 1985, Figure no. 8)}$$

$$k_{l,O_2}^0 = \frac{k_{L,O_2}^0 a}{a} = \frac{1.623 \times 10^{-3}}{1.3} = 1.248 \times 10^{-3} \text{ cm/s}$$

$$k_{l,O_2}^0 a = 1.623 \times 10^{-3} \text{ s}^{-1}$$

$$\text{At } 20^\circ\text{C}, D_A = D_{SO_2} = 1.728 \times 10^{-5} \text{ cm}^2/\text{s}$$

$$D_{O_2} = 2.35 \times 10^{-5} \text{ cm}^2/\text{s}$$

Substituting these values, we get

$$\text{Then, } k_{l,SO_2}^0 = 1.248 \times 10^{-3} \left( \frac{1.728 \times 10^{-5}}{2.35 \times 10^{-5}} \right)^{2/3} = 1.02 \times 10^{-3} \text{ s}^{-1}$$

The value of  $k_l^0$  agree closely with those reported by Sharma and Danckwerts, (1970).

#### 4B.3 Gas-side mass transfer coefficient from experimental data

The extent of gas phase mixing in the bubble column has been determined through the estimation of Peclet number in the column for the experimental conditions used in this study. It was observed that the reported values of Peclet number vary from 0.001 to 1 (Table 3C.2.1) and in general gas-phase pattern is assumed to be in plug flow for the design of bubble columns. For the present experimental conditions, the value of gas phase Peclet number ranged from 0.2 to 0.472 for MLIL and 2.08 for Ca(OH)<sub>2</sub> slurry. For the liquid phase, it was 0.374 for MLIL and Ca(OH)<sub>2</sub> slurry. Hence, the gas flow pattern was approximate as plug flow. Therefore only partial back-mixing of both the phases occur in the column and for simplicity, calculations are made assuming plug

flow. The gas phase concentration for estimation of parameter values was therefore taken as the average of inlet and exit concentration of SO<sub>2</sub>.

$k_{gSO_2} \cdot a$  was calculated from the experimental data as described in chapter 3, section 3.7.2 where:

$$k_{gSO_2} \cdot a = \frac{W_{SO_2}}{V_{disp} \cdot P_{SO_2b avg}}$$

$$P_{SO_2b avg} = \frac{P_{SO_2in} + P_{SO_2out}}{2} = \frac{(500+10) \times 10^{-6}}{2} = 2.55 \times 10^{-4} \text{ atm}$$

$$V_{dis} = V_L + V_L \frac{\varepsilon_G}{1 - \varepsilon_G} = 250 + 250 \frac{0.22}{1 - 0.22} = 320 \text{ cm}^3$$

$$W_{SO_2} = \frac{333.33 (5 \times 10^{-4} - 10 \times 10^{-6})}{82.05 \times 303} = 6.57 \times 10^{-6} \text{ g mol/s}$$

$$\text{Thus, } k_{gSO_2} \cdot a = \frac{6.57 \times 10^{-6}}{320 \times 2.55 \times 10^{-4}} = 8.05 \times 10^{-5} \text{ g mol cm}^{-3} \text{ s}^{-1} \text{ atm}^{-1}$$

$$k_{gSO_2} = \frac{k_{gSO_2} \cdot a}{a} = \frac{8.05 \times 10^{-5}}{1.3} = 6.19 \times 10^{-5} \text{ g mol cm}^{-2} \text{ s}^{-1} \text{ atm}^{-1}$$

This value of  $k_{gSO_2}$  is in the range of values reported in the literature (Mashelkar, R. A., 1970)

#### 4B.4 Verification of the instantaneous reaction

For the verification of condition of instantaneous reaction for the present system, a value for  $E_{inst}$  is needed. For this an assessment of  $C_{Ai}$  is essential. In the present investigation, concentration of component  $B$  maintained being substantially high and there being a source for continuous supply of  $B$  within the film itself, partial pressure of SO<sub>2</sub> at the interface was assumed close to zero (Chapter 3, Figure 3.7). As a close approximation the exit concentration of SO<sub>2</sub> which is normally 10 ppm in almost all the experiments, is taken for calculation purposes.

$$Ha. > 10E_{inst}$$

$$Ha = \frac{\sqrt{D_A k_2 C_{B0}}}{k_{l,SO_2}^0}$$

$$D_A = 1.728 \times 10^{-5} \text{ cm}^2/\text{s}$$

$$k_2 \text{ (second order rate constant)} = 10^{12} \text{ cm}^3 \text{ g mol}^{-1} \text{ s}^{-1} \quad (\text{Saal, R.N.J., 1928})$$

$$C_{B0} = 2.3 \times 10^{-5} \text{ g mol/cm}^3$$

$$k_{L,SO_2}^0 = 1.02 \times 10^{-3} \text{ cm/s}$$

$$Ha = \frac{\sqrt{1.728 \times 10^{-5} \times 10^{12} \times 2.3 \times 10^{-5}}}{1.02 \times 10^{-3}} = 19544$$

$$E_{inst} = 1 + \frac{D_B C_{B0}}{D_A C_{Ai}}$$

$$P_{Ai} = 10 \times 10^{-6} \text{ atm}$$

$$H = 6.8 \times 10^2 \text{ atm cm}^3 \text{ mol}^{-1} \quad (\text{Deckwer, W. D., 1992})$$

$$C_{Ai} = \frac{P_{Ai}}{H} = \frac{10 \times 10^{-6}}{6.8 \times 10^2} = 1.47 \times 10^{-8} \text{ mol/cm}^3$$

$$E_{inst} = 1 + \frac{1.6 \times 10^{-5} \times 2.3 \times 10^{-5}}{1.728 \times 10^{-5} \times 1.47 \times 10^{-8}} = 1449.15$$

Here,  $Ha > 10E_{inst}$

#### 4B.5 Percent gas phase resistance from experimental data

The expression for percentage of gas-phase resistance was formulated in chapter 3, section 3.6 and may be written as

$$\beta = \frac{\frac{1}{k_{gSO_2} H}}{\frac{1}{k_{LSO_2}^0 E_{inst}} + \frac{1}{k_{gSO_2} H}} \times 100$$

$$k_{gSO_2} = 6.23 \times 10^{-5} \text{ g mol cm}^{-2} \text{ atm}^{-1} \text{ s}^{-1}$$

$$k_{L,SO_2}^0 = 1.02 \times 10^{-3} \text{ cm s}^{-1}$$

$$H = 6.8 \times 10^2 \text{ atm cm}^3 \text{ mol}^{-1}$$

Substituting these values in the above expression one gets,

$$\beta = \frac{\frac{1}{6.19 \times 10^{-5} \times 6.8 \times 10^2}}{\frac{1}{6.19 \times 10^{-5} \times 6.8 \times 10^2} + \frac{1}{1.02 \times 10^{-3} \times 1449}} \times 100 = 97.22\%$$

**4B.6 Checking from the experimental data whether the system is gas-film controlling**

$$k_{gSO_2} = 6.19 \times 10^{-5} \text{ g mol cm}^{-2} \text{ atm}^{-1} \text{ s}^{-1}$$

$$k_{l,SO_2}^0 = 1.02 \times 10^{-3} \text{ cm s}^{-1}$$

$$k_{gSO_2} p_{SO_2,b,avg} = 6.19 \times 10^{-5} \times 2.55 \times 10^{-4} = 1.58 \times 10^{-8}$$

$$D_A = 1.728 \times 10^{-5} \text{ cm}^2/\text{s}$$

$$D_B = 1.6 \times 10^{-5} \text{ cm}^2/\text{s}$$

$$Z = 1$$

$$\frac{k_{l,SO_2}^0 D_B C_{BO}}{z D_A} = \frac{1.02 \times 10^{-3} \times 1.6 \times 10^{-5} \times 2.3 \times 10^{-5}}{1.728 \times 10^{-5}} = 2.17 \times 10^{-8}$$

$$\text{Here, } k_{gSO_2} p_{SO_2,avg} < \frac{k_{l,SO_2}^0 D_B C_{BO}}{z D_A}$$

Thus, absorption is accompanied by entirely completely gas film controlled

**4B.7 Solid-liquid interfacial area from experimental data**

Solid-liquid interfacial area is calculated by the expression (Ramachandran and Sharma, 1969):

$$A_p = \frac{6w}{\rho_p d_{p,avg}}$$

$w$  = Amount of solid per volume of dispersion,  $\text{g/cm}^3$

Amount of solid = 1 g

Volume of dispersion =  $393.7 \text{ cm}^3$

Therefore,  $w = 1/393.7 \text{ g/cm}^3$  slurry dispersion

$$\rho_p = 2.21 \text{ g/cm}^3$$

$$d_{p,avg} = 6.84 \text{ } \mu\text{m} = 6.84 \times 10^{-4} \text{ cm}$$

Substituting these values, we get

$$A_p = \frac{6}{2.21 \times 6.84 \times 10^{-4} \times 393.7} = 10.08 \text{ cm}^2/\text{cm}^3$$

#### 4B.8 Solid-liquid mass transfer coefficient from experimental data

The expression for solid-liquid mass-transfer coefficient estimation was obtained in chapter 3, section 3.7.6 and can be calculated by using the expression:

$$k_{sl} = \frac{R_B}{A_p C_{B0} V_{disp}}$$

Molar rate of dissolution of  $B$  = Molar rate of absorption of  $A$  =  $6.63 \times 10^{-6}$  g mol/s  
(shown at page no. 25)

$$C_{B0} = 2.3 \times 10^{-5} \text{ g mol/cm}^3$$

$$V_{dis} = V_L + V_L \frac{\epsilon_G}{1 - \epsilon_G} = 250 + 250 \frac{0.365}{1 - 0.365} = 393.7 \text{ cc}$$

$$A_p = 10.08 \text{ cm}^2/\text{cm}^3 \text{ (from 4B.7)}$$

Substituting these values, we get

$$k_{sl} = \frac{6.63 \times 10^{-6}}{10.08 \times 2.3 \times 10^{-5} \times 393.7} = 7.26 \times 10^{-5} \text{ cm}^2/\text{s}$$

#### 4B.9 Mass balance verification from experimental data

Expressions for mass balance verification were obtained in chapter 3, section 3.5 Mass of  $\text{SO}_2$  absorbed is calculated using the expression,

$$\text{Mass of } \text{SO}_2 \text{ absorbed} = M_A \int_0^{t_{br}} \frac{(Q_{gtot}) (1000/60) (C_{\text{SO}_2in} - C_{\text{SO}_2out}) \times 10^{-6}}{RT} dt$$

Here:

$$w_B = 1 \text{ g of Ca(OH)}_2 \text{ sample}$$

$$Q_{gtot} = 20 \text{ lpm}$$

$$C_{\text{SO}_2in} = 500 \text{ ppm}$$

$$t_{br} = 35 \text{ min} = 2100 \text{ s}$$

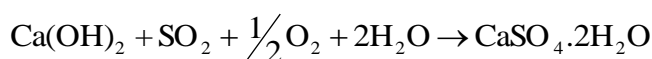
$$M_A = 64$$

$$C_{\text{SO}_2out} = \text{concentration of } \text{SO}_2 \text{ in exit gas till the breakthrough time, } t_{br}$$

Thus putting these values in the equation above

$$\begin{aligned} \text{Mass of SO}_2 \text{ absorbed} &= M_A \int_0^{t_{br}} \frac{(Q_{gtot}) (1000/60) (C_{\text{SO}_2\text{in}} - C_{\text{SO}_2\text{out}}) \times 10^{-6}}{RT} dt \\ &= 64 \times \text{area representing the integration} \\ &= 64 \times 0.01326 \text{ g} = 0.849 \text{ g SO}_2 \end{aligned}$$

Stoichiometric requirement



1 g mole of Ca(OH)<sub>2</sub> reacts with 64 g of SO<sub>2</sub>

74 g of Ca(OH)<sub>2</sub> reacts with 64 g of SO<sub>2</sub>

∴ 1 g of Ca(OH)<sub>2</sub> reacts with 64/74 g of SO<sub>2</sub> = 0.8648 g

*Calculation of stoichiometric amount of SO<sub>2</sub> absorbed by 1 g Ca(OH)<sub>2</sub> sample:*

The purity of Ca(OH)<sub>2</sub> sample was analyzed by iodometric titration details of which has been shown in Appendix 4A.1. The sample contained 96% Ca(OH)<sub>2</sub>. XRD analysis confirmed that impurities are present mainly in the form of CaCO<sub>3</sub>. It is assumed that 3.5% impurity is CaCO<sub>3</sub> and the rest 0.5 % are others.

Mass of sample that reacts with SO<sub>2</sub> = 0.96 g Ca(OH)<sub>2</sub> and 0.035 g CaCO<sub>3</sub>

From the stoichiometry (reactions are shown in chapter 3, section 3), 1 g mol of each Ca(OH)<sub>2</sub> and CaCO<sub>3</sub> react with 1 g mol of SO<sub>2</sub>.

Therefore, moles of SO<sub>2</sub> absorbed by 1 g of the sample is obtained as

$$= \frac{\text{weight of Ca(OH)}_2 \text{ in sample}}{\text{Molecular weight of Ca(OH)}_2} + \frac{\text{weight of CaCO}_3 \text{ in sample}}{\text{Molecular weight of CaCO}_3}$$

Moles of SO<sub>2</sub> reacted = (0.96/74) + (0.035/100) = 0.01332 g mol

Mass of SO<sub>2</sub> reacted = 0.01332 x 64 = 0.8526 g

$$\text{Percent error} = \frac{\text{Deviation from the stoichiometric value}}{\text{SO}_2 \text{ absorbed by stoichiometry}} \times 100$$

$$= \frac{0.8526 - 0.849}{0.8526} \times 100 = 0.43\%$$

**4B.10 Transient percent removal efficiency from experimental data**

Transient values of SO<sub>2</sub> removal efficiency is calculated from the experimental data using the expression:

$$\eta(t) = \frac{C_{in} - C_{e1}}{C_{in}} \times 100 \quad (6)$$

where,  $\eta(t)$  = % of transient SO<sub>2</sub> removal efficiency

$C_{in}$  = concentration of SO<sub>2</sub> at the inlet to reactor (invariant) at time  $t$  after start of experiment, ppm

$C_{e1}(t)$  = exit concentration of SO<sub>2</sub> after one small time interval  $\Delta t=10$  s of the gas inlet time  $t$ , ppm

if,  $C_{in}= 500$  ppm and  $C_{e1} = 5$  ppm

**CHAPTER-5****RESULTS & DISCUSSION**

Experiments on desulfurization studies from simulated gaseous mixtures using a variety of absorbents have been described in Chapter 4. Two distinct categories of low-cost absorbents were used in this investigation, the one organic in nature was synthesized in-house, characterized for its important solvent properties, and, then used for desulfurization and solvent regeneration studies for its reuse. Calcium-based slurries, the other category of absorbents, extensively used in industries for desulfurization of flue gas using a spray scrubber were also used for studies of additional aspects. Performance data of a bubble column reactor for this system reported in the literature are found to be meagre and considering this aspect desulfurization in bubble column reactor was investigated in this study.

This chapter has been broadly divided into two parts: PART I and PART II. The former has once again been divided into three sections and the latter into two sections. Results based on experiments using ILs have been taken up in PART I while that on Ca-based slurries in PART II. Characterization of ILs, absorption of SO<sub>2</sub> as functions of different variables and regeneration of solvents have been discussed in Sections I, II and III, respectively of PART I. In Section I of PART II, absorption of SO<sub>2</sub> in Ca-based slurries as functions of different variables and the other, characterization of FGD products have been discussed.

Several experimental observations have been attributed to the strongly gas-phase resistance controlled process for the absorption of SO<sub>2</sub>, and the latter fact is reported in the literature as well. For determination of percent resistance to mass transfer, the required theory has been discussed in Chapter 3 and the concerned parameter values determined experimentally, the details of which have been described in Chapter 4.

In the present studies, superficial velocity of gaseous mixture was kept relatively high ( $3.85 \times 10^{-2}$  to  $7.70 \times 10^{-2}$  m/s) to avoid settling of particles and choking of the gas distributor plate and that at relatively lower velocities, weeping occurred through the holes in the distributor plate. A few sets of experiments were conducted with addition of (i) a nonionic surfactant, Triton X-100 (546 ppmw) and Tween 80 (582 ppmw), (ii) a cationic surfactant, CTAB (100 ppmw), and (iii) an anionic surfactant, SDS (400



ppmw) and Teepol (625 ppmw), for comparison of the slurry reactor with a foam reactor and also to determine the effect of the type of a surfactant on the foam-reactor performance.

A series of experiments were performed specifically to generate experimental reactor-performance data with respect to important operational parameters of a gas-liquid or gas-liquid-solid mass transfer system, viz. gas-flow rate, initial loading of solid particles, and concentration of SO<sub>2</sub> in the feed gas and volume of slurry charged into the reactor. The other experiments performed were, measurements of the liquid hold-up, physical mass-transfer coefficient values, FGD product characterization, viz., XRD, SEM, TGA and FT-IR analyses.

A similar set of experiments were performed using ionic liquid (ILs) solvents, viz., synthesis, SO<sub>2</sub> absorption studies and solvent regeneration. NMR, TGA and FTIR analyses were also performed.

## **PART I: IONIC LIQUID – Characterization of synthesized ILs, absorption of SO<sub>2</sub> in ILs and solvent regeneration**

### **5.1 Characterization of synthesized ILs**

Physical properties of the synthesized ionic liquids, viz., density, viscosity, surface tension and refractive index were measured (Table 5.1) for assessing the suitability of these liquids as the solvent for gas absorption operations. The measured values of these properties are shown in Table 5.1. All the synthesized ILs were liquid at room temperature except MSIL. Densities of these ionic liquids are marginally higher than that of water, but viscosity values were observed to be substantially higher (243-647 mPa.s) and probably the major disadvantage of ILs for its use as absorbing solvents. Because of the very high surface tension values, about 44 to 56 mN/m of the synthesized ILs, gas bubbles rising through the pool of absorbent liquid were found to burst immediately, and no foaming could be observed on the liquid pool. Measured values of refractive index, useful for identification of an unknown substance or its concentration in a given liquid mixture, are found to vary in the range 1.457 to 1.511. Temperature stability of MLIL was determined through measurement of its decomposition temperature by TGA analysis. The data obtained from Perkin-Elmer DSC-7 Differential Scanning Calorimetry (DSC) clearly showed the decomposition temperature to be 230 °C (Figure 5.1). Yuan et al. (2007) found this temperature to be 247 °C. It is important that these authors specially purified the virgin IL before using

this as absorbent. The marginally lower temperature obtained in the present investigation was attributed to the presence of impurities, primarily ethanol and water.

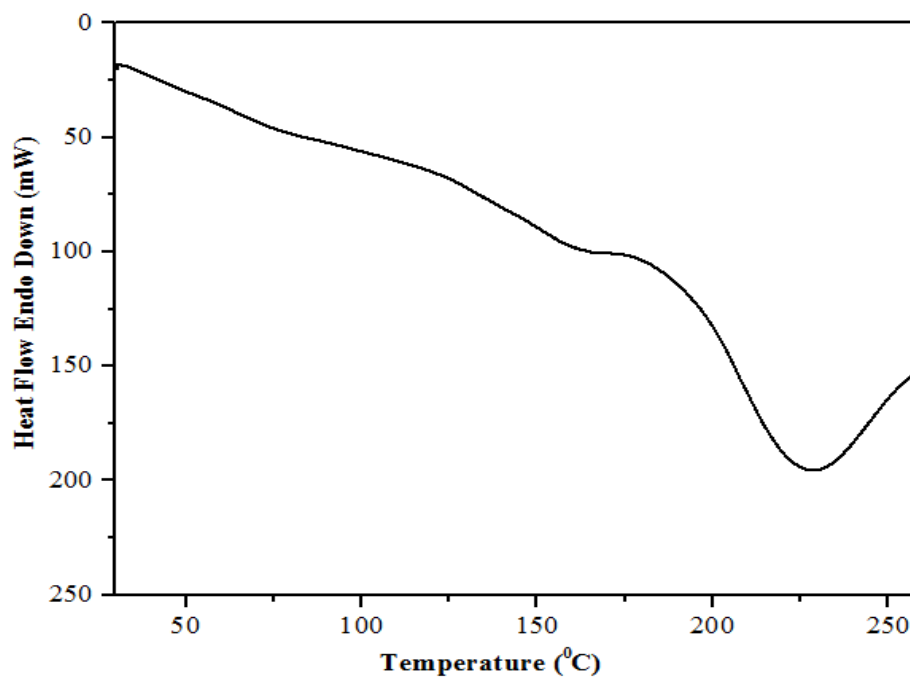


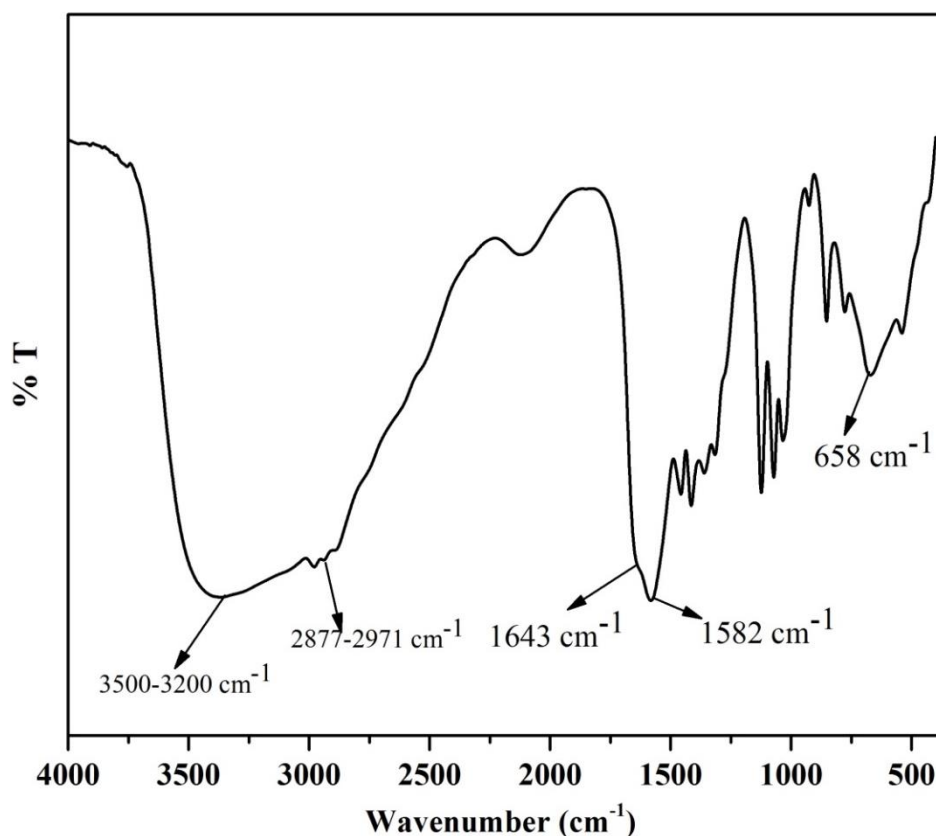
Figure 5.1 DSC analysis of MLIL

Table 5.1 Physical properties of synthesized ionic liquids at 303 K

Ionic liquid	Density (kg/m <sup>3</sup> ) x 10 <sup>-3</sup>	Viscosity (mPa.s)	Refractive index	Surface Tension (mN/m)
MLIL	1.172	647	1.469	43.81
TLIL	1.176	234.6	1.457	44.26
TSIL	1.165	518.5	1.511	56.36
MSIL	Synthesized material was in solid phase			

### 5.1.1 FT-IR and $^1\text{H}$ NMR spectra of ILs for micro structure analysis

To obtain information about the micro structure of the synthesized ionic liquids, and chemical interaction between the absorbed  $\text{SO}_2$  and the IL solvents, FT-IR and  $^1\text{H}$  NMR spectra of ILs were measured.



**Figure 5.2a: FT-IR of virgin MLIL**

*FT-IR* spectra of 2- hydroxyethylammonium lactate (MLIL) are presented in Figure 5.2a. *FT-IR* spectrum showed characteristic vibrational peaks at wavenumber (3500–3200  $\text{cm}^{-1}$ ) (Bicak, 2005; E. Duan et al., 2011) which corresponded to N-H and O-H, C-H stretch (2877, 2931 and 2971  $\text{cm}^{-1}$ ) (Liu et al., 2013), broad band centered combined band of the carbonyl (1643  $\text{cm}^{-1}$ ), N–H plane bending vibrations (1582  $\text{cm}^{-1}$ ) (Bicak, 2005) and N-H oop (658  $\text{cm}^{-1}$ ) (Pavia et al., 1973).

*FT-IR* spectra of Tri-hydroxyethylammonium lactate (TLIL) has been presented in Figure 5.2b. *FT-IR* spectrum showed characteristic vibrational peaks at wavenumber (3500–3200  $\text{cm}^{-1}$ ) (Bicak, 2005; E. Duan et al., 2011) which corresponded to N-H and O-H, C-H stretch (2871, 2931 and 2971  $\text{cm}^{-1}$ ) (Liu et al., 2013), carbonyl, C=O bent (1737  $\text{cm}^{-1}$ ), N–H plane bending vibrations (1595  $\text{cm}^{-1}$ ) (Bicak, 2005) and N-H oop (668  $\text{cm}^{-1}$ ) (Pavia et al., 1973).

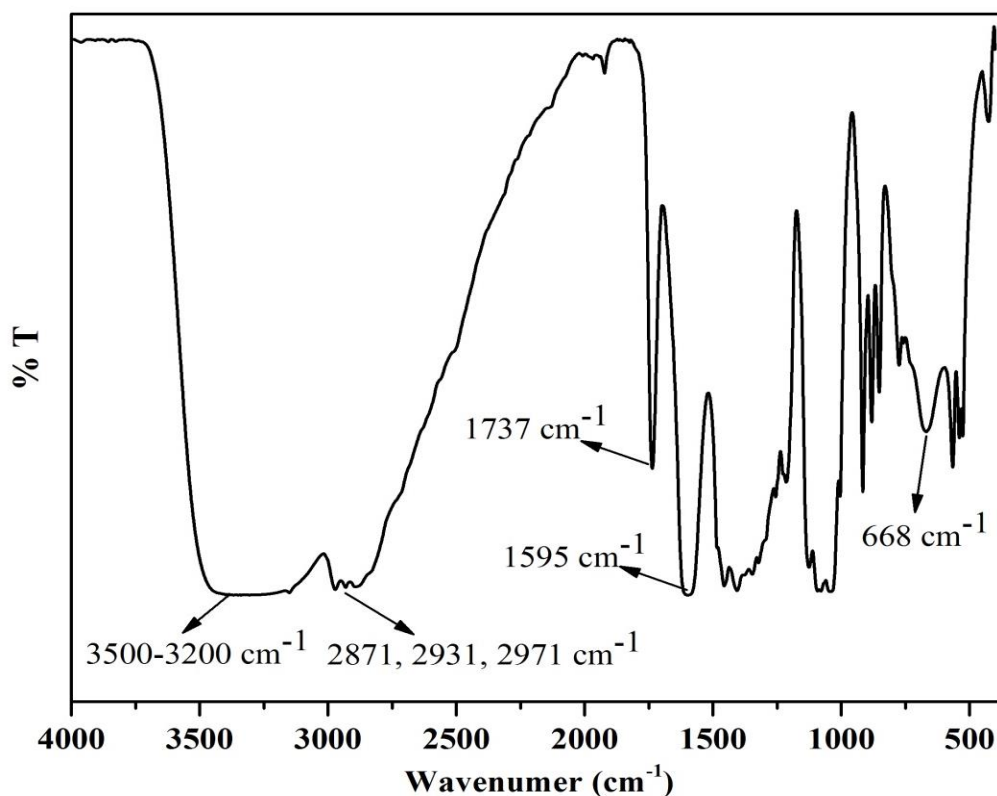


**Figure 5.2b: FT-IR of virgin TLIL**

The FT-IR spectra of TSIL acid is shown in Figure 5c. FT-IR spectrum showed characteristic vibrational peaks at wavenumber 3300-3200  $\text{cm}^{-1}$  which corresponded to N-H and O-H stretch, 2999-2831  $\text{cm}^{-1}$  that were assigned to OH and C-H stretching, respectively. The C=O ( $\text{COO}^-$ ) asymmetric and symmetric stretching were assigned to IR peaks observed at 1626  $\text{cm}^{-1}$  and 1384  $\text{cm}^{-1}$ , respectively. Further, IR peaks appeared at 1558-1610  $\text{cm}^{-1}$  were attributed to C=C (phenolic) multiple peaks. The C-C stretching peaks were observed at 1444-1503  $\text{cm}^{-1}$ . The O-H (phenolic) bending was assigned to IR peak appeared at 1342  $\text{cm}^{-1}$ . The vibrational peaks appeared at 763-666  $\text{cm}^{-1}$  were attributed to =C-H bending. The observed FT-IR data of salicylic acid was well supported by the literature data (Guan et al., 2007).

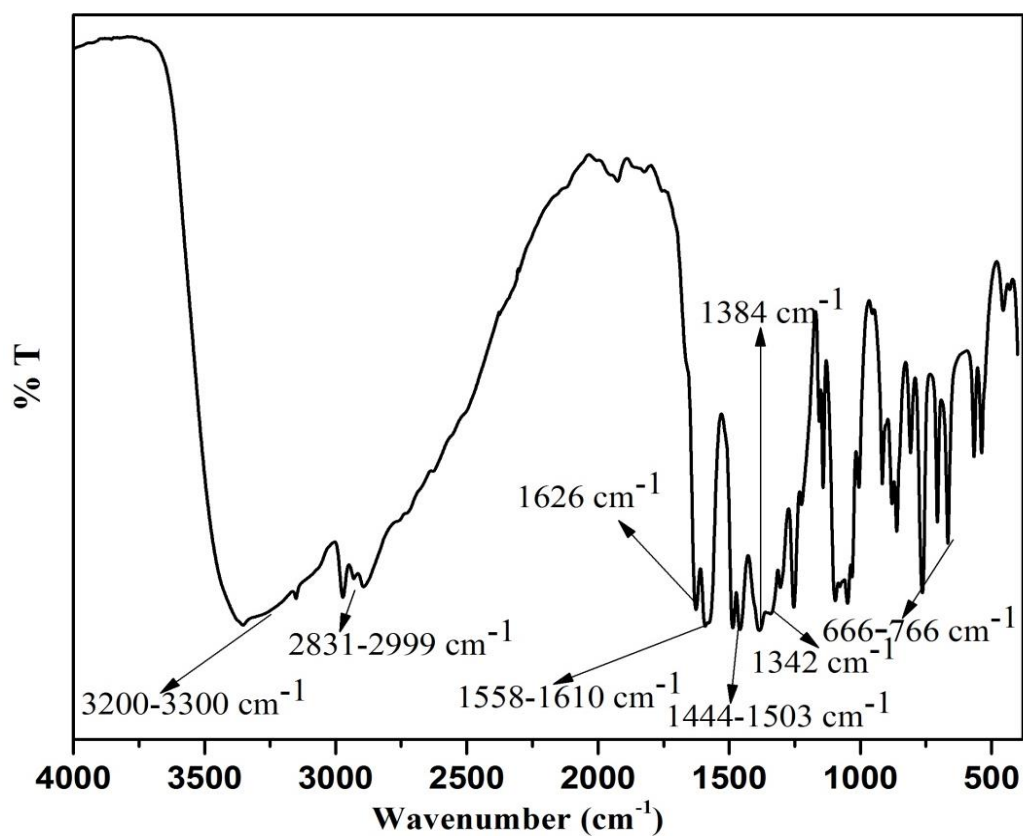
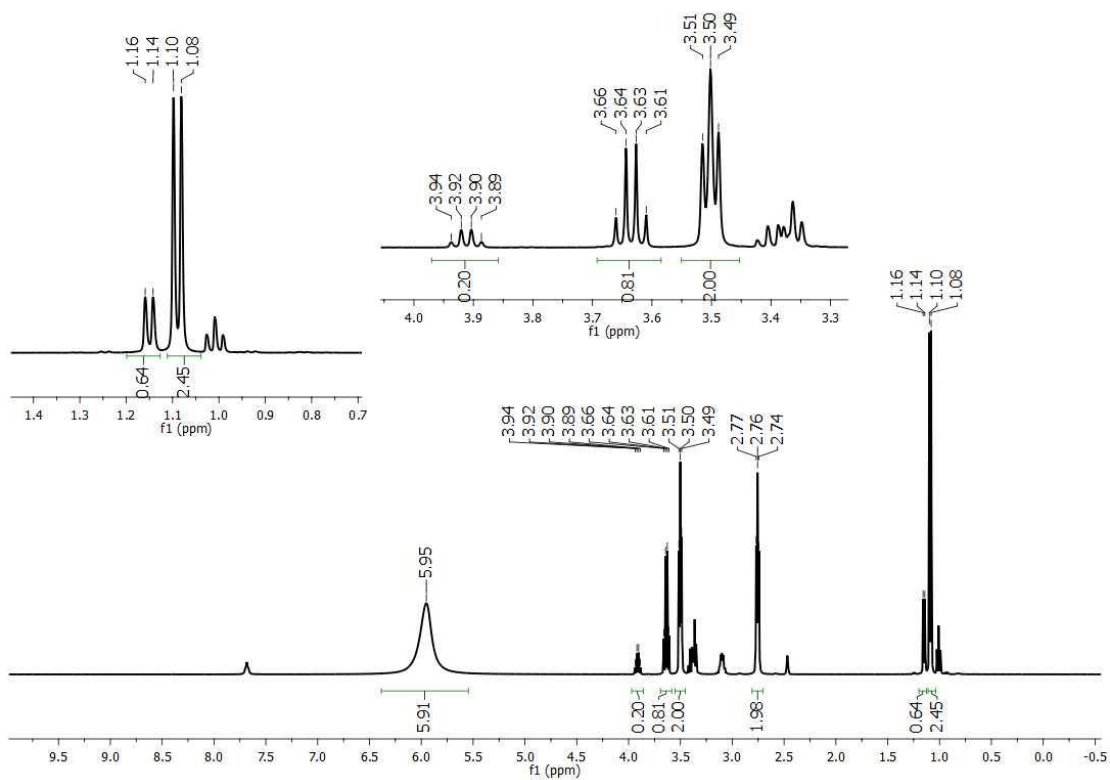


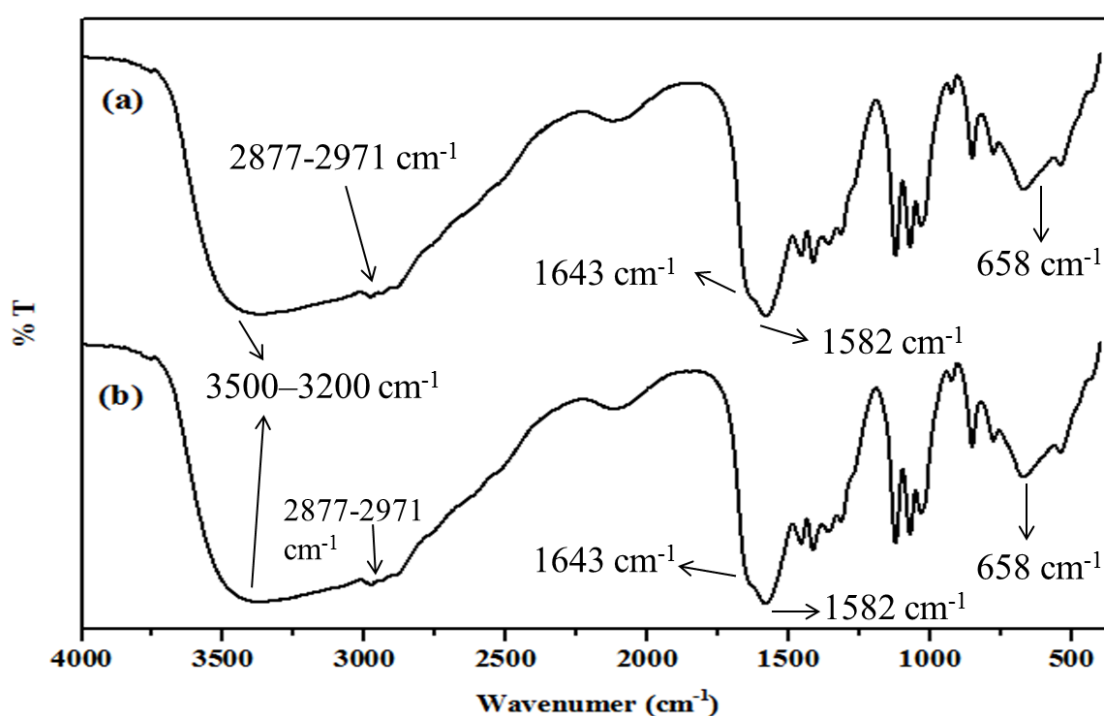
Figure 5.2c: FT-IR of virgin TSIL

Figure 5.2d: <sup>1</sup>H NMR spectra of virgin MLIL

$^1\text{H-NMR}$  spectra (the frequency of signal or *Chemical shift*,  $\delta$  ppm) measured on a Bruker 400 MHz spectrometer using  $\text{DMSO-d}_6$  as the solvent of the ‘as synthesized MLIL’ shown in Figure 5.2d. The noticeable signals lead to the following observations.  $\delta$ : 5.95 ppm (broad singlet, sum of ammonium and OH protons), 3.61, 3.63, 3.64, 3.66 ppm and 3.89, 3.90, 3.92, 3.94 ppm (q, 1H,  $\text{CH}_3\text{-CH}$ , D(+) and L(-) lactic acid respectively), 3.49, 3.50, 3.51 ppm (t, 2H,  $\text{OH-CH}_2\text{-CH}_2$ ), 2.74, 2.76, 2.77 ppm (t, 2H,  $\text{OH-CH}_2\text{-CH}_2$ ), 1.08, 1.10 ppm and 1.14-1.16 ppm (d, 3H,  $\text{CH}_3\text{-CH}$ , D(+) and L(-) lactic acid respectively) (Yuan et al., 2007; Pavia et al. 2008).

Traces of solvent ethanol 3.35, 3.36, 2.37, 3.38 ppm (q, 2H,  $\text{CH}_3\text{-CH}_2\text{-OH}$ ), 0.99-1.03 ppm (t, 3H,  $\text{CH}_3\text{-CH}_2\text{-OH}$ ) (Gottlieb et al., 1997) and moisture in the form of HDO at 3.34 ppm (Gottlieb et al., 1997).

A comparison of the IR spectra and  $^1\text{H NMR}$  of  $\text{SO}_2$ -absorbed with the virgin MLIL shown in Figure 5.3a and 5.3b reveals that no new absorption bands form in the  $\text{SO}_2$ -absorbed IL. Also, no difference in the proton chemical shift was observed in (a) and (b) of Figure 5.3b. From these observations, it was concluded that ionic liquids investigated in the present work, absorb  $\text{SO}_2$  by physical absorption (Huang et al., 2006; Qu et al., 2013);



**Figure 5.3a: FTIR analysis of MLIL (a) before absorption and (b) after absorption**

and in all probability, the absorbed SO<sub>2</sub> gas remained in the molecular state without any formation of the chemical bond. The interaction between the two species was weak and probably occurred through hydrogen bonds, van der Waals forces,  $\pi - \pi$  interactions or the interaction may be Coulumbic.

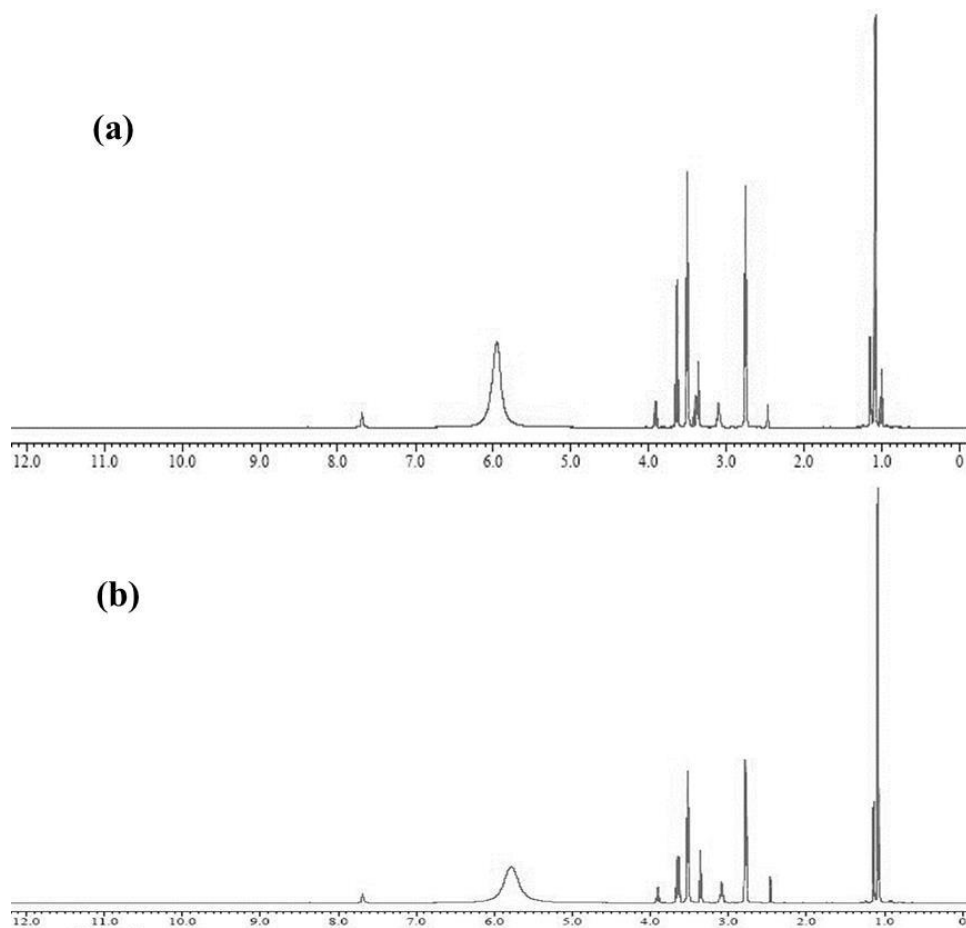


**Figure 5.3b: <sup>1</sup>H NMR spectra of MLIL (a) before absorption and (b) after absorption**

## 5.2 Absorption of SO<sub>2</sub> in IL

A close look at the graphs of the exit concentration of SO<sub>2</sub> in the exit gas, versus the time presented in this section, leads to the following statements. The time associated with the commencement of fall in the concentration of SO<sub>2</sub> in the exit gas, evident from the display on the data logger screen, was taken as the start of the experiment. Hence, the experimental data reported in this work does not include the time lag associated with the process of sampling of the exit gas at the suction point located at the apex of the reactor for its analysis, moisture removal in the condenser, generation of analyzer response and display on the VDU screen. This time lag continuously shifted to the end of the experimental run and the display of data.

It may also be observed in Figures 5.4 to 5.8, that it took about 2-3 minutes for the analyzer response to reach and remain at or above 90 percent of the maximum transient SO<sub>2</sub> removal efficiency of the ILs. This is attributed to two major reasons. Firstly, the batch of liquid is fed into the reactor when the gas flow rate and the predetermined SO<sub>2</sub> concentration in it have already attained a steady value. The former aspect is confirmed to avoid weeping through the distributor plate. The batch of liquid is carefully poured through the inlet port at the top of the column to avoid any escape of the liquid through the orifices of the distributor plate. The period, over which the batch of liquid-feed addition is completed, the depth of liquid in the reactor gradually increases. The concentration of SO<sub>2</sub> in the exit gas would, therefore, reduce with time depending on the depth of absorbent on the distributor plate at that particular instant. Secondly, immediately after complete addition of the batch of solvent to the reactor, about 96 percent of the reactor volume above the pool of reactant solution/ slurry remains occupied by the gas with an SO<sub>2</sub> concentration equal to that present in the feed stream. This occurs because when the solvent addition is started, the column remains full with the gaseous mixture with a SO<sub>2</sub> concentration, equal to that present in the feed gas. With the propagation of SO<sub>2</sub> absorption, the exit gas from the absorbent with a lower concentration of SO<sub>2</sub> first gets mixed up with this gas on the upper part of the reactor and therefore the analyzer shows higher values of SO<sub>2</sub> concentration or equivalently lower percent of transient SO<sub>2</sub> removal efficiency. In actual practice, the reduction in SO<sub>2</sub> concentration is substantially fast and a steep decrease in the SO<sub>2</sub> concentration after a very small period of the start of the



experiment can be seen if the above factors are taken into account in the design of reactor inclusive of the sampling and data analysis system.

### 5.2.1 Effects of different variables on the removal efficiency of SO<sub>2</sub>

#### 5.2.1.1 Effect of the nature of constituting ions in the ILs on absorption behavior

Figure 5.4a and Figure 5.4b show the effects of a combination of the hydroxyl ammonium cation and the two anions (lactate and salicylate ions) on transient SO<sub>2</sub> removal efficiency for virgin IL and regenerated IL respectively. Figure 5.4c shows the absorption capacities of the regenerated ILs.

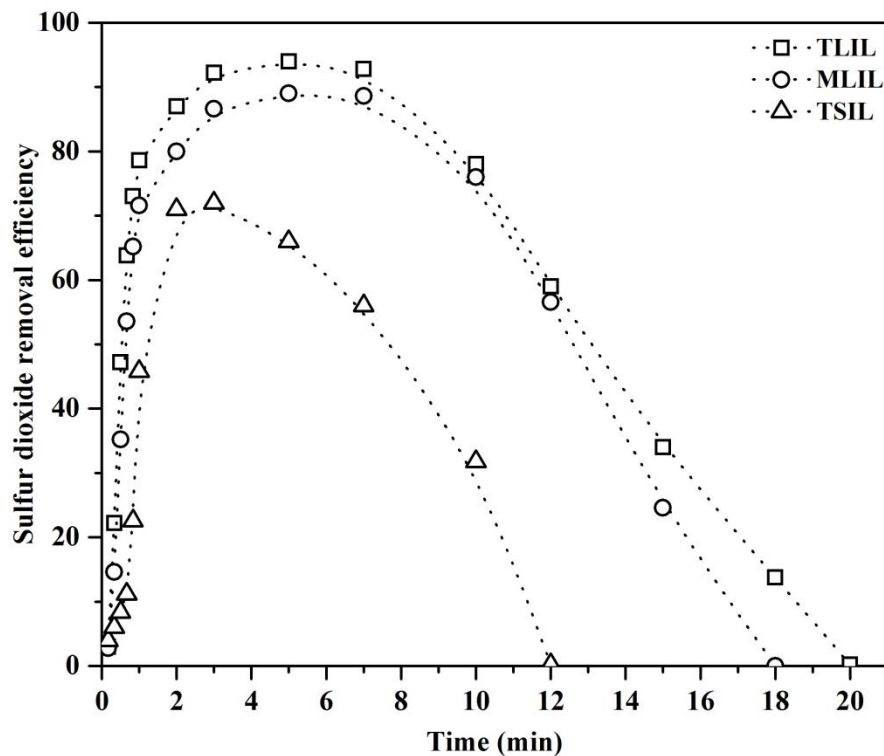


**Figure 5.4a** Variation of SO<sub>2</sub> absorption efficiency of virgin TLIL, MLIL and TSIL with time ( $u_G = 5.77 \times 10^{-2} \text{ ms}^{-1}$ ;  $C_{\text{SO}_2} = 500 \text{ ppm}$ ;  $V_{\text{IL}} = 2.5 \times 10^{-4} \text{ m}^3$ ); (Experimental data has been shown in Table 5A.1a)

It is observed in Figure 5.4a that when either 2-hydroxyethylammonium or tri-(2-hydroxyethyl) ammonium cation is associated with the lactate anion, each attains the magnitude, 89 and 94 percent respectively, of the transient values of maximum SO<sub>2</sub> removal efficiency. 70 % removal efficiency was observed when tri-(2-hydroxyethyl) ammonium cation is associated with salicylate anion.

In Figure 5.4b it is observed that the saturation time was more as compared to virgin ILs that concludes increase in absorption capacity after regeneration. The reason

attributed to this observation was analyzed with the help of NMR analysis. By  $^1\text{H}$  NMR peaks analysis, the amount of ethanol present in virgin IL was approx. 10% and the peaks before and after absorption do not show chemical shift. Apparently the core  $\text{SO}_2$  absorption behavior of virgin liquid is attributed to be formation of hydrogen bond of ethanol of IL and thus it hindrance the  $\text{SO}_2$  absorption by blocking the active sites of virgin IL.

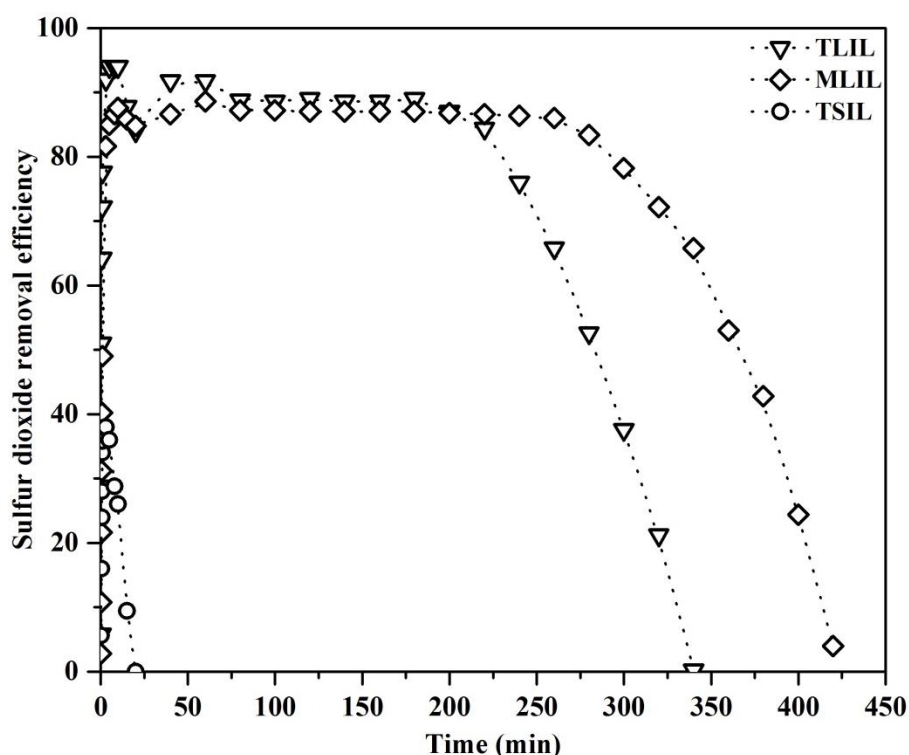


**Figure 5.4b Variation of  $\text{SO}_2$  absorption efficiency of 1<sup>st</sup> regenerated TLIL, MLIL and TSIL with time ( $u_G = 5.77 \times 10^{-2} \text{ ms}^{-1}$ ;  $C_{\text{SO}_2} = 500 \text{ ppm}$ ;  $V_{\text{IL}} = 2.5 \times 10^{-4} \text{ m}^3$ ); (Experimental data has been shown in Table 5A.1b)**

In Figure 5.4c, the  $\text{SO}_2$  absorption *capacity* of these ILs, was calculated by writing a mass balance for  $\text{SO}_2$  in the gas phase over the bubble column (equation mention in 4B.9). The experiments were conducted till the IL get exhausted or saturated with  $\text{SO}_2$ . Saturated point was considered when  $\text{SO}_2$  analyzer showed value near to inlet concentration (i.e. 500 ppm). The saturation time for 1<sup>st</sup> regenerated TLIL, MLIL and TSIL was 5.67 hrs, 7.0 hrs and 0.25 hr, respectively.

The absorption capacities of TLIL, MLIL and TSIL were obtained as 12.262 gm  $\text{SO}_2$ , 9.811 gm  $\text{SO}_2$  and 0.158 gm  $\text{SO}_2$  per  $2.5 \times 10^{-4} \text{ m}^3$  IL, respectively. Absorption capacity of MLIL was observed to be higher than TLIL (Yuan et al. 2007). It may, however, be observed that the IL synthesized using tri(2- hydroxyethyl ammonium),

and the salicylate ions showed very low level of the transient values of the maximum  $\text{SO}_2$  removal efficiency as well as the absorption capacity.

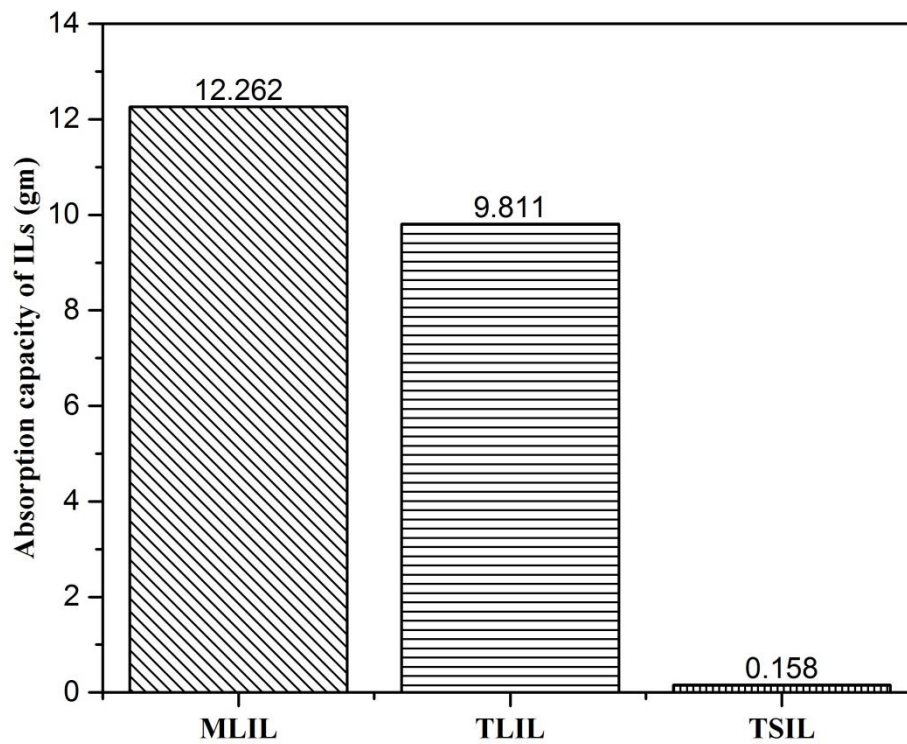


**Figure 5.4c. Complete  $\text{SO}_2$  absorption characteristics of MLIL, TLIL and TSIL after 1<sup>st</sup> regeneration of these ILs ( $u_G = 5.77 \times 10^{-2} \text{ m s}^{-1}$ ,  $C_{\text{SO}_2} = 500 \text{ ppm}$ ,  $V_{\text{IL}} = 2.5 \times 10^{-4} \text{ m}^3$ ); (Experimental data has been shown in Table 5A.2)**

Due to the very poor absorption behavior, TSIL is not considered as a desired alternative absorbent. Hence, further experiments were not performed with TSIL.

### 5.2.1.2 Effect of superficial velocity of gas on transient SO<sub>2</sub> removal efficiency

Effects of superficial velocity of gas on transient values of the SO<sub>2</sub> removal efficiency of the ionic liquids have been shown in Figure 5.5a.

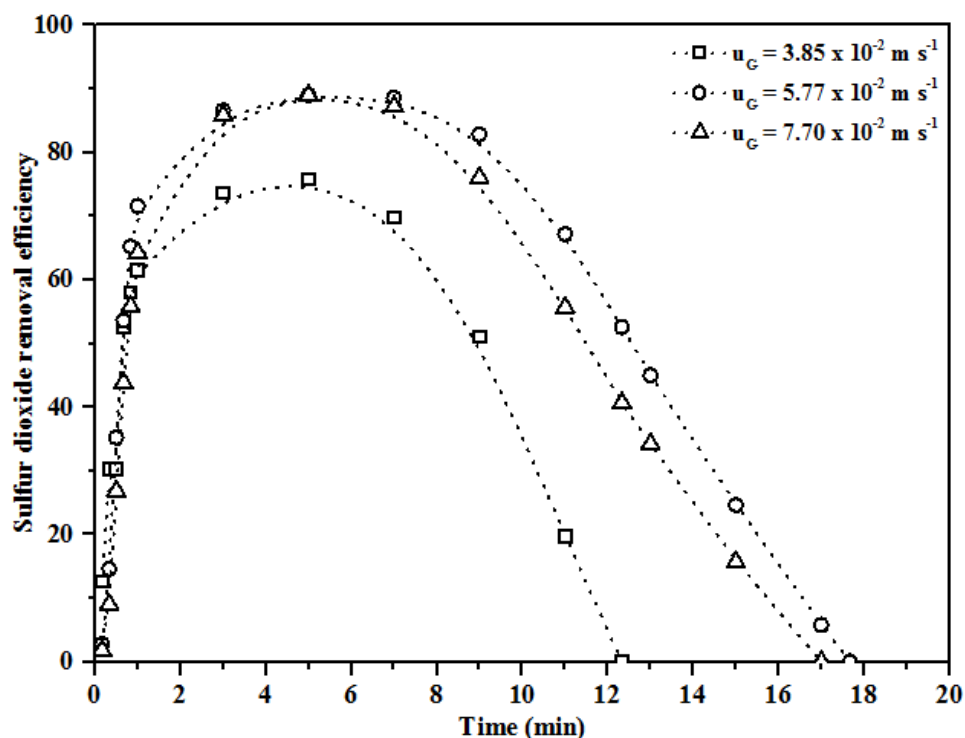


**Figure 5.5a: Effect of superficial velocity of gas on percent SO<sub>2</sub> removal efficiency by virgin MLIL ( $C_{\text{SO}_2} = 500 \text{ ppm}$ ,  $V_{\text{IL}} = 2.5 \times 10^{-4} \text{ m}^3$ ); (Experimental data has been shown in Table 5A.3)**

Three different superficial velocities, viz.,  $3.85 \times 10^{-2}$ ,  $5.77 \times 10^{-2}$  and  $7.7 \times 10^{-2} \text{ m s}^{-1}$  were used for this study at constant values of the other variables. It is observed that at a constant inlet SO<sub>2</sub> concentration of 500 ppm, as the superficial velocity of the gas is increased, maximum SO<sub>2</sub> removal efficiency increases from 76 percent and then approximately remains constant at about 89 percent. For the present experimental conditions, this maximum value of the transient removal efficiency remains effective over the time interval 3<sup>rd</sup> -7<sup>th</sup> min after the start of the experiment when either TLIL or MLIL is used as the absorbing liquid. With an increase in the superficial velocity of the gas, intensity of turbulence in the short bubble column increases due to the high viscosity of ionic liquid resulting in an increase in the mass-transfer coefficient for gas absorption. The increased amount of SO<sub>2</sub> is thereby absorbed from each bubble during its rise through the pool of liquid and removal efficiency is thereby increased. This is observed to occur as the superficial velocity is increased from  $3.85 \times 10^{-2}$  to  $5.77 \times 10^{-2}$

$^2 \text{ m s}^{-1}$ . However, rise-velocity of bubbles also increases with an increase in the superficial velocity of the gas. The gas bubbles then remain in the liquid pool for a shorter period and the contact time of the gas in a bubble with the surrounding liquid reduces. This, therefore, tends to reduce the amount of  $\text{SO}_2$  absorbed from the bubbles. While in the lower range of gas velocities the former effect predominates and removal efficiencies are increased, at the relatively higher range of gas velocities, these opposing factors possibly off-set each other's effect and maximum removal efficiency remains unchanged at about 89 percent.

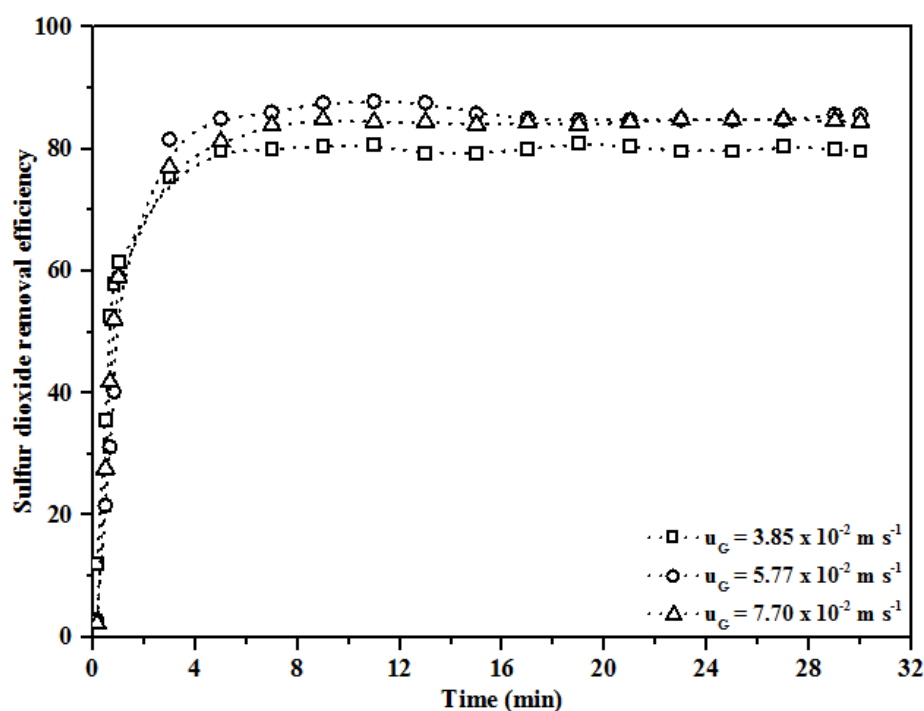


**Figure 5.5b.:** Effect of superficial velocity of gas on percent removal efficiency by 1<sup>st</sup> regenerated MLIL ( $C_{\text{SO}_2} = 500 \text{ ppm}$ ,  $V_{\text{IL}} = 2.5 \times 10^{-3} \text{ m}^3$ ); (Experimental data has been shown in Table 5A.4)

Reuse of MLIL after first regeneration for the absorption of  $\text{SO}_2$  at different superficial velocities of gas has been shown in Figure 5.5b. While the virgin IL got exhausted shortly after about 12-18 min of absorption operation depending on the value of the superficial velocity of the gas,  $u_G$ , the absorption capacity of the regenerated solvent after the first absorption increased enormously. This is because, after 1<sup>st</sup> absorption, ethanol was removed from IL which can be observed from  $^1\text{H}$ NMR spectra of IL after absorption (Figure 5.3b) that shows there is no peak of hydrogen due to ethanol. The experiments were discontinued after 30 min (or 60 min

as shown in Figures 5.8a and 5.8b) of reactor operation and till this period, virtually no decline in the transient SO<sub>2</sub> removal efficiency could be observed.

### 5.2.1.3 Effect of volume of solvent on percent SO<sub>2</sub> removal efficiency

Three different volumes,  $2.5 \times 10^{-4}$ ,  $3.5 \times 10^{-4}$  and  $5.0 \times 10^{-4} \text{ m}^3$  of the ionic liquid MLIL were used to study the effects of the volume of solvent on maximum SO<sub>2</sub> removal efficiency

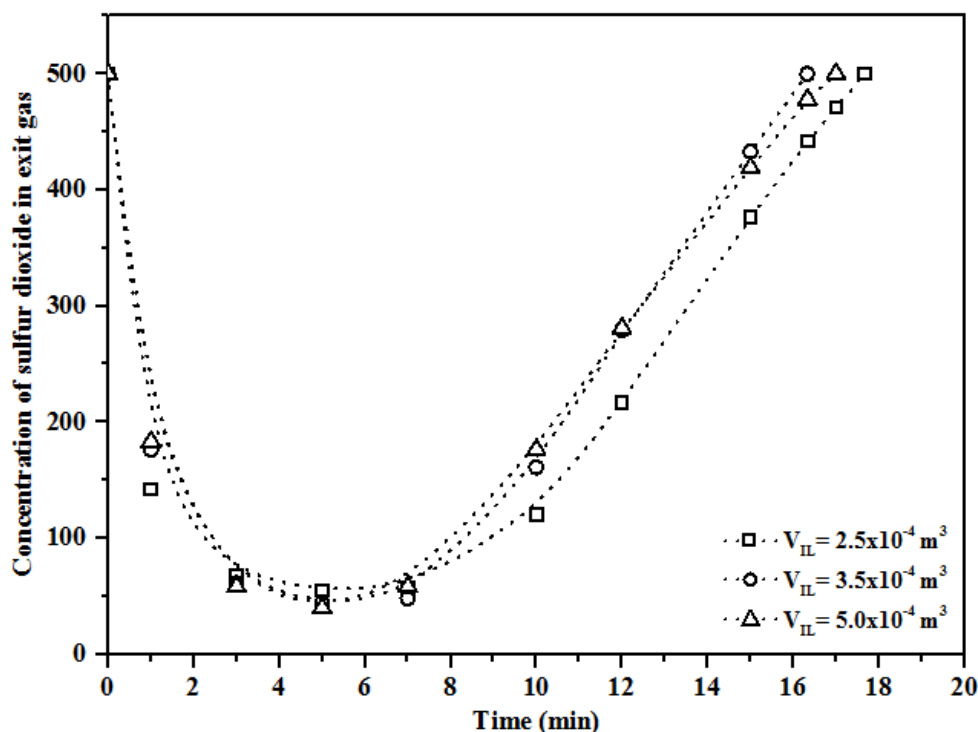


**Figure 5.6a** Effect of volume of virgin MLIL on exit concentration of SO<sub>2</sub> ( $u_G = 5.77 \times 10^{-2} \text{ m s}^{-1}$ ;  $C_{\text{SO}_2} = 500 \text{ ppm}$ ); (Experimental data has been shown in Table 5A.5)

and capacity of absorption. It is observed that SO<sub>2</sub> concentration at the reactor exit reduces from 500 ppm at the inlet to a minimum of 70, 50 and 40 ppm at the exit when the volumes of solvents used are  $2.5 \times 10^{-4}$ ,  $3.5 \times 10^{-4}$  and  $5.0 \times 10^{-4} \text{ m}^3$ , respectively (Figure 5.6a). It is also found that the maximum value of the SO<sub>2</sub> removal efficiency increases from 88 to 92 percent with an increase in the volume of IL used for absorption operation. Superficial velocity of feed gas being the same in each case, intensity of turbulence reduces with an increase in the volume of solvent used for absorption. The resulting lower value of mass-transfer coefficient tends to reduce the amount of SO<sub>2</sub> absorbed from each bubble for rising a definite height in the liquid pool. However, the depth of the clear liquid as well as the dispersion height increases

with an increase in the volume of solvent. The contact time of gas bubbles with the liquid in the dispersion increases and more  $\text{SO}_2$  is absorbed from each bubble.

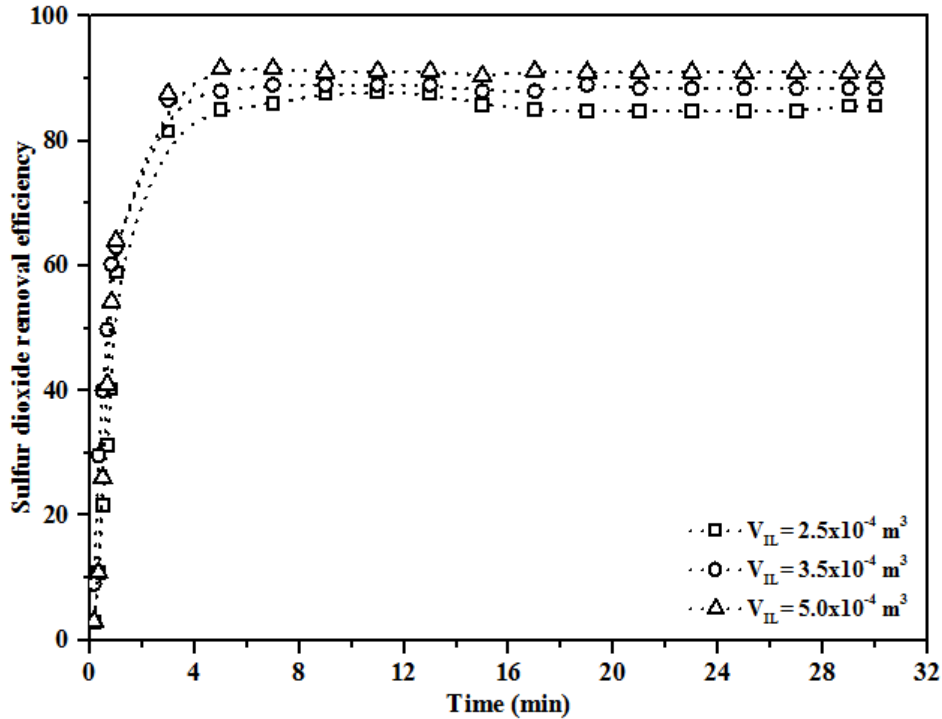


**Figure 5.6b** Effect of volume of regenerated MLIL after first regeneration on its transient  $\text{SO}_2$  removal efficiency ( $u_G = 5.77 \times 10^{-2} \text{ m s}^{-1}$ ;  $C_{\text{SO}_2} = 500 \text{ ppm}$ ); (Experimental data has been shown in Table 5A.6)

Maximum  $\text{SO}_2$  removal efficiency is thereby increased with an increase in the volume of feed solvent. Unlike superficial velocity of the gas, the effect of volume of solvent is found to be very important considering that for a given concentration of  $\text{SO}_2$  in the feed gas, volume of solvent can be increased to obtain the higher maximum  $\text{SO}_2$  removal efficiency.

Considering that at the time of pouring the solvent into the reactor, an excess of  $2.5 \times 10^{-4}$  (Run 1) and  $1.0 \times 10^{-4} \text{ m}^3$  (Run 2) of gas containing 500 ppm  $\text{SO}_2$  over that present at the start of Run 3, were occupying the reactor volume above the liquid phase reactant. For an analysis, one can divide the time-concentration graph into three parts. The first part extends up to about 3 min in which exit concentration of  $\text{SO}_2$  reduces with time, the middle part ranging from 3 to 6.5 min where it remains virtually constant and the third part which extends up to the end of the experiment. The latter shows a continuous increase in the exit concentration of the solute gas. The initial volume of gas containing 500 ppm  $\text{SO}_2$  over the batch of solvent at the start for

Run 3 being the minimum and solvent volume maximum, one would expect lowest exit concentration of SO<sub>2</sub> in all the three parts of the graph. However, except for the middle part, the reverse phenomena are found to occur. The total quantity of SO<sub>2</sub> absorbed is found to be more when the volume of solvent is least under otherwise identical operating conditions. Possible reasons for this unexpected observation may be as follows.

Absorption of SO<sub>2</sub> especially from a lean gaseous mixture is known to be a strongly gas-phase controlled process. The intensity of mixing in the gas phase and the consequent decrease in the gas-phase resistance to mass transfer is considered crucial to enhance the rate of mass transfer. In addition to this, although the intensity of mixing in the liquid phase for this situation is considered unimportant, a too high value of the solvent viscosity causes a substantial reduction in the value of the effective diffusivity or equivalently the mass-transfer coefficient. According to

Stokes-Einstein Equation  $\frac{D\mu}{T} = \text{Constant}$ ; the diffusivity is inversely proportional to

viscosity. A value of the dimensionless Peclet number,  $Pe$  equal to zero indicates complete mixing while a value equal to infinity signifies plug flow. The Peclet number in a bubble column is a function of axial gas dispersion coefficient,  $Pe = H \cdot V_g / (D_g \cdot \varepsilon_g)$ . The value of  $D_g$ , in turn, depends on the superficial velocity of the gas and the column diameter but independent of physicochemical properties of the system (Table 3C.2.1). Values of  $V_g$  and  $\varepsilon_g$  being the same, that of  $D_g$  remains constant for all the three experiments. Values of  $Pe$ , therefore, reduce with a reduction in the volume of liquid in the column and the intensity of mixing in the gas phase increases. Gas-phase mass-transfer resistance gets reduced, and the rate of SO<sub>2</sub> absorption is thereby enhanced. The similar argument is applicable for the liquid phase mass-transfer enhancement as well.

Regeneration and reuse of the different volumes of the ionic liquids for gas absorption resulted in exceptionally high SO<sub>2</sub> absorption capacity. While SO<sub>2</sub> removal efficiency in the case of virgin IL remains at its maximum value over only a short period, 4<sup>th</sup> to 6<sup>th</sup> min, with the regenerated IL it is found to remain uniformly high over exceptionally longer period and the experiments were discontinued after 30 min of reactor operation for the same reason as it was done in the case of superficial velocity of gas.



#### 5.2.1.4 Effect of initial concentration of SO<sub>2</sub> in feed gas on mass of SO<sub>2</sub> absorbed

Figure 5.7a shows the effect of initial concentration of SO<sub>2</sub> in feed gas on the variation of its transient removal efficiency by MLIL. The concentration of SO<sub>2</sub> in the feed was varied from 250 to 1500 ppm by diluting with air. Superficial velocity of gas and volume of solvent charged into the reactor were kept constant at  $5.77 \times 10^{-2} \text{ m s}^{-1}$  and  $2.50 \times 10^{-4} \text{ m}^3$ , respectively. It is observed (Figure 5.7a) that the maximum value of the SO<sub>2</sub> removal efficiency firstly reduces and then increases with an increase in the concentration of SO<sub>2</sub> in the feed gas.

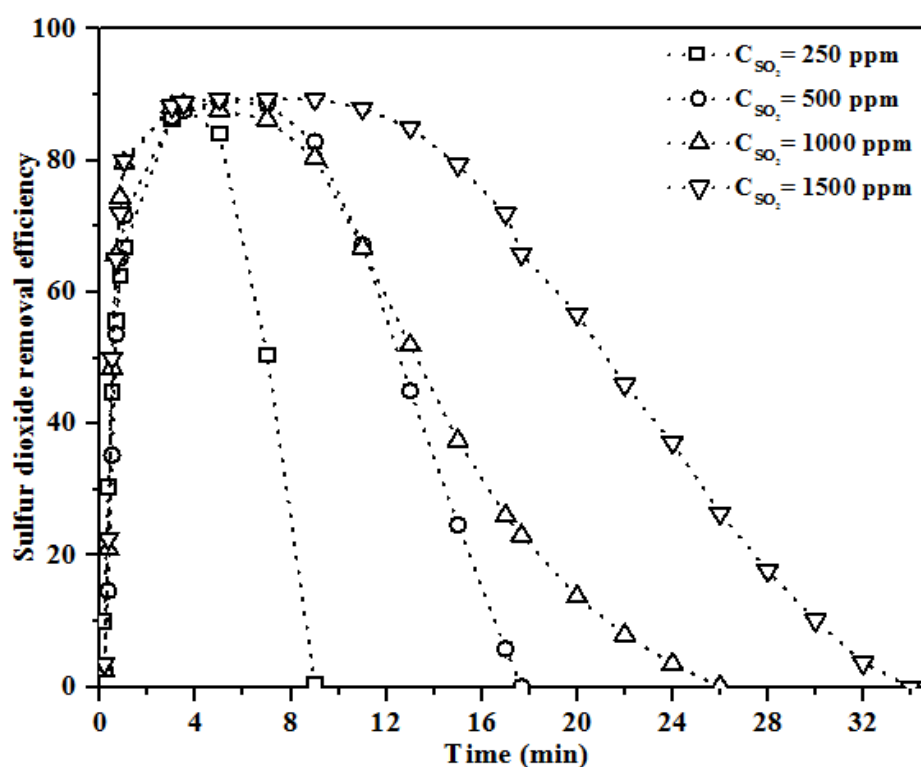


**Figure 5.7a:** Effect of initial concentration of SO<sub>2</sub> in feed gas on its percent removal efficiency by virgin MLIL ( $u_G = 5.77 \times 10^{-2} \text{ m s}^{-1}$ ;  $V_{IL} = 2.5 \times 10^{-4} \text{ m}^3$ ); (Experimental data has been shown in Table 5A.7)

At a given temperature and operating pressure, the solubility of SO<sub>2</sub> in the ionic liquid gets enhanced with an increase in its concentration in the gas phase. Total moles of SO<sub>2</sub> absorbed from each bubble and hence the rate of absorption, at a fixed superficial velocity of the gas, is thereby increased. On the other hand, SO<sub>2</sub> removal efficiency tends to reduce because of the definition used for its calculation. The latter signifies that the concentration of SO<sub>2</sub> in the feed gas appears in the denominator of the expression used for estimation of its removal efficiency. It is however observed in Fig.

5.7a that these two opposing factors cancel each other's effect and the reduction in the maximum value of SO<sub>2</sub> removal efficiency is only marginal. However, if the further increase in SO<sub>2</sub> concentration causes a substantial reduction in bubble size due to the larger amount of SO<sub>2</sub> absorbed from it, the mass transfer is further accelerated by turbulence at the bubble surface, and the removal efficiency is increased further, as seen for 1500 ppm. SO<sub>2</sub> absorption capacity, defined as mol of SO<sub>2</sub> absorbed per mol of IL, is found to decrease with a reduction in the partial pressure of SO<sub>2</sub> in the feed gas. Similar observations have also been reported by Li et al., 2017; Huang et al., 2006 and Cui et al., 2015. In the present investigation also, for the semi-batch operation of the contactor, absorption saturation time is observed to be the shortest for 250 ppm SO<sub>2</sub> gas.

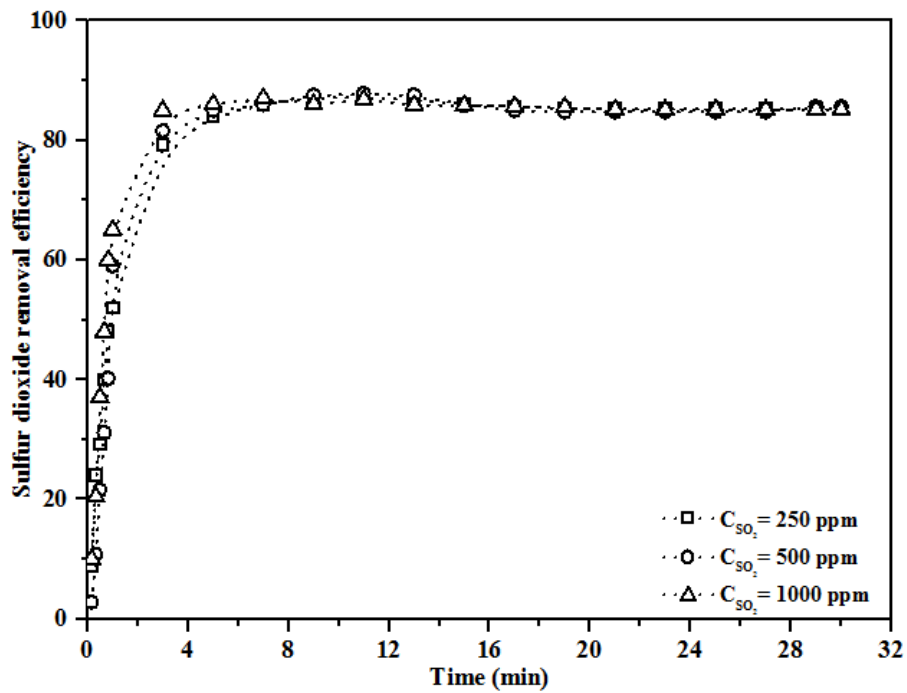


**Figure 5.7b: Effect of initial concentration of SO<sub>2</sub> in feed gas on its removal efficiency by use of regenerated (after 1<sup>st</sup> absorption) MLIL ( $u_G = 5.77 \times 10^{-2} \text{ m s}^{-1}$ ;  $V_{IL} = 2.5 \times 10^{-4} \text{ m}^3$ ); (Experimental data has been shown in Table 5A.8)**

Effect of variation of SO<sub>2</sub> concentration in the feed gas on its removal efficiency by absorption in regenerated (after the first absorption) IL has been shown in Figure 5.7b. At the end of 11<sup>th</sup> min from the start of absorber operation, SO<sub>2</sub> removal efficiencies attain the maximum values of 87.2, 87.8 and 86.8 percent for SO<sub>2</sub> feed concentrations of 250, 500 and 1000 ppm, respectively. At the end of 28<sup>th</sup> min, the respective removal efficiencies attain steady values of 85.2, 85.6 and 85.1 percent. It is believed

that these removal efficiencies can be increased further by a simultaneous increase in the volume of feed solvent and superficial velocity of the gas. As already stated, the absorption capacity of the regenerated IL increased to a large extent compared to the virgin liquid and the experiments were discontinued after 30 min of absorber operation.

### 5.2.1.5 Comparison of transient SO<sub>2</sub> removal efficiencies of virgin and regenerated ILs

The regeneration and recyclability performance of ionic liquids are very important aspects for their application in gas absorption operations as these play a significant role in the economic feasibility of the process. In the present investigation, it is observed that unlike the common regenerative solvents, the ionic liquids do not show the reduction in their absorption capacities even after successive absorption and regeneration operations. This is best explained in the light of the experimental data shown in Figures 5.8a and 5.8b.

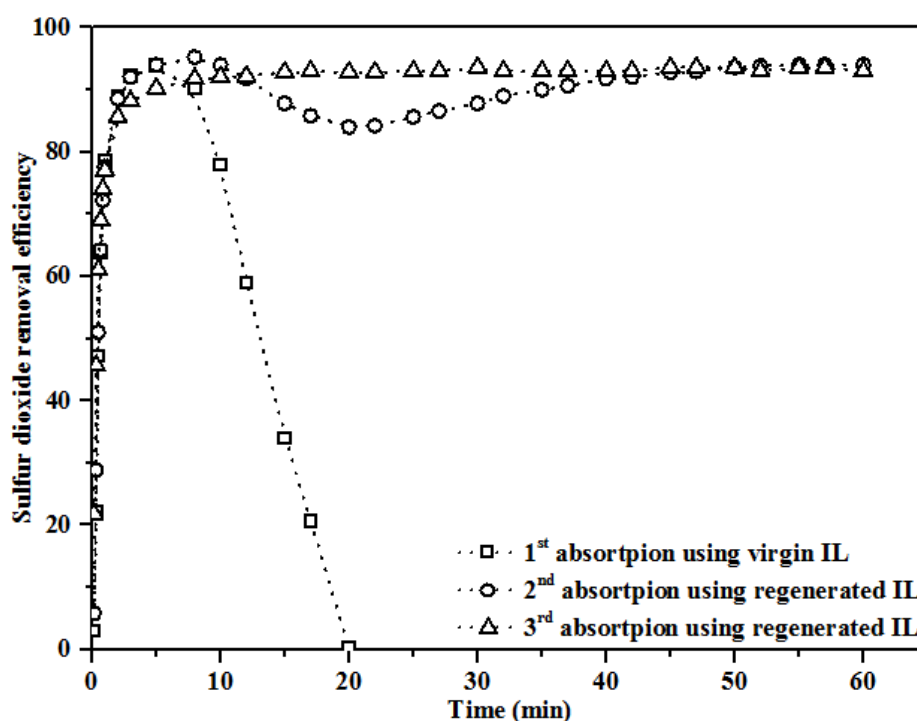


**Figure 5.8a:** Variation of percent SO<sub>2</sub> removal efficiency by TLIL with time for three consecutive absorption cycle ( $u_G = 5.77 \times 10^{-2} \text{ m s}^{-1}$ ;  $C_{\text{SO}_2} = 500 \text{ ppm}$ ;  $V_{IL} = 2.5 \times 10^{-4} \text{ m}^3$ ); (Experimental data has been shown in Table 5A.9)

It is also observed from Figures 5.8a and 5.8b that the virgin IL absorbents got exhausted in the shorter period during the first absorption compared to those of the

regenerated ionic liquids. This is attributed to the presence of traces of ethanol in virgin ILs (Figure 3a) that result in the formation of additional hydrogen bonds or analogous weak interactions with the amine group of ionic liquids and being not accessible to accommodate the  $\text{SO}_2$  molecules, lead to a reduction in the absorption capacity of each of the two virgin ILs.

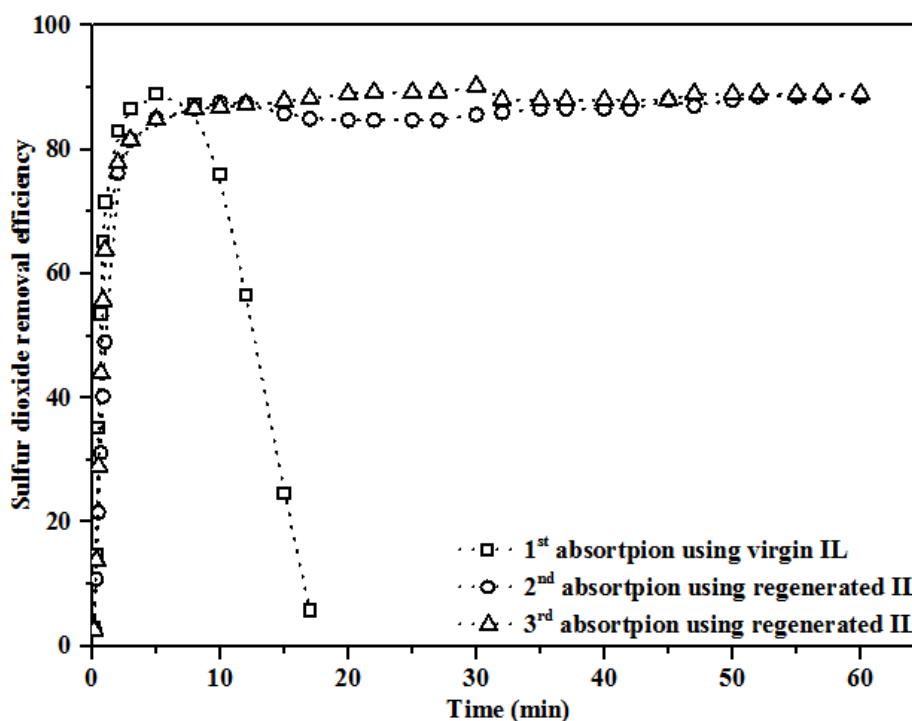


**Figure 5.8b:** Variation of percent  $\text{SO}_2$  removal efficiency by MLIL with time for three consecutive absorption regeneration cycles ( $u_G = 5.77 \times 10^{-2} \text{ m s}^{-1}$ ;  $C_{\text{SO}_2} = 500 \text{ ppm}$ ;  $V_{\text{IL}} = 2.5 \times 10^{-4} \text{ m}^3$ ); (Experimental data has been shown in Table 5A.10)

On regeneration of the exhausted ILs, the residual amount of ethanol gets evaporated (Figure 3b) and the absorption capacity of the ILs is thereby largely enhanced. Absorption capacities and transient removal efficiencies of both the ionic liquids after successive regenerations are observed to increase even after 60 min of absorption operation. These observations are certainly very important to explore the further beneficial effects of these ionic liquids for desulfurization.

## PART-II: Absorption of SO<sub>2</sub> in aqueous slurries of Ca(OH)<sub>2</sub> and CaCO<sub>3</sub>

### 5.3 Effects of different variables on SO<sub>2</sub> removal efficiency by Ca(OH)<sub>2</sub> and CaCO<sub>3</sub> slurries in bubble column and foam-bed reactors

#### 5.3.1 Simultaneous variation of exit concentration of SO<sub>2</sub>, pH of reactant slurry and gas hold-up with time in bubble column reactor for a typical experimental run

Figure 5.9 shows the interrelation of SO<sub>2</sub> concentration in the exit gas, pH of reacting slurry and gas hold-up at the time of operation of a bubble column reactor. The data shown in the figure corresponds to  $C_{SO_2} = 500$  ppm,  $V_{sl} = 250 \times 10^{-6} \text{ m}^3$  and  $u_G = 5.77 \times 10^{-3} \text{ ms}^{-1}$ . Under the experimental conditions the reaction is observed to satisfy the condition of instantaneous reaction and until 15 minutes from the start of the reaction, pH remains constant at 12.5. During this time interval, exit gas concentration is constant about 5-10 ppm, as shown in Figure 5.9. At the start of the reaction, the feed slurry contains the saturated solution of *B* along with its suspended particles, about 10 volume percent of which comprises of particles of  $d_p \leq 1/\delta$  ( $\delta$  is film thickness).

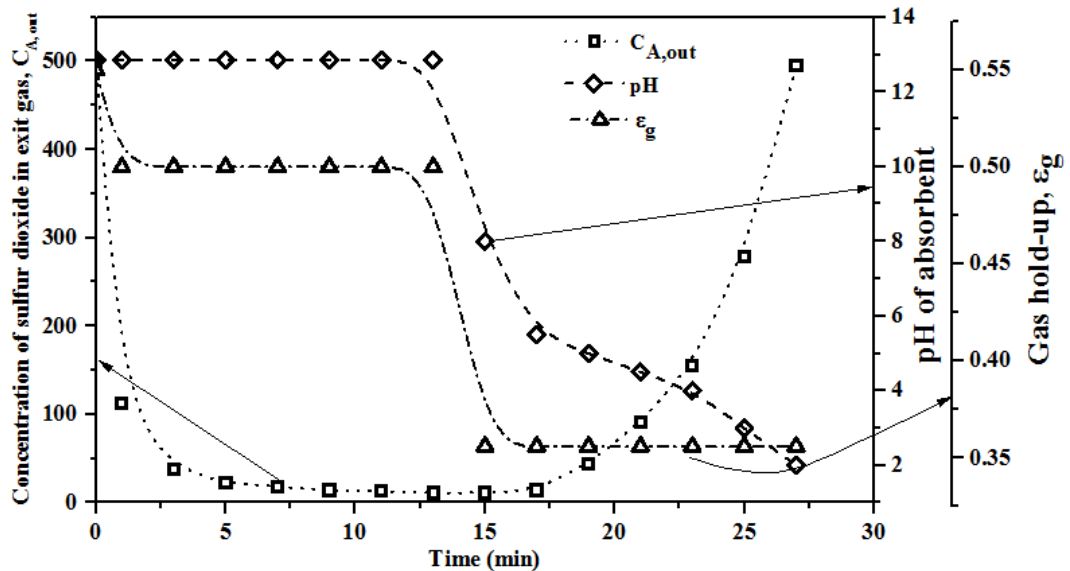


Figure 5.9. Variation of the concentration of SO<sub>2</sub> in exit gas, pH of absorbent and gas hold-up with time in the bubble column reactor ( $u_G = 5.77 \times 10^{-2} \text{ m s}^{-1}$ ,  $C_{SO_2} = 500$  ppm and  $V_{sl} = 2.5 \times 10^{-4} \text{ m}^3$ ); (Experimental data has been shown in Table 5B.1)

Therefore reaction of dissolved *B* with the absorbed SO<sub>2</sub> occurs in parallel with the continuous supply of *B* by dissolution of particles within the film and the reaction

plane shifts very close to the gas-liquid interface. But because initially, about 96 percent of the reactor volume remains occupied with the gas having a concentration of  $\text{SO}_2$  equal to that in the feed, denoted here as residual gas, it takes about 3 to 5 min. to remove this residual gas by the exit gas flow. The data logger, therefore, shows, due to mixing with the residual gas, higher values than the actual exit concentration of  $\text{SO}_2$ . When the amount and size of particles reduces to such an extent that particle dissolution rate has reduced substantially and maximum extent of  $\text{SO}_2$  absorption and reaction is no more possible, exit concentration of  $\text{SO}_2$  starts increasing and simultaneously pH of the slurry starts decreasing gradually. When the exit gas contains primarily air (very low concentration of  $\text{SO}_2$ ) and the reacting slurry contains particles of hydrated lime, the gas bubbles are stabilized by the particles and the dispersion height vis a vis gas holdup remains at a high value. As soon as the particles in the slurry get exhausted, the residual amount of dissolved lime reacts. Water then starts acting as the absorbent, pH decreases until it reaches to 2 and  $\text{SO}_2$  gas bubbles merely passes through the solution without any further absorption and reaction. The gas bubbles break, there being no mechanism to stabilize it and lead to a reduction in the height of dispersion and gas holdup.

### 5.3.2 Gas hold-up ( $\epsilon_g$ ) in the bubble column

Gas holdup was studied in semi-batch bubble column reactor using hydrated lime and calcium carbonate slurry with a solids loading of  $4.0 \text{ kg m}^{-3}$  each (Figure 10). Superficial velocity of gas was varied from  $3.85 \times 10^{-2}$  -  $7.70 \times 10^{-2} \text{ m s}^{-1}$ .

It is observed that gas hold-up increases with an increase in the superficial velocity of gas for both slurries. Gas holdup for the case of the lime slurry is found to be higher, varies from 0.36 to 0.71, over the entire range of superficial gas velocity than those, ranging from 0.31 to 0.64, with the calcium carbonate slurry. Hydrated lime with lower density  $\rho_{hl} = 2.2 \times 10^3 \text{ kg m}^{-3}$  has been observed to stabilize gas bubbles compared to the heavier particles of calcium carbonate,  $\rho_{cc} = 2.711 \times 10^3 \text{ kg m}^{-3}$ . The latter possess the lesser wetting ability and result in a lower dispersion height and gas holdup.

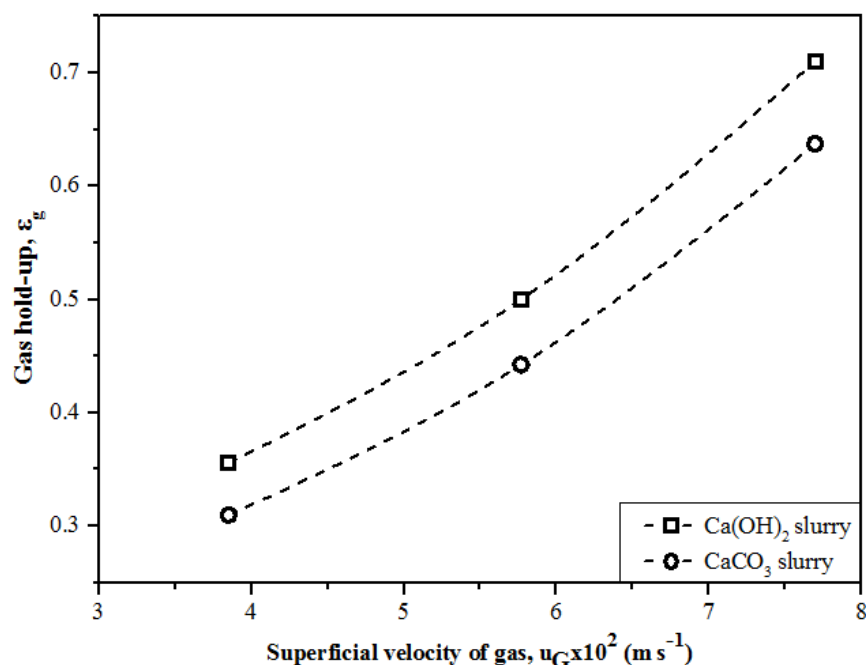


**Figure 5.10** Variation of gas hold-up with superficial velocity of gas in the slurry bubble column ( $C_{\text{SO}_2} = 500$  ppm and  $V_{sl} = 2.5 \times 10^{-4} \text{ m}^3$ ,  $m_B^T(0) = 4.0 \text{ kg m}^{-3}$ ); (Experimental data has been shown in Table 5B.2)

### 5.3.3 Effects of different variables on SO<sub>2</sub> removal efficiency

#### 5.3.3.1 Effect of initial concentration of sulfur dioxide in feed gas on its removal efficiency

Concentration of sulfur dioxide gas in the feed gas mixture was varied from 250 to 1500 ppm to study its effect on percent removal of SO<sub>2</sub>. Experimental results have been shown in Figure 11a. SO<sub>2</sub> removal efficiency instantly increases to 99 percent and remains there till the reactant particles get reduced in size as well as in amount to such an extent that the system ceases its capacity to absorb any appreciable amount of SO<sub>2</sub>. Thereafter only the solvent gradually gets saturated with the absorbed SO<sub>2</sub> and its concentration in the exit gas becomes equal to that in the feed gas. As the concentration of SO<sub>2</sub> in the feed gas is increased, gas phase resistance to mass transfer reduces and interfacial concentration of sulfur dioxide in the liquid phase increases. This increases the rate of gas absorption and reaction, and, the concentration of dissolved solid in the liquid phase is thereby reduced at a faster rate. This phenomenon lends more solid to dissolve in the liquid to restore its solubility. Thus, the rate of gas absorption, solid dissolution and its reaction increases with an increase in the concentration of SO<sub>2</sub> in the feed gas.

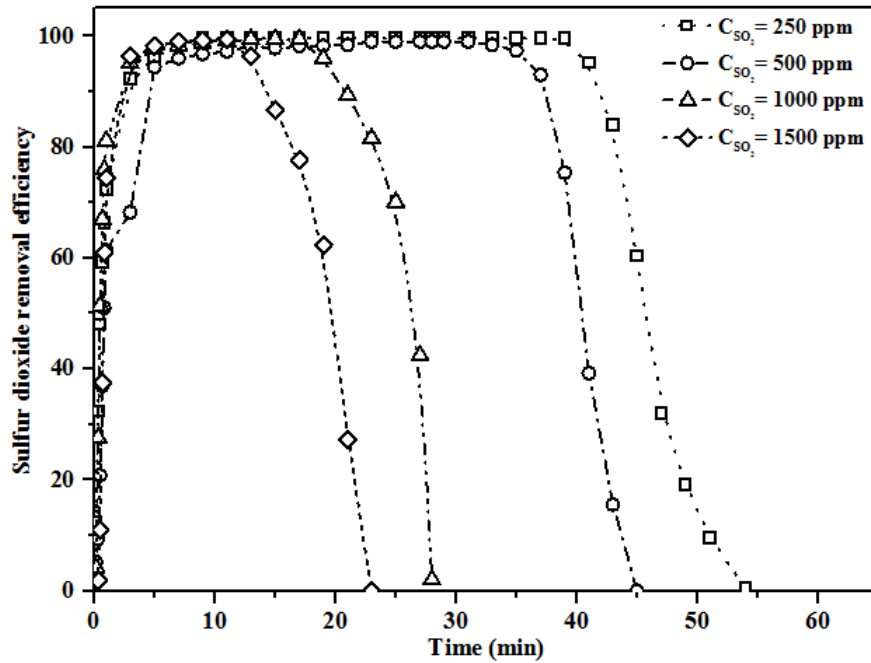


Figure 5.11a Effect of initial  $\text{SO}_2$  concentration in the feed gas on its percent removal efficiency by  $\text{Ca}(\text{OH})_2$  slurry ( $u_G = 3.85 \times 10^{-2} \text{ m s}^{-1}$ ,  $m_B^T(0) = 4 \text{ kg m}^{-3}$  and  $V_{sl} = 2.5 \times 10^{-4} \text{ m}^3$ ); (Experimental data has been shown in Table 5B.3)

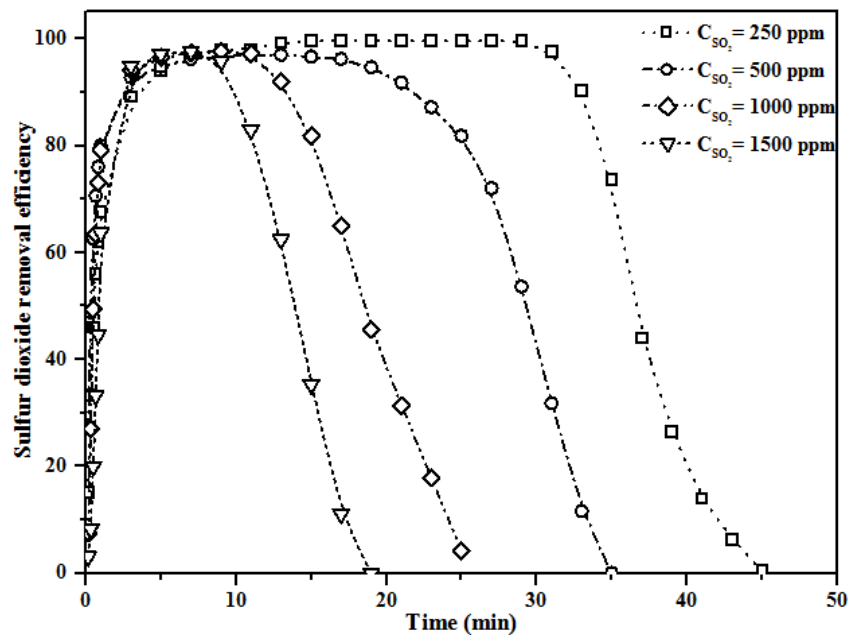


Figure 5.11b Effect of initial  $\text{SO}_2$  concentration of inlet gas on percent removal efficiency by  $\text{CaCO}_3$  ( $u_G = 3.85 \times 10^{-2} \text{ m s}^{-1}$ ,  $m_B^T(0) = 4 \text{ kg m}^{-3}$  and  $V_{sl} = 2.5 \times 10^{-4} \text{ m}^3$ ); (Experimental data has been shown in Table 5B.4)



For a comparison of the  $\text{Ca}(\text{OH})_2$  slurry- $\text{SO}_2$  system with that incorporating  $\text{CaCO}_3$  slurry, desulfurization of simulated flue gas was studied using the same loading of calcium carbonate as that used for the hydrated lime system. It was observed that in addition to the gas-phase resistance to  $\text{SO}_2$  absorption, the dissolution rate of limestone in the liquid phase plays an important role in determining the rate of reaction. The position of the reaction plane in the film is established by the rate of diffusion of absorbed  $\text{SO}_2$  and that of dissolved calcium carbonate. When the inlet  $\text{SO}_2$  concentration is increased, the flux of  $\text{SO}_2$  gets enhanced. However, the dissolution rate of calcium carbonate does not increase so fast to accommodate the effect of increased flux of  $\text{SO}_2$ . Therefore, the reaction plane within the liquid film gets shifted further away from the gas-liquid interface.

Additionally, increased rate of back diffusion of  $\text{CO}_2$  generated by the reaction and dissolved in the liquid reduces the effective flux of dissolved reactants to the reaction plane. Although total moles of  $\text{SO}_2$  absorbed and reacted with component  $B$  increases with an increase in the initial concentration of  $\text{SO}_2$ , its maximum removal efficiency reduces as the inlet concentration is increased from 250 ppm to 1500 ppm, owing to the definition used for its calculation in addition to the reasons mentioned above.

### 5.3.3.2 Effect of superficial gas velocity

Effect of superficial velocity of gas on  $\text{SO}_2$  removal efficiency by use of hydrated lime slurry as an absorbent in a bubble column reactor has been shown in Figure 5.12a. Three different values of superficial velocity of gas:  $3.85 \times 10^{-2}$ ,  $5.77 \times 10^{-2}$  and  $7.70 \times 10^{-2} \text{ m s}^{-1}$  were used to study its effect on the  $\text{SO}_2$  removal efficiency under otherwise identical experimental conditions. Partial pressure in the feed gas being very low, 0.001 atm, and absorption of  $\text{SO}_2$  occurred under purely gas-phase controlled conditions as shown in chapter 3.

With an increase in the superficial velocity of gas, gas phase mass-transfer resistance reduced, one of the most important parameters governing the rate of mass transfer for a gas phase controlled process. In addition to  $k_G$ ,  $k_l$  and  $k_{sl}$  also increase and cause an increase in the rate of absorption of  $\text{SO}_2$ . This is confirmed from Figure 5.13a. When the gas velocity is increased by a factor of two, the rate of reaction becomes twice and consequently the time required to completely consume  $1.0 \times 10^{-3} \text{ kg}$  of reactant  $B$  reduces to half (Figure 5.12a). When the gas flow rate is doubled, the number of bubbles entering the reactor is expected to be less than twice, as bubble size increases

with an increase in the gas rate. In spite of this, the proportionate increase in the rate of gas absorption and reaction signifies that liquid phase mass-transfer coefficient for gas absorption increases.

Concentration of  $\text{SO}_2$  in the exit gas depends on the total moles of  $\text{SO}_2$  absorbed by each bubble which in turn varies with the residence time of bubbles in the slurry. With an increase in the superficial velocity of the gas, moles of  $\text{SO}_2$  absorbed by each bubble reduce due to a reduction in the residence time of bubbles in the slurry. This tends to reduce the  $\text{SO}_2$  removal efficiency. The observed decrease in the transient values of maximum  $\text{SO}_2$  removal efficiency by about 1 percent is, therefore, the resultant of the two opposing effects mentioned above.

As the superficial gas velocity is increased, the rate of gas absorption and reaction increase and concentration of component  $B$  in the slurry reduces at an increased rate. Amount of lime fed into the reactor being same in each case, further reaction and  $\text{SO}_2$  removal efficiency follows a downward trend at an earlier time as the gas velocity is increased. For the case of highest

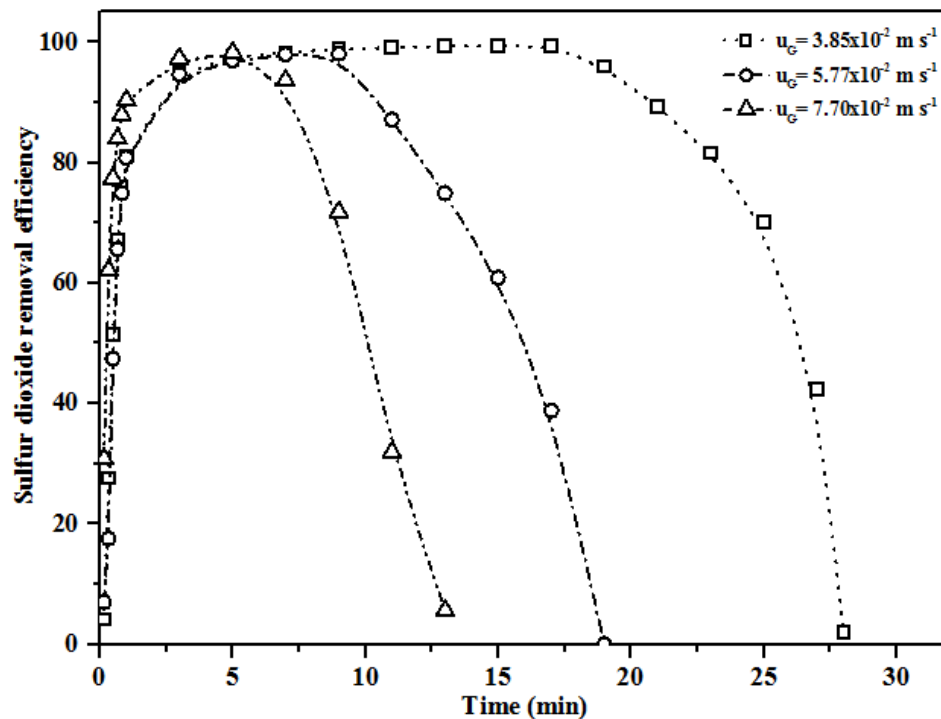


**Figure 5.12a** Effect of superficial velocity of gas on  $\text{SO}_2$  removal efficiency by  $\text{Ca}(\text{OH})_2$  slurry ( $C_{\text{SO}_2} = 1000 \text{ ppm}$ ,  $m_B^T(0) = 4.0 \text{ kg m}^{-3}$  and  $V_{sl} = 2.50 \times 10^{-4} \text{ m}^3$ ); (Experimental data has been shown in Table 5B.5)

superficial gas velocity,  $7.70 \times 10^{-2} \text{ ms}^{-1}$  used in this study, the maximum removal efficiency possibly occurs very early but the measured data cannot capture this as about 96 percent of the reactor volume initially remains filled with  $\text{SO}_2$  with a concentration equal to that in the feed gas and the instantaneous value of actual concentration not accessible at the sampling point. The apparent decrease by 1 percent, in the maximum  $\text{SO}_2$  removal efficiency, is attributed to the already decreased concentration of component  $B$  in the slurry rather than to the reduced residence time of bubbles caused by an increase in the superficial velocity of the gas.

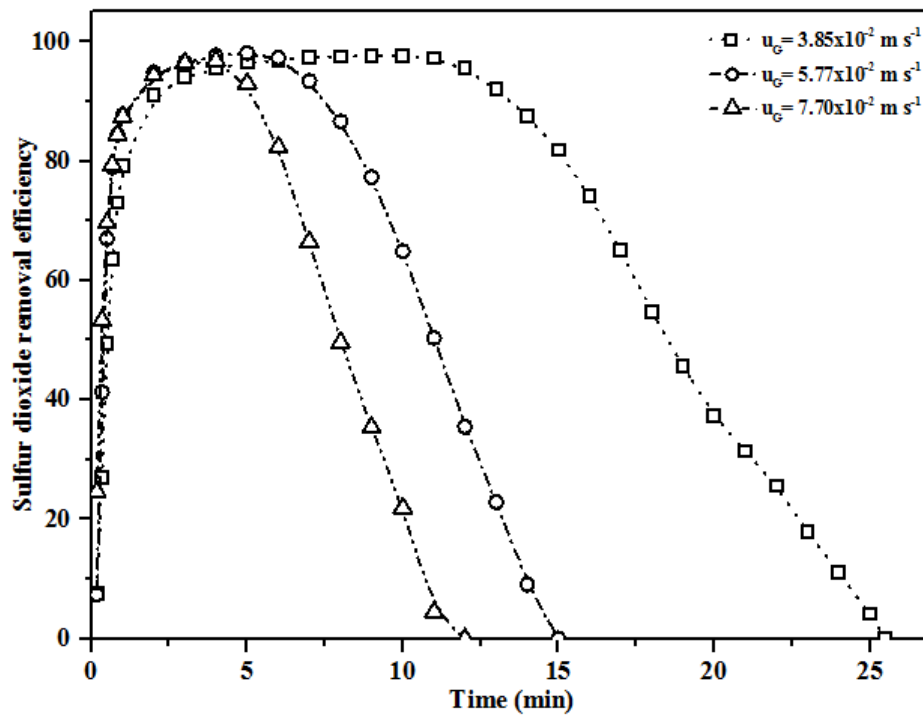


**Figure 5.12b** Effect of superficial velocity of gas on percent  $\text{SO}_2$  removal efficiency by  $\text{CaCO}_3$  slurry ( $C_{\text{SO}_2} = 1000 \text{ ppm}$ ,  $m_B^T(0) = 4.0 \text{ kg m}^{-3}$  and  $V_{sl}$  of  $2.50 \times 10^{-4} \text{ m}^3$ ); (Experimental data has been shown in Table 5B.6)

It is observed that a maximum removal efficiency of 99.4% is achieved at the lowest superficial velocity of gas of  $3.85 \times 10^{-2} \text{ ms}^{-1}$  that decreases to 98% for higher values of  $u_G$ ,  $5.77 \times 10^{-2}$  and  $7.70 \times 10^{-2} \text{ m s}^{-1}$ . But in the case of calcium carbonate, the removal efficiency increases from 97.7 to 98.1 possibly due to an increase in the dissolution rate of suspended particles of calcium carbonate. The solubility of  $\text{CaCO}_3$  in water is 143.5 times lower than that of  $\text{Ca(OH)}_2$  and that sulfur-dioxide is highly soluble in water. With further increase in  $u_G$ , viz.,  $7.70 \times 10^{-2} \text{ m s}^{-1}$ , removal efficiency reduced

to 96.8 percent possibly due to the dominating effect of the reduced residence time of bubbles in the slurry over the increased rate of gas absorption and reaction.

### 5.3.3.3 Effect of initial solids loading

Effects of the initial loading of hydrated lime and calcium carbonate on  $\text{SO}_2$  removal efficiency in the bubble column reactor have been shown in Figures 5.13 (a) and 5.13 (b), respectively. Initial solids loading in the feed slurry was varied from 4 to 8  $\text{kg m}^{-3}$  while values of all the other variables and parameters were kept unchanged for the different set of experiments. It is observed that the time required for complete consumption of  $4.0 \times 10^{-3}$  kg of hydrated lime is 28 min and for  $6.0 \times 10^{-3}$  kg, it increases proportionately to 28 min.

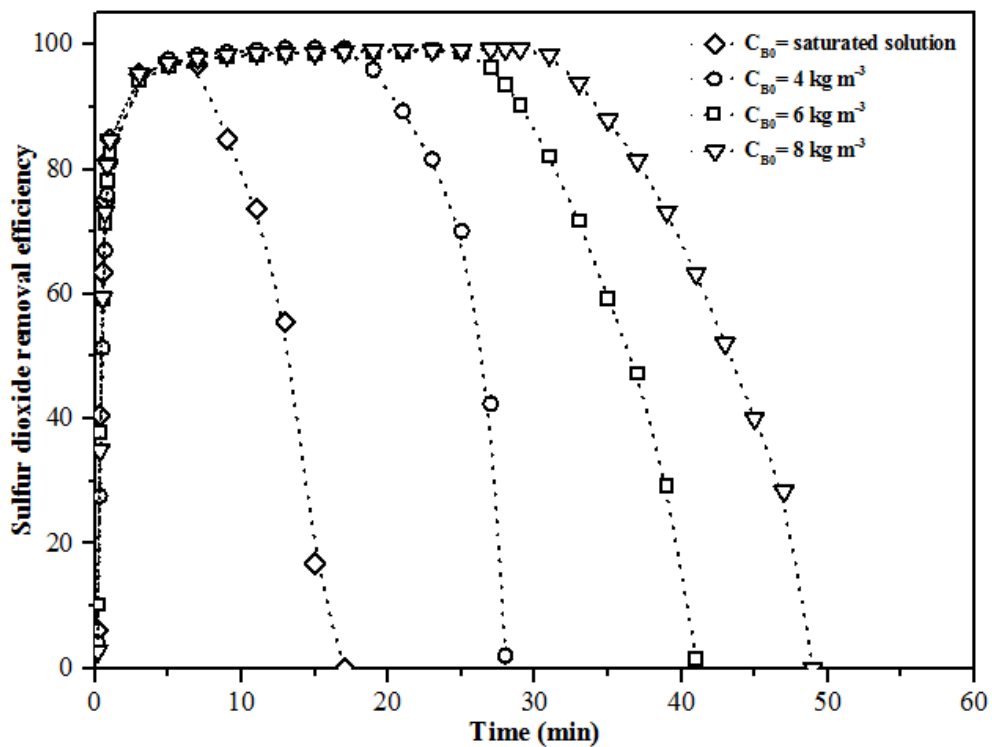


**Figure 5.13a: Effect of initial solids loading on percent  $\text{SO}_2$  removal efficiency by  $\text{Ca}(\text{OH})_2$  slurry in a bubble column reactor ( $u_G = 3.85 \times 10^{-2} \text{ m s}^{-1}$ ,  $C_{\text{SO}_2} = 1000$  ppm and  $V_{sl} = 2.50 \times 10^{-4} \text{ m}^3$ ); (Experimental data has been shown in Table 5B.7)**

Although, solid-liquid interfacial area increased by a factor of 1.5, important to increase the rate of solid dissolution, the rate of  $\text{SO}_2$  absorption and reaction is observed to remain unchanged. This is attributed to the high gas phase resistance at the very low partial pressure of  $\text{SO}_2$ , not causing any increase in its rate of absorption and hence no increase in the rate of reaction. When the feed is a saturated solution of

lime,  $\text{SO}_2$  removal efficiency is found to be less, 97.6 percent as compared to the feed containing sparingly soluble fine suspended particles of lime. In the present case the rate of reaction increases due to dissolution of fine particle ( $dp \leq \delta/5$ ) within the film itself. Reaction and particle dissolution occur in parallel (Ramachandran and Sharma, 1969) within the film surrounding the gas bubbles with the consequent shifting of the reaction plane towards the gas-liquid interface and increase in the rate of reaction.

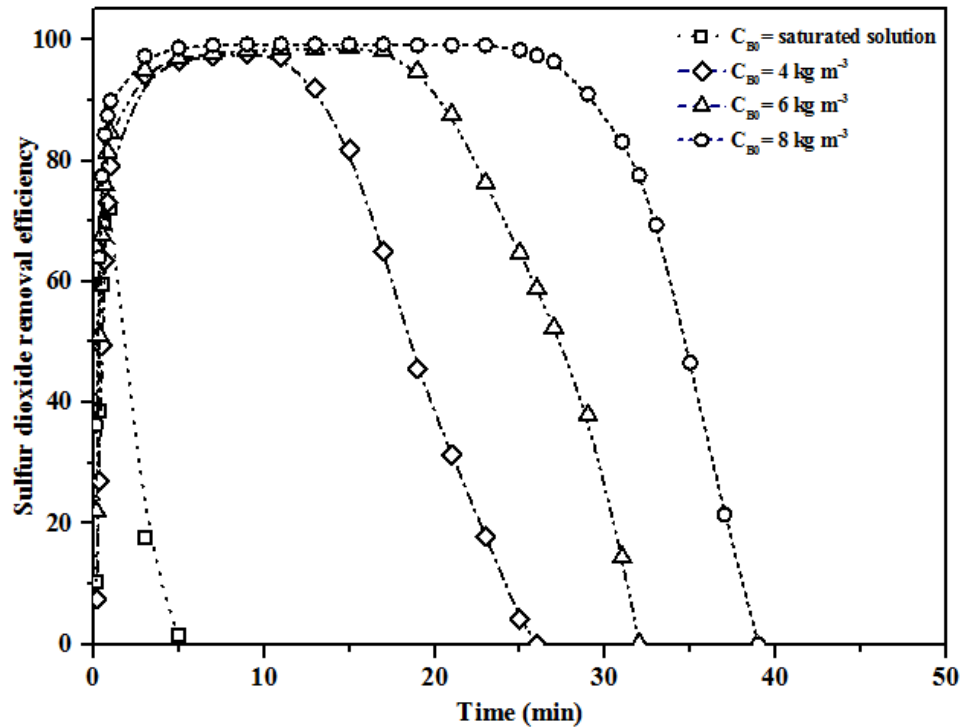


**Figure 5.13b: Effect of initial solids loading on  $\text{SO}_2$  removal efficiency by limestone slurry in a bubble column reactor ( $u_G = 3.85 \times 10^{-2} \text{ m s}^{-1}$ ,  $C_{\text{SO}_2} = 1000 \text{ ppm}$  and  $V_{sl} = 2.50 \times 10^{-4} \text{ m}^3$ ); (Experimental data has been shown in Table 5B.8)**

These experiments were also performed with calcium carbonate slurry as the absorbent. The mass ratio of CaO present in calcium carbonate to that in hydrated lime being 0.76, for the equal rate of reaction if hydrated lime needs 28 min, calcium carbonate slurry would require 21.28 min, when the same mass of the reactants are present in the two feed slurry. But, the actual time consumed by the calcium carbonate slurry is found to be about 26 min. Such variations may be observed for other solids loading also. The solubility of  $\text{CaCO}_3$  at  $30^\circ\text{C}$  is 143.5 times lower than  $\text{Ca(OH)}_2$ . The much lower dissolution rate of calcium carbonate compared to that of hydrated lime and reduction in the flux of  $\text{SO}_2$  due to back diffusion of the  $\text{CO}_2$  generated by

the reaction and dissolved in the liquid is considered to be the main reason for this lower reaction rate of calcium carbonate.

### 5.3.3.4 Comparison of removal efficiency in bubble column- and foam-bed reactors

A comparison of the SO<sub>2</sub> removal efficiency in bubble column and foam-bed reactors under otherwise identical conditions by use of hydrated lime slurry has been shown in Figure 5.14a. The FGD products, CaSO<sub>3</sub> and CaSO<sub>4</sub>·2H<sub>2</sub>O, have been reported to seriously choke the spray nozzles and the filtration devices. In a study with a different Ca-slurry system, it has also been reported by other authors that use of a surface active agent for carbonation of hydrated lime in a bubble column reactor can substantially enhance the carbonation rate and reduce the choking problem of the gas distributor plate (Jana, S.K., 2007). To overcome this problem in the FGD operations, while extended aeration facility in the desulfurization process has been incorporated in industries, in the present work, it was decided to try out adding a surface active agent to the reaction mass to overcome the choking problem.

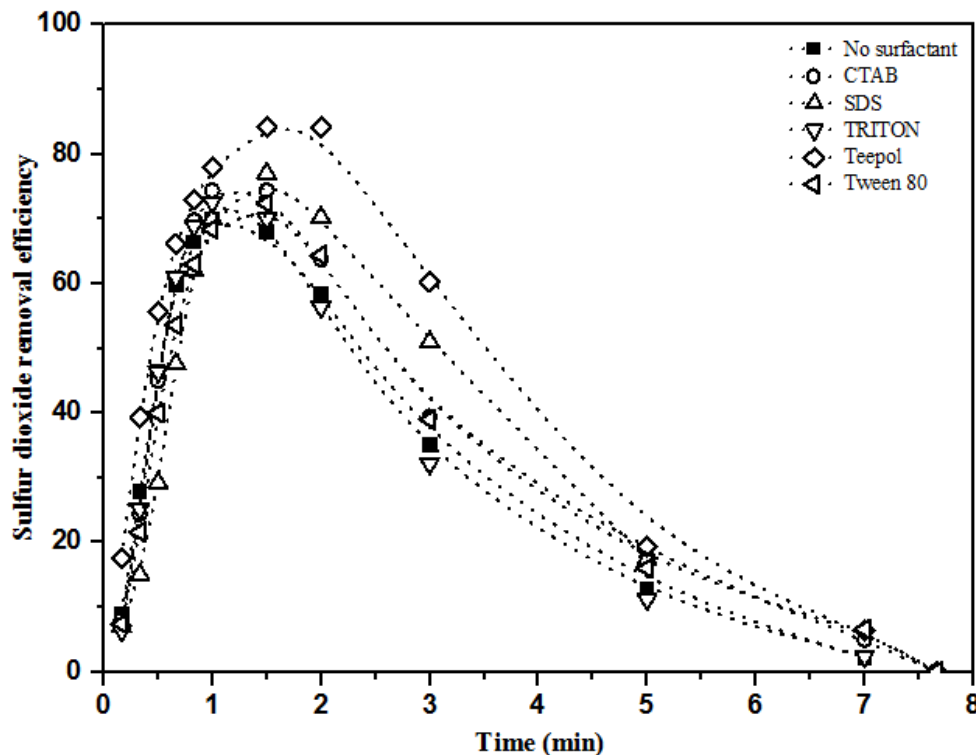


**Figure 5.14a Comparison of percent SO<sub>2</sub> removal efficiency by use of distilled water as absorbent in bubble column and foam-bed reactors ( $u_G = 3.85 \times 10^{-2} \text{ m s}^{-1}$ ,  $C_{SO_2} = 1000 \text{ ppm}$ ,  $m_B^T(0) = 4.0 \text{ kgm}^{-3}$  and  $V_{sl} = 2.50 \times 10^{-4} \text{ m}^3$ ); (Experimental data has been shown in Table 5B.9)**

In a *bubble column contactor*, the orifices on the gas distributor plate was observed in the present investigation to get choked at the time of product withdrawal for solids loading beyond  $8 \text{ kg m}^{-3}$ , but in the foam-bed reactor with a surfactant concentration of only 4 ppm CTAB, no such choking was observed up to  $16 \text{ kg m}^{-3}$  of solids loading beyond which experiments were not performed. Experiments were also conducted with and without addition of several other surfactants at constant values of the other variables and parameters:  $u_G = 3.85 \times 10^{-2} \text{ m s}^{-1}$ ,  $C_{\text{SO}_2} = 1000 \text{ ppm}$ ,  $m_B^T(0) = 4.0 \text{ kg m}^{-3}$  and  $V_{sl} = 2.50 \times 10^{-4} \text{ m}^3$ .

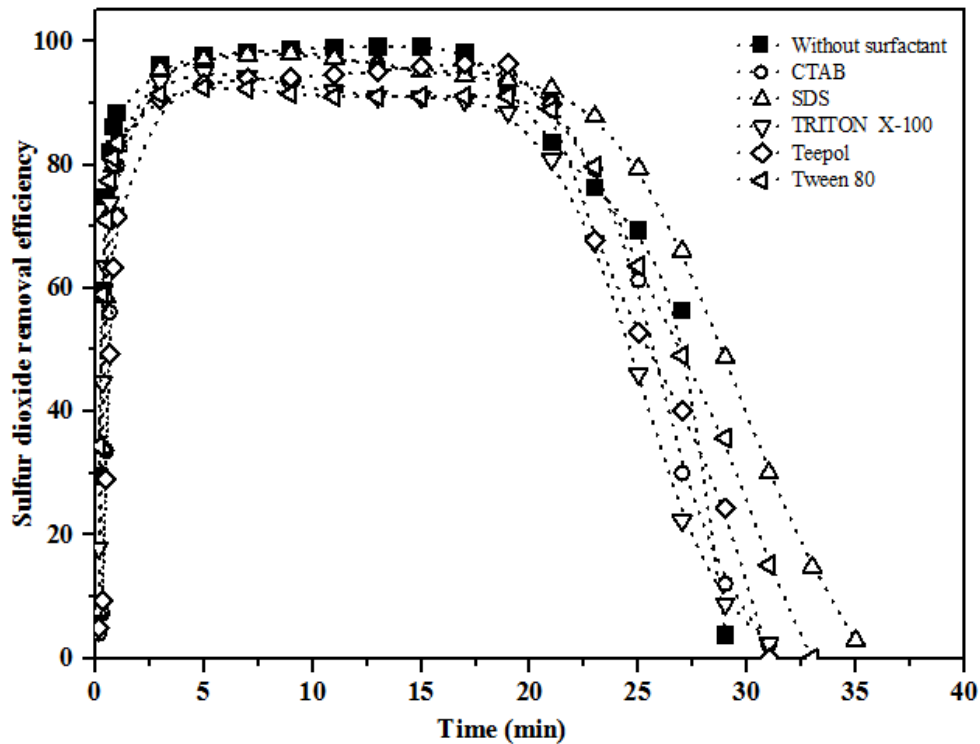


**Figure 5.14b Comparison of percent  $\text{SO}_2$  removal efficiency by use of  $\text{Ca}(\text{OH})_2$  slurry as absorbent in bubble column and foam-bed slurry reactors ( $u_G = 3.85 \times 10^{-2} \text{ m s}^{-1}$ ,  $C_{\text{SO}_2} = 1000 \text{ ppm}$ ,  $m_B^T(0) = 4.0 \text{ kg m}^{-3}$  and  $V_{sl} = 2.50 \times 10^{-4} \text{ m}^3$ ); (Experimental data has been shown in Table 5B.10)**

It was observed that percent  $\text{SO}_2$  removal efficiency reduced in the foam-bed reactor as compared to that in the bubble column reactor in presence of each of the surfactants when added at a relatively higher concentration but remained unaffected at 4 ppm CTAB as mentioned above. This latter surfactant at its very low concentration was found to be effective compared to other surfactants. However, there appears no marked difference in the exit concentration when  $\text{SO}_2$  is absorbed in distilled water in the presence or absence of surfactants. Partial surface coverage of the particles with

the surfactant molecules leading to reduced rate of its dissolution and additional resistance formed on the liquid film of the alkaline solution results in a reduction in the absorption rate of  $\text{SO}_2$  and hence, a reduction in the removal efficiency of this gas is observed.

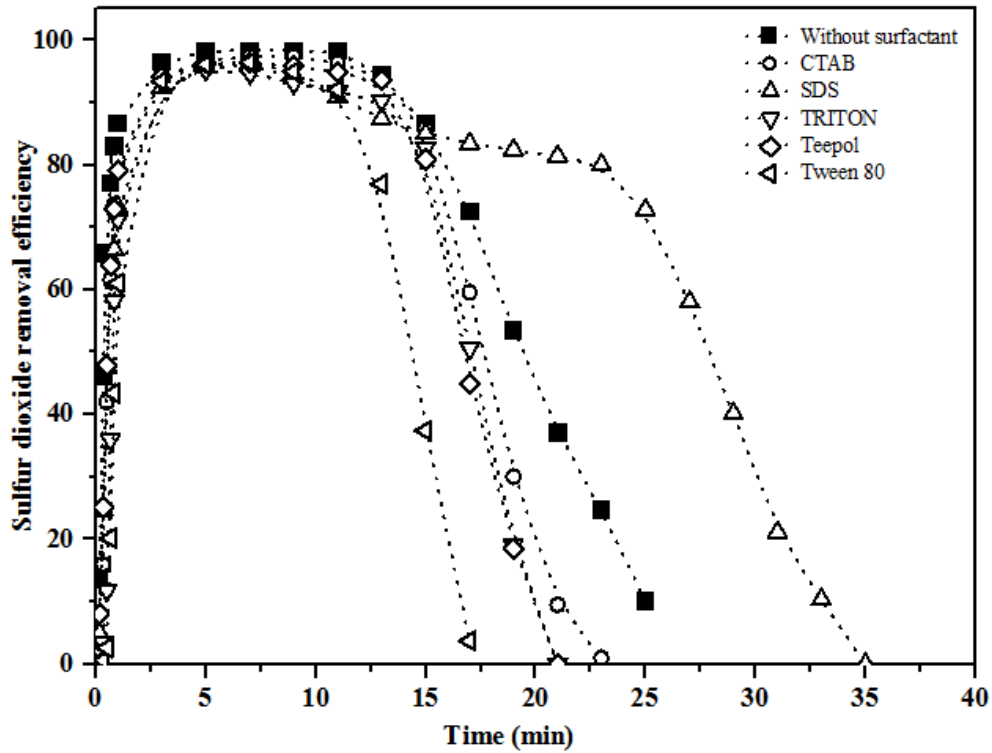


Figure 5.14c: Comparison of percent  $\text{SO}_2$  removal efficiency by use of  $\text{CaCO}_3$  slurry as absorbent in bubble column and foam-bed slurry reactors ( $u_G = 3.85 \times 10^{-2} \text{ ms}^{-1}$ ,  $C_{\text{SO}_2} = 1000 \text{ ppm}$ ,  $m_B^T(0) = 4.0 \text{ kgm}^{-3}$  and  $V_{sl} = 2.50 \times 10^{-4} \text{ m}^3$ ); (Experimental data has been shown in Table 5B.11)



## 5.4 Characterization of Reactants and FGD products

### 5.4.1 Analysis of Ca(OH)<sub>2</sub> and CaCO<sub>3</sub> sample

#### 5.4.1.1 Particle size distribution of Ca(OH)<sub>2</sub> and CaCO<sub>3</sub> sample

Particle size distribution of Ca(OH)<sub>2</sub> and CaCO<sub>3</sub> sample supplied by Merck Pvt. Ltd. were measured by Malvern Mastersizer 2000E and the data are shown in Table 5.2a and 5.2b respectively. The volume average particle diameters of Ca(OH)<sub>2</sub> and CaCO<sub>3</sub> sample are 6.84 μm and 6.36 μm respectively.

**Table 5.2a Particle size distribution of Ca(OH)<sub>2</sub> sample**

Sr. No. of fraction	Particle size (μm)	Volume (%)	Sr. No. of fraction	Particle size (μm)	Volume (%)
1.	0.4925	0.68	9.	21.8421	10.71
2.	1.1298	1.92	10.	40.3842	1.31
3.	2.2192	6.4	11.	276.7392	0.14
4.	10.7375	11.96	12.	392.4591	1.96
5.	5.035	12.17	13.	552.1671	2.9
6.	6.6377	14.47	14.	677.6965	1.51
7.	8.7515	14.64	15.	835.7392	2.1
8.	12.411	17.12			

**Table 5.2b Particle size distribution of CaCO<sub>3</sub> sample**

S.No.	Size Classes (µm)	Volume Density (%)	S.NO.	Size Classes (µm)	Volume Density (%)
1.	0.4909	0.0000	27.	13.5646	6.1773
2.	0.5577	0.0043	28.	15.4116	5.9456
3.	0.6336	0.0591	29.	17.5101	5.4960
4.	0.7199	0.2479	30.	19.8943	4.8216
5.	0.8179	0.5179	31.	22.6032	3.9585
6.	0.9293	0.8611	32.	25.6809	2.9844
7.	1.0558	1.2478	33.	29.1776	2.0125
8.	1.1996	1.6485	34.	33.1505	1.1738
9.	1.3630	2.0410	35.	37.6644	0.5736
10.	1.5485	2.4091	36.	42.7928	0.2580
11.	1.7594	2.7438	37.	48.6196	0.0799
12.	1.9990	3.0501	38.	55.2397	0.0065
13.	2.2711	3.3426	39.	62.7613	0.0001
14.	2.5804	3.6317	40.	104.5811	0.0002
15.	2.9317	3.9230	41.	118.8211	0.0099
16.	3.3309	4.2184	42.	135.0001	0.0990
17.	3.7845	4.5136	43.	153.3820	0.1798
18.	4.2998	4.7992	44.	174.2668	0.2355
19.	4.8852	5.0651	45.	197.9954	0.2502
20.	5.5504	5.3041	46.	224.9549	0.2209
21.	6.3062	5.5155	47.	255.5853	0.1612
22.	7.1648	5.7046	48.	290.3863	0.0947
23.	8.1404	5.8785	49.	329.9260	0.0411
24.	9.2488	6.0377	50.	374.8495	0.0040

25.	10.5082	6.1676	51.	425.8898	0.0001
26.	11.9390	6.2322	52.	1040.8298	0.0000

#### 5.4.1.2 XRD analysis of $\text{Ca(OH)}_2$ sample

XRD analysis of  $\text{Ca(OH)}_2$  sample was done for determining the impurities present in the sample and the data is shown in Figure 5.15. Peaks at 2 theta degree of 18.06, 28.65, 34.11, 47.15, 50.81, 54.39 and 56.06 are compared with the JCPDS no. 00-004-0733 and it was observed that these peaks are of  $\text{Ca(OH)}_2$ . The peak at 2 theta degree of 29.39 was compared with the JCPDS no. 01-078-4615. It shows that this peak is for  $\text{CaCO}_3$  (calcite).  $\text{CaCO}_3$  is present as an impurity in the sample.

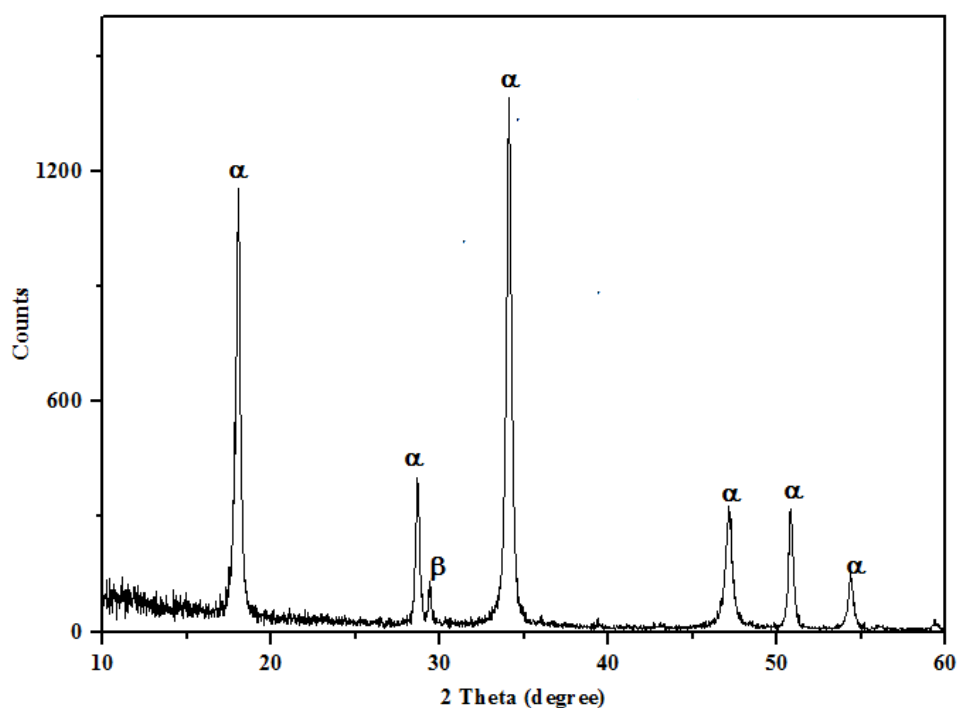
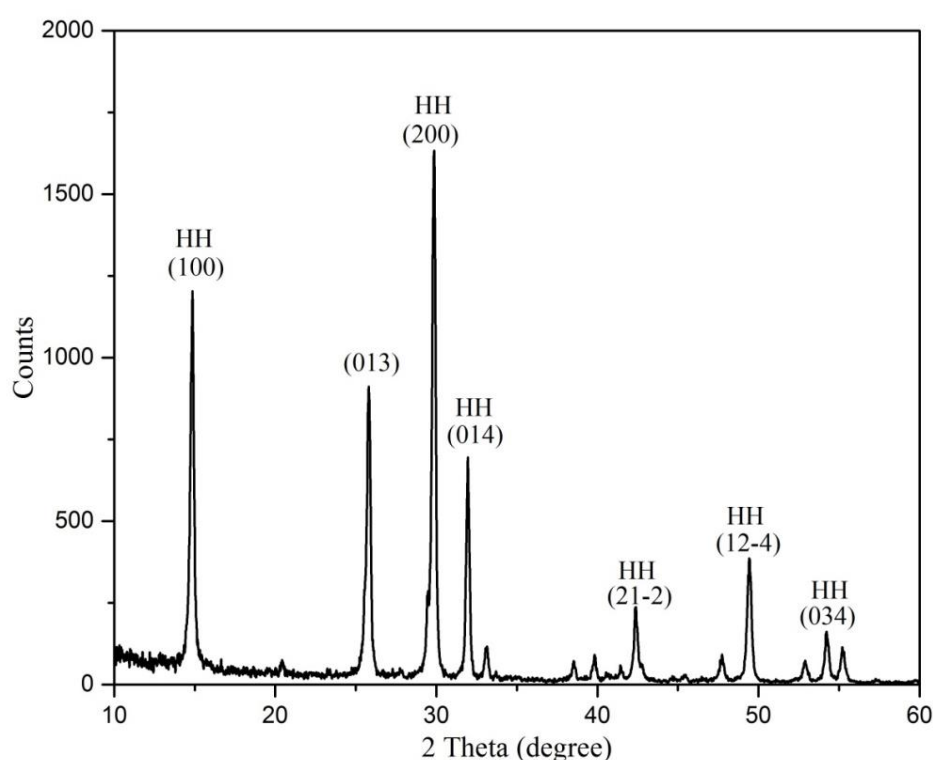


Figure 5.15 XRD analysis of  $\text{Ca(OH)}_2$  sample ( $\alpha$ :  $\text{Ca(OH)}_2$  and  $\beta$ :  $\text{CaCO}_3$ )

#### 5.4.2 XRD analysis of FGD products obtained from bubble column reactor

Diffraction patterns were compared with the reference standards (International Powder Diffraction File (JCPDS No.-01-078-5228) database), for identification of phases. For the products obtained from calcium hydroxide slurry (Figure 5.16a), the different peaks were observed at 2 theta values of 14.7, 25.7, 29.8, 31.9, 42.3, 49.4 and 54.2 correspond to the *hkl* values of 100, 013, 200, 014, 21-2, 12-4 and 034 respectively. In case of calcium carbonate slurry (Figure 5.16b), the different peaks observed at 2 theta values of 14.8, 25.7, 29.7, 31.8, 42.3, 49.3 and 54.1 corresponds to the *hkl* values of 100, 013, 200, 014, 21-2, 12-4 and 034 respectively.



**Figure 5.16a: XRD pattern of the product, obtained by SO<sub>2</sub> absorption in the bubble column using the Ca(OH)<sub>2</sub> slurry**

In the Figs. 5.16a and 5.16b HH indicates hemihydrate phase. Similar results were obtained by Pan et al. (2013) in which calcium sulphate hemihydrate was formed with the hexagonal crystal structure. Calcium sulfate hemihydrate with controlled crystal morphology has attracted broad interests due to its superior physical and chemical properties, as well as excellent biological performance. The peak broadening of XRD diffraction has been used to estimate the mean crystalline size (*D*) of synthesized calcium sulphate hemihydrate powder using Debye- Scherrer formula:  $D \text{ (\AA)} =$

$(0.89\lambda)/(\beta \cdot \cos\theta)$ ; Where  $\lambda = 1.5406 \text{ \AA}$  is the X-ray wavelength of Cu K radiation,  $\beta$  is full width measured at half of the maximum intensity peak (FWHM) and  $\theta$  is angle of diffraction. The mean crystalline size for the product obtained in case of calcium hydroxide and calcium carbonate slurries were 31.275 nm and 35.2 nm respectively. Therefore, it can be concluded that the product obtained in the case of calcium carbonate slurry is more crystalline than in the product obtained using calcium hydroxide slurry.

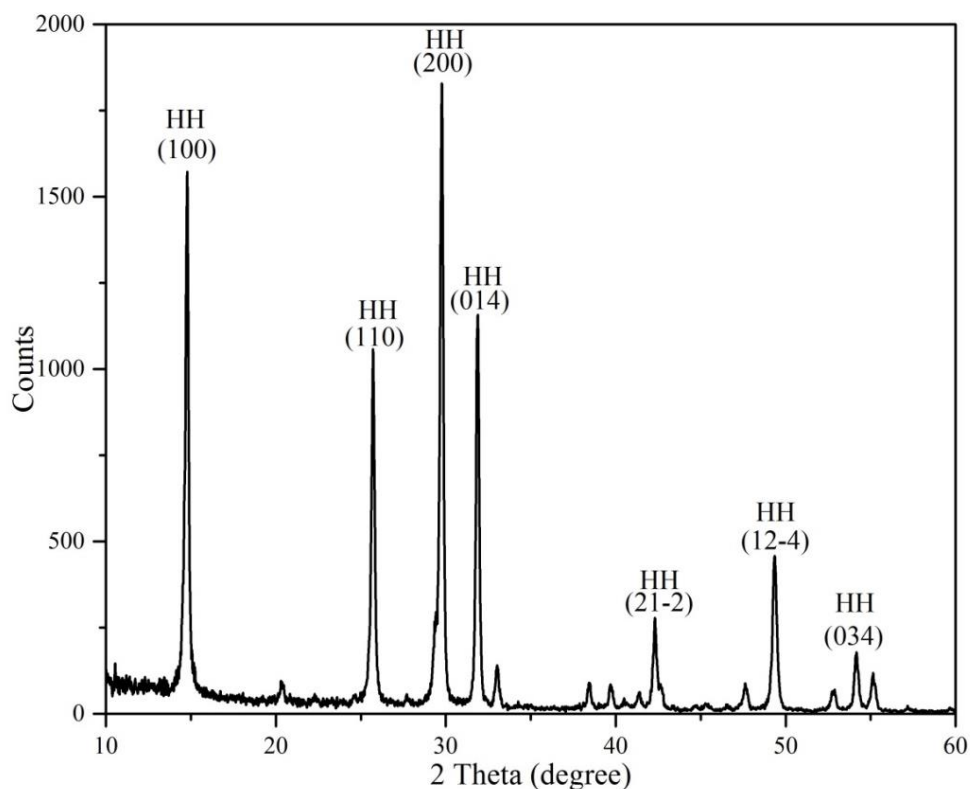


**Figure 5.16b: XRD pattern of the product, obtained by SO<sub>2</sub> absorption in bubble column reactor using the CaCO<sub>3</sub> slurry**

### 5.4.3 FT-IR spectra of FGD product in presence and absence of the surface active agent

One can acquire information on the functional groups present in the product molecules obtained from the desulfurization operation through its FTIR analysis. FT-IR spectra of the FGD products obtained from bubble column and foam-bed reactors are presented in Figures 5.17a and 5.17b. The presence of water in the molecules has

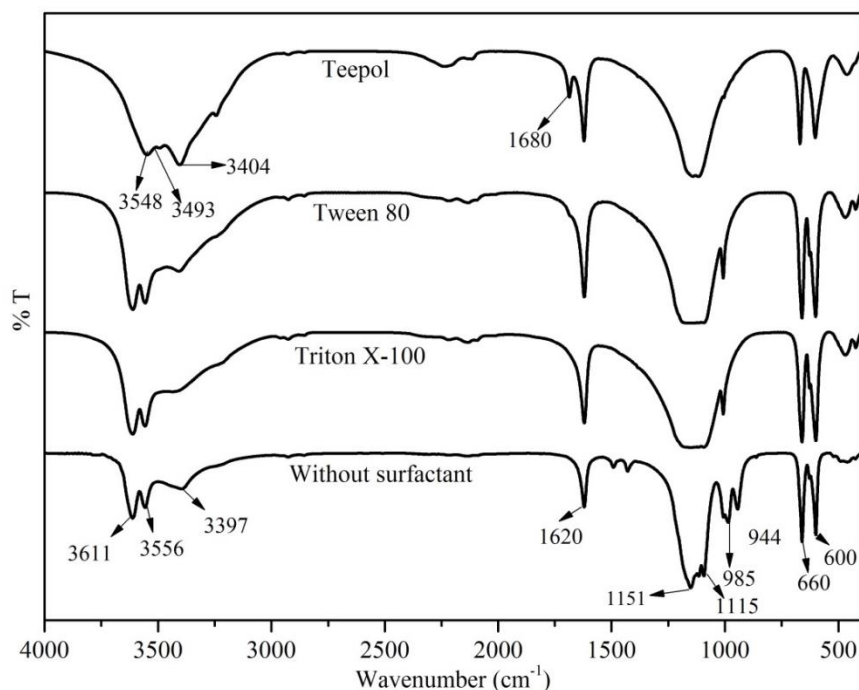


**Figure 5.17a. FT-IR analysis of the FGD the products, obtained by  $\text{SO}_2$  absorption in the bubble and foam-bed contactors using  $\text{Ca}(\text{OH})_2$  slurry**

held anion water and therefore possess unique band at  $1620\text{ cm}^{-1}$  due to bending vibration of water molecule. Only the dihydrate is known to contain the loosely held water molecules and the corresponding band occurs at  $1680\text{ cm}^{-1}$  (Nosov et al., 1976), not noticeable in the IR spectra shown in Figures 5.17a or 5.17b except for the case when Teepol is used as the surfactant. The two bands at  $3557$  and  $3611\text{ cm}^{-1}$ , referred to as O—H stretches and observed in the IR spectra in the above figures are attributed due to the presence of water in hemi-hydrate molecules only. Therefore, the FGD product obtained using calcium carbonate slurry contains only hemihydrates. One more O—H bend at  $1680\text{ cm}^{-1}$  can be seen in the IR of the FGD product obtained from a foam-bed reactor using Teepol as the surfactant and hydrated lime as the absorbent. This band is for loosely held water molecules and indicates that this

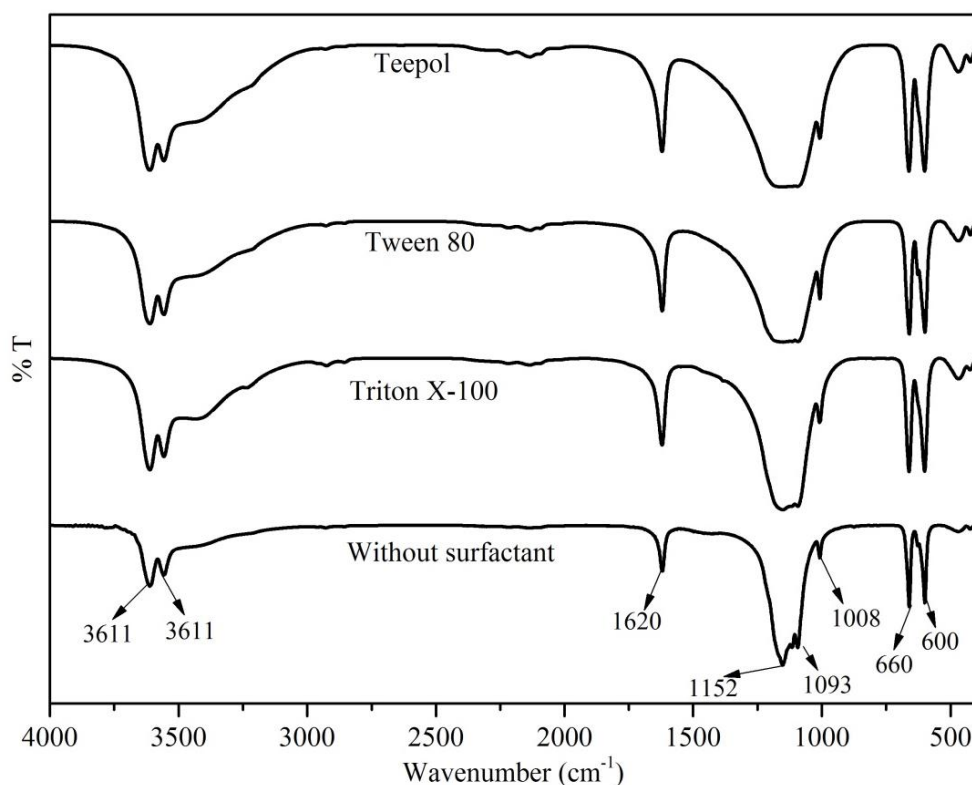


**Figure 5.17b. FT-IR analysis of the FGD the products, obtained by SO<sub>2</sub> absorption in bubble and foam-bed contactors using CaCO<sub>3</sub> slurry**

particular FGD product contains a mixture of both hemihydrates and dihydrate. The region of stretching vibrations  $\nu_4$  of the SO<sub>4</sub><sup>2-</sup> ion in CaSO<sub>4</sub>·0.5H<sub>2</sub>O occurs in the frequency range 700-500 cm<sup>-1</sup> and in the Figure 5.17a, it is found to occur at 660 and 600 cm<sup>-1</sup>.

#### **5.4.4 TGA of the FGD products in presence and absence of surface active agent**

Thermogravimetric analysis (TGA) of FGD product was performed to study the weight loss determine the specific phase present in the product sample and therefore the product quality. Theoretically, the gypsum phase (CaSO<sub>4</sub>·2H<sub>2</sub>O) contains about 20.91% of the water of hydration, and the hemihydrate phase (CaSO<sub>4</sub>·0.5H<sub>2</sub>O) contains 6.20%. Experimental data of TGA of the FGD products obtained from bubble column- and foam-bed reactors have been shown in Figures 5.18a and 5.18b, respectively. It is observed that the products obtained from both the bubble column and foam-bed reactors using hydrated lime slurry suffer a weight loss of about 6.11% at about 145 °C except when Teepol is used as the surface active agent in a foam-bed reactor. In this latter case the weight loss is about 20% at 170 °C. All the former products are therefore calcium sulfate hemihydrate and the latter is recognized as the

dihydrate phase. The results from FT-IR analysis also agree with these observations. Products obtained from calcium carbonate slurry (Figure 5.18b) are also observed to follow the similar trend but no dihydrate was formed. Similar observations were obtained from FTIR analysis.

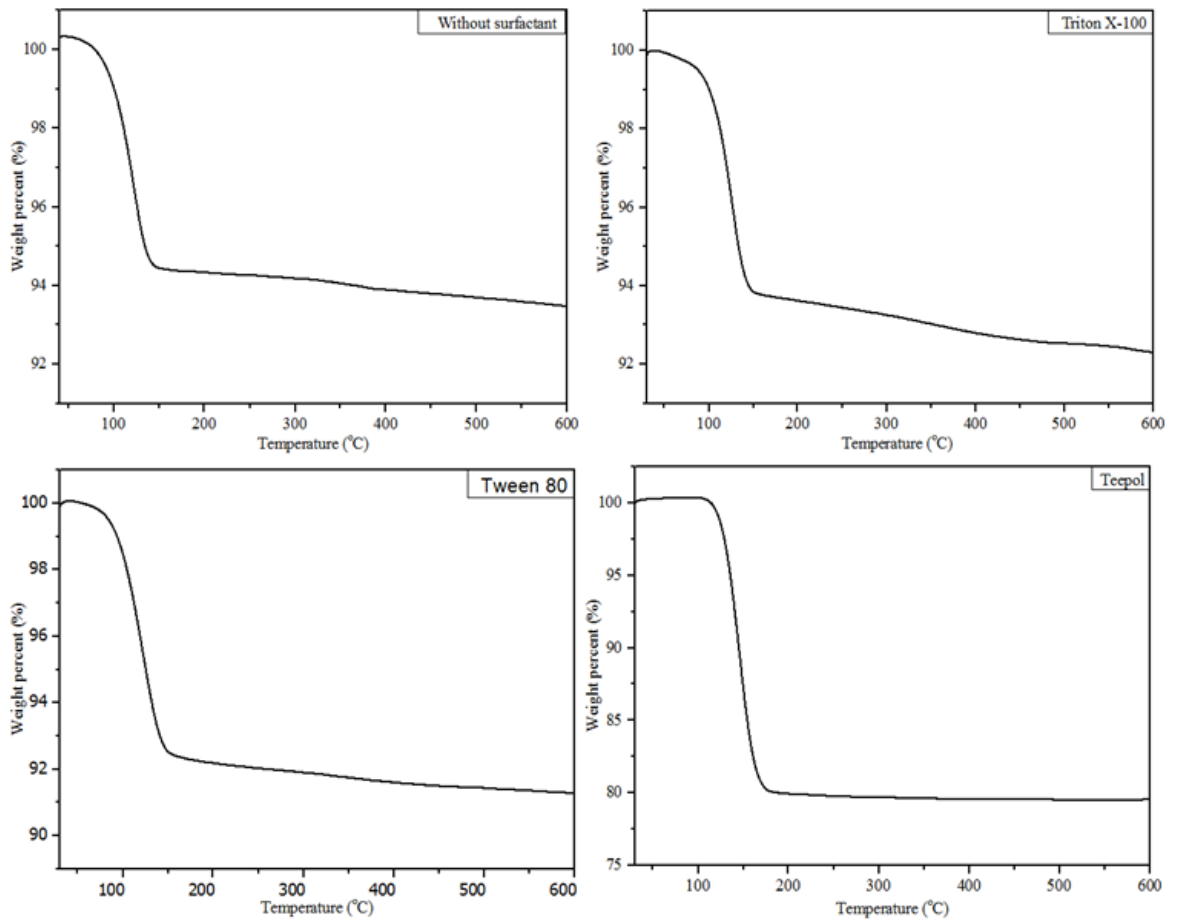


**Figure 5.18a.** TGA of the FGD product, obtained by SO<sub>2</sub> absorption in bubble column- and foam-bed reactors using Ca(OH)<sub>2</sub> slurry



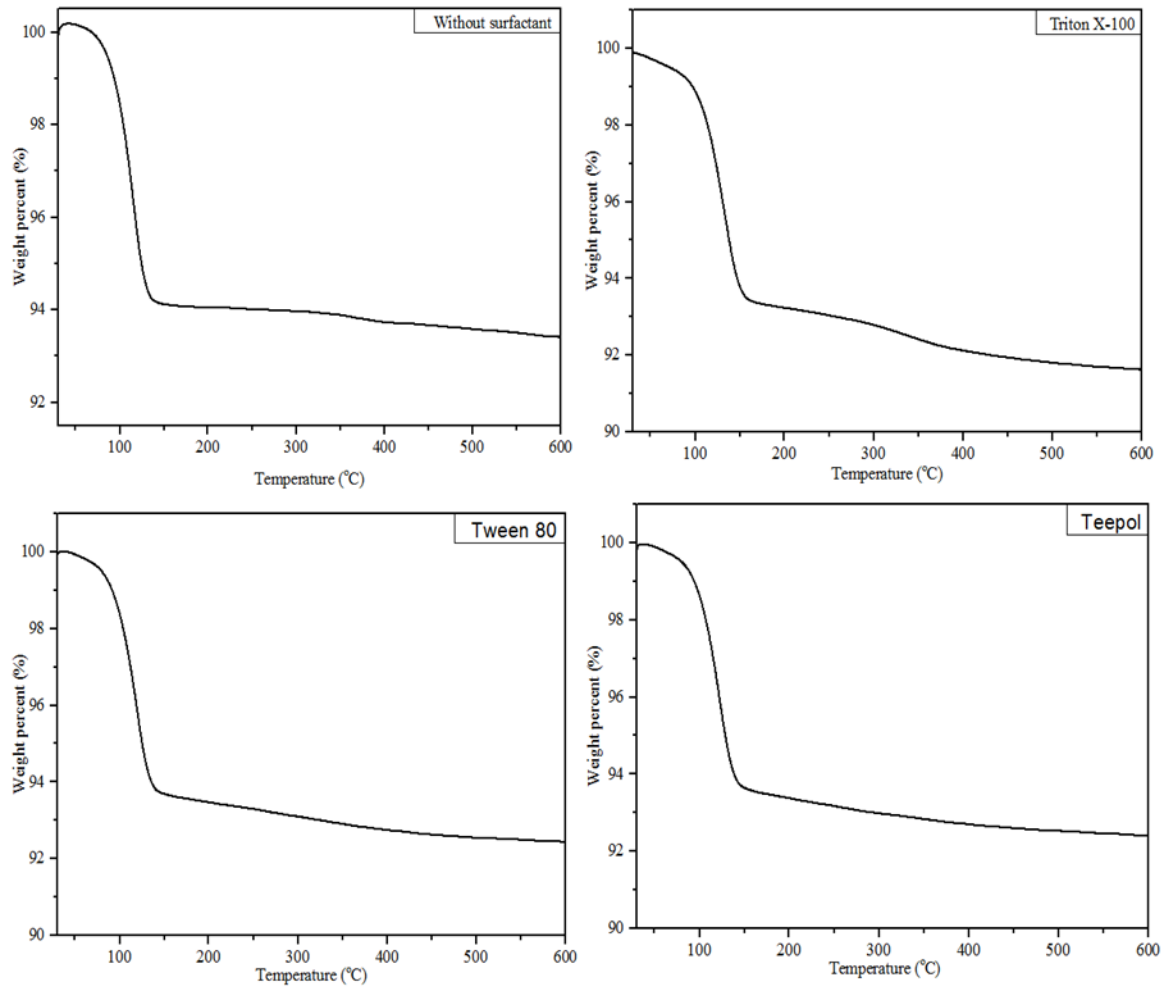


**Figure 5.18b. TGA of the FGD product, obtained by SO<sub>2</sub> absorption in bubble column- and foam-bed reactors using the CaCO<sub>3</sub> slurry**

#### 5.4.5 Morphology of FGD products in presence and absence of the surface active agent

Shape and size of particles are important parameters that govern specific applications of fine particles produced in industries. SEM micrographs provide complete knowledge of the morphology of the particles. SEM micrographs of the FGD products obtained in the presence and absence of surface active agents have been shown in Figures 5.19 and 5.22. Three different surfactants, viz., Triton X-100, Tween 80 and Teepol were used as surfactants during desulfurization operation in a foam-bed reactor.

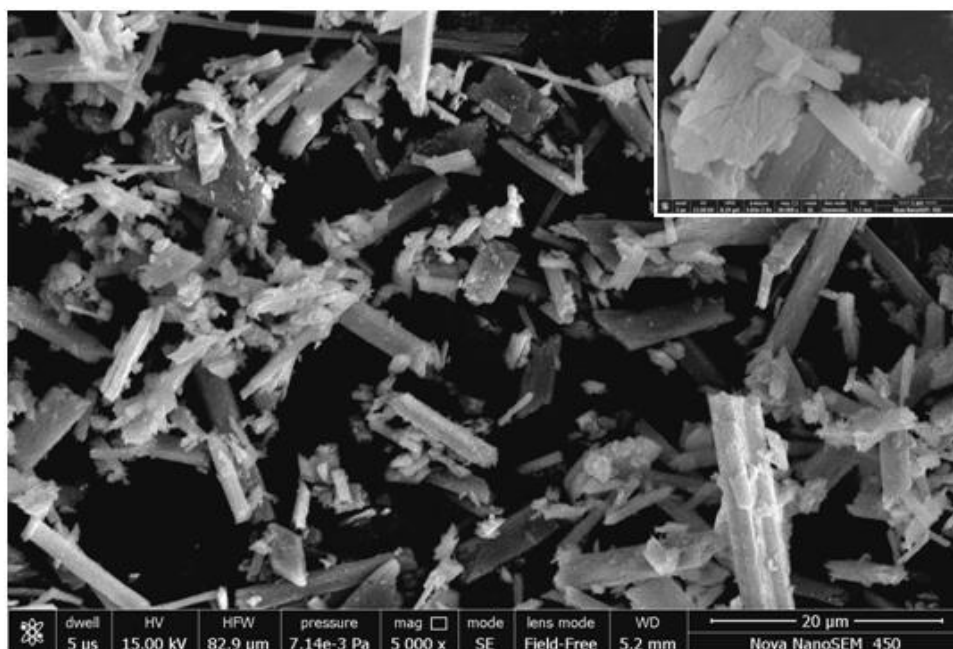
Figure 19-22 provide the SEM micrographs for the calcium sulfate hemihydrate samples obtained in presence and absence of surface active agent which helps in investigating about the morphology of the calcium sulfate hemihydrate crystals. It can be observed that the morphology of the gypsum crystals was needle-shaped and rod-like as discussed by Rashad et al. (2004). The size analysis was described in Table.5.3

**Table 5.3 Size analysis of FGD product crystals using FE-SEM**

Absorbent	Surfactant	Length (μm)	Width (μm)	Aspect ratio
Ca(OH) <sub>2</sub> slurry	Without surfactant	7.84	2.12	3.70:1
	Triton X-100	155.15	22.76	6.82:1
	Tween 80	273.55	12.05	22.66:1
	Teepol	116.29	18.44	6.31:1
CaCO <sub>3</sub> slurry	Without surfactant	28.89	6.8	4.25:1
	Triton X-100	9.11	2.24	4.07:1
	Tween 80	80.53	11.45	7.03:1
	Teepol	52.61	14.33	3.67:1

Figure 5.19a depicts the morphology of the FGD product obtained after gas absorption using calcium hydroxide slurry in the absence of surfactant. It can be observed from Table 5.3, the length of the particles is 7.84  $\mu\text{m}$  and width is 2.12  $\mu\text{m}$  with an aspect ratio of 3.70:1.

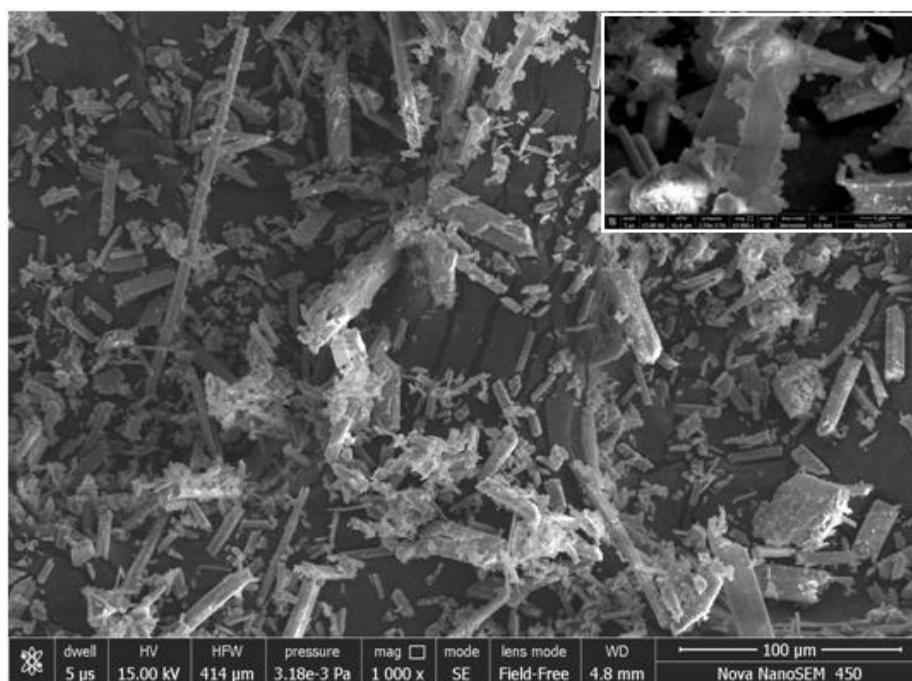
Figure 5.19b depicts the morphology of the FGD product obtained after gas absorption using calcium carbonate slurry in the absence of surfactant. It can be observed from Table 5.3, length of the particles is 28.89  $\mu\text{m}$  and width is 6.8  $\mu\text{m}$  with an aspect ratio of 4.25:1.



**Figure 5.19a. SEM image of the FGD product, obtained by  $\text{SO}_2$  absorption in bubble column reactors using  $\text{Ca}(\text{OH})_2$  slurry (without surfactant)**

Figure 5.20a shows the morphology of the FGD product obtained in the foam-bed reactor using calcium hydroxide slurry in the presence of Triton X-100 (surfactant). The size of the particles was of 155  $\mu\text{m}$  in length and 22.86  $\mu\text{m}$  in width with an aspect ratio of 6.82:1. Figure 5.20b shows the morphology of the FGD product obtained in the foam-bed reactor using calcium carbonate slurry in the presence of Triton X-100 (surfactant). The size of the particles was of 9.11  $\mu\text{m}$  in length and 2.24  $\mu\text{m}$  in width with an aspect ratio of 4.07:1 as depicted in Table 5.3. The size of the particles was smaller as compared to the particles formed in the case of calcium hydroxide slurry. The aspect ratio was also comparatively lesser.

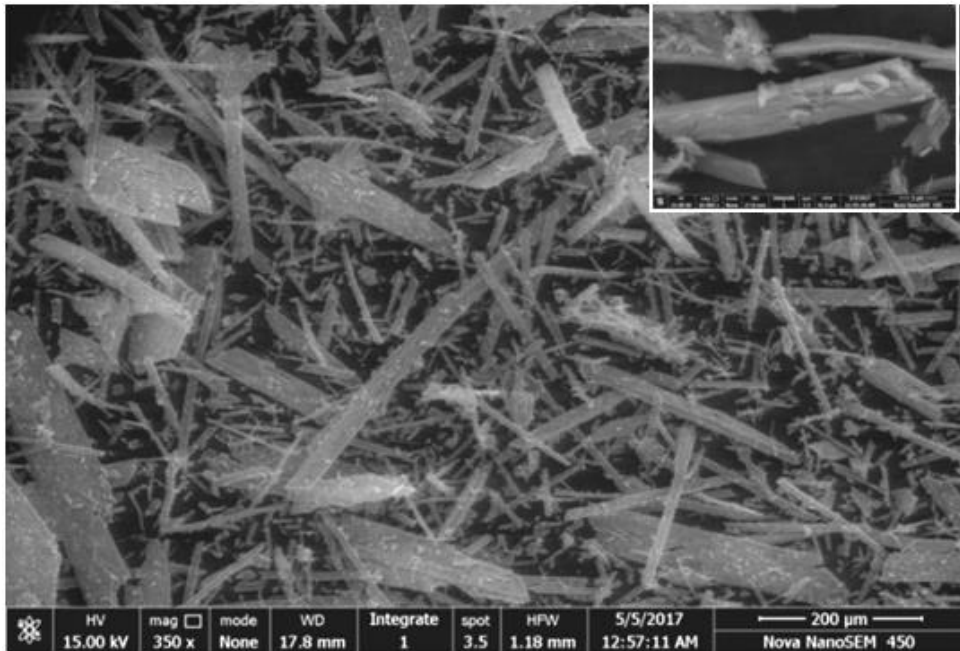
Figure 5.21a shows the morphology of the FGD product obtained in the foam-bed reactor using calcium hydroxide slurry in the presence of Tween 80 (surfactant). The length of the particle was 12.05  $\mu\text{m}$  wide and 273.55  $\mu\text{m}$  in length resulting in an aspect ratio of 22.66:1. As reported by Guan et al. (2011), there was fibiform crystals of CSH were formed which are similar to the results shown here. Figure 5.21b depicts the morphology of the product obtained when  $\text{CaCO}_3$  slurry was used in the presence of Tween 80 surfactant for  $\text{SO}_2$  gas removal. The length of CSH whisker was 52.61  $\mu\text{m}$  wide and 14.3  $\mu\text{m}$  in length resulting in an aspect ratio of 3.67:1. Calcium sulphate hemihydrate (CSH) whiskers were successfully obtained in reasonable reaction time in the presence of impurities except when calcium hydroxide slurry was used with the Teepol surfactant. It is therefore viable to use FGD product, without beforehand removing the impurities (Miao et al., 2015).



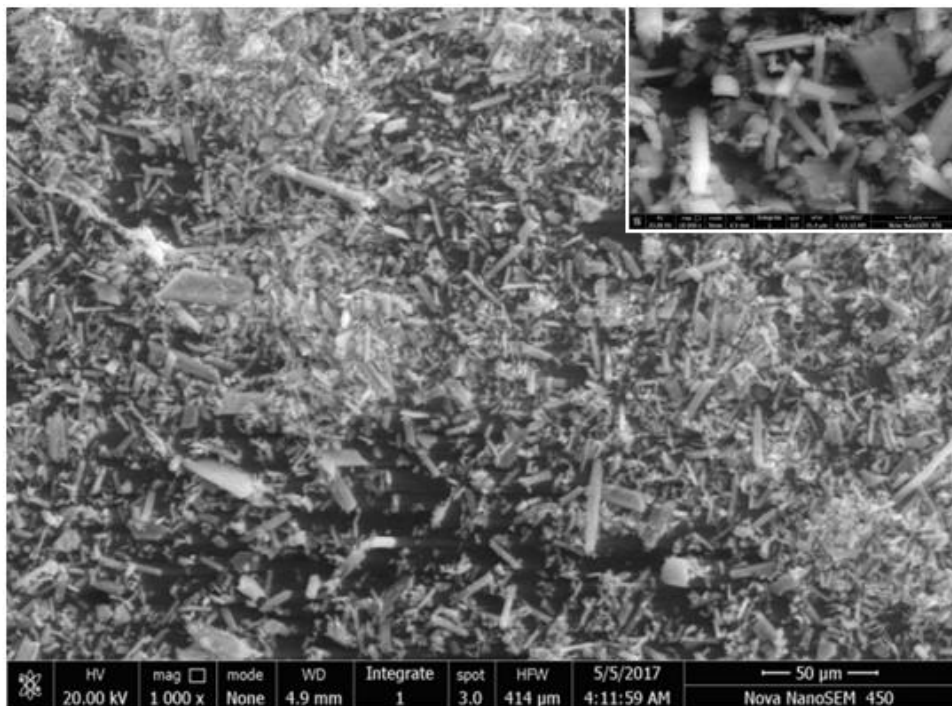
**Figure 5.19b: SEM image of the FGD product, obtained by  $\text{SO}_2$  absorption in bubble column reactors using  $\text{CaCO}_3$  slurry (without surfactant)**

Figure 22a provides the SEM micrographs for the synthesized gypsum when calcium hydroxide slurry was used along with Teepol surfactant for gas absorption. It can be observed that the morphology of the gypsum crystals was tabular as discussed by Ausset et al. (2000) as well as needle-shaped and rod-like as discussed by Shih et al. 2005 and Ashrit et al. (2015). The size (length= 16.29  $\mu\text{m}$  & width = 18.44  $\mu\text{m}$ ) and aspect ratio (6.31:1) of the product has been tabulated in Table 5.1. It can also be seen

that in between the gypsum crystals clusters of silica are present, as can be seen from the SEM microstructures at 500X magnification. Therefore, SEM analysis confirms the identity of the synthetic gypsum synthesized in the laboratory.



**Figure 5.20a.** SEM image of the FGD product, obtained by SO<sub>2</sub> absorption in the foam-bed reactor using Ca(OH)<sub>2</sub> slurry (surfactant: Triton X-100)



**Figure 5.20b.** SEM image of the FGD product, obtained by SO<sub>2</sub> absorption in the foam-bed reactor using CaCO<sub>3</sub> slurry (surfactant: Triton X-100)

Figure 5.22b depicts the morphology of the product obtained when  $\text{CaCO}_3$  slurry was used in the presence of Teepol surfactant for  $\text{SO}_2$  gas removal. The length of CSH whisker  $80.53 \mu\text{m}$  was wide and  $11.45 \mu\text{m}$  in length resulting in an aspect ratio of 7.03:1.

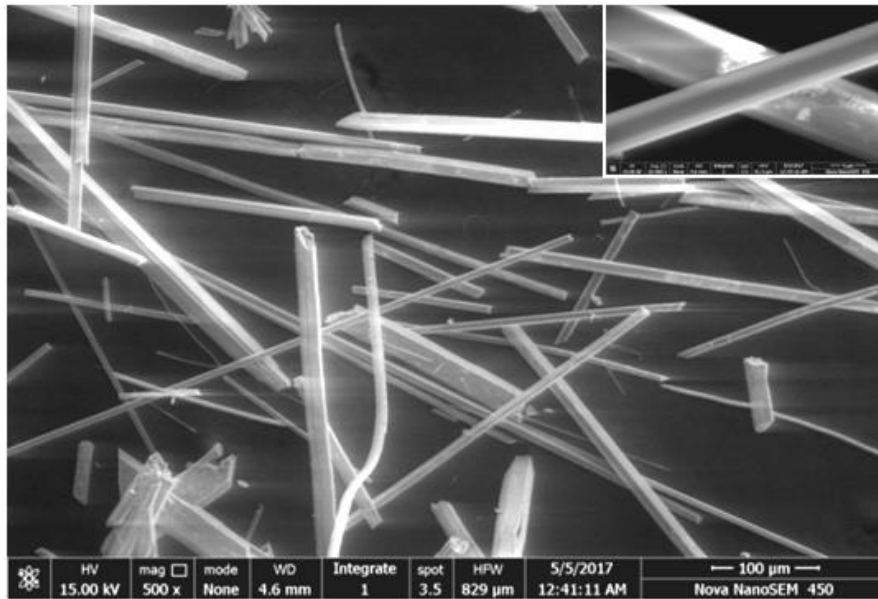


**Figure 5.21a. SEM image of the FGD product, obtained by  $\text{SO}_2$  absorption in the foam-bed reactor using  $\text{Ca}(\text{OH})_2$  slurry (surfactant: Tween 80)**

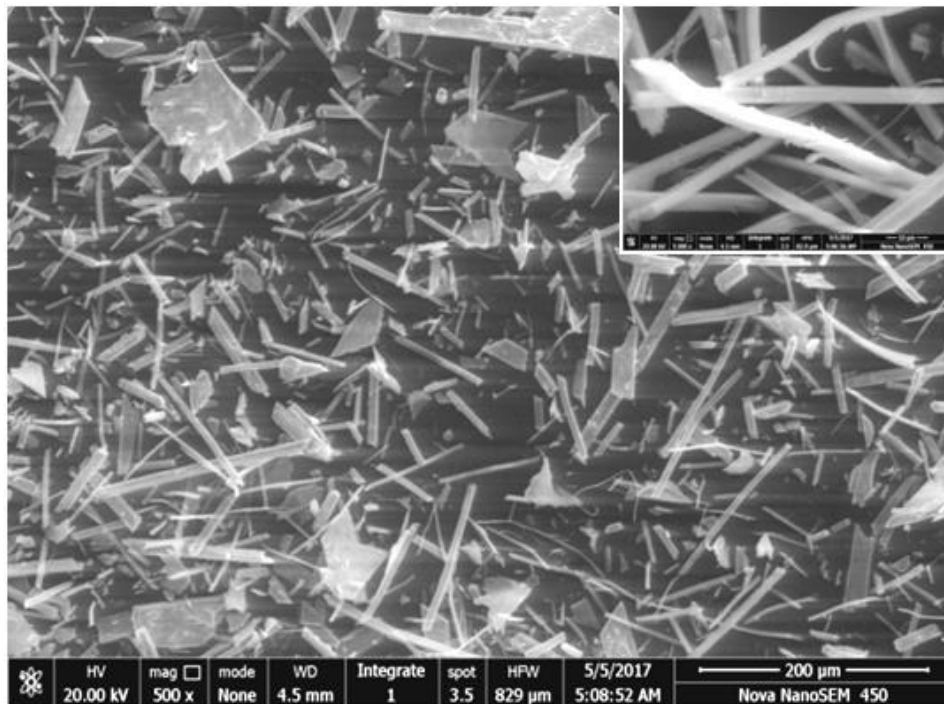


**Figure 5.21b. SEM image of the FGD product, obtained by  $\text{SO}_2$  absorption in the foam-bed reactor using  $\text{CaCO}_3$  slurry (surfactant: Tween 80)**

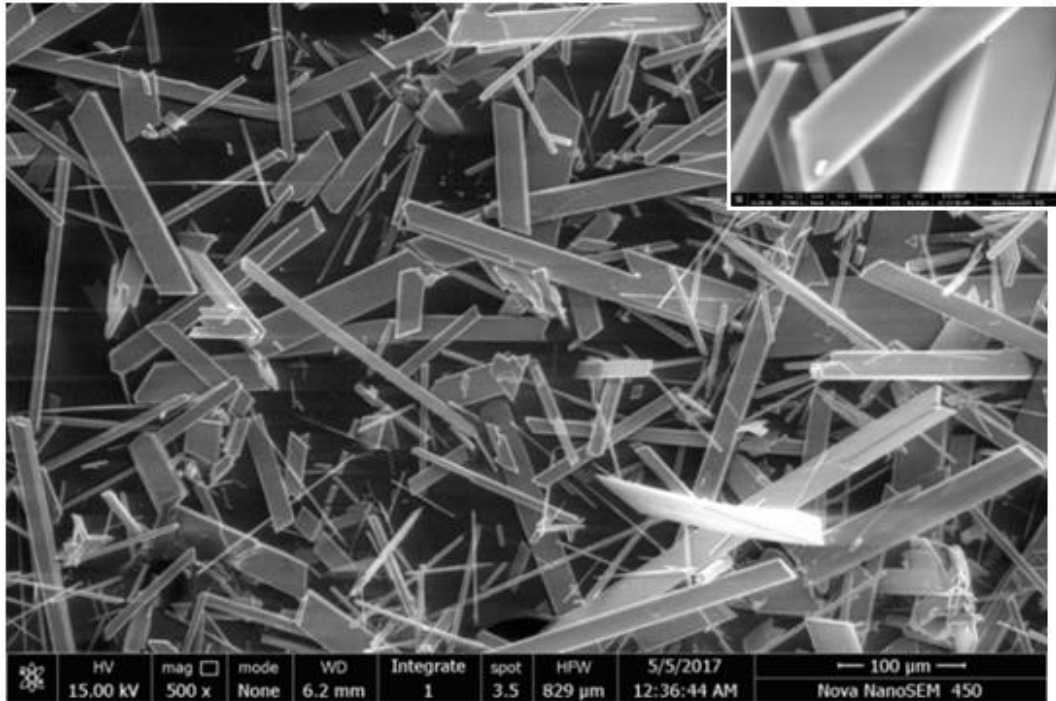


**Figure 5.22a.** SEM image of the FGD product, obtained by  $\text{SO}_2$  absorption in the foam-bed reactor using  $\text{Ca}(\text{OH})_2$  slurry (surfactant: Teepol)

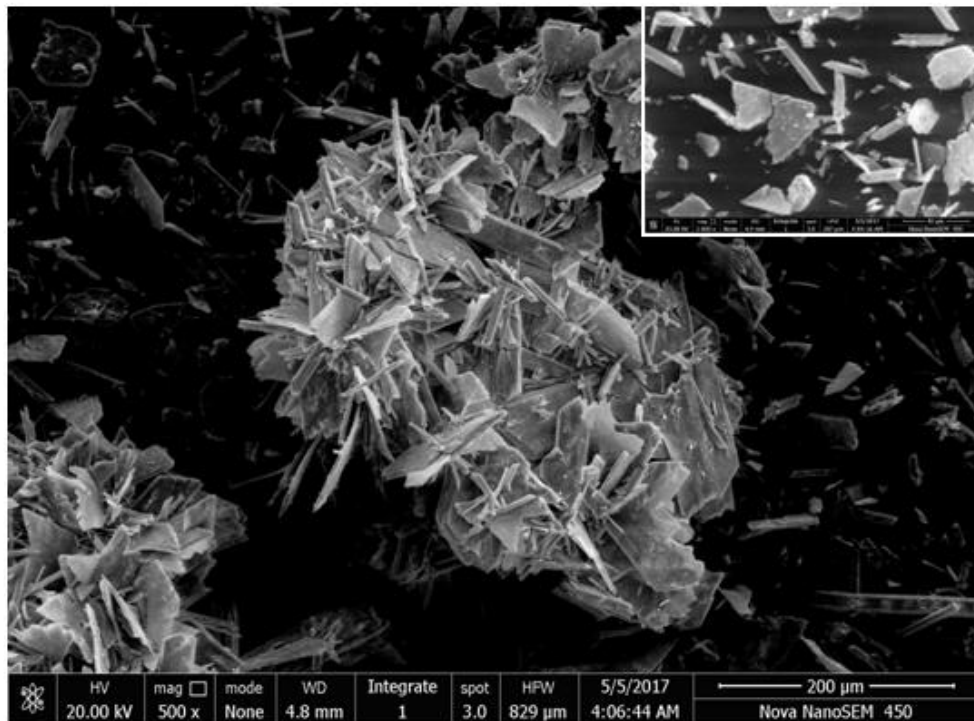


**Figure 5.22b.** SEM image of the FGD product, obtained by  $\text{SO}_2$  absorption in the foam-bed reactor using  $\text{CaCO}_3$  slurry (surfactant: Teepol)

## APPENDIX -5A

5A. Experimental data for the absorption of SO<sub>2</sub> in ILTable 5A.1a. Variation of SO<sub>2</sub> absorption efficiency of virgin TLIL, MLIL and TSIL with time (Figure 5.4a)Parameters: Initial concentration of SO<sub>2</sub> in the feed gas,  $C_{SO_2} = 500$  ppmSuperficial velocity of gas,  $u_G = 5.77 \times 10^{-2} \text{ m s}^{-1}$ Volume of solvent,  $V_{IL} = 2.50 \times 10^{-4} \text{ m}^3$ 

Time (min)	Sulfur dioxide removal efficiency		
	TLIL	MLIL	TSIL
0.1667	4	1.8	0.8
0.3333	27.6	9	2.2
0.5	50.8	26.8	3.8
1	76	64.2	34
1.5	81.2	76	69.6
2	85.8	81.2	73.2
3	87.8	85.8	72.2
5	88.6	89	63.2
8	86.6	83	29.8
9.6667	79.6	70.6	0
10	76.8	67	
12	52	44.6	
15	16.6	15.6	
17	0	0	



**Table 5A.1b. Variation of SO<sub>2</sub> absorption efficiency of 1<sup>st</sup> regenerated TLIL, MLIL and TSIL with time (Figure 5.4b)**

Parameters: Initial concentration of SO<sub>2</sub> in the feed gas,  $C_{SO_2} = 500$  ppm

Superficial velocity of gas,  $u_G = 5.77 \times 10^{-2}$  m s<sup>-1</sup>

Volume of solvent,  $V_{IL} = 2.50 \times 10^{-4}$  m<sup>3</sup>

Time (min)	Sulfur dioxide removal efficiency		
	TLIL	MLIL	TSIL
0	0	0	0
0.166667	5.8	2.8	5.6
0.333333	28.8	10.8	16
0.5	51	21.6	24
0.666667	64.2	31.2	28
0.833333	72.2	40.2	34
1	77.6	49	35.8
3	92	81.6	38
5	94	85	36
8	94	86.6	28.8
10	94	87.6	26
15	87.8	85.8	9.4
20	84	84.8	0
40	91.8	86.6	
60	91.8	88.6	

---

---

80	88.8	87.2	
100	88.6	87.2	
120	89	87	
140	88.6	87	
160	88.6	87	
180	89	87	
200	87	86.8	
220	84.4	86.6	
240	76	86.4	
260	65.8	86	
280	52.6	83.4	
300	37.6	78.2	
320	21.2	72.2	
340	0.2	65.8	
360		53	
380		42.8	
400		24.4	
420		4	

**Table 5A.2. Complete SO<sub>2</sub> absorption characteristics of MLIL, TLIL and TSIL after 1<sup>st</sup> regeneration of these ILs ( $u_G = 5.77 \times 10^{-2} \text{ m s}^{-1}$ ,  $C_{\text{SO}_2} = 500 \text{ ppm}$ ,  $V_{\text{IL}} = 250 \text{ ml}$ ); (Figure 5.4c)**

Parameters: Superficial velocity of gas,  $u_G = 5.77 \times 10^{-2} \text{ m s}^{-1}$

Initial concentration of SO<sub>2</sub> in the feed gas,  $C_{\text{SO}_2} = 500 \text{ ppm}$

Volume of solvent,  $V_{\text{IL}} = 2.50 \times 10^{-4} \text{ m}^3$

Time (min)	Absorption capacity (gm)
MLIL	12.416
TLIL	9.103
TSIL	0.253

**Table 5A.3. Effect of superficial velocity of gas on percent SO<sub>2</sub> removal efficiency of virgin MLIL (Figure 5.5a)**Parameters: Initial concentration of SO<sub>2</sub> in feed gas,  $C_{SO_2} = 500$  ppmVolume of solvent,  $V_{IL} = 2.50 \times 10^{-4} \text{ m}^3$ 

Time (min)	Sulfur dioxide removal efficiency		
	$3.85 \times 10^{-4} \text{ m s}^{-1}$	$5.775 \times 10^{-4} \text{ m s}^{-1}$	$7.70 \times 10^{-4} \text{ m s}^{-1}$
0.1667	12.6	2.8	1.8
0.3333	30.2	14.6	9
0.5	30.2	35.2	26.8
0.6667	52.6	53.6	43.8
0.8333	58	65.2	55.8
1	61.6	71.6	64.2
3	73.6	86.6	85.8
5	75.8	89	89
7	69.8	88.6	87.2
9	51	82.8	76
11	19.8	67.2	55.6
12.3333	0	52.6	40.6
13		45	34.2
15		24.6	15.6
17		5.8	0
17.6667		0	

**Table 5A.4. Effect of the superficial velocity of gas on percent removal efficiency of 1<sup>st</sup> regenerated MLIL (Figure 5.5b)**Parameters: Initial concentration of SO<sub>2</sub> in the feed gas,  $C_{SO_2} = 500$  ppmVolume of solvent,  $V_{IL} = 2.50 \times 10^{-4} \text{ m}^3$ 

Time (min)	Sulfur dioxide removal efficiency		
	$3.85 \times 10^{-4} \text{ m s}^{-1}$	$5.775 \times 10^{-4} \text{ m s}^{-1}$	$7.70 \times 10^{-4} \text{ m s}^{-1}$
0.1667	12	2.8	2.2
0.5	52.6	31.2	41.8
0.6667	58	40.2	52
1	61.6	59	59
3	75.4	81.6	77
5	79.6	85	81.2
7	80	86	83.8
9	80.4	87.6	84.8
11	80.8	87.8	84.4
13	79.2	87.6	84.4
15	79.2	85.8	84
17	80	85	84.4
19	81	84.8	84
21	80.4	84.8	84.4
23	79.6	84.8	84.8
25	79.6	84.8	84.8
27	80.4	84.8	84.8
29	80	85.6	84.6
30	79.6	85.6	84.4

**Table 5A.5. Effect of volume of virgin MLIL on exit concentration of SO<sub>2</sub> (Figure 5.6a)**Parameters: Initial concentration of SO<sub>2</sub> in the feed gas,  $C_{SO_2} = 500$  ppmSuperficial velocity of gas,  $u_G = 5.77 \times 10^{-2} \text{ m s}^{-1}$ 

Time (min)	Exit concentration of SO <sub>2</sub> (ppm)		
	$2.50 \times 10^{-4} \text{ m}^3$	$3.50 \times 10^{-4} \text{ m}^3$	$5.0 \times 10^{-4} \text{ m}^3$
0	500	500	500
1	142	176	183
3	67	61	58
5	55	44	40
7	57	48	58
10	120	161	176
12	217	279	281
15	377	433	419
16.3333	442	500	478
17	471		500
17.6667	500		

**Table 5A.6. Effect of volume of regenerated MLIL after first regeneration on its transient SO<sub>2</sub> removal efficiency (Figure 5.6b)**Parameters: Initial concentration of SO<sub>2</sub> in the feed gas,  $C_{SO_2} = 500$  ppmSuperficial velocity of gas,  $V_G = 5.77 \times 10^{-2} \text{ m s}^{-1}$ 

Time (min)	Sulfur dioxide removal efficiency		
	$2.50 \times 10^{-4} \text{ m}^3$	$3.50 \times 10^{-4} \text{ m}^3$	$5.0 \times 10^{-4} \text{ m}^3$
0.1667	2.8	9	3
0.3333	10.8	29.6	10.8
0.5	21.6	40	26
0.6667	31.2	49.8	41
0.8333	40.2	60.2	54.2
1	59	63	64
3	81.6	86.6	87.6
5	85	88	91.6
7	86	89	91.6
9	87.6	89	91
11	87.8	89	91.2
13	87.6	89	91.2
15	85.8	88	90.4
17	85	88	91.2
19	84.8	89	91
21	84.8	88.4	91

## RESULTS & DISCUSSION

---

23	84.8	88.4	91
25	84.8	88.4	91
27	84.8	88.4	91
29	85.6	88.4	91
30	85.6	88.4	91



**Table 5A.7 Effect of initial concentration of SO<sub>2</sub> in the feed gas on its percent removal efficiency by virgin MLIL (Figure 5.7a)**Parameters: Volume of solvent,  $V_{IL} = 2.50 \times 10^{-4} \text{ m}^3$ Superficial velocity of the gas,  $u_G = 5.77 \times 10^{-2} \text{ m s}^{-1}$ 

Time (min)	Sulfur dioxide removal efficiency			
	250 ppm	500 ppm	1000 ppm	1500 ppm
0.1667	10	2.8	2.4	3.6
0.3333	30.4	14.6	20.9	22.6
0.5	44.8	35.2	48.5	50
0.6667	55.6	53.6	65.6	65
0.8333	62.4	65.2	74.4	72
1	66.8	71.6	79.6	80
3	86.4	86.6	88.1	88.2
3.5	88	87.6	88.4	88.6667
5	84	89	87.6	89.3333
7	50.4	88.6	86.2	89.2667
9	0.4	82.8	80.4	89.3333
11		67.2	66.7	87.9333
13		45	51.9	85
15		24.6	37.4	79.3333
17		5.8	26	71.9333
17.6667		0	23	65.8

## RESULTS & DISCUSSION

---

20			13.7	56.6667
22			7.9	45.9333
24			3.5	37.1333
26			0.1	26.4
28				17.6667
30				10.1333
32				3.6667
34				0

**Table 5A.8. Effect of initial concentration of SO<sub>2</sub> in the feed gas on its percent removal efficiency by the use of regenerated (after 1<sup>st</sup> absorption) MLIL (Figure 5.7b)**

Parameters: Volume of solvent,  $V_{IL} = 2.50 \times 10^{-4} \text{ m}^3$

Superficial velocity of the gas,  $V_G = 5.77 \times 10^{-2} \text{ m s}^{-1}$

Time (min)	Sulfur dioxide removal efficiency		
	250 ppm	500 ppm	1000 ppm
0.1667	8.8	2.8	10
0.3333	24	10.8	20.4
0.5	29.2	21.6	37
0.6667	40	31.2	48
0.8333	48	40.2	60
1	52	59	65
3	79.2	81.6	85
5	84	85	86
7	86	86	87
9	87.2	87.6	86
11	87.2	87.8	86.8
13	86.8	87.6	85.9
15	86	85.8	85.8
17	85.6	85	85.7
19	85.2	84.8	85.5

---

21	85.2	84.8	85.1
23	85.2	84.8	85.1
25	85.2	84.8	85.1
27	85.2	84.8	85.1
29	85.2	85.6	85.1
30	85.2	85.6	85.1

**Table 5A.9. Variation of percent SO<sub>2</sub> removal efficiency of TLIL with time for three consecutive absorption regeneration cycles (Figure 5.8a)**Parameters: Volume of solvent,  $V_{IL} = 2.50 \times 10^{-4} \text{ m}^3$ Superficial velocity of gas,  $u_G = 5.77 \times 10^{-2} \text{ m s}^{-1}$ 

Time (min)	Sulfur dioxide removal efficiency		
	1 <sup>st</sup> absorption with virgin IL	2 <sup>nd</sup> absorption using regenerated IL	3 <sup>rd</sup> absorption using regenerated IL
0.1667	3	5.8	21.8
0.3333	22.2	28.8	45.6
0.5	47.2	51	61
0.6667	63.8	64.2	69
0.8333	73	72.2	74
1	78.6	77.6	77
2	89	88.6	85.6
3	92.2	92	88.2
5	94	94	90.2
8	90.2	95.2	91.8
10	78	94	92
12	59	91.8	92.2
15	34	87.8	92.8
17	20.6	85.8	93
20	0.2	84	92.8

---

22		84.2	92.8
25		85.6	93
27		86.6	93
30		87.8	93.6
32		89	93
35		90	93
37		90.6	93
40		91.8	93
42		92	93
45		92.8	93.6
47		93	93.6
50		93.6	93.6
52		93.8	93
55		94	93.6
57		94	93.6
60		94	93

**Table 5A.10. Variation of percent SO<sub>2</sub> removal efficiency of MLIL with time for three consecutive absorption cycles (Figure 5.8b)**Parameters: Volume of solvent,  $V_{IL} = 2.50 \times 10^{-4} \text{ m}^3$ Superficial velocity of the gas,  $V_G = 5.77 \times 10^{-2} \text{ m s}^{-1}$ 

Time (min)	Sulfur dioxide removal efficiency		
	1 <sup>st</sup> absorption with virgin IL	2 <sup>nd</sup> absorption using regenerated IL	3 <sup>rd</sup> absorption using regenerated IL
0.1667	2.8	2.8	2.6
0.3333	14.6	10.8	13.8
0.5	35.2	21.6	29
0.6667	53.6	31.2	44
0.8333	65.2	40.2	55.6
1	71.6	49	63.8
2	83	76.2	77.8
3	86.6	81.6	81.6
5	89	85	84.8
8	87.2	86.6	86.6
10	76	87.6	86.8
12	56.6	87.6	87.2
15	24.6	85.8	87.8
17	5.8	85	88.2
20		84.8	89

---

---

22		84.8	89.2
25		84.8	89.2
27		84.8	89.2
30		85.6	90.2
32		86	88
35		86.6	88
37		86.6	88
40		86.6	88
42		86.6	88
45		88	88
47		87	89
50		88	89
52		88.6	89
55		88.6	89
57		88.6	89
60		88.6	89



## APPENDIX -5B

**5B. Experimental data for the absorption of SO<sub>2</sub> in aqueous slurries of Ca(OH)<sub>2</sub> and CaCO<sub>3</sub>****Table 5B.1. Variation of the concentration of SO<sub>2</sub> in exit gas, pH of absorbent and gas hold-up with time (Figure 5.9)**Parameters: Superficial velocity of the gas,  $u_G = 5.77 \times 10^{-2} \text{ m s}^{-1}$ Initial concentration of SO<sub>2</sub> in the feed gas,  $C_{\text{SO}_2} = 500 \text{ ppm}$ Volume of slurry,  $V_{sl} = 2.5 \times 10^{-4} \text{ m}^3$ 

Time (min)	Concentration of SO <sub>2</sub> in exit gas (ppm)	pH of Ca(OH) <sub>2</sub> slurry	Gas hold-up of Ca(OH) <sub>2</sub> slurry
0	500	12.85	0.55
1	112	12.85	0.5
3	38	12.85	0.5
5	23	12.85	0.5
7	18	12.85	0.5
9	14	12.85	0.5
11	13	12.85	0.5
13	11	12.85	0.5
15	11	8	0.3556
17	14	5.5	0.3556
19	44	5	0.3556
21	91	4.5	0.3556
23	155	4	0.3556

## RESULTS & DISCUSSION

---

25	279	3	0.3556
27	495	2	0.3556

**Table 5B.2. Variation of gas hold-up with the superficial velocity of the gas in the slurry bubble column (Figure 5.10)**Parameters: Superficial velocity of gas,  $u_G = 5.77 \times 10^{-2} \text{ m s}^{-1}$ Initial concentration of  $\text{SO}_2$  in feed gas,  $C_{\text{SO}_2} = 500 \text{ ppm}$ Volume of slurry,  $V_{sl} = 2.5 \times 10^{-4} \text{ m}^3$ 

Superficial velocity of gas, ( $u_G$ ), $\text{m s}^{-1}$	$\text{Ca(OH)}_2$ slurry $C_{B0}^T = 4.0 \text{ kg m}^{-3}$	$\text{CaCO}_3$ slurry $C_{B0}^T = 4.0 \text{ kg m}^{-3}$
$3.85 \times 10^{-2}$	0.3555	0.3095
$5.77 \times 10^{-2}$	0.5	0.4423
$7.7 \times 10^{-2}$	0.71	0.6375

**Table 5B.3. Effect of initial SO<sub>2</sub> concentration in the feed gas on its percent removal efficiency by Ca(OH)<sub>2</sub> slurry (Figure 5.11a)**Parameters: Superficial velocity of the gas,  $u_G = 3.85 \times 10^{-2} \text{ m s}^{-1}$ Initial concentration of SO<sub>2</sub> in the feed gas,  $C_{\text{SO}_2} = 1000 \text{ ppm}$ Volume of slurry,  $V_{sl} = 2.50 \times 10^{-4} \text{ m}^3$ 

Time (min)	Sulfur dioxide removal efficiency			
	250 ppm	500 ppm	1000 ppm	1500 ppm
0.1667	12.4	5.2	4.1	1.4
0.3333	32.4	9.4	27.6	1.8667
0.5	48	20.8	51.4	10.9333
0.6667	59.2	37	67	37.5333
0.8333	66.4	51	75.9	61.0667
1	72.4	61.4	81.1	74.4
3	92.4	68.2	95.1	96.4
5	96.4	94.4	97.6	98.2
7	98.4	96	98.3	99
9	99.6	96.8	98.8	99.2
11	99.6	97.2	99.1	99.4
13	99.6	98.2	99.4	96.4
15	99.6	97.8	99.4	86.6667
17	99.6	98.2	99.4	77.6667
19	99.6	98.2	96	62.3333

---

---

21	99.6	98.4	89.3	27.4
23	99.6	99	81.6	0
25	99.6	99	70.1	
27	99.6	99	42.4	
28	99.6	99	2	
29	99.6	99		
31	99.6	99		
33	99.6	98.4		
35	99.6	97.4		
37	99.6	93		
39	99.6	75.4		
41	95.2	39.2		
43	84	15.6		
45	60.4	0		
47	32			
49	19.2			
51	9.6			
54	0.4			

**Table 5B.4. Effect of initial SO<sub>2</sub> concentration of inlet gas on percent removal efficiency by calcium carbonate slurry (Figure 5.11b)**Parameters: Superficial velocity of the gas,  $u_G = 3.85 \times 10^{-2} \text{ m s}^{-1}$ Initial solid loading,  $C_{B0}^T = 4.0 \text{ kg m}^{-3}$ Volume of slurry,  $V_{sl} = 2.50 \times 10^{-4} \text{ m}^3$ 

Time (min)	Sulfur dioxide removal efficiency			
	250 ppm	500 ppm	1000 ppm	1500 ppm
0.1667	15.2	27	7.5	3.1333
0.3333	33.2	48.8	27	8.2667
0.5	46	62.6	49.4	20
0.6667	56	70.6	63.5	33.3333
0.8333	62	76	73	44.7333
1	67.6	80	79.2	63.7333
3	89.2	92.8	94.1	94.9333
5	94	94.8	96.5	97.1333
7	97.2	96.2	97.4	97.6667
9	98	96.6	97.7	95.8
11	98	97	97.2	82.9333
13	99.2	97	92	62.4
15	99.6	96.6	81.9	35.3333
17	99.6	96.2	65	11.0667
19	99.6	94.6	45.6	0

---

21	99.6	91.8	31.4	
23	99.6	87.2	17.9	
25	99.6	81.8	4.2	
27	99.6	72		
29	99.6	53.6		
31	97.6	31.8		
33	90.4	11.6		
35	73.6	0		
37	44			
39	26.4			
41	14			
43	6.4			
45	0.4			

**Table 5B.5. Effect of superficial velocity of gas on SO<sub>2</sub> removal efficiency of Ca(OH)<sub>2</sub> slurry (Figure 5.12a)**Parameters: Initial concentration of SO<sub>2</sub> in the feed gas,  $C_{SO_2} = 1000$  ppmInitial solid loading,  $C_{B0}^T = 4.0$  kg m<sup>-3</sup>Volume of slurry,  $V_{sl} = 2.50 \times 10^{-4}$  m<sup>3</sup>

Time (min)	Sulfur dioxide removal efficiency		
	$3.85 \times 10^{-4}$ m s <sup>-1</sup>	$5.775 \times 10^{-4}$ m s <sup>-1</sup>	$7.70 \times 10^{-4}$ m s <sup>-1</sup>
0.1667	4.1	7	30.8
0.3333	27.6	17.6	62.1
0.5	51.4	47.4	77.4
0.6667	67	65.6	84
0.8333	75.9	74.9	87.9
1	81.1	80.8	90.3
3	95.1	94.6	97.3
5	97.6	96.9	98.3
7	98.3	97.9	93.6
9	98.8	98.1	71.8
11	99.1	87.1	31.9
13	99.4	74.9	5.6
15	99.4	60.9	
17	99.4	38.8	
19	96	0	



---

21	89.3		
23	81.6		
25	70.1		
27	42.4		
28	2		

**Table 5B.6. Effect of superficial velocity of gas on SO<sub>2</sub> removal efficiency of CaCO<sub>3</sub> slurry (Figure 5.12b)**Parameters: Initial concentration of SO<sub>2</sub> in the feed gas,  $C_{SO_2} = 1000$  ppmInitial solid loading,  $C_{B0}^T = 4.0$  kg m<sup>-3</sup>Volume of slurry,  $V_{sl} = 2.50 \times 10^{-4}$  m<sup>3</sup>

Time (min)	Sulfur dioxide removal efficiency		
	$3.85 \times 10^{-4}$ m s <sup>-1</sup>	$5.775 \times 10^{-4}$ m s <sup>-1</sup>	$7.70 \times 10^{-4}$ m s <sup>-1</sup>
0.1667	7.5	7.4	24.6
0.3333	27	41.3	53.3
0.5	49.4	67	69.6
0.6667	63.5	79	79.4
0.8333	73	84.4	84.4
1	79.2	87.6	87.5
2	91	94.8	94.3
3	94.1	96.5	96.4
4	95.5	97.6	96.8
5	96.5	98.1	93
6	96.9	97.3	82.3
7	97.4	93.4	66.5
8	97.5	86.6	49.6
9	97.7	77.3	35.4
10	97.7	64.9	21.9

---

---

11	97.2	50.4	4.5
12	95.5	35.5	0
13	92	22.9	
14	87.6	9.1	
15	81.9	0	
16	74.1		
17	65		
18	54.7		
19	45.6		
20	37.4		
21	31.4		
22	25.6		
23	17.9		
24	11.1		
25	4.2		
25.5	0		

**Table 5B.7. Effect of initial solids loading on percent SO<sub>2</sub> removal efficiency by Ca(OH)<sub>2</sub> slurry (Figure 5.13a)**

Parameters: Superficial velocity of the gas,  $u_G = 3.85 \times 10^{-2} \text{ m s}^{-1}$

Initial concentration of SO<sub>2</sub> in feed gas,  $C_{\text{SO}_2} = 1000 \text{ ppm}$

Volume of slurry,  $V_{sl} = 2.50 \times 10^{-4} \text{ m}^3$

Time (min)	Sulfur dioxide removal efficiency			
	saturated sol <sup>n</sup>	4 kg m <sup>-3</sup>	6 kg m <sup>-3</sup>	8 kg m <sup>-3</sup>
0.1667	6.1	4.1	10.2	2.8
0.3333	40.6	27.6	37.9	34.9
0.5	63.5	51.4	59.3	59.4
0.6667	75	67	71.3	73.2
0.8333	81.4	75.9	78.1	80.7
1	84.8	81.1	82.6	84.7
3	95.3	95.1	94.4	95.4
5	97.3	97.6	96.7	97.1
7	96.8	98.3	97.6	97.9
9	84.9	98.8	98.1	98.4
11	73.6	99.1	98.2	98.6
13	55.5	99.4	98.6	98.7
15	16.8	99.4	98.7	98.7
17	0	99.4	98.9	98.9
19		96	98.9	99.1

## RESULTS &amp; DISCUSSION

---

---

21		89.3	98.9	99.1
23		81.6	99.1	99.1
25		70.1	98.9	99.1
27		42.4	96.3	99.3
28		2	93.6	99.3
29			90.4	99.3
31			82.1	98.4
33			71.8	93.9
35			59.3	87.9
37			47.3	81.4
39			29.3	73.2
41			1.5	63.3
43				52.1
45				40.1
47				28.4
49				0

**Table 5B.8. Effect of initial solid loading on SO<sub>2</sub> removal efficiency of CaCO<sub>3</sub> slurry Figure (5.13b)**Parameters: Superficial velocity of the gas,  $u_G = 3.85 \times 10^{-2} \text{ m s}^{-1}$ Initial concentration of SO<sub>2</sub> in feed gas,  $C_{\text{SO}_2} = 1000 \text{ ppm}$ Volume of slurry,  $V_{sl} = 2.50 \times 10^{-4} \text{ m}^3$ 

Time (min)	Sulfur dioxide removal efficiency			
	saturated sol <sup>n</sup>	4 kg m <sup>-3</sup>	6 kg m <sup>-3</sup>	8 kg m <sup>-3</sup>
0.1667	10.3	7.5	22	36.3
0.3333	38.5	27	51	64
0.5	59.5	49.4	67.6	77.4
0.6667	69.6	63.5	75.9	84.3
0.8333	72.9	73	81.4	87.5
1	72	79.2	84.5	89.9
3	17.6	94.1	95	97.3
5	1.5	96.5	96.9	98.6
7		97.4	97.8	99.1
9		97.7	98.1	99.2
11		97.2	98.4	99.2
13		92	98.4	99.2
15		81.9	98.6	99.2
17		65	98.1	99.2
19		45.6	94.8	99.1

## RESULTS & DISCUSSION

---

21		31.4	87.6	99.1
23		17.9	76.3	99.1
25		4.2	64.7	98.3
26		0	58.8	97.4
27			52.3	96.4
29			37.9	91
31			14.4	83.1
32			0.2	77.6
33				69.4
35				46.6
37				21.5
39				0

**Foam-bed reactor****Table 5B.9. Comparison of percent SO<sub>2</sub> removal efficiency by use of distilled water as the absorbent in the bubble column and foam-bed slurry reactor (Figure 5.14a)**Parameters: Superficial velocity of the gas,  $u_G = 3.85 \times 10^{-2} \text{ m s}^{-1}$ Initial concentration of SO<sub>2</sub> in feed gas,  $C_{\text{SO}_2} = 1000 \text{ ppm}$ Volume of water,  $V_{sl} = 2.50 \times 10^{-4} \text{ m}^3$ 

Time (min)	Sulfur dioxide removal efficiency					
	Without surfactant	CTAB	SDS	Triton X- 100	Teepol	Tween 80
0.1667	9	8	7	6.4	17.6	7.4
0.3333	27.8	24.4	15	25.2	39.4	21.6
0.5	46.4	45	29.2	46.4	55.6	40
0.6667	59.8	60.8	47.6	61	66.2	53.6
0.8333	66.4	69.8	62	69	73	63
1	70	74.4	70	72.6	78	68.4
1.5	68	74.4	77	70	84.2	72.4
2	58.4	63.8	70.2	56.4	84.2	64.4
3	35	39.4	51	32.2	60.2	39
5	12.8	17.8	17.4	11.2	19.4	16
7	2.2	5		2.4	6.4	6.6
7.66		0			0	0



**Table 5B.10. Comparison of percent SO<sub>2</sub> removal efficiency by use of Ca(OH)<sub>2</sub> slurry as absorbent in bubble column and the foam-bed slurry reactor (Figure 5.14b)**

Parameters: Superficial velocity of the gas,  $u_G = 3.85 \times 10^{-2} \text{ m s}^{-1}$

Initial concentration of SO<sub>2</sub> in feed gas,  $C_{\text{SO}_2} = 1000 \text{ ppm}$

Volume of slurry,  $V_{sl} = 2.50 \times 10^{-4} \text{ m}^3$

Time (min)	Sulfur dioxide removal efficiency					
	Without surfactant	CTAB	SDS	Triton X- 100	Teepol	Tween 80
0.1667	29.5	4	7.6	18	5	34.4
0.3333	59.5	7.3	34.3	44.8	9.4	59
0.5	74.8	33.6	58.5	63.5	29	71
0.6667	82.1	56.1	72.3	73.8	49.3	77.4
0.8333	86.1	71.3	79.9	79.9	63.3	81.1
1	88.4	79.8	83.9	83	71.5	83.5
3	96.1	95.4	95.4	93.5	90.6	91.4
5	97.6	97.3	97.1	95	93.1	92.5
7	98.3	98.3	97.8	94.3	94	92.3
9	98.6	98.5	98	92.8	94.1	91.5
11	99	97.4	97.3	91.9	94.6	91
13	99.1	96.3	96	91.1	95.1	91
15	99.1	95.4	95.1	90.9	95.9	91.1
17	98.3	95	94.3	90.5	96.3	91.1

## RESULTS &amp; DISCUSSION

---

19	92.5	94.9	93.6	88.6	96.3	91.1
21	83.6	90.5	92.3	80.9	89.8	88.9
23	76.3	79.4	87.8	67.5	67.8	79.7
25	69.4	61.3	79.4	46.1	52.8	63.6
27	56.4	30	66	22.3	40.1	49.1
29	3.8	12.1	48.8	8.9	24.3	35.7
31		2.1	30	2.4	0	15.1
33			14.8			0
35			2.9			

**Table 5B.11. Comparison of percent SO<sub>2</sub> removal efficiency by use of CaCO<sub>3</sub> slurry as absorbent in bubble column and the foam-bed slurry reactor (Figure 5.14c)**

Parameters: Superficial velocity of the gas,  $u_G = 3.85 \times 10^{-2} \text{ m s}^{-1}$

Initial concentration of SO<sub>2</sub> in feed gas,  $C_{\text{SO}_2} = 1000 \text{ ppm}$

Volume of slurry,  $V_{sl} = 2.50 \times 10^{-4} \text{ m}^3$

Time (min)	Sulfur dioxide removal efficiency					
	Without surfactant	CTAB	SDS	Triton X- 100	Teepol	Tween 80
0.1667	13.5	2.6	4.9	2.1	8.1	0.4
0.3333	46	16	24.6	3.5	25.1	0.6
0.5	65.8	42	47.6	11.8	47.9	2.6
0.6667	77.1	61.6	65	36	63.9	20.2
0.8333	83	73.6	66.4	58.2	72.9	43.4
1	86.6	80.8	73.2	71.2	79.1	61
3	96.5	94.6	92.4	93.3	94.1	93.4
5	98.3	96.8	95.8	95.2	96.3	96.1
7	98.3	97.4	96	94.7	96.4	96.4
9	98.3	97.4	94	93.1	95.9	94.9
11	98.3	96.4	90.8	91.7	94.8	92
13	94.5	94.3	87.4	90.3	93.6	76.9
15	86.6	85.8	85	82.7	80.9	37.4
17	72.5	59.6	83.4	50.6	45	3.7

---

19	53.5	30	82.4	19.1	18.5	
21	37.1	9.5	81.4	0	0	
23	24.8	1	80			
25	10.1		72.8			
27			58			
29			40.1			
31			21.1			
33			10.3			
35			0			

## APPENDIX -5C

## 5C.1. Experimental data liquid-side mass-transfer coefficient of pure Oxygen

Table 5C.1. Variation of dissolve O<sub>2</sub> and liquid-side mass-transfer coefficient of pure Oxygen with time in bubble column (Appendix 4B.2)Parameters: Superficial velocity of O<sub>2</sub>,  $u_G = 3.85 \times 10^{-2} \text{ m s}^{-1}$ Volume of distilled water,  $V_L = 2.50 \times 10^{-4} \text{ m}^3$ 

Time (min)	Dissolve oxygen, (mg/l)	Instantaneous $k_{l,O_2}^0 a$ , $\text{s}^{-1}$
0	0.8	-
1	17	$66.1 \times 10^{-4}$
3	21	$11.0 \times 10^{-4}$
5	23	$6.64 \times 10^{-4}$
10	25.2	$3.27 \times 10^{-4}$
15	26.4	$1.976 \times 10^{-4}$
20	27.3	$1.587 \times 10^{-4}$
25	28	$1.305 \times 10^{-4}$
30	28.6	$1.173 \times 10^{-4}$
35	29.4	$1.65 \times 10^{-4}$
40	30	$1.31 \times 10^{-4}$

Detail calculations are described in Appendix 4B.2

## CONCLUSIONS AND RECOMMENDATIONS FOR FUTURE WORK

### Gas absorption in ionic liquids:

- I. A series of low-cost regenerative hydroxyl ammonium ionic liquids have been synthesized and used for absorptive removal of SO<sub>2</sub> from its mixture with air to find out its transient SO<sub>2</sub> removal efficiency under different experimental conditions. The variables studied were the superficial velocity of the gas, depth of solvent in the semi-batch reactor and nature of constituting ions in the ionic liquids on the SO<sub>2</sub> absorption capacity. A maximum of 89 percent transient SO<sub>2</sub> removal efficiency was achieved when MLIL and TLIL were used as solvents which could be further enhanced by an increase in the depth of solvent in the semi-batch reactor.
- II. Exhausted ILs were found to be capable of getting fully regenerated and could be used repeatedly for gas absorption. Sulfur dioxide absorption capacities of these regenerated ionic liquids were found to be enormously higher than those of the virgin ILs. Contrary to this, only a maximum of 70 percent SO<sub>2</sub> removal efficiency could be achieved when TSIL was used as the solvent. For the same constituent cation in the ionic liquid, the lactate anion was found to be substantially more effective than its salicylate counterpart. Pure SO<sub>2</sub> gas obtained by desorption operation can be utilized for suitable industrial usages.
- III. Physico-chemical and micro structural analyses of all the reagents used in the absorption studies were performed. FT-IR and <sup>1</sup>HNMR spectrum analyses of the synthesized, exhausted and regenerated ionic liquids show that the mechanism of physical absorption plays the major role for the absorption of SO<sub>2</sub> under the experimental conditions employed in the present investigation.
- IV. As the SO<sub>2</sub> removal efficiency continued to remain at a very high level for several hours and that the viscosity of the IL absorbents was substantially high, two semi-batch contactors with a shallow pool of absorbents could operate in parallel. Gravity flow of the exhausted solvent to the regenerator would reduce the pumping cost and likely to be beneficial.

### Sulfur dioxide absorption in Ca-based slurries:

- I. A comparative study of a bubble column reactor with that of a foam-bed reactor has been made with respect to different variables for absorption studies of SO<sub>2</sub> in calcium-based aqueous slurries primarily those of hydrated lime and calcium carbonate.
- II. In both the reactors, the concentration of SO<sub>2</sub> in the feed gas was able to be reduced to 5 ppm for feed gas concentrations ranging from 250 to 1500 ppm and maximum SO<sub>2</sub> removal efficiency of 99 percent was achieved.
- III. Gas side, liquid side and solid-liquid mass transfer coefficients, gas hold-up in the bubble column, particle size distribution of the solid phase reactant have been determined experimentally. It was verified that the reaction in each of these cases is instantaneous and gas phase controlled.
- IV. Under identical operating conditions, the rate of absorption of SO<sub>2</sub> in Ca(OH)<sub>2</sub> slurry in a foam-bed reactor was found to be lower than that in a bubble column reactor. This is, however, is not the case when SO<sub>2</sub> is absorbed in pure water in the two types of reactor. In alkaline medium, the reaction being instantaneous, additional resistance due the surfactant film at the gas-liquid interface and partial surface coverage of the dissolving particles by the surfactant molecules is considered to be the main reason for this decrease. It has been reported that at this low concentration of surfactant, its effect on Ca(OH)<sub>2</sub>-CO<sub>2</sub> system was negligible, although it was reported to be important at high concentrations.
- V. Orifices on the gas distributor plate of the *bubble column* got choked at the time of product withdrawal for solids loading beyond 8 kg m<sup>-3</sup>. But, in the foam-bed reactor with the addition of only 4 ppm CTAB, about 7-10 x 10<sup>-2</sup> m of foam column was formed and no choking were observed up to 16 kg m<sup>-3</sup> of solids loading beyond which experiments were not performed. The maximum value of SO<sub>2</sub> removal efficiencies was found to reduce at higher concentration of surfactants.
- VI. Analysis of products formed by reaction of the dissolved solute with the absorbed gas indicated that either calcium sulfate hemihydrates or dihydrate was formed and depend on the nature and use of surfactant type.
- VII. Semi-batch operation has the advantage that residual lime content in the gypsum can be reduced to a very low value as desired by continuing the operation for the

## **CONCLUSIONS AND RECOMMENDATIONS FOR FUTURE WORK**

---

required period. FGD product quality can thereby be improved, but it then requires operation of two semi-batch reactors in parallel.

### **Recommendations for further work**

- I. Future work may be carried out using gaseous mixtures having compositions identical to those of flue gases containing the major components, viz.  $\text{SO}_x$ ,  $\text{NO}_x$  and  $\text{CO}_2$  emitted from different industries. Each gas component will have its own mass-transfer rate.
- II. The scale-up of this system requires to be working in deep. The rise of bubbles will be many greater in case of real industrial system.
- III. The strange absorption behavior of virgin ILs need to study more in detail.
- IV. Studies of the parameter dependence of choking problem in bubble column need to be performed in more detail.



---

## NOTATION

$\Delta C$	Amount of gas phase component $A$
$a$	Specific interfacial area per unit volume of dispersion, $m^2/m^3$
$a'$	Specific interfacial area per unit volume of solvent, $m^2/m^3$
$A_c$	Cross sectional area of column, $m^2$
$A_p$	Total surface area of particles, $m^2/m^3$
$A_{pi}$	Surface area of particles in $i^{\text{th}}$ fraction, $m^2$
$A_{sl}$	Solid-liquid interfacial area, $m^2/m^3$
$A_T$	Defined in chapter 3
$A_{Td}$	Defined in chapter 3
$C_A$	Concentration of $A$ in liquid at any time $t$ , $k \text{ mol m}^{-3}$
$C_{Ai}$	Concentration of $A$ at gas-liquid interface, $k \text{ mol m}^{-3}$
$C_B$	Concentration of $B$ at any time $t$ , $k \text{ mol m}^{-3}$
$C_{Bb}$	Concentration of $B$ in bulk, $k \text{ mol m}^{-3}$
$C_{BO}$	Saturation solubility of solid ( $B$ ), $k \text{ mol m}^{-3}$
$C_B^T(0)$	Defined in eqn. (3.19) in chapter 3
$C_B^T(t)$	Defined in eqn. (3.19) in chapter 3
$C_e(t)$	Defined in eqn. (3.17) in chapter 3
$C_{in}$	Defined in eqn. (3.17) in chapter 3
$C_{OH^-}^0$	Saturation solubility of $OH^-$ , $k \text{ mol m}^{-3}$
$C_{SO_2}$	Initial concentration of $SO_2$ in inlet gas, ppm
$C_{SO_2,in}$	Inlet $SO_2$ gas concentration, ppm
$C_{SO_2,out}$	Outlet $SO_2$ gas concentration, ppm
$C_{SO_2}(t)$	Concentration of $SO_2$ at any time $t$ , $k \text{ mol m}^{-3}$
$C_l(t)$	Concentration of $SO_2$ in liquid at any time $t$ , $k \text{ mol m}^{-3}$
$C_{O_2}^*$	Saturation concentration of oxygen in water, $kmol \text{ m}^{-3}$
$C_{O_2}$	Concentration of oxygen in water at any time $t$ , $kmol \text{ m}^{-3}$
$C_{O_2,i}$	Initial concentration of oxygen in water, $k \text{ mol m}^{-3}$

---

$C_{O_2,f}$	Final concentration of oxygen in water, $\text{k mol m}^{-3}$
$D_A$	Liquid phase diffusivity of $A$ in water, $\text{m}^2/\text{s}$
$D_B$	Liquid phase diffusivity of $B$ in water, $\text{m}^2/\text{s}$
$D_{O_2}$	Liquid phase diffusivity of oxygen in water, $\text{m}^2/\text{s}$
$D_{OH^-}$	Diffusivity of $\text{OH}^-$ in water, $\text{m}^2/\text{s}$
$d_c$	Column diameter, $\text{m}$
$D_g$	Gas phase dispersion coefficient, $\text{m}^2/\text{s}$
$D_l$	Liquid-phase dispersion coefficient, $\text{m}^2/\text{s}$
$d_{pi}$	Diameter of particle in $i^{\text{th}}$ volume fraction, $\text{m}$
$E_{inst}$	Instantaneous enhancement factor
$f_{SO_2}$	Defined in eqn. 3C.1 in chapter 3
$H$	Henry's constant for gas absorption, $\text{atm m}^3 \text{ kmol}^{-1}$
$h_{disp}$	Dispersion height, $\text{m}$ , defined in chapter 3
$H_a, \sqrt{M}$	Hatta number
$h_d$	defined in eqn. 3.44 in chapter 3
$h_l$	defined in eqn. 3.44 in chapter 3
$k$	Rate constant
$K$	Equilibrium constant of reactions
$k_1$	Second order reaction rate constant, $\text{l gmol}^{-1} \text{ s}^{-1}$
$K_l$	Overall liquid-phase mass-transfer coefficient,
$k_l$	Liquid phase mass transfer-coefficient for chemical absorption
$k_g$	Gas-phase mass transfer coefficient, $\text{m s}^{-1}$
$k_l^0$	Liquid phase mass-transfer coefficient for physical absorption, $\text{m/s}$
$k_{lO_2}^0$	Liquid phase mass-transfer coefficient for physical absorption of $\text{O}_2$ , $\text{m/s}$
$k_{lSO_2}^0$	Liquid phase mass-transfer coefficient for physical absorption of $\text{SO}_2$ , $\text{m/s}$
$k_{lO_2}^0 a$	Volumetric liquid phase mass-transfer coefficient for physical

---

	absorption of O <sub>2</sub> , s <sup>-1</sup>
$k_{lSO_2}^0 a$	Volumetric liquid phase mass-transfer coefficient for physical absorption of SO <sub>2</sub> , s <sup>-1</sup>
$K_{SO_2-H_2O}$	Defined in eqn. 3.5(ii)
$k_{SO_2-H_2O}$	Forward reaction rate constant of reaction 3.5(ii), s <sup>-1</sup>
$K_{SO_2-OH^-}$	Equilibrium reaction rate constant of reaction 3.9a, l/g mol
$k_{SO_2-OH^-}$	Forward reaction rate constant of reaction 3.8, l/g mol s <sup>-1</sup>
$k_{HSO_3^-SO_3^{2-}}$	Forward reaction rate constant of reaction 3.9b, l/g mol
$K_{HCO_3^-}$	Equilibrium reaction rate constant of reaction 3.14(xiii), l/g mol
$k_{mn}$	Reaction rate constant for m-n <sup>th</sup> order,
$k_{sl}$	Solid-liquid mass transfer coefficient, m s <sup>-1</sup>
$K_w$	Equilibrium constant of reaction 3.5(iv)
$m$	Reaction order for species A
$M_B$	Molecular weight of component B
$n$	Reaction order for species B
$m_B^T(0)$	Defined in eqn. (3.18) in chapter 3
$m_B^T(t)$	Defined in eqn. (3.18) in chapter 3
$n_{pi}$	Initial no. of particles present in slurry
$P_{Ab}$	Partial pressure of A in bulk, atm
$P_{Ai}$	Partial pressure of A interface, atm
$Pe_g$	Peclet no. for gas-phase
$Pe_l$	Peclet no. for liquid- phase
$p_{SO_2b}$	Partial pressure of SO <sub>2</sub> in bulk, atm
$p_{SO_2i}$	Partial pressure of SO <sub>2</sub> at interfacial, atm
$p_{SO_2in}$	Concentration of SO <sub>2</sub> in feed gas, ppm
$p_{SO_2out}$	Concentration of SO <sub>2</sub> in outlet gas, ppm
$R_A$	Reaction rate, k mol/m <sup>2</sup> s

---

$\overline{R}_A$	Rate of absorption of A, $\text{kmol/m}^3 \text{ s}$
$R_{SO_2}$	Defined in eqn. 3.32 in chapter 3
$R_B$	Rate of dissolution of particles, $\text{kmol s}^{-1}$
$u$	Superficial velocity of gas, $\text{m/s}$
$V_{IL}$	Volume of ionic liquid, $\text{m}^3$
$V_{sl}$	Volume of slurry, $\text{m}^3$
$V_l$	Volume of liquid, $\text{m}^3$
$V_{disp}$	Volume of dispersion of slurry, $\text{m}^3$
$Q_o$	Defined in eqn. 3A.i, in appendix 3A
$Q_{gtot}$	Total inlet gas flow rate, $\text{m}^3/\text{s}$
$W_i$	Defined in chapter 3
$W_{SO_2}$	Rate of gas absorption in bubble column, $\text{g mol/s}$
$X$	Percentage conversion of dissolved species, <b>B</b>
$Z, R_{BA}$	Stoichiometry coefficient, <b>m</b>
<i>Greek symbols</i>	
$\delta$	Film thickness, <b>m</b>
$\varepsilon_g$	Gas hold-up
$\varepsilon_l$	Liquid hold-up
$\beta$	Percent of gas-phase resistance to mass transfer
$\rho$	Density of particles, $\text{kg m}^{-3}$
$\eta(t)$	Percent of transient $\text{SO}_2$ removal efficiency, defined in chapter 3
<i>Symbol</i>	
<b>A</b>	$\text{SO}_2$
<b>B</b>	Solid
<b>G,g</b>	Gas
<b>P</b>	Particle

---

## REFERENCES

- [1]. Abraham, M. and Sawant, S. B. (1990). Hydrodynamics and mass transfer characteristics of packed bubble columns. *The Chemical Engineering Journal*, 43(3), 95-105.
- [2]. Adewuyi, Y. G., He, X., Shaw, H. and Lolertpihop, W. (1999). Simultaneous absorption and oxidation of NO and SO<sub>2</sub> by aqueous solutions of sodium chlorite. *Chemical Engineering Communications*, 174(1), 21-51.
- [3]. Akita, K. and Yoshida, F. (1974). Bubble size, interfacial area, and liquid-phase mass transfer coefficient in bubble columns. *Industrial and Engineering Chemistry Process Design and Development*, 13(1), 84-91.
- [4]. Alva, A. K. (1994). Possible utilization of fuel-gas desulfurization gypsum and fly ash for citrus production: evaluation of crop growth response. *Waste management*, 14(7), 621-627.
- [5]. Anderson, J. L., Dixon, J. K., Maginn, E. J. and Brennecke, J. F. (2006). Measurement of SO<sub>2</sub> solubility in ionic liquids. *The Journal of Physical Chemistry B*, 110(31), 15059-15062.
- [6]. Arif, A., Stephen, C., Branken, D., Everson, R., Neomagus, H. and Piketh, S. (2015). Modeling wet flue gas desulfurization. In *Conference of the National Association for Clean Air (NACA 2015)*, Bloemfontein, South Africa.
- [7]. Armand, M., Endres, F., MacFarlane, D. R., Ohno, H. and Scrosati, B. (2009). Ionic-liquid materials for the electrochemical challenges of the future. *Nature materials*, 8(8), 621-629.
- [8]. Babu, D. R., Narsimhan, G. and Phillips, C. R. (1984). Absorption of sulfur dioxide in calcium hydroxide solutions. *Industrial and engineering chemistry fundamentals*, 23(3), 370-373.
- [9]. Bandyopadhyay, A. and Biswas, M. N. (2006). Prediction of the removal efficiency of a novel two-stage hybrid scrubber for flue gas desulfurization. *Chemical Engineering and Technology*, 29(1), 130–145.
- [10]. Bandyopadhyay, A. and Biswas, M. N. (2006). SO<sub>2</sub> scrubbing in a tapered bubble column scrubber. *Chemical Engineering Communications*, 193(12), 1562–1580.
- [11]. Bandyopadhyay, A. and Biswas, M. N. (2007). Modeling of SO<sub>2</sub> scrubbing in spray towers. *Science of the Total Environment*, 383(1), 25-40.

- 
- [12]. Basu, R. K. and Dutta, B. K. (1987). Kinetics of absorption of sulfur dioxide in dimethylaniline solution. *The Canadian Journal of Chemical Engineering*, 65(1), 27-35.
- [13]. Bates, E. D., Mayton, R. D., Ntai, I. and Davis, J. H. (2002). CO<sub>2</sub> capture by a task-specific ionic liquid. *Journal of the American Chemical Society*, 124(6), 926-927.
- [14]. Bhattacharya, S., Dutta, B. K., Shyamal, M. and Basu, R. K. (1996). Absorption of sulfur dioxide in aqueous dispersions of dimethyl aniline. *The Canadian Journal of Chemical Engineering*, 74(3), 339-346.
- [15]. Bhavaraju, S. M., Mashelkar, R. A. and Blanch, H. W. (1978). Bubble motion and mass transfer in non-Newtonian fluids. *AIChE Journal*, 24(6), 1063–1070.
- [16]. Bhoi, S., Banerjee, T. and Mohanty, K. (2016). Beneficiation of Indian coals using Ionic Liquids. *Fuel Processing Technology*, 151, 1-10.
- [17]. Bicak, N. (2005). A new ionic liquid: 2-hydroxy ethylammonium formate. *Journal of Molecular Liquids*, 116(1), 15-18.
- [18]. Bicer, A. and Kar, F. (2017). Thermal and mechanical properties of gypsum plaster mixed with expanded polystyrene and tragacanth. *Thermal Science and Engineering Progress*, 1, 59-65.
- [19]. Bjerle, I., Bengtsson, S. and Färnkvist, K. (1972). Absorption of SO<sub>2</sub> in CaCO<sub>3</sub>-slurry in a laminar jet absorber. *Chemical Engineering Science*, 27(10), 1853-1861.
- [20]. Braulick, W. J., Fair, J. R. and Lerner, B. J. (1965). Mass transfer in a sparged contactor: Part I. Physical mechanisms and controlling parameters. *AIChE Journal*, 11(1), 73-79.
- [21]. Bravo, R. V., Camacho, R. F., Moya, V. M. and García, L. A. I. (2002). Desulphurization of SO<sub>2</sub>-N<sub>2</sub> mixtures by limestone slurries. *Chemical Engineering Science*, 57(11), 2047-2058.
- [22]. Brogren, C. and Karlsson, H. T. (1997). Modeling the absorption of SO<sub>2</sub> in a spray scrubber using the penetration theory. *Chemical Engineering Science*, 52(18), 3085-3099.
- [23]. Bukur, D. B. and Daly, J. G. (1987). Gas hold-up in bubble columns for Fischer-Tropsch synthesis. *Chemical engineering science*, 42(12), 2967-2969.

- 
- [24]. Chandara, C., Azizli, K. A. M., Ahmad, Z. A. and Sakai, E. (2009). Use of waste gypsum to replace natural gypsum as set retarders in portland cement. *Waste management*, 29(5), 1675-1679.
- [25]. Chang, C. S. and Rochelle, G. T. (1981). SO<sub>2</sub> absorption into aqueous solutions. *AIChE Journal*, 27(2), 292-298.
- [26]. Chang, C. S. and Rochelle, G. T. (1985). SO<sub>2</sub> absorption into NaOH and Na<sub>2</sub>SO<sub>3</sub> aqueous solutions. *Industrial and Engineering Chemistry Fundamentals*, 24(1), 7-11.
- [27]. Chien, T. W. and Chu, H. (2000). Removal of SO<sub>2</sub> and NO from flue gas by wet scrubbing using an aqueous NaClO<sub>2</sub> solution. *Journal of Hazardous Materials*, 80(1), 43-57.
- [28]. Chien, T. W., Chu, H. and Hsueh, H. T. (2003). Kinetic study on absorption of SO<sub>2</sub> and NO<sub>x</sub> with acidic NaClO<sub>2</sub> solutions using the spraying column. *Journal of Environmental Engineering*, 129(11), 967-974.
- [29]. Chu, H., Chien, T. W. and Li, S. Y. (2001). Simultaneous absorption of SO<sub>2</sub> and NO from flue gas with KMnO<sub>4</sub>/NaOH solutions. *Science of the Total Environment*, 275(1), 127-135.
- [30]. Codolo, M. C. (2012). Experimental Evaluation of the Removal Efficiency of SO<sub>2</sub> in A Spray Tower Using Different Spray Nozzles, 14th Brazilian Congress of Thermal Sciences and Engineering, Nov. 18-22.
- [31]. Cui, G., Zhang, F., Zhou, X., Huang, Y., Xuan, X. and Wang, J. (2015). Acylamido-based anion-functionalized ionic liquids for efficient SO<sub>2</sub> capture through multiple-site interactions. *ACS Sustainable Chemistry and Engineering*, 3(9), 2264-2270.
- [32]. Dagaonkar, M. V., Beenackers, A. A. and Pangarkar, V. G. (2001). Enhancement of gas-liquid mass transfer by small reactive particles at realistically high mass transfer coefficients: absorption of sulfur dioxide into aqueous slurries of Ca(OH)<sub>2</sub> and Mg (OH)<sub>2</sub> particles. *Chemical Engineering Journal*, 81(1), 203-212.
- [33]. Daly, J. G., Patel, S. A. and Bukur, D. B. (1992). Measurement of gas holdups and sauter mean bubble diameters in bubble column reactors by dynamics gas disengagement method. *Chemical engineering science*, 47(13-14), 3647-3654.
- [34]. Danckwerts and Sharma M. M. (1966). The Absorption of Carbon Dioxide into Solutions of Alkalis and Amines: (with Some Notes on Hydrogen

- 
- Sulphide and Carbonyl Sulphide). Institution of Chemical Engineers, CE244-CE280.
- [35]. Dankwerts, P. V. Gas-liquid reactions. McGraw-Hill, New York, 1970.
- [36]. Dantuluri, S. R., Davis, W. T., Counce, R. M. and Reed, G. D. (1990). Mathematical model of sulfur dioxide absorption into a calcium hydroxide slurry in a spray dryer. *Separation Science and Technology*, 25(13-15), 1843-1855.
- [37]. De Visscher, A. (2013). Air dispersion modeling: foundations and applications. John Wiley and Sons.
- [38]. Deckwer, W. D. (1992). Bubble column reactors (Vol. 200). R. W. Field (Ed.). New York: Wiley.
- [39]. Deckwer, W. D., Louisi, Y., Zaidi, A. and Ralek, M. (1980). Hydrodynamic properties of the Fischer-Tropsch slurry process. *Industrial and Engineering Chemistry Process Design and Development*, 19(4), 699-708.
- [40]. Degaleesan, S., Dudukovic, M. and Pan, Y. (2001). Experimental study of gas-induced liquid-flow structures in bubble columns. *AIChE Journal*, 47(9), 1913-1931.
- [41]. Doraiswamy, L. K. and Sharma, M. M. (1984). Heterogeneous reactions: Analysis examples and reactor design. Vol1: Gas solid and solid-solid reactions.
- [42]. Dou, B., Byun, Y. C. and Hwang, J. (2008). Flue gas desulfurization with an electrostatic spraying absorber. *Energy and Fuels*, 22(2), 1041-1045.
- [43]. Dou, B., Pan, W., Jin, Q., Wang, W. and Li, Y. (2009). Prediction of SO<sub>2</sub> removal efficiency for wet flue gas desulfurization. *Energy Conversion and Management*, 50(10), 2547-2553.
- [44]. Duan, E., Guo, B., Zhang, D., Shi, L., Sun, H. and Wang, Y. (2011). Absorption of NO and NO<sub>2</sub> in caprolactam tetrabutyl ammonium halide ionic liquids. *Journal of the Air and Waste Management Association*, 61(12), 1393-1397.
- [45]. Duan, E., Guo, B., Zhang, M., Yang, B. and Zhang, D. (2010). pH measurements of caprolactam tetrabutyl ammonium bromide ionic liquids in solvents. *Journal of Chemical and Engineering Data*, 55(9), 3278-3281.



- 
- [46]. Ebrahimi, S., Picioreanu, C., Kleerebezem, R., Heijnen, J. J. and Van Loosdrecht, M. C. M. (2003). Rate-based modelling of SO<sub>2</sub> absorption into aqueous NaHCO<sub>3</sub>/Na<sub>2</sub>CO<sub>3</sub> solutions accompanied by the desorption of CO<sub>2</sub>. *Chemical Engineering Science*, 58(16), 3589-3600.
- [47]. ECOBA. (2010). Production and Utilisation of CCPs in 2010 in Europe (EU 15). European Coal Combustion Products Association. Retrieved from <http://www.ecoba.com/ecobaccpprod.html>
- [48]. Erdöl-Aydın, N. and Nasün-Saygılı, G. (2007). Modelling of trona based spray dry scrubbing of SO<sub>2</sub>. *Chemical Engineering Journal*, 126(1), 45-50.
- [49]. Fang, P., Cen, C., Tang, Z., Zhong, P., Chen, D. and Chen, Z. (2011). Simultaneous removal of SO<sub>2</sub> and NO<sub>x</sub> by wet scrubbing using urea solution. *Chemical Engineering Journal*, 168(1), 52-59.
- [50]. Field, R. W. and Davidson, J. F. (1980). Axial dispersion in bubble columns. *Transaction Institute Chemical Engineers*, 58(4), 228-236.
- [51]. Fogler, H. S. (1999). *Elements of chemical reaction engineering*. 3rd edition, PHI, New Delhi, Eastern Economy Edition.
- [52]. Frandsen, J. B., Kiil, S. and Johnsson, J. E. (2001). Optimisation of a wet FGD pilot plant using fine limestone and organic acids. *Chemical Engineering Science*, 56(10), 3275-3287.
- [53]. Gao, X., Ding, H., Du, Z., Wu, Z., Fang, M., Luo, Z. and Cen, K. (2010). Gas-liquid absorption reaction between (NH<sub>4</sub>)<sub>2</sub>SO<sub>3</sub> solution and SO<sub>2</sub> for ammonia-based wet flue gas desulfurization. *Applied Energy*, 87(8), 2647-2651.
- [54]. García-Abuín, A., Gómez-Díaz, D., Navaza, J. M. and Sanjurjo, B. (2015). Influence of surfactant upon SO<sub>2</sub> absorption with and without chemical reaction.
- [55]. Gerbec, M., Stergaršek, A. and Kocjančič, R. (1995). Simulation model of wet flue gas desulphurization plant. *Computers and Chemical Engineering*, 19, 283-286.
- [56]. Ghosh, D., Lal, S., and Sarkar, U. (2017). Variability of tropospheric columnar NO<sub>2</sub> and SO<sub>2</sub> over eastern Indo-Gangetic Plain and impact of meteorology. *Air Quality, Atmosphere and Health*, 10(5), 565-574.
- [57]. Glasscock, D. A. and Rochelle, G. T. (1989). Numerical simulation of theories for gas absorption with chemical reaction. *AIChE journal*, 35(8), 1271-1281.

- 
- [58]. Gómez, A., Fueyo, N. and Tomás, A. (2007). Detailed modelling of a flue-gas desulfurisation plant. *Computers and Chemical Engineering*, 31(11), 1419-1431.
- [59]. Gopal, J. S. and Sharma, M. M. (1982). Hydrodynamic and mass transfer characteristics of bubble and packed bubble columns with downcomer. *The Canadian Journal of Chemical Engineering*, 60(3), 353-362.
- [60]. Gottlieb, H. E., Kotlyar, V. and Nudelman, A. (1997). NMR chemical shifts of common laboratory solvents as trace impurities. *The Journal of organic chemistry*, 62(21), 7512-7515.
- [61]. Guan, X. H., CHEN, G. H., & Shang, C. (2007). ATR-FTIR and XPS study on the structure of complexes formed upon the adsorption of simple organic acids on aluminium hydroxide. *Journal of Environmental Sciences*, 19(4), 438-443.
- [62]. Guan, B., Jiang, G., Wu, Z., Mao, J. and Kong, B. (2011). Preparation of  $\alpha$ -Calcium Sulfate Hemihydrate from Calcium Sulfate Dihydrate in Methanol–Water Solution under Mild Conditions. *Journal of the American Ceramic Society*, 94(10), 3261-3266.
- [63]. Guo, B., Duan, E., Zhong, Y., Gao, L., Zhang, X. and Zhao, D. (2010). Absorption and oxidation of H<sub>2</sub>S in caprolactam tetrabutyl ammonium bromide ionic liquid. *Energy and Fuels*, 25(1), 159-161.
- [64]. Guo, B., Duan, E., Zhong, Y., Gao, L., Zhang, X. and Zhao, D. (2010). Absorption and oxidation of H<sub>2</sub>S in caprolactam tetrabutyl ammonium bromide ionic liquid. *Energy and Fuels*, 25(1), 159-161.
- [65]. Gupta, S.K., Singh, H. and Sahgal, P.N. (1986). Gas absorption in a falling film with a finite gas phase resistance. *Indian Chemical Engineer*, 28, 3-8.
- [66]. Halhouli, K. A., Aly, A. I. and Abu-Ashour, B. M. (1999). Flue gas desulfurization using methanol as a solvent and bromine or iodine as an oxidant. *Chemosphere*, 38(13), 3181-3192.
- [67]. Hallett, J. P. and Welton, T. (2011). Room-temperature ionic liquids: solvents for synthesis and catalysis. 2. *Chemical reviews*, 111(5), 3508-3576.
- [68]. Hamed, Mohamed (2012). Hydrodynamics, Mixing, and Mass Transfer in Bubble Columns with Internals. *All Thesis and Dissertations (ETDs)*. 1006.

- 
- [69]. Hamm, H., Kersten, H. J. and Hueller, R. (2004). 25 year experience gained in the European Gypsum Industry with the use of FGD gypsum. *Cement International*, 4, 92-102.
- [70]. Helsby, F. W. and Birt, D. C. P. (1955). Foam as a medium for gas absorption. *Journal of Chemical Technology and Biotechnology*, 5(7), 347-352.
- [71]. Helsby, F. W., and Birt, D. C. P. (1955). Foam as a medium for gas absorption. *Journal of Chemical Technology and Biotechnology*, 5(7), 347-352.
- [72]. Herbolzheimer, E. and Iglesia, E. (1994). U.S. Patent No. 5,348,982. Washington, DC: U.S. Patent and Trademark Office.
- [73]. Hikita, H. and Konishi, Y. (1983). The absorption of SO<sub>2</sub> into aqueous Na<sub>2</sub>CO<sub>3</sub> solutions accompanied by the desorption of CO<sub>2</sub>. *Chemical Engineering Journal*, 27(3), 167-176.
- [74]. Hikita, H., Asai, S. and Tsuji, T. (1977). Absorption of sulfur dioxide into aqueous sodium hydroxide and sodium sulfite solutions. *AIChE Journal*, 23(4), 538-544.
- [75]. Hikita, H., Asai, S. and Tsuji, T. (1978). Absorption of sulfur dioxide into aqueous ammonia and ammonium sulfite solutions. *Journal of Chemical Engineering of Japan*, 11(3), 236-238.
- [76]. Hikita, H., Asai, S. and Takatsuka, T. (1972). Gas absorption with a two-step instantaneous chemical reaction. *The Chemical Engineering Journal*, 4(1), 31-40.
- [77]. Hikita, H., Asai, S., Tanigawa, K., Segawa, K. and Kitao, M. (1981). The volumetric liquid-phase mass transfer coefficient in bubble columns. *The Chemical Engineering Journal*, 22(1), 61-69.
- [78]. Hills, J. H. (1974). Radial non-uniformity of velocity and voidage in a bubble column. *Transactions of the Institution of Chemical Engineers*, 52(1), 1-9.
- [79]. Hills, J. H. (1976). The operation of a bubble column at high throughputs: I. Gas holdup measurements. *The Chemical Engineering Journal*, 12(2), 89-99.
- [80]. Huang, J., Riisager, A., Berg, R. W. and Fehrmann, R. (2008). Tuning ionic liquids for high gas solubility and reversible gas sorption. *Journal of Molecular Catalysis A: Chemical*, 279(2), 170-176.

- 
- [81]. Huang, J., Riisager, A., Wasserscheid, P. and Fehrmann, R. (2006). Reversible physical absorption of SO<sub>2</sub> by ionic liquids. *Chemical Communications*, (38), 4027-4029.
- [82]. Huang, K., Chen, Y. L., Zhang, X. M., Xia, S., Wu, Y. T., and Hu, X. B. (2014). SO<sub>2</sub> absorption in acid salt ionic liquids/sulfolane binary mixtures: experimental study and thermodynamic analysis. *Chemical Engineering Journal*, 237, 478-486.
- [83]. Huang, K., Lu, J. F., Wu, Y. T., Hu, X. B. and Zhang, Z. B. (2013). Absorption of SO<sub>2</sub> in aqueous solutions of mixed hydroxylammonium dicarboxylate ionic liquids. *Chemical Engineering Journal*, 215, 36-44.
- [84]. Huang, K., Wang, G. N., Dai, Y., Wu, Y. T., Hu, X. B. and Zhang, Z. B. (2013). Dicarboxylic acid salts as task-specific ionic liquids for reversible absorption of SO<sub>2</sub> with a low enthalpy change. *RSC Advances*, 3(37), 162, 64-69.
- [85]. Huddleston, J. G., Willauer, H. D., Swatoski, R. P., Visser, A. E. and Rogers, R. D. (1998). Room temperature ionic liquids as novel media for 'clean' liquid-liquid extraction. *Chemical Communications*, (16), 1765-1766.
- [86]. Hughmark, G. A. (1967). Holdup and mass transfer in bubble columns. *Industrial and Engineering Chemistry Process Design and Development*, 6(2), 218-220.
- [87]. Hyndman, C. L., Larachi, F. and Guy, C. (1997). Understanding gas-phase hydrodynamics in bubble columns: a convective model based on kinetic theory. *Chemical Engineering Science*, 52(1), 63-77.
- [88]. Jana, S. K. and Bhaskarwar, A.N. (2010). Modeling gas absorption accompanied by chemical reaction in bubble column and foam-bed slurry reactors. *Chemical Engineering Science*, 65(11), 3649-3659.
- [89]. Jana, S. K. and Bhaskarwar, A. N. (2011). Gas absorption accompanied by chemical reaction in a system of three-phase slurry-foam reactors in series. *Chemical Engineering Research and Design*, 89(6), 793-810.
- [90]. Jana, S.K. (2007). Studies on a slurry foam reactor for carbonation of hydrated-lime slurry using pure carbon-dioxide gas. Ph.D. thesis, IIT Delhi.
- [91]. Jia, Y., Zhong, Q., Fan, X., Chen, Q. and Sun, H. (2011). Modeling of ammonia-based wet flue gas desulfurization in the spray scrubber. *Korean Journal of Chemical Engineering*, 28(4), 1058-1064.

- 
- [92]. Jiang, L., Liguang, B. A. I., Jiqin, Z. H. U. and Biaohua, C. H. E. N. (2013). Thermodynamic Properties of Caprolactam Ionic Liquids. *Chinese Journal of Chemical Engineering*, 21(7), 766-769.
- [93]. Jin, D. S., Deshwal, B. R., Park, Y. S. and Lee, H. K. (2006). Simultaneous removal of SO<sub>2</sub> and NO by wet scrubbing using aqueous chlorine dioxide solution. *Journal of Hazardous Materials*, 135(1), 412-417.
- [94]. Joshi, J. B. and Sharma, M. M. (1979). A circulation cell model for bubble columns. *Transactions of the Institution of Chemical Engineers*, 57(4), 244.
- [95]. Ju-Hui, J., Hao, Y., Ya-Hong, L., Wei-Jie, X., Long-Hai, L. and Wei-Min, C. (2008). SO<sub>2</sub> removal with ferric sulfate solution. *Environmental technology*, 29(4), 445-449.
- [96]. Kalekar, M. S. and Bhagwat, S. S. (2006). Dynamic behavior of surfactants in solution. *Journal of dispersion science and technology*, 27(7), 1027-1034.
- [97]. Kallinikos, L. E., Farsari, E. I., Spartinos, D. N. and Papayannakos, N. G. (2010). Simulation of the operation of an industrial wet flue gas desulfurization system. *Fuel Processing Technology*, 91(12), 1794-1802.
- [98]. Kantak, M. V., Shetty, S. A., and Kelkar, B. G. (1994). Liquid phase backmixing in bubble column reactors—a new correlation. *Chemical Engineering Communications*, 127(1), 23-34.
- [99]. Kantarci, N., Borak, F. and Ulgen, K. O. (2005). Bubble column reactors. *Process Biochemistry*, 40(7), 2263-2283.
- [100]. Karatepe, N. (2000). A comparison of flue gas desulfurization processes. *Energy Sources*, 22(3), 197-206.
- [101]. Kawagoe, K., Inoue, T., Nakao, K. and Otake, T. (1976). Flow-Pattern and Gas-Holdup Conditions in Gas-Sparged Contactors. *International Chemical Engineering*, 16(1), 176-183.
- [102]. Kawase, Y. and Moo-Young, M. (1987). Heat transfer in bubble column reactors with Newtonian and non-Newtonian fluids. *Chemical Engineering Research and Design*, 65 (2), 121-126.
- [103]. Kawase, Y., Umeno, S. and Kumagai, T. (1992). The prediction of gas hold-up in bubble column reactors: Newtonian and non-Newtonian fluids. *The Chemical Engineering Journal*, 50(1), 1-7.

- 
- [104]. Krishna, R., De Swart, J. W., Ellenberger, J., Martina, G. B., and Maretto, C. (1997). Gas holdup in slurry bubble columns: effect of column diameter and slurry concentrations. *AIChE Journal*, 43(2), 311-316.
- [105]. Krishna, R., De Swart, J. W., Hennephof, D. E., Ellenberger, J. and Hoefsloot, H. C. (1994). Influence of increased gas density on hydrodynamics of bubble-column reactors. *AIChE journal*, 40(1), 112-119.
- [106]. Kumar, A., Degaleesan, T. E., Laddha, G. S. and Hoelscher, H. E. (1976). Bubble swarm characteristics in bubble columns. *The Canadian Journal of Chemical Engineering*, 54(6), 503-508.
- [107]. Kumar, R. and Kuloor, N. K. (1970). The formation of bubbles and drops. *Advances in Chemical Engineering*, 8, 255-368.
- [108]. Lancia, A., Musmarra, D. and Pepe, F. (1997). Modeling of SO<sub>2</sub> absorption into limestone suspensions. *Industrial and Engineering Chemistry Research*, 36(1), 197-203.
- [109]. Lancia, A., Musmarra, D., Pepe, F. and Volpicelli, G. (1994). SO<sub>2</sub> absorption in a bubbling reactor using limestone suspensions. *Chemical Engineering Science*, 49(24), 4523-4532.
- [110]. Laohavichitra, C., Muroyama, K., Weng, S. H., and Fan, L. S. (1982). Absorption of sulfur dioxide by calcium hydroxide solution in a wetted-wall column: effect of magnesium hydroxide, magnesium carbonate and magnesium su. *Chemical Engineering Science*, 37(10), 1572-1575.
- [111]. Lee, K. Y., Kim, C. S., Kim, H., Cheong, M., Mukherjee, D. K. and Jung, K. D. (2010). Effects of halide anions to absorb SO<sub>2</sub> in ionic liquids. *Bulletin of the Korean Chemical Society*, 31(7), 1937-1940.
- [112]. Leibson, I., Holcomb, E. G., Cacosso, A. G. and Jacmic, J. J. (1956). Rate of flow and mechanics of bubble formation from single submerged orifices. II. Mechanics of bubble formation. *AIChE journal*, 2(3), 300-306.
- [113]. Leiva, C., Arenas, C. G., Vilches, L. F., Vale, J., Gimenez, A., Ballesteros, J. C. and Fernández-Pereira, C. (2010). Use of FGD gypsum in fire resistant panels. *Waste Management*, 30(6), 1123-1129.
- [114]. Li, H. and Prakash, A. (1997). Heat transfer and hydrodynamics in a three-phase slurry bubble column. *Industrial and Engineering Chemistry Research*, 36(11), 4688-4694.

- 
- [115]. Li, H., Chen, W. R., and Liu, D. Z. (2003). Desulfurizing absorbent for flue gas and its absorption mechanism. *Journal of Environmental Sciences*, 15(1), 92-96.
- [116]. Li, W., Liu, Y., Wang, L. and Gao, G. (2017). Using Ionic Liquid Mixtures To Improve the SO<sub>2</sub> Absorption Performance in Flue Gas. *Energy and Fuels*, 31(2), 1771-1777.
- [117]. Li, X., Zhang, L., Zheng, Y. and Zheng, C. (2015). Effect of SO<sub>2</sub> on CO<sub>2</sub> absorption in flue gas by ionic liquid 1-ethyl-3-methylimidazolium acetate. *Industrial and Engineering Chemistry Research*, 54(34), 8569-8578.
- [118]. Li, X., Zhu, C., Lu, S. and Ma, Y. (2013). Mass transfer of SO<sub>2</sub> absorption with an instantaneous chemical reaction in a bubble column. *Brazilian Journal of Chemical Engineering*, 30(3), 551-562.
- [119]. Liu, B., Zhao, J. and Wei, F. (2013). Characterization of caprolactam based eutectic ionic liquids and their application in SO<sub>2</sub> absorption. *Journal of Molecular Liquids*, 180, 19-25.
- [120]. Liu, S. Y. and Xiao, W. D. (2006). Modeling and simulation of a bubbling SO<sub>2</sub> absorber with granular limestone slurry and an organic acid additive. *Chemical Engineering and Technology*, 29(10), 1167-1173.
- [121]. Lou, W., Guan, B. and Wu, Z. (2011). Dehydration behavior of FGD gypsum by simultaneous TG and DSC analysis. *Journal of Thermal Analysis and Calorimetry*, 104(2), 661-669.
- [122]. Lu, Z., Streets, D. G., de Foy, B. and Krotkov, N. A. (2013). Ozone Monitoring Instrument observations of interannual increases in SO<sub>2</sub> emissions from Indian coal-fired power plants during 2005–2012. *Environmental Science and Technology*, 47(24), 13993-14000.
- [123]. Lu, Z., Streets, D. G., Zhang, Q., Wang, S., Carmichael, G. R., Cheng, Y. F. and Tan, Q. (2010). Sulfur dioxide emissions in China and sulfur trends in East Asia since 2000. *Atmospheric Chemistry and Physics*, 10(13), 6311-6331.
- [124]. Lu, Z., Zhang, Q. and Streets, D. G. (2011). Sulfur dioxide and primary carbonaceous aerosol emissions in China and India, 1996–2010. *Atmospheric Chemistry and Physics*, 11(18), 9839-9864.
- [125]. Mangartz, K. H., and Pilhofer, T. (1981). Interpretation of mass transfer measurements in bubble columns considering dispersion of both phases. *Chemical Engineering Science*, 36(6), 1069-1077.

- 
- [126]. Mansour, M. B., Soukaina, C. A., Benhamou, B. and Jabrallah, S. B. (2013). Thermal characterization of a Tunisian gypsum plaster as construction material. *Energy Procedia*, 42, 680-688.
- [127]. Marocco, L. (2010). Modeling of the fluid dynamics and SO<sub>2</sub> absorption in a gas-liquid reactor. *Chemical Engineering Journal*, 162(1), 217-226.
- [128]. Marocco, L. and Inzoli, F. (2009). Multiphase Euler-Lagrange CFD simulation applied to wet flue gas desulphurisation technology. *International Journal of Multiphase Flow*, 35(2), 185-194.
- [129]. Martias, C., Joliff, Y. and Favotto, C. (2014). Effects of the addition of glass fibers, mica and vermiculite on the mechanical properties of a gypsum-based composite at room temperature and during a fire test. *Composites Part B: Engineering*, 62, 37-53.
- [130]. Mashelkar, R. A. (1970). Bubble columns. *British Chemical Engineering*, 15(10), 1297.
- [131]. Mashelkar, R. A. and Sharma, M. M. (1970). Mass transfer in bubble and packed bubble columns. *Transactions of the Institution of Chemical Engineers and the Chemical Engineer*, 48(4-6).
- [132]. Matsuura, A. and Fan, L. S. (1984). Distribution of bubble properties in a gas-liquid-solid fluidized bed. *AICHE journal*, 30(6), 894-903.
- [133]. Mc Kinney M.L., Schoch R.M. and Yonavjak L. *Environmental Science: Systems and Solutions*. Fourth edi. Jones and Bartlett Learning, Inc.; 2007.
- [134]. McKinney, M. L. and Schoch, R. M. (2003). *Environmental science: Systems and solutions*. Jones and Bartlett Learning.
- [135]. Mehra, A. (1996). Gas absorption in reactive slurries: particle dissolution near gas-liquid interface. *Chemical Engineering Science*, 51(3), 461-477.
- [136]. Meikap, B. C., Kundu, G. and Biswas, M. N. (2002). A novel modified multi-stage bubble column scrubber for SO<sub>2</sub> removal from industrial off gases. *Separation Science and Technology*, 37(15), 3421-3442.
- [137]. Meikap, B. C., Kundu, G. and Biswas, M. N. (2002). Modeling of a novel multi-stage bubble column scrubber for flue gas desulfurization. *Chemical Engineering Journal*, 86(3), 331-342.
- [138]. Metzner, A. B. and Brown, L. F. (1956). Mass transfer in foams. *Industrial and Engineering Chemistry*, 48(11), 2040-2045.



- 
- [139]. Miller, D. N. (1974). Scale-up of agitated vessels gas-liquid mass transfer. *AICHE Journal*, 20(3), 445-453.
- [140]. Mohammadi, M. and Foroutan, M. (2014). Molecular investigation of SO<sub>2</sub> gas absorption by ionic liquids: Effects of anion type. *Journal of Molecular Liquids*, 193, 60-68.
- [141]. Mondal, A. and Balasubramanian, S. (2016). Understanding SO<sub>2</sub> capture by ionic liquids. *The Journal of Physical Chemistry B*, 120(19), 4457-4466.
- [142]. Mondal, M. K., and Chelluboyana, V. R. (2013). New experimental results of combined SO<sub>2</sub> and NO removal from simulated gas stream by NaClO as low-cost absorbent. *Chemical Engineering Journal*, 217, 48-53.
- [143]. Moo-Young, M. and Blanch, H. W. (1981). Design of biochemical reactors mass transfer criteria for simple and complex systems. In *Reactors and Reactions* (1-69). Springer, Berlin, Heidelberg.
- [144]. Noble, R. D. and Gin, D. L. (2011). Perspective on ionic liquids and ionic liquid membranes. *Journal of Membrane Science*, 369(1), 1-4.
- [145]. Nolan, P. S. (2000). Flue gas desulfurization technologies for coal-fired power plants. In *The Babcock and Wilcox Company, US*, presented by Michael X. Jiang at the Coal-Tech 2000 International Conference.
- [146]. Nosov, V. N., Frolova, N. G. and Kamyshov, V. F. (1976). IR spectra of calcium sulfate semihydrates. *Journal of Applied Spectroscopy*, 24(4), 509-511.
- [147]. Nygaard, H. G., Kiil, S., Johnsson, J. E., Jensen, J. N., Hansen, J., Fogh, F. and Dam-Johansen, K. (2004). Full-scale measurements of SO<sub>2</sub> gas phase concentrations and slurry compositions in a wet flue gas desulphurisation spray absorber. *Fuel*, 83(9), 1151-1164.
- [148]. Olander, D. R. (1960). Simultaneous mass transfer and equilibrium chemical reaction. *AICHE Journal*, 6(2), 233-239.
- [149]. Olausson, S., Wallin, M. and Bjerle, I. (1993). A model for the absorption of sulphur dioxide into a limestone slurry. *The Chemical Engineering Journal*, 51(2), 99-108.
- [150]. Ozturk, S.S., Schumpe, A., and Deckwer, W. D. (1987). Organic liquids in a bubble column: holdups and mass transfer coefficients. *AICHE journal*, 33(9), 1473-1480.

- 
- [151]. Pandey, R. A., Biswas, R., Chakrabarti, T. and Devotta, S. (2005). Flue gas desulfurization: physicochemical and biotechnological approaches. *Critical reviews in environmental science and technology*, 35(6), 571-622.
- [152]. Park, H. W. and Park, D. W. (2017). Removal kinetics for gaseous NO and SO<sub>2</sub> by an aqueous NaClO<sub>2</sub> solution mist in a wet electrostatic precipitator. *Environmental Technology*, 38(7), 835-843.
- [153]. Park, H. W., and Park, D. W. (2017). Removal kinetics for gaseous NO and SO<sub>2</sub> by an aqueous NaClO<sub>2</sub> solution mist in a wet electrostatic precipitator. *Environmental technology*, 38(7), 835-843.
- [154]. Pasiuk-Bronikowska, W. and Rudziński, K. J. (1991). Absorption of SO<sub>2</sub> into aqueous systems. *Chemical Engineering Science*, 46(9), 2281-2291.
- [155]. Pavia, D. L., Lampman, G. M., Kriz, G. S. and Vyvyan, J. A. (2008). *Introduction to Spectroscopy*. Cengage Learning.
- [156]. Perez-Lopez, R., Montes-Hernandez, G., Nieto, J. M., Renard, F. and Charlet, L. (2008). Carbonation of alkaline paper mill waste to reduce CO<sub>2</sub> greenhouse gas emissions into the atmosphere. *Applied Geochemistry*, 23(8), 2292-2300.
- [157]. Pilhofer, T. H., Bach, H. F., and Mangartz, K. H. (1978). Determination of fluid dynamic parameters in bubble column design.
- [158]. Prasad, B. R. and Senapati, S. (2009). Explaining the differential solubility of flue gas components in ionic liquids from first-principle calculations. *The Journal of Physical Chemistry B*, 113(14), 4739-4743.
- [159]. Qu, G., Zhang, J., Li, J. and Ning, P. (2013). SO<sub>2</sub> absorption/desorption characteristics of two novel phosphate ionic liquids. *Separation Science and Technology*, 48(18), 2876-2879.
- [160]. Ramachandran, P. A. and Sharma, M. M. (1969). Absorption with fast reaction in a slurry containing sparingly soluble fine particles. *Chemical Engineering Science*, 24(11), 1681-1686.
- [161]. Reilly, I. G., Scott, D. S., De Bruijn, T., Jain, A. and Piskorz, J. (1986). A correlation for gas holdup in turbulent coalescing bubble columns. *The Canadian Journal of Chemical Engineering*, 64(5), 705-717.
- [162]. Ren, S., Hou, Y., Wu, W. and Jin, M. (2010). Oxidation of SO<sub>2</sub> absorbed by an ionic liquid during desulfurization of simulated flue gases. *Industrial and Engineering Chemistry Research*, 50(2), 998-1002.

- 
- [163]. Ren, S., Hou, Y., Wu, W., and Jin, M. (2010). Oxidation of SO<sub>2</sub> absorbed by an ionic liquid during desulfurization of simulated flue gases. *Industrial and Engineering Chemistry Research*, 50(2), 998-1002.
- [164]. Rennie, J. and Evans, F. (1962). The formation of froth and foams above sieve plates. *Brit. Chem. Eng*, 7, 498.
- [165]. Ridgway, D., Sharma, R. N., and Hanley, T. R. (1991). Fast to instantaneous reaction regime transition in a gas-liquid vessel. *AIChE journal*, 37(4), 633-635.
- [166]. Rochelle, G. T. (1992). Comments on absorption of SO<sub>2</sub> into aqueous systems. *Chemical Engineering Science*, 47(12), 3169-3171.
- [167]. Rogers, R. D. and Seddon, K. R. (2003). Ionic liquids-solvents of the future. *Science*, 302(5646), 792-793.
- [168]. Rosenberg, H. S. (1986). Byproduct gypsum from flue gas desulfurization processes. *Industrial and Engineering Chemistry Product Research and Development*, 25(2), 348-355.
- [169]. Saal, R. N. J. (1928). The velocity of ionic reactions, II. *Recueil des Travaux Chimiques des Pays-Bas*, 47(4), 264-285.
- [170]. Sada, E., Kumazawa, H. and Butt, M. A. (1979). Chemical absorption into a finite slurry. *Chemical Engineering Science*, 34(5), 715-718.
- [171]. Sada, E., Kumazawa, H. and Butt, M. A. (1980). Absorption of sulfur dioxide in aqueous slurries of sparingly soluble fine particles. *Chemical Engineering Journal*, 19(2), 131-138.
- [172]. Sada, E., Kumazawa, H. and Hashizume, I. (1983). Chemical absorption of two gases into a slurry containing fine catalyst particles. *Chemical Engineering Journal*, 26(3), 239-244.
- [173]. Sada, E., Kumazawa, H. and Hoshino, T. (1979). Absorption of lean SO<sub>2</sub> in aqueous solutions of Na<sub>2</sub>CO<sub>3</sub> and desorption of CO<sub>2</sub>. *Chemical Engineering Journal*, 18(1), 125-130.
- [174]. Sada, E., Kumazawa, H. and Lee, C. H. (1983). Chemical absorption in a bubble column loading concentrated slurry. *Chemical engineering science*, 38(12), 2047-2051.
- [175]. Sada, E., Kumazawa, H. and Lee, C. H. (1984). Chemical absorption into concentrated slurry: absorptions of carbon dioxide and sulfur dioxide into

- 
- aqueous concentrated slurries of calcium hydroxide. *Chemical engineering science*, 39(1), 117-120.
- [176]. Sada, E., Kumazawa, H. and Butt, M. A. (1977). Simultaneous absorption of three reacting gases. *Chemical Engineering Journal*, 13(3), 225-231.
- [177]. Sada, E., Kumazawa, H., Hashizume, I. and Kamishima, M. (1981). Desulfurization by limestone slurry with added magnesium sulfate. *Chemical Engineering Journal*, 22(2), 133-141.
- [178]. Sada, E., Kumazawa, H., Hashizume, I. and Nishimura, H. (1982). Absorption of dilute SO<sub>2</sub> into aqueous slimes of 3. *Chemical Engineering Science*, 37(9), 1432-1435.
- [179]. Sada, E., Kumazawa, H., Lee, C. and Fujiwara, N. (1985). Gas-liquid mass transfer characteristics in a bubble column with suspended sparingly soluble fine particles. *Industrial and Engineering Chemistry Process Design and Development*, 24(2), 255-261.
- [180]. Sada, E., Kumazawa, H., Lee, C. H. and Narukawa, H. (1987). Gas-liquid interfacial area and liquid-side mass-transfer coefficient in a slurry bubble column. *Industrial and Engineering Chemistry Research*, 26(1), 112-116.
- [181]. Satriana, M. (1981). *New developments in flue gas desulfurization technology*. United States: Noyes Data Corp., Park Ridge, NJ.
- [182]. Sawant, S. B., Pangarkar, V. G. and Joshi, J. B. (1979). Gas hold-up and mass transfer characteristics of packed bubble columns. *Chemical Engineering Journal*, 18(1), 143-149.
- [183]. Saxena, S. C., Rao, N. S. and Saxena, A. C. (1990). Heat-transfer and gas-holdup studies in a bubble column: air-water-glass bead system. *Chemical Engineering Communications*, 96(1), 31-55.
- [184]. Scala, F. (2002). Gas absorption with instantaneous irreversible chemical reaction in a slurry containing sparingly soluble fine reactant particles. *Industrial and Engineering Chemistry Research*, 41(21), 5187-5195.
- [185]. Scala, F. and D'Ascenzo, M. (2002). Absorption with instantaneous reaction in a droplet with sparingly soluble fines. *AIChE journal*, 48(8), 1719-1726.
- [186]. Schultes, M. (1998). Absorption of Sulphur Dioxide with Sodium Hydroxide Solution. *Chemical Engineering and Technology*, 21(2), 2.

- 
- [187]. Schumpe, A. and Grund, G. (1986). The gas disengagement technique for studying gas holdup structure in bubble columns. *The Canadian Journal of Chemical Engineering*, 64(6), 891-896.
- [188]. Shainberg, I., Sumner, M. E., Miller, W. P., Farina, M. P. W., Pavan, M. A. and Fey, M. V. (1989). Use of gypsum on soils: A review. In *Advances in soil science* (1-111). Springer US.
- [189]. Shang, Y., Li, H., Zhang, S., Xu, H., Wang, Z., Zhang, L. and Zhang, J. (2011). Guanidinium-based ionic liquids for sulfur dioxide sorption. *Chemical Engineering Journal*, 175, 324-329.
- [190]. Shannon, M. S., Irvin, A. C., Liu, H., Moon, J. D., Hindman, M. S., Turner, C. H. and Bara, J. E. (2014). Chemical and physical absorption of SO<sub>2</sub> by N-functionalized imidazoles: experimental results and molecular-level insight. *Industrial and Engineering Chemistry Research*, 54(1), 462-471.
- [191]. Sharma, M. M. and Mashelkar, R. A. (1968). Absorption with reaction in bubble columns. *Inst. Chem. Eng. Symp. Ser*, 28(10).
- [192]. Sharma, M. M., and Danckwerts, P. V. (1970). Chemical methods of measuring interfacial area and mass transfer coefficients in 2-fluid systems. *British Chemical Engineering*, 15(4), 522.
- [193]. Shen, Z., Chen, X., Tong, M., Guo, S., Ni, M. and Lu, J. (2013). Studies on magnesium-based wet flue gas desulfurization process with oxidation inhibition of the byproduct. *Fuel*, 105, 578-584.
- [194]. Shiflett, M. B. and Yokozeki, A. (2009). Chemical absorption of sulfur dioxide in room-temperature ionic liquids. *Industrial and Engineering Chemistry Research*, 49(3), 1370-1377.
- [195]. Shiflett, M. B. and Yokozeki, A. (2009). Separation of carbon dioxide and sulfur dioxide using room-temperature ionic liquid [bmim][MeSO<sub>4</sub>]. *Energy and Fuels*, 24(2), 1001-1008.
- [196]. Shih, F. S. and Lemlich, R. (1971). Continuous foam drainage and overflow. *Industrial and Engineering Chemistry Fundamentals*, 10(2), 254-259.
- [197]. Shulman, H. L. and Molstad, M. C. (1950). Gas-bubble columns for gas-liquid contacting. *Industrial and Engineering Chemistry*, 42(6), 1058-1070.

- 
- [198]. Stangle, G. C. and Mahalingam, R. (1990). Mass transfer with chemical reaction in a three-phase; phase foam-slurry reactor. *AIChE journal*, 36(1), 117-125.
- [199]. Steiner, L., Hunkeler, R. and Hartland, S. (1977). Behaviour of dynamic cellular foams. *Transactions of Industrial Chemical Engineers*, 55, 153-163.
- [200]. Stern, D., Bell, A. T., and Heinemann, H. (1983). Effects of mass transfer on the performance of slurry reactors used for Fischer-Tropsch synthesis. *Chemical Engineering Science*, 38(4), 597-605.
- [201]. Stolojanu, V. and Prakash, A. (1997). Hydrodynamic measurements in a slurry bubble column using ultrasonic techniques. *Chemical Engineering Science*, 52(21-22), 4225-4230.
- [202]. Sung, J. S. and Burgess, J. M. (1987). A laser-based method for bubble parameter measurement in two-dimensional fluidised beds. *Powder technology*, 49(2), 165-175.
- [203]. Tang, Z. G., Zhou, C. C., and Chen, C. (2004). Studies on flue gas desulfurization by chemical absorption using an ethylenediamine– phosphoric acid solution. *Industrial and engineering chemistry research*, 43(21), 6714-6722.
- [204]. Thorat, B. N. and Joshi, J. B. (2004). Regime transition in bubble columns: experimental and predictions. *Experimental Thermal and Fluid Science*, 28(5), 423-430.
- [205]. Tian, S., Hou, Y., Wu, W., Ren, S. and Qian, J. (2014). Hydrophobic task-specific ionic liquids: Synthesis, properties and application for the capture of SO<sub>2</sub>. *Journal of hazardous materials*, 278, 409-416.
- [206]. Towell, G. D., and Ackerman, G. H. (1972, May). Axial mixing of liquid and gas in large bubble reactors. In *Proceedings of 2nd International Symposium on Chemical Reaction Engineering*. Amsterdam, The Netherlands B (Vol. 3, pp. 1-B3).
- [207]. Tzouvalas, G., Dermatas, N. and Tsimas, S. (2004). Alternative calcium sulfate-bearing materials as cement retarders: part I. Anhydrite. *Cement and Concrete Research*, 34(11), 2113-2118.

- 
- [208]. Uchida, S. and Wen, C. Y. (1977). Rate of gas absorption into a slurry accompanied by instantaneous reaction. *Chemical Engineering Science*, 32(11), 1277-1281.
- [209]. Uchida, S., Koide, K. and Shindo, M. (1975). Gas absorption with fast reaction into a slurry containing fine particles. *Chemical Engineering Science*, 30(5-6), 644-646.
- [210]. Uchida, S., Miyachi, M. and Ariga, O. (1981). Penetration model of gas absorption into slurry accompanied by an instantaneous irreversible chemical reaction. *The Canadian Journal of Chemical Engineering*, 59(4), 560-562.
- [211]. Uchida, S., Miyazaki, M. and Masumoto, S. (1984). Absorption of sulfur dioxide into melamine slurry. *Chemical Engineering Science*, 39(10), 1527-1528.
- [212]. Uchida, S., Moriguchi, H., Maejima, H., Koide, K. and Kageyama, S. (1978). Absorption of sulfur dioxide into limestone slurry in a stirred tank reactor. *The Canadian Journal of Chemical Engineering*, 56(6), 690-697.
- [213]. Van Dam, M. H. H., Corriou, J. P., Midoux, N., Lamine, A. S. and Roizard, C. (1999). Modeling and measurement of sulfur dioxide absorption rate in a laminar falling film reactor. *Chemical Engineering Science*, 54(21), 5311-5318.
- [214]. Van Vuuren, D. S. and Heydenrych, M. D. (1985). Multicomponent modelling of Fischer-Tropsch slurry reactors (No. PB-86-116720/XAB; CSIR-CENG-581). Council for Scientific and Industrial Research, Pretoria (South Africa). Chemical Engineering Research Group.
- [215]. Varshney, A., Agrawal, P. and Bhaskarwar, A. N. (2003). Gas absorption with zero-order chemical reaction in a foam-bed reactor. *Chemical Engineering Science*, 58(15), 3413-3424.
- [216]. Vázquez, G., Antorrena, G., Chenlo, F. and Paleo, F. (1988). Absorption of SO<sub>2</sub> by aqueous NaOH solutions in the presence of a surfactant. *Chemical Engineering and Technology*, 11(1), 156-162.
- [217]. Vazquez, G., Cancela, M. A., Riverol, C., Alvarez, E. and Navaza, J. M. (2000). Determination of interfacial areas in a bubble column by different chemical methods. *Industrial and Engineering Chemistry Research*, 39(7), 2541-2547.

- 
- [218]. Wang, C., Cui, G., Luo, X., Xu, Y., Li, H. and Dai, S. (2011). Highly efficient and reversible SO<sub>2</sub> capture by tunable azole-based ionic liquids through multiple-site chemical absorption. *Journal of the American Chemical Society*, 133(31), 11916-11919.
- [219]. Wang, K. B. and Fan, L. T. (1978). Mass transfer in bubble columns packed with motionless mixers. *Chemical Engineering Science*, 33(7), 945-952.
- [220]. Wang, L. K., Williford, C. and Chen, W. Y. (2005). Desulfurization and emissions control. In *Advanced Air and Noise Pollution Control* (pp. 35-95). Humana Press.
- [221]. Wang, L. K., Williford, C., and Chen, W. Y. (2005). Desulfurization and emissions control. In *Advanced Air and Noise Pollution Control* (pp. 35-95). Humana Press.
- [222]. Wang, X. and Deng, J. (2015). Advances in Utilization of Flue Gas Desulfurization Gypsum, 5th International Conference on Advanced Design and Manufacturing Engineering, 1205-1213.
- [223]. Warych, J. and Szymanowski, M. (2001). Model of the wet limestone flue gas desulfurization process for cost optimization. *Industrial and Engineering Chemistry Research*, 40(12), 2597-2605.
- [224]. Wu, Y., Li, Q. and Li, F. (2007). Desulfurization in the gas-continuous impinging stream gas-liquid reactor. *Chemical Engineering Science*, 62(6), 1814-1824.
- [225]. Wu, Y., Ong, B. C. and Al-Dahhan, M. H. (2001). Predictions of radial gas holdup profiles in bubble column reactors. *Chemical Engineering Science*, 56(3), 1207-1210.
- [226]. Yagi, H. and Hikita, H. (1987). Gas absorption into a slurry accompanied by chemical reaction with solute from sparingly soluble particles. *Chemical Engineering Journal*, 36(3), 169-174.
- [227]. Yang, Z. and Pan, W. (2005). Ionic liquids: Green solvents for non-aqueous bio-catalysis. *Enzyme and Microbial Technology*, 37(1), 19-28.
- [228]. Yeager, K. E. (1980). Coal Clean up Technology. *Annu. Rev. Energy*, 5, 357.
- [229]. Yu, Q. L. and Brouwers, H. J. H. (2011). Microstructure and mechanical properties of  $\beta$ -hemihydrate produced gypsum: an insight from its hydration process. *Construction and Building Materials*, 25(7), 3149-3157.



- 
- [230]. Yu, Q. L. and Brouwers, H. J. H. (2012). Development of a self-compacting gypsum-based lightweight composite. *Cement and Concrete Composites*, 34(9), 1033-1043.
- [231]. Yuan, X. L., Zhang, S. J. and Lu, X. M. (2007). Hydroxyl ammonium ionic liquids: synthesis, properties, and solubility of SO<sub>2</sub>. *Journal of Chemical and Engineering Data*, 52(2), 596-599.
- [232]. Zeng, S., Gao, H., Zhang, X., Dong, H., Zhang, X. and Zhang, S. (2014). Efficient and reversible capture of SO<sub>2</sub> by pyridinium-based ionic liquids. *Chemical Engineering Journal*, 251, 248-256.
- [233]. Zhang, Y. C., Dai, S. B., Huang, J., Duan, S. G. and Zhi, Z. Z. (2016). Preparation of Thermal Insulation Plaster with FGD Gypsum. *Kemija u Industriji*, 65(5/6), 283-288.
- [234]. Zhang, Y., Guo, S., Zhou, J., Li, C. and Wang, G. (2010). Flue gas desulfurization by FeSO<sub>4</sub> solutions and coagulation performance of the polymeric ferric sulfate by-product. *Chemical Engineering and Processing: Process Intensification*, 49(8), 859-865.
- [235]. Zhao, Y., Guo, T. X., Chen, Z. Y. and Du, Y. R. (2010). Simultaneous removal of SO<sub>2</sub> and NO using M/NaClO<sub>2</sub> complex absorbent. *Chemical Engineering Journal*, 160(1), 42-47.
- [236]. Zhao, Y., Liu, F., Guo, T. and Zhao, Y. (2009). Experiments and reaction characteristics of liquid phase simultaneous removal of SO<sub>2</sub> and NO. *Science in China Series E: Technological Sciences*, 52(6), 1768-1775.
- [237]. Zhao, Y., Wen, X., Guo, T. and Zhou, J. (2014). Desulfurization and denitrogenation from flue gas using Fenton reagent. *Fuel Processing Technology*, 128, 54-60.
- [238]. Zheng, Y., Kiil, S. and Johnsson, J. E. (2003). Experimental investigation of a pilot-scale jet bubbling reactor for wet flue gas desulphurisation. *Chemical Engineering Science*, 58(20), 4695-4703.
- [239]. Zhu, J., Ye, S. C., Bai, J., Wu, Z. Y., Liu, Z. H. and Yang, Y. F. (2015). A concise algorithm for calculating absorption height in spray tower for wet limestone–gypsum flue gas desulfurization. *Fuel Processing Technology*, 129, 15-23.

## **PUBLICATIONS FROM THESIS**

### ***International Journal:***

- Kumar, A., and Jana, S. K. (2017). "Absorption of SO<sub>2</sub> in a three-Phase Bubble Column and Foam-Bed Slurry Reactor", IJETSRSR, volume 4(5), page 328-332, 2017.

### ***International conferences:***

- Kumar, A., and Jana, S. K. (2017). "Absorption of SO<sub>2</sub> in a three-Phase Bubble Column and Foam-Bed Slurry Reactor", ICNFESMH-2017, by Conference Proceeding at NITTTR Chandigarh / p495-499/ May 2017.
- Kumar, A., Shrivastava, P. and Jana, S. K. , "Studies on Absorption of SO<sub>2</sub> in a Three-Phase Bubble Column Slurry Reactor" CHEMCON 2016 by Conference Proceeding at Anna University, Chennai / 788 / 2016.
- Kumar, A. and Jana S. K. , "A Critical Review of the Reaction Kinetics, Reactor Modeling, Diverse Absorbents and Contactors for Flue Gas Desulfurization" 67th Annual Session of Indian Institute of Chemical Engineers (CHEMCON- 2014) by IChE at SSBUI CET, Chandigarh / 538-539 / 2014.
- Jana, S. K., Arya, I and Kumar, A., "Analysis of Gas-Liquid and Gas-Liquid-Solid Foam-Bed Reactor" 67th Annual Session of Indian Institute of Chemical Engineers (CHEMCON- 2014) by IChE at SSBUI CET Chandigarh / 1104-1105 / 2014.

## BIO-DATA

Name : AVANISH KUMAR

Father's Name : Shri Yougeshwar Pd. Singh

Mother's Name : Smt. Manju Sinha

Date of Birth : 31/01/1987

Marital Status : Married

Educational Qualification : M.Tech., Clean Coal & Energy Technology, (2011),  
*ISM (IIT) Dhanbad*  
B.E., Chemical Engineering, (2008), *R.G.P.V. University, Bhopal*

Job Experience : 03 years teaching

Scientific Memberships : 01 (Life associate member- Indian Institute of Chemical Engineers)

Publications : International Journal (01)  
International conference (04)